Global Sensitivity Analysis of Impedance Measurement Algorithms Implemented in Intelligent Electronic Devices

by

Nanang Rohadi

Bachelor of Engineering,
The University of Indonesia, Indonesia, 1998

Master of Engineering,
Institute Technology of Bandung, Indonesia, 2005

Thesis is submitted for the degree of

Doctor of Philosophy

in

School of Electrical and Electronic Engineering
Faculty of Engineering, Computer, and Mathematical Sciences
The University of Adelaide, Australia

June 2013

Abstract

A novel methodology for testing performance of impedance measurement algorithms used in transmission line protection schemes is developed. Nowadays, impedance measurement algorithms are software functions implemented in the multifunction Intelligence Electronic Devices (IEDs) responsible for overall monitoring, protection and control of transmission lines. Accurate impedance measurement during fault conditions is the key in successful performance of the line protection as well as fault location functions of an IED. This thesis investigates a typical practical situation where only short-term fault records of voltage and current measurements from one side of a transmission line are used as inputs in the impedance measurement algorithm. Current flowing into the fault from the remote terminal of transmission line as well as fault impedance can influence significantly accuracy of impedance measurement. Since these two quantities are not measured, we require a systematic tool which will assess sensitivity of impedance measurement to those factors. At present, these sensitivities are obtained in heuristic and ad hoc manner during application testing done by utilities before commissioning of new IEDs. Situation in practice can be increasingly complex and this kind of unsystematic testing approach can fail. The thesis addresses those practical complex cases in the systematic manner. In these cases we encounter the following configurations of transmission lines with new not measured factors:

- parallel closely spaced lines, where the effect of electromagnetic mutual coupling can be significant;
- series capacitive compensation of transmission line, where capacitance of the compensation device can be unknown;
- three-terminal lines, where measurements on the tapped line are not available.

The proposed systematic sensitivity testing tool comprises of a transmission line electromagnetic simulation module and a Global Sensitivity Analysis (GSA) module. The

software packages commonly used by industry are employed to implement those modules: the DIgSILENT software for the line simulation module and the SIMLAB software for the GSA module. The simulation module is used to simulate large number of fault scenarios for all samples in the factor space, while the GSA module is responsible for creating a set of specific samples in the factor space as well as for sensitivity analysis. The commercial multifunctional IED SEL-421 from the Schweitezer Engineering Laboratories has been used to demonstrate the proposed sensitivity analysis tool. The IED functions has been modelled in DIgSILENT environment and integrated into the simulation module. Test automation program has been written using the DIgSILENT Programming Language (DPL) so fully automatic and integrated performance of the simulation and the GSA modules has been achieved. The GSA module relies on the Quasi-Monte Carlo (QMC) technique with the Sobol's quasi random sampling and the Morris method is used in fast factor pre-screening in order to remove non-influential factors before applying the QMC GSA. The results of systematic tests of the impedance measurement algorithm implemented in the SEL-421 IED, for various line configuration cases, are presented in this thesis. The results verify the usefulness of the proposed testing methodology for practical applications.

Statement of Originality

I certify that this work contains no material which has been accepted for the award of any other degree or diploma in my name, in any university or other tertiary institution and, to the best of my knowledge and belief, contains no material previously published or written by another person, except where due reference has been made in the text. In addition, I certify that no part of this work will, in the future, be used in a submission in my name, for any other degree or diploma in any university or other tertiary institution without the prior approval of the University of Adelaide and where applicable, any partner institution responsible for the joint-award of this degree.

I give consent to this copy of my thesis when deposited in the University Library, being made available for loan and photocopying, subject to the provisions of the Copyright Act 1968.

The author acknowledges that copyright of published works contained within this thesis resides with the copyright holder(s) of those works.

I also give permission for the digital version of my thesis to be made available on the web, via the University's digital research repository, the Library Search and also through web search engines, unless permission has been granted by the University to restrict access for a period of time.

Signed: ……. Date: …….

This page is blank

Acknowledgements

This research has been carried out at the School of Electrical and Electronic Engineering, The University of Adelaide, South Australia.

I would like to express my gratitude and appreciation for Dr. Rastko Zivanovic for his supervision, encouragement, support, patience, and invaluable inputs for this research. His vision and guidance in the preparation of this thesis are gratefully acknowledged. I also wish to thank my advisory committee member, Assoc.Prof. Nesimi Ertugrul, for his suggestions and advice.

I greatly acknowledge the Directorate General of Higher Education (DIKTI), Department of National Education, for providing financial support during my studies. I also acknowledge the financial support, during the last year of this project, provided by Graduate Studies (Research Operations), and also the support from the State Polytechnique of Jakarta.

I would also like to thank Robert Moric, a Ph.D. candidate, at the School of Electrical and Electronic Engineering, University of Adelaide, for his help in editing this thesis. I also acknowledge the support provided by the IT staff, and also the staff of the School of Electrical and Electronic Engineering at the University of Adelaide.

I am also grateful for SIMLAB (2009) version 2.2.1, the software tool developed by the Joint Research Centre of the European Commission, for providing a simulation environment for sensitivity analysis.

To my wife, kind acknowledgements and special thanks are conveyed for your continued love, support and patience in the making of this thesis. To my family members: my late father, my mother, sister, and brother, thank you for your loving and constant encouragement.

To my friends, and research partners, thank you very much for your support during this research. The completion of this project would not have been possible without support from you.

Nanang Rohadi, June 2013

This page is blank

Contents

List of Figures

This page is blank

List of Tables

This page is blank

Glossary of Symbols

$\underline{E}_S$, $\underline{E}_R$, $\underline{E}_T$	source voltage behind terminal S , R, T, respectively	V
$\underline{E}_{1S}$	positive-sequence voltage behind terminal S	V
F	fault location	p.u.
$\underline{I}_1$, $\underline{I}_2$, $\underline{I}_0$	positive-, negative-, and zero-sequence current, respectively	A
$\underline{I}_{1S}$, $\underline{I}_{2S}$, $\underline{I}_{0S}$	positive-, negative-, zero-sequence current at terminal S, respectively	A
$\underline{I}_{AB}$	phase A-B current at the end S during the fault	A
$\underline{I}_{BC}$	phase B-C current at the end S during the fault	A
$\underline{I}_{CA}$	phase C-A current at the end S during the fault	A
$\underline{V}_{AB}$	phase A-B voltage at the end S during the fault	V
$\underline{V}_{BC}$	phase B-C voltage at the end S during the fault	V
$\underline{V}_{CA}$	phase C-A voltage at the end S during the fault	V
$\underline{I}_F$	pure-fault current flowing through the fault resistance	A
$\underline{V}_F$	voltage drop from relaying point to fault location F	V
$\Delta\underline{V}$	random errors of measured voltage distributed value	V
$\Delta\underline{I}$	random errors of measured current distributed value	I
$\underline{I}_S$	total line current at the end S during the fault	A

$\underline{I_A}$, $\underline{I_B}$, $\underline{I_C}$	phase-A, Phase-B, Phase-C current at the end S during the fault, respectively	A
$\underline{I_S^C}$	total compensated current at the end S during the fault	A
$\underline{I_A^C}$	phase-A compensated current at the end S during the fault	A
$\underline{k}_0$	zero-sequence current compensation factor	
k_{0M}	zero-sequence current compensation factor of mutual coupling	
$\underline{I}_{0P}$	zero-sequence current parallel line with both lines in active	A
$\underline{I}'_{0P}$	zero-sequence current parallel line with one is switched off and grounded at both sides	A
$\underline{k}_{0(mod)}$	modified of zero-sequence current compensation factor	
p	proportional of the total line from terminal S	p.u.
r	zone reach from terminal S	p.u.
$R_{1L,}\, R_{0L}$	positive- and zero-sequence line resistances, respectively	Ω
$R_{1S,}\, R_{1R}$	positive -sequence source resistance at station S and R, respectively	Ω
R_F	fault resistance	Ω
X_C	capacitor reactance	Ω
X_L	inductor reactance	Ω
R'_F	resistance and capacitve/inductive reactance	Ω
$\underline{V_1}, \underline{V_2}, \underline{V_0}$	positive-, negative-, and zero-sequence voltage, respectively	V
$\underline{V_{1S}}, \underline{V_{2S}}, \underline{V_{0S}}$	positive-, negative-, and zero-sequence voltage at terminal S, respectively	V

$\underline{V_S}$	total voltage at the line end S during the fault	V
$X_{1L,}X_{0L}$	positive- and zero-sequence line reactance, respectively	Ω
$\Delta\underline{Z_m}$	error calculated in apparent fault impedance on the line at terminal S	Ω
$\underline{Z_{Ref}}$	expected value of apparent fault impedance	Ω
$\underline{Z_{m(\text{sec.})}}$	secondary part of measured impedance on the line at terminal S	Ω
$\underline{Z_m}$	measured fault impedance on the line at terminal S	Ω
$\underline{Z_{1S}}, \underline{Z_{1R}}$	positive-sequence source impedance behind bus S and R, respectively	Ω
$\underline{Z_{0S}}, \underline{Z_{0R}}$	zero-sequence source impedance behind bus S and R, respectively	Ω
$\underline{Z_{1L}}, \underline{Z_{0L}}$	positive- and zero- sequence line impedance, respectively	Ω
$\underline{Z_S}, \underline{Z_R}, \underline{Z_T}$	source impedance behind bus *S,* R, and T respectively	Ω
$\underline{Z_L}$	total line impedance	Ω
$\underline{Z_{OM}}$	mutual impedance of line for the zero-sequence network	Ω
$\underline{Z_{est}}$	estimated impedance of line	Ω
$\underline{Z_{act}}$	actual impedance of line	Ω
$\underline{Z_{tot}}$	total impedance of line (total protected line impedance)	Ω
$\underline{Z_{012}}$	sequence impedance matric	Ω
$\underline{Z_{E1,}}\ \underline{Z_{E2}}, \underline{Z_{E3}}$	equivalent of external line impedance	Ω
θ_L	the angle of maximum reach	deg
$\underline{S_{Pol}}$	polarizing quantity	Ω

$\underline{S}_{op}$	operating quantity	Ω
$\underline{V}^*_{pol}$	polarising voltage	V
Θ	impedance relay operation angle	deg
ϕ_i	angle of the measured current	deg
ϕ_V	angle of the measured voltage	deg
$error_{ss}$	error steady state	%
δ_F	pre-fault power flow angle	deg
$\underline{Z}_{1L1}$, $\underline{Z}_{1L2}$, $\underline{Z}_{1L3}$	positive- sequence line impedance, Line-1, Line-2, and Line-3, respectively	Ω
$\boldsymbol{x}_i$	a number of factors	
$\underline{v}_s(t)$	time varying of measured voltage from terminal S of transmission line	V
$\underline{i}_s(t)$	time varying of measaured line current	A
Δt	sampling interval	s
τ	time constant	s
N	number of samples per period	
Δ	difference	
$H(s)$	transfer function	
s_i	poles of transfer function	
π	mathematical constant	3.14
A	constant value	
$\delta_S, \delta_R, \delta_T$	power flow angle of source impedance in bus S, R, T respectively	deg

x_k	sample of signal with dc-offset	
φ	phase angle	deg
$\underline{V_{peak}}$	maksimum voltage	V
ω	machine angular speed	rad/s
t	time	s
ρ	conductivity of material	Ω.m
l	length of the conductor	m
A	cross sectional area	m^2
R_{dc}	dc-resistance	Ω
L_{int}	internal inductance	H
L_{ext}	external inductance	H
L_{tot}	total inductance	H
R_{t1}	dc-resistance at termperature t_1	Ω
R_{t2}	dc-resistance at termperature t_2	Ω
t_1, t_2	first temperature, second temperature	$°C$
M	temperature constant	
H	magnetic intencity	A/m
B	magnetic dencity	T
λ	flux linkage	Wb-turn/m
$d\emptyset$	differential flux	Wb/m
X_A	inductive reactance of phase A	Ω
$\emptyset_{AB}, \emptyset_{AC}$	flux due to I_B and I_C	Wb

$\underline{Z}_{xy}$	line impedance, xx for self impedance and xy mutual impedance, where $xy = a, b, c$	Ω
$\underline{V}_{AS}, \underline{V}_{BS}, \underline{V}_{CS},$	phase to ground voltage measured from terminal S of	V
$\underline{V}_{AR}, \underline{V}_{BR}, \underline{V}_{CR,}$	phase to ground voltage measured from terminal R of	V
$\underline{V}_{C1}, \underline{V}_{C2}, \underline{V}_{C0},$	sequence voltage of series capacitor	V
$\emptyset_{AA,self},$	self flux in phase A	Wb
$\emptyset_{AA,self}$	another self-flux of phase A	Wb
$\underline{V}_{real}$	real voltage value	V
$\underline{V}_{imag}$	imaginary voltage value	V
$\underline{V}_{mag}$	magnitude voltage	V
$\underline{V}_{angle}$	voltage angle	deg
$\underline{S}_{k}.$	sampled value	
E_i	'elementary effect' calculation for Morris method	
d	number of discretization grid levels	
μ	mean	
σ	Standard deviation	
$E\{*\}$	expected operator	
$V\big(f(\mathbf{x})\big)$	Total variance	
S_i	sensitivity indice	
x_i, x_j	two independence factors	

$Re\{\underline{Z}_{0S}\}$, $Re\{\underline{Z}_{0R}\}$	real value of zero-sequence of source impedance in terminal S and terminal R	Ω
$Im\{\underline{Z}_{0S}\}$, $Im\{\underline{Z}_{0R}\}$	imaginary value of zero-sequence of source impedance in terminal S and terminal R	Ω
$Re\{\underline{Z}_{1S}\}$, $Re\{\underline{Z}_{1R}\}$	real value of positive-sequence of source impedance in terminal S and terminal R	Ω
$Im\{\underline{Z}_{1S}\}$, $Im\{\underline{Z}_{1R}\}$	imaginary value of positive-sequence of source impedance in terminal S and terminal R	Ω
$Re\{\underline{Z}_{1L}\}$, $Re\{\underline{Z}_{0L}\}$	real value of positive- and zero-sequence of line impedance	Ω
$Im\{\underline{Z}_{1L}\}$, $Im\{\underline{Z}_{0L}\}$	imaginary value of positive- and zero-sequence of line impedance	Ω
f	non linear complex function	
$\underline{\boldsymbol{P}}_{\boldsymbol{S}}$	group of positive- and zero-sequence sources impedance	
$\underline{\boldsymbol{P}}_{\boldsymbol{E}}$	group of sources of voltage	
$\underline{\boldsymbol{P}}_{\boldsymbol{L}}$	group of positive- and zero-sequence line impedance	
$\underline{V}_{REF}$	reference voltage	V
$\underline{V}_{V}$	voltage drop across the capacitor	V
q	exponent	
P	reference current	A
R'_C	equivalent series resistance	Ω
X'_C	equivalent series reactance	Ω
X_{CO}	capacitor bank reactance	Ω

This page is blank

Abbreviations

A/D	Analogue to Digital converter
ANOVA	Analysis of Variance
CT	Current Transformer
CVT	Capacitor Voltage Transformer
EMT	Electromagnetic Transient
GSA	Global Sensitivity Analysis
IEDs	Intelligent Electronic Devices
DPL	DIgSILENT Programming Language
QMC	Quasi-Monte Carlo
MCF	Modified Compensation Factor
GMR	Geometric Mean Radius
CB	Circuit Breaker

SCs	Series Capacitors
DFT	Discrete Fourier Transform
MOVs	Metal Oxide Varistors
SA	Sensitivity Analysis
GUI	Graphical User Interface
DSL	Dynamic Simulation Language

List of Publications

[P1] M.N. Ibrahim, **N. Rohadi** and R. Zivanovic, "Methodology for Automated Testing of Transmission Line Fault Locator Algorithms", Australasian Universities Power Engineering Conference (AUPEC 2009), 27-30 September 2009, Adelaide-Australia.

[P2] **N. Rohadi** and R. Zivanovic, "Sensitivity Analysis of Impedance Measurement Algorithms Used in Distance Protection", IEEE TENCON 2011, Bali, Indonesia, November 22-24, 2011.

[P3] **N. Rohadi** and R. Zivanovic, "Sensitivity Analysis of Fault Impedance Measurement Algorithm Used in Protection of Three-Terminal Lines", Australasian Universities Power Engineering Conference (AUPEC 2012), 26-29 September 2012, Bali-Indonesia.

[P4] **N. Rohadi** and R. Zivanovic, " Sensitivity Analysis of a Fault Impedance Measurement Algorithm Applied in Protection of Parallel Transmission Lines", The 9th IET International Conference on Advances in Power System Control, Operation and Management (APSCOM 2012), 18-21 November 2012, Hong Kong

[P5] **N. Rohadi**, R. Zivanovic, "A Method for Sensitivity Analysis of Impedance Measurement Algorithm", Journal of Electrical Engineering, Springer, 2013 (under reviewed).

[P6] **N. Rohadi**, R. Zivanovic, "Sensitivity Analysis of Impedance Measurement Algorithms Used in Series-Compensated Power Transmission Line", Journal of IET Generation, Transmission & Distribution, 2013 (under reviewed)

This page is blank

Chapter 1

Introduction

1.1. Uncertainty in Impedance Measurement and Performance Testing

Impedance measurement algorithm is an important part of an Intelligent Electronic Device (IED) that is used for transmission line protection and monitoring. The algorithm used to calculate fault impedance is based on voltage and current signals measured by the IED at the relaying point. This calculation is used to estimate a positive sequence fault-loop impedance which is influenced by a number of 'uncertain factors' [1]. Understanding the impact of these factors on the accuracy of impedance estimations requires application of a systematic procedure for testing IEDs.

Testing of Impedance Measurement Algorithm is aimed at investigating the accuracy of the calculated transmission line impedance. Testing involves the application of the relay algorithm for estimating the faulted line impedance. This enables the identification of factors that are important for operation of the impedance measurement function and quantifies the impact of those factors using performance measures. Various testing

methods have been proposed in [2-5] that consider the variation of only one factor at a time. However, they are not able to quantify the impact of interactions between two or more factors. A systematic sensitivity analysis of the impedance measurement algorithm using uncertain factors and their interdependencies, as well as full statistical analysis of the measurement variance due to variability of factors has not been considered yet.

Uncertainty sources will contribute to the impedance measurement error, therefore testing of the IED must take this measurement error into account. Testing is not only focused on the protective relay function response and analysis of the accuracy of fault impedance measurement results, but also identifies the factors that influence the impedance measurement algorithm performance during fault conditions. In this case, the factors should be considered simultaneously during error fault impedance calculation. This can be achieved through comprehensive relay testing using a systematic methodology to determine the effects of factors that contribute to the estimation of line fault impedance, $\underline{Z}_m$, which contains some error, $\Delta\underline{Z}_m$, resulting from a non-linear function of uncertain inputs in many fault conditions. The statistical calculation in this case is used for investigating the variability of the output model, $f(\boldsymbol{x})$, the relay algorithm. This model is influenced by the uncertainty of the input factors, $\boldsymbol{x}$.

The approach to comprehensive testing should use a combination of software packages for power system protection and statistical software calculation. Test set software should have the capability to not only investigate the performance of operating characteristics [6], such as response time and steady-state accuracy, but also the effects of individual factors and interactions between factors that impact on operating characteristics [1, 7-9]. This form of relay testing, i.e. for a distance relay, is extremely important for IEDs when applied in complex electrical networks including parallel lines, three-terminal lines, and lines with series compensation where some additional factors such as mutual coupling, current remote infeed of the tapped line, and series compensation will affect their operation.

Factors that impact the measurement algorithm accuracy are classified as follows [10]: System Factors, including fault resistance, non-homogeneous system, system infeeds, series compensation, insufficient detail of a line model, mutual coupling; Setting Factors, including inaccurate line modelling parameters, inaccurate local and remote source modelling parameters, zero-sequence compensation parameter; Measuring Factors,

including inaccuracies in measurement system and measurement conditions. In order to observe which inaccurate value of parameters most impact measurement precision, a method is applied that is based on a large number of tests that are using injection signals produced in simulation of faulted transmission line with factors varied within possible practical intervals. This approach would be recommendable in the systematic testing of the IEDs.

The methods for testing IED have been the subject of extensive research. However, this research did not consider the importance of interaction between uncertainty factors that impact the performance of measurement and protection functions. Complete analysis of the measurement and protection functions output sensitivity to uncertain factors, and statistical analysis of the error in function response has not been considered yet.

The systematic method of relay testing by considering uncertainty factors is performed to analyse the sensitivity of relay algorithm performance. Extensive research has been conducted to develop IED testing scenarios [3, 4, 11-13]. Several methods have been developed that integrate tools including software and hardware. However, these methods did not include an analysis of the global sensitivity. To identify which factors mostly impact on relay performance, a new systematic methodology of testing is required.

In this thesis, we propose a test-based method, where the tests are organized in a systematic way using the Global Sensitivity Analysis (GSA) methodology [14]. The GSA method is demonstrated by testing the specific algorithm implemented in SEL-421 multifuntional feeder protection and automation system [15]. The practical implementation of the method integrates two computation environments: SIMLAB [16] and DIgSILENT [17]. As a power system tool, DIgSILENT *PowerFactory* [17] is used for simulating transmission line faults, calculating the performance index of relay algorithm output during faults and for modelling IED, while the SIMLAB software environment [16] is used to generate factor samples according to the Sobol's quasi-random sequence, and to perform uncertainty and sensitivity analysis using collected test data. The automation task is required to vary the values of factors in a power system protection model. To implement this automation task, we developed an algorithm as a script using the DIgSILENT Programming Language (DPL). The main challenge of the method lies in implementation of large numbers of test cases when there are many factors. For this reason, we need to apply a screening method [1, 7, 8, 18] to identify and disregard unimportant factors in

order to reduce the dimension of the factor space, and hence reduce the number of test cases.

1.2. Objectives of this Thesis

The objective of this thesis is to develop a novel systematic approach in testing impedance measurement algorithms implemented in present day IEDs. This methodology is designed to facilitate the process of multifunctional testing of distance relays by considering the uncertainty parameters of inputs that influence the expected output of the IED. The methodology covers several parts as follows:

- Analysing the performance of IED (i.e., SEL-421 protective relay functions).
- Global sensitivity technique for testing protective relays functions.
- Power system modelling and fault simulation design using DIgSILENT PowerFactory version 14, while SIMLAB is used for the sensitivity analysis.
- Developing a DPL scripting program for automation tasks.

1.3. Outline of the Thesis

Throughout the thesis we describe the design of a systematic methodology for testing the IED based on the GSA. During the research this methodology has been implemented in testing impedance measurement of SEL-421.

Chapter 2 presents a review of the distance protection function. This chapter also details the factors that impact on the performance of the fault impedance calculated by relay. The procedure for the fault impedance calculation, the characteristics of distance protection, and the structure of protection relay are described.

Chapter 3 desirable transmission line faults and fault impedance calculation. The calculation of fault impedance and how distance protection sees this fault impedance are discussed. A ‘system equivalent’ for protection study is applied in conditions where the power system network is complex. In this study, two terminal equivalent and multiport equivalent systems are implemented to study the faults where the IED is located to protect the faulted transmission line.

Chapter 4 and chapter 5, discuss the proposed methodology of testing and the developed technique for Global Sensitivity Analysis (GSA). Two different techniques of sensitivity analysis using Moris, and Quasi-Monte Carlo (QMC) are applied in this study. The fault simulation procedure is described in Chapter 5. Chapter 6 presents several case studies where this methodology has been used. Chapter 7 summarises this work.

Chapter 2

Review of Distance Protection Functions

2.1. Introduction

The main IED function that is used for transmission line protection is called a numerical distance relay. This IED function is an automatic device that is used for short circuit line protection for all medium to ultra high voltage levels. This device is a vital part of power system protection, as it provides a reliable function for detecting and isolating the path of the faulted transmission line, minimises damage to equipment and the disturbance to the electrical power system during fault conditions.

Distance protection relay operates by monitoring the sampled currents and voltages of the power system from the relaying point to detect power system problems (i.e., the faulted line). For a faulted transmission line, the current and voltage to relay are supplied via Current Transformer (CT) and Capacitor Voltage Transformer (CVT). These current and voltage are used by the relay algorithm to determine the apparent fault impedance, $\underline{Z}_m$. Appropriate characteristics are then applied to decide on the disconnection of a faulted transmission line. This IED function is highly effective in protecting a simple transmission

line, such as a single line with two voltage sources, since the fault impedance, $\underline{Z}_m$, is calculated based on the ratio between voltage and current (i.e., $\underline{Z}_m = \underline{V}_S/\underline{I}_S$) [19], and the most common characteristic, self-polarization mho characteristic, which is formed from comparators and various combinations of measured voltages and currents [20].

A wide range of relay application can be investigated with different networks such as parallel line, line with tapping, and line with series compensation. A number of factors, such as fault resistance, inception angle, and additional factors related to mutual coupling, different remote-end infeed/outfeed as well as effect of series compensation, may impact on the performance of the relay algorithm [1, 7, 8, 18]. Underreaching or overreaching problems can affect the non-pilot distance relays as a result of the limiting function in calculating the line fault impedance.

This chapter will discuss the distance relay function for the ground fault on the protected transmission line shown in Figure 2.1. One-ended impedance based fault calculation method is used. The discussion will begin with the operating principles of the distance relay function followed by a description of the distance relay characteristic using self-polarization mho distance relay characteristic, zone classification and setting, and zero-sequence current compensation. The discussion will also review the main functionality of internal modules of the distance relay, such as anti-aliasing filter, phasor estimation algorithm, as well as the relay algorithm function.

2.2. Distance Protection

2.2.1. Principle of Operation of the Distance Protection Function

The principle operation of distance protection function for protecting the faulted transmission line is illustrated in Figure 2.1. This function compares the voltage, $\underline{V}_S$, and current, $\underline{I}_S$, signals measured from the relaying point to obtain a measure of apparent fault impedance, $\underline{Z}_m$, at the fundamental frequency between the distance relay located at substation S and the fault point *F*. This measured fault impedance, $\underline{Z}_m$, is then compared with the known reach point impedance, $\underline{Z}_{Ref}$. If the measured impedance is less than the

set line impedance, $\underline{Z}_{Ref}$ (i.e., $\underline{Z}_m < \underline{Z}_{Ref}$), then the fault is detected and the trip command to the circuit breaker is issued to isolate the fault [21].

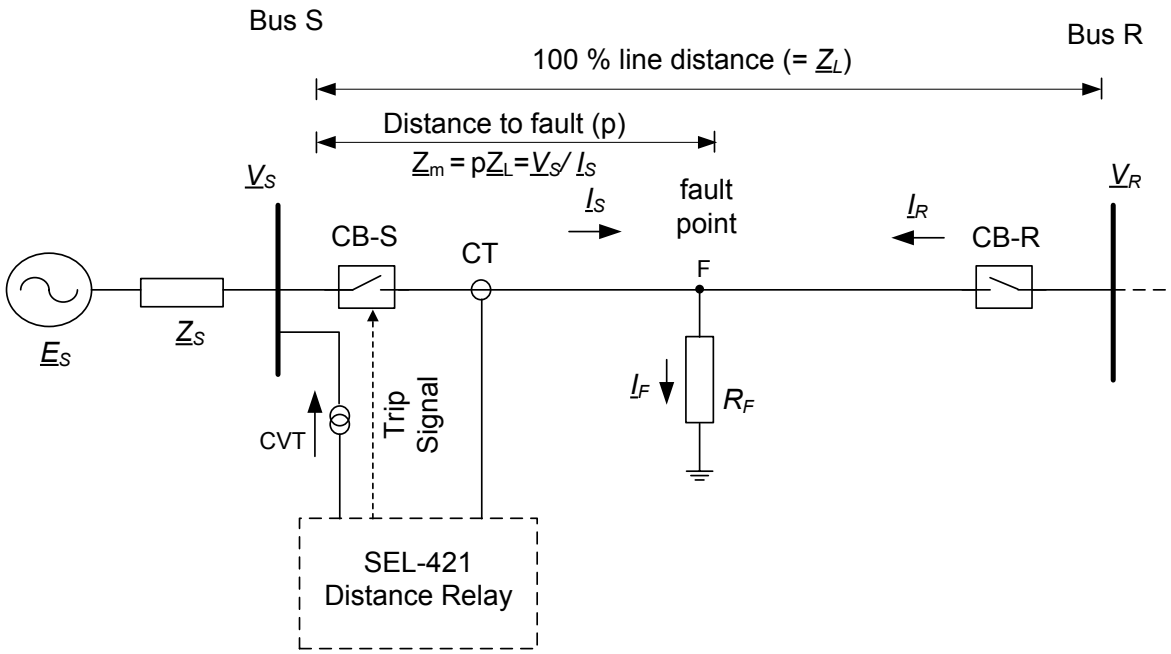

Figure 2.1: Distance protection principle of measured fault impedance.

In simple fault impedance calculations, only voltage and current signals are required. This means that no additional information is required for the traditional distance relay, and the fault calculation does not depend on the factors that contribute to their accuracy. Equations (2.1) to (2.3) show the ideal fault impedance calculation that is directly proportional to the distance between the faults located at F and the relay located at substation S.

Fault impedance calculation is derived according to Figure 2.1 as follows:

$$\underline{V}_S = \frac{\underline{E}_S p \underline{Z}_{1L}}{\underline{Z}_S + p\underline{Z}_{1L}} \tag{2.1}$$

$$\underline{I}_S = \frac{\underline{E}_S}{\underline{Z}_S + p\underline{Z}_{1L}} \tag{2.2}$$

$$\underline{Z}_{m(\text{sec.})} = \frac{\underline{V_S}/_{CVT\ ratio}}{\underline{I_S}/_{CTratio}} = \ p\underline{Z}_{1L(prim.)}\frac{CTratio}{CVT\ ratio} \tag{2.3}$$

From Equations (2.1) and (2.2), $\underline{V_S}$ and $\underline{I_S}$ are the primary voltage and current of voltage transformer, CVT, and current transformer, CT, respectively. The apparent impedance, $\underline{Z_m}$, which is called a secondary impedance [22], is calculated based on the ratio between the secondary value of voltage and current signals in the phasor domain.

In reality, a number of internal and external factors will impact the accuracy of fault impedance calculations and result in measurement error. Therefore, in practice it is not possible to apply the relay to 100% of the line distance (see Figure 2.1). A security limit of 10% - 20% of the line length needs to be applied in order to ensure the selectivity of no delay time response of zone 1 during the faults. The rest of the line length is covered by zone 2 in which different time delay response is applied (see Figure 2.4).

2.2.2. Self- Polarization Mho Characteristic

A simple mho characteristic with a reach of 0.8 $\underline{Z}_{1L}$ and the maximum reach angle, θ_L, is shown in Figure 2.2. The impedance reference value, $\underline{Z}_{Ref}$, sets the point along the line impedance locus that is intersected by the boundary characteristic of the relay. This self-polarization mho characteristic is used for analysing the performance of the impedance measurement algorithm, where the loci of calculated fault impedance, $\underline{Z_m}$, are plotted in the same diagram to study the performance. The algorithm function included in the distance relay located at terminal R (see Figure 2.1) determines whether the measured fault impedance, $\underline{Z_m}$, is plotted within the boundary of the self-polarization mho characteristic. The trip command is then issued to open the circuit breaker. The fault impedance is obtained by measuring the total impedance seen from the relaying point to the fault location *F* and is based on the measured voltage, $\underline{V_S}$, and current, $\underline{I_S}$, on the primary CVT and CT at the relaying point. The fault beyond this reach setting should not be tripped immediately by the relay located at terminal S but will be cleared when the relay located at terminal R issues the trip command to open circuit breaker R (CB-R). A fault close to a reach point of 80% should be picked-up by the relay located at terminal S.

The impedance measurement at relay S is a function of all system parameters [23]. These are: fault resistance, impedance in the network, inception angle, and the Thevenin's equivalent circuit representing sources S and R, as well as internal factors, e.g. setting of zero-sequence impedance of distance relay. These factors may affect the current and voltage measured by the relay located at terminal S, and consequently results in underreach and overreach of the distance relay function [7, 8, 18].

Distance protection has a settable maximum angle, which is the angle of the current compared to the voltage angle at which the relay is most sensitive. Figure 2.3 shows a typical self-polarization mho characteristic using cosine-phase comparator to measure the phase angle, $-90° \leq \Theta \leq 90°$, between operating, $\underline{S}_{op} = r\underline{Z}_{1L}\underline{I}_S^C - \underline{V}_S$, and polarizing signals, $\underline{S}_{Pol} = \underline{V}_S$, which is characterized as circular. The mho comparator P, which is used to test the measured fault impedance against a self-polarizing mho characteristic, is derived using Equation (2.4) [20, 23-26]:

$$P = R_e\left[\underline{S}_{op}\underline{S}_{Pol}\right] = R_e\left[\left(r\underline{Z}_{1L}\underline{I}_S^C - \underline{V}_S\right)\underline{V}_P^*\right], \tag{2.4}$$

where:

$\underline{S}_{op} = r\underline{Z}_{1L}\underline{I}_S^C - \underline{V}_S$, compensated line voltage-drop,

$\underline{S}_{op} = \underline{V}_P$, polarizing voltage,

$\underline{V}_S$, measured voltage at terminal S,

$\underline{I}_S^C = \underline{I}_S + \underline{k}_0\underline{I}_0$, compensated current measured at terminal S,

$\underline{k}_0 = \left(\underline{Z}_{0L} - \underline{Z}_{1L}\right)/\underline{Z}_{1L}$,

R_e, real portion,

r, per-unit reach,

*, complex conjugate.

To determine the boundary characteristic of the reach, $r\underline{Z}_{1L}$, of self-polarized mho characteristic, $P = 0$ is set and substitute $\underline{S}_{Pol} = \underline{V}_S$. Hence equation (2.4) is rewritten as follows:

$$R_e\left[\left(r\underline{Z}_{1L}\underline{I}_S^C - \underline{V}_S\right)\underline{V}_S{}^*\right] = 0, \tag{2.5a}$$

$$R_e\left[\left(r\underline{Z}_{1L}\underline{I}_S^C\underline{V}_S{}^*\right) - \left|\underline{V}_S\right|^2\right] = 0. \tag{2.5b}$$

If $r\underline{Z}_{1L} = \left|r\underline{Z}_{1L}\right|\angle\theta_L$ then

$$r\underline{Z}_{1L} = \frac{|\underline{V}_S|^2}{R_e\left(\underline{I}_S^C \, 1\angle\theta_L \underline{V}_S^*\right)}, \tag{2.6a}$$

$$|r\underline{Z}_{1L}| = \frac{|\underline{V}_S|}{|\underline{I}_S^C| cos[\theta_L - (\phi_v - \phi_i)]}, \tag{2.6b}$$

$$|\underline{Z}_m| = |r\underline{Z}_{1L}| cos[\theta_L - \phi] \ , \tag{2.7}$$

where:

$\phi = \phi_v - \phi_i$, the angle of the protected line (angle setting),

ϕ_v, angle of the measured voltage,

ϕ_i, angle of the measured current,

θ_L, maximum angle of self-polarization mho characteristic.

If $\phi = \theta_L$, then the apparent fault impedance can be stated as:

$$|\underline{Z}_m| = {|\underline{V}_S|}/{|\underline{I}_S^C|} = |r\underline{Z}_{1L}| \tag{2.8}$$

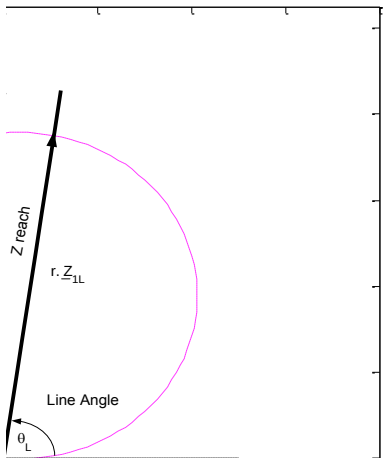

Figure 2.2: Self-Polarized Mho Characteristic with a reach of $r\underline{Z}_{1L}$.

A voltage diagram describing the self-polarization mho characteristic is shown in Figure 2.3. A different phasor between line-drop compensated voltage, $\underline{S}_{OP}$, and polarizing

voltage, $\underline{S}_{pol}$, is used for the analysis. Replica of line impedance characteristic of $r\underline{Z}_{1L}\underline{I}_S^C$ is the maximum reach of the circle, and $\underline{V}_S$ is based on the location of the fault (i.e., the measured fault voltage). A difference phasor between $\underline{S}_{OP}$ and $\underline{S}_{pol}$ that is 90 degrees apart indicates that all faults are located in the border of the circle. If the fault moves near the relaying point, it is inside the circle or inside the protection zone. If this condition is met, the magnitude of the measured voltage, $\underline{V}_S$, will decrease and the magnitude of the operating signal will increase. At this value, the angle of A will be more than 90 degrees while the angle of B will be less than 90 degrees. Alternatively, if the fault moves farther from the relaying point, that is outside of the circle, the magnitude of $\underline{V}_S$ will increase relative to the magnitude of operating signal and the angle of A will be less than 90 degrees while the angle of B will be more than 90 degrees.

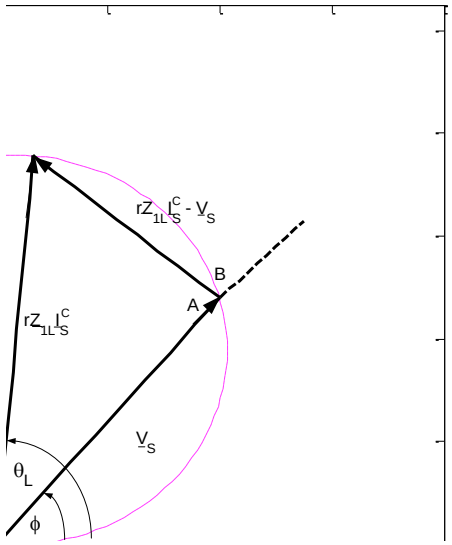

Figure 2.3: Voltage Diagram of Self-Polarizing Mho Characteristic [23, 24].

2.2.3. Zone Classification and Setting

The feeder length protected by the distance relay is normally divided into three protection zones. These zones are classified based on the impedance reaches combined with different

time delays [27]. As shown in Figure 2.4, directional Zone 1 protection is an instantaneous (high-speed, no intentional delay) tripping zone that is normally set to provide less than 100% coverage of the protected line, SR, of Zone 1 and should never reach the next bus R. The distance relay is designed to trip first when the fault is detected in the 1st zone. The resulting 15-20% safety margin ensures that there is no risk of the Zone 1 protection overreaching the protected line due to uncertain factors of the power systems protection, including errors in CVT and CT for relay setting.

A special condition is taken into account when Zone 1 of the conventional distance relay, in Figure 2.4, is applied in circuits containing parallel lines, lines with series compensation, and multi-terminal lines, where the accuracy of fault loop impedance measurements are substantially affected when the conventional distance relay is applied to these types of circuits. Consequently, a change in the Zone 1 distance protection reach may occur. This condition presents a difficult task for utility engineers or manufactures in setting the first zone. The following considerations need to be applied when the conventional distance relays are used in such complex line cases.

Complexity may occur when the Zone 1 distance function is applied on the protected line with a series compensated system (see Figure 2.17). The setting of Zone 1, in this case, is difficult since the performance of the protection system will depend on the status of the capacitor, effects of subharmonic-frequency transient, and distance relay filter response when the fault is simulated behind series capacitor SCs [28, 29]. The overreaching or underreaching of distance relay reach may occur in cases where faults occur behind the series capacitor. To properly set the distance relay, the following items may need to be considered when setting Zone 1 [29]:

- Line impedance and level of capacitor compensation value.
- The location of series capacitor.
- Type of capacitor protection.
- Protection level of capacitor protection.

The complexity of the Zone 1 relay setting is observed when the distance relay is applied to parallel circuits. In this condition, the overreaching and underreaching of the distance relay reach may occur due to the effect of the mutual coupling of zero-sequence currents between parallel lines [30, 31]. If the system impedance, bus configuration, and line operating conditions do not change during normal operation, the effect of mutual

coupling can be compensated using the proper relay setting. Thus, we can change the zero-sequence compensation factor, or the relay zone coverage setting, to obtain a typical 80%-85% relay setting [30]. However, the operating condition of parallel lines could change due to scheduled maintenance and forced outage, or load distances. In these cases, different effects of mutual coupling on the first zone reach will contribute to overreaching or underreaching in distance relay operation. Figure 2.19 shows these phenomena when the second line is switched off and grounded at both ends and both lines are in operation. Use of an adaptive scheme is required to overcome this problem.

The final consideration regarding the complexity in setting Zone 1 reach occurs when the distance relay is applied to multi-terminal lines. Overreaching and underreaching occurs when the conventional distance relay (or non-pilot distance relay) is applied to multi-terminal lines [32]. This limitation, acknowledged in [33], is due to the different characteristics of remote-end infeed/outfeed and is not measured by conventional distance relay. To achieve proper setting and avoid underreaching, the covering of the distance relay reach of Zone 1 is set to 80-90% of the line length of the nearest remote terminal [32].

Zone 2 is a time delayed tripping zone that covers the protected line (SR) beyond Zone 1 (see Figure 2.4). This zone also provides backup for a failed Zone 1 element, both in the protected line (SR) and in the next line. Zone tripping must be time-delayed to ensure grading with the primary relaying applied to the adjacent circuit that falls within the Zone 2 reach and it should be set to a delay of at least 20-30 cycles. The Zone 2 setting is set to at least 120% of the protected transmission line. In many applications the setting of Zone 2 is +50% of the protected section line.

Zone 3 is a time delayed tripping zone for backup protection on adjacent line faults and should be set for 0.5-3.0 seconds. Zone 1 and Zone 2 preserve continuity of service or preserve system stability whereas Zone 3 is a remote backup to clear a fault in the event a remote breaker does no trip.

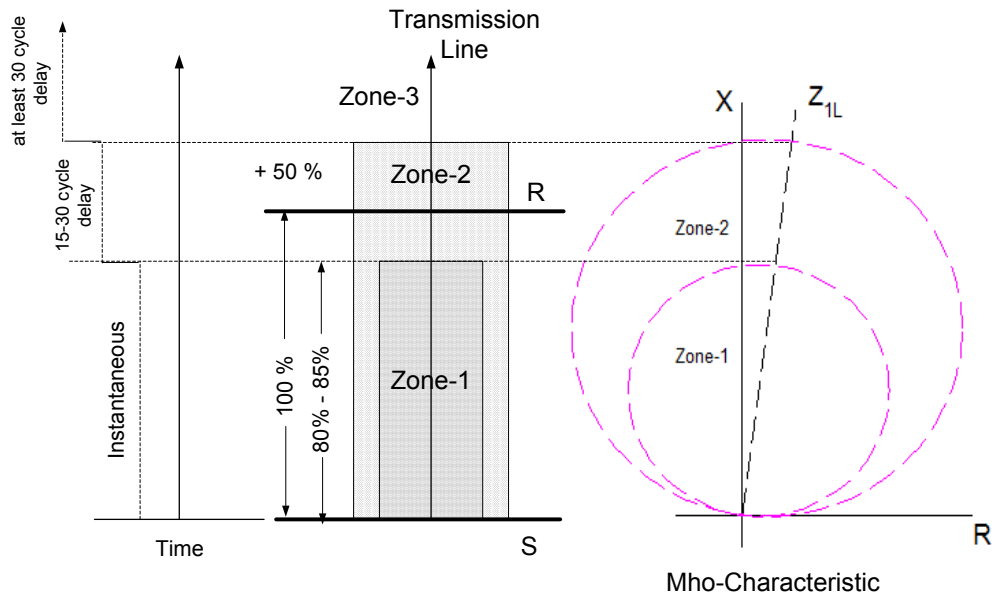

Figure 2.4: Zone classification and stepped time of distance relay operation.

2.2.4. Fault Impedance Measurement

Processing Signals for Fault Impedance Measurement

Figure 2.5 demonstrates waveforms of three-phases of voltage, current, and measured fault impedance, for single phase to ground fault, simulated using DIgSILENT software. The recorded waveforms of voltages and currents are used as input signals that provide the information necessary for the signal processing of fault impedance demonstrated in Figure 2.10. Signal processing that consists of a low-pass analog anti-aliasing 2^{nd} Order Butterworth filter and and A/D converter is used to discretize the filtered analog input signals which is then used to describe the faulted line. The output of this function is used by a discrete filter, comprised of Fourier transforms, and describes the state of the faulted line using the phasor approach.

In order to calculate the fault impedance using the phasor approach, the sinusoidal input of voltage and current signals, and symmetrical components are represented in the form of magnitude and angle velocity ω. This approach is called frequency domain circuit analysis [34]. The measured fault impedance is described entirely using voltage/current phasors and the line impedance, where symmetrical components are used to determine the fault impedance that can be stated as positive-sequence or negative-sequence.

Additionally, uncertain values of zero-sequence impedance data of transmission lines, and present effects of voltage and current zero-sequence of parallel lines, are used in measuring the fault impedance calculated by the relay algorithm. To avoid this, zero-sequence current compensation and zero-sequence compensation of parallel lines are applied.

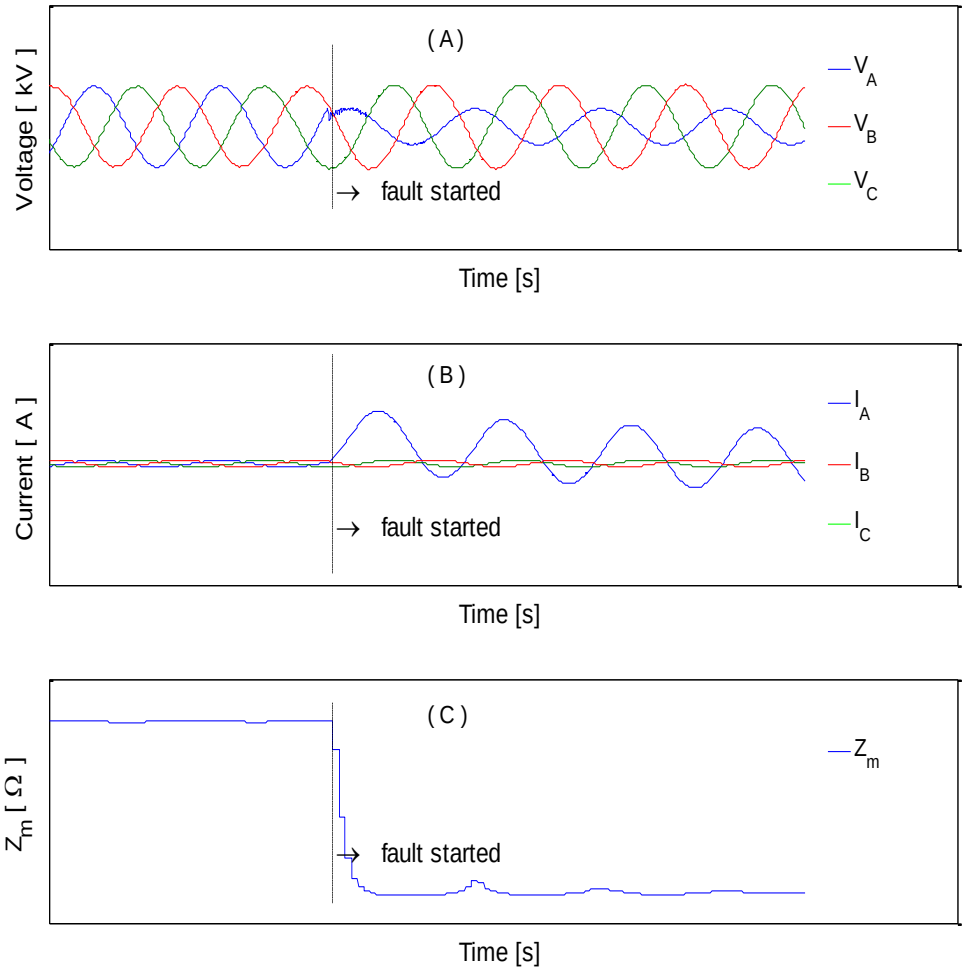

Figure 2.5: Fault input signals and fault impedance: (a) phase voltage, (b) phase current, (c) and fault impedance, at the relaying point.

Fault Impedance Measurement Technique

We consider the impedance unit of the distance relay (see Figure 2.10) that is used to calculate the apparent fault impedance of the fault in Figure 2.1. The apparent fault

impedance, $\underline{Z}_m$, is calculated as the ratio of the relay voltage, $\underline{V}_S$, to the relay current, $\underline{I}_S$ (i.e., $\underline{Z}_m = \underline{V}_S/\underline{I}_S$). This equation is unique since only one fault impedance calculation is needed per fault loop for the use of multi-zones in analysing impedance unit algorithm performance during faults.

In relation to Figure 2.1, the calculation of phase to ground fault impedance, shown in Figure 2.6, is typically calculated based on the positive-sequence impedance. Figure 2.7 shows the impedance seen by the relaying point that is calculated using a combination of the positive-, negative-, and zero-sequence impedances of the system [24]. The positive- and negative-sequence impedances are generally equal in magnitude and angle except for the zero-sequence impedance. For this reason, a zero-sequence current compensation of $\underline{k}_0$ is required to be in phase with the ground fault in order to adjust the apparent measured impedance to reflect the actual system impedance.

We assume in Figure 2.1 that the phase, A, to ground fault with the fault current, $\underline{I}_F$, flows through the fault resistance, R_F. Hence, the fault voltage measured from the relaying point can be stated as [20] :

$$\underline{V}_S = p\underline{Z}_{1L}\left(\underline{I}_A + \underline{k}_0\underline{I}_0\right) + R_F\underline{I}_F\,. \tag{2.9}$$

Equation (2.9) could be converted into the impedance equation by dividing it with the current measured from the relaying point, $\underline{I}_S$, where $\underline{I}_S^C = \underline{I}_A + \underline{k}_0\underline{I}_F$. This results in:

$$\underline{Z}_m = \frac{\underline{V}_S}{I_S^C} = p\underline{Z}_{1L} + R_F\frac{\underline{I}_F}{\underline{I}_S^C}, \tag{2.10}$$

$$= \frac{\underline{V}_S}{\underline{I}_S^C} = pZ_{1L}\,, \quad \text{for } R_F = 0. \tag{2.11}$$

If $\underline{Z}_m$ is assumed to be the primary impedance, $\underline{Z}_{m(pri)}$, the secondary impedance for use in the distance relay, that reflects the actual value of primary impedance, is given in Equation (2.12).

$$\underline{Z}_{m(\text{sec})} = \underline{Z}_{m(pri)}\frac{CT_{ratio}}{CVT_{ratio}}, \tag{2.12}$$

where CT_{ratio} is the ratio between the high voltage and the current (i.e., primary current) to the relay current (i.e., secondary current), and CVT_{ratio} is the ratio of the primary voltage (i.e., high voltage) to the secondary voltage (i.e., relay voltage).

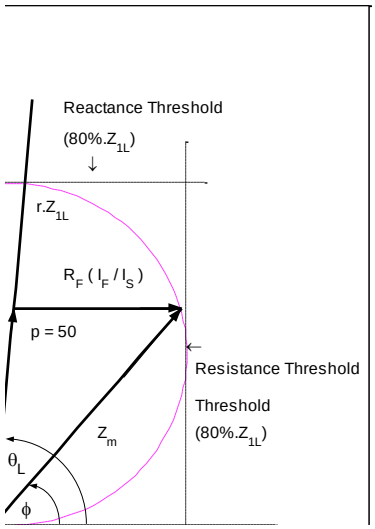

Figure 2.6: AG apparent impedance plane (including fault resistance, R_F).

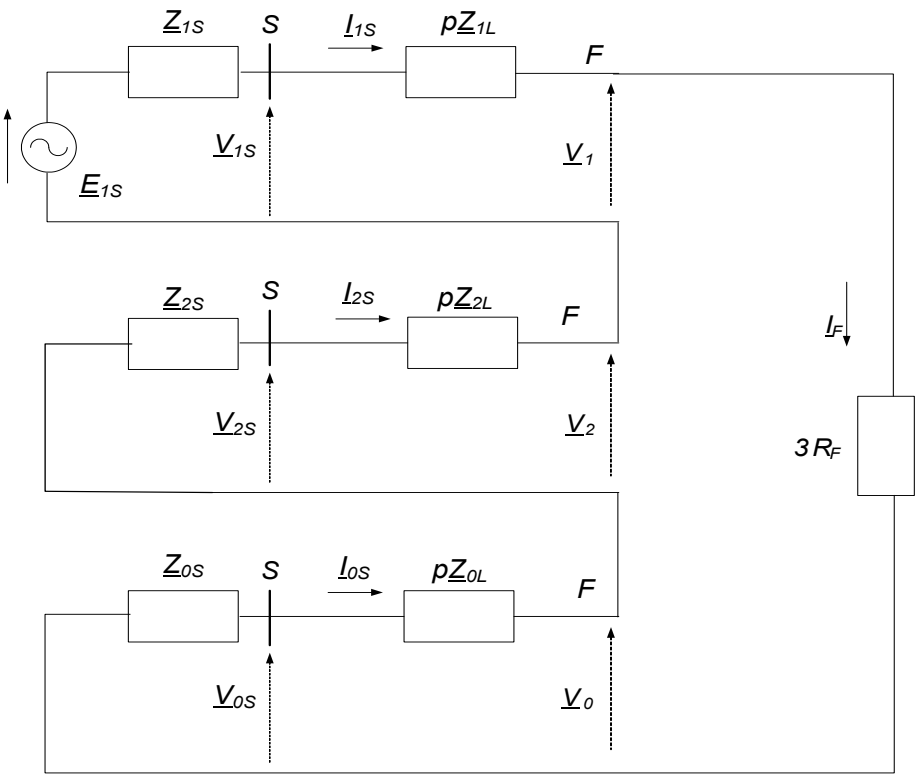

Figure 2.7: Sequence network connection for SLG fault.

Zero Sequence Current Compensation

It has been shown that the voltage measured at the relaying point in a multi-phase fault (balancing fault) is equal to the voltage drop along the line between the relaying point and fault location [26]. However, this is the case for an unbalanced fault, with phase A to ground fault (unbalanced fault), that was introduced in the previous section. The measured voltage by a ground distance function uses only the faulted phase, the fault current and setting value. The voltage drop of phase A is not simply made up of the drop in the positive-sequence of line impedance, $\underline{Z}_{1L}$, as with a balanced fault. This is due to factors such as: zero-sequence of line impedance, $\underline{Z}_{0L}$, zero-sequence of current, $\underline{I}_0$ [26], and fault resistance, R_F. The voltage drop of $\underline{I}_A\underline{Z}_{1L}$ is equal to the measured voltage $\underline{V}_A$ only if zero-sequence compensation, $\underline{k}_0$, and $R_F = 0$ are applied.

From the sequence network connection for phase A to ground fault (see Figure 2.7), the voltage at the relaying point ($\underline{V}_S$) is derived as follows [26]:

$$\underline{V}_S = \underline{V}_{1S} + \underline{V}_{2S} + \underline{V}_{0S}, \tag{2.13}$$

where

$$\underline{V}_{1S} = \underline{I}_{1S}p\underline{Z}_{1L} + \underline{V}_1, \tag{2.14a}$$

$$\underline{V}_{2S} = \underline{I}_{2S}p\underline{Z}_{2L} + \underline{V}_2, \tag{2.14b}$$

$$\underline{V}_{0S} = \underline{I}_{0S}p\underline{Z}_{0L} + \underline{V}_0. \tag{2.14c}$$

Therefore, Equation (2.13) can be restated as:

$$\underline{V}_S = \underline{I}_{1S}p\underline{Z}_{1L} + \underline{I}_{2S}p\underline{Z}_{2L} + \underline{I}_{0S}p\underline{Z}_{0L} + \left(\underline{V}_1 + \underline{V}_2 + \underline{V}_0\right), \tag{2.15}$$

$$\left(\underline{V}_1 + \underline{V}_2 + \underline{V}_0\right) = 0 \text{ if } R_F = 0.$$

Assuming that $p\underline{Z}_{1L}$, we have

$$\underline{V}_S = \left(\underline{I}_{1S} + \underline{I}_{2S}\right)p\underline{Z}_{1L} + \underline{I}_{0S}p\underline{Z}_{0L.} \tag{2.16}$$

This voltage drop of $\underline{V}_S$ would not be equal to the voltage drop on the positive-sequence on the faulted line, $p\underline{Z}_{1L}$, not as for the multi phase fault. In order for $\underline{V}_S$ to be equal to the voltage drop on the faulted line, a proportional factor to the zero-sequence impedance is included. If a distance relay only measures the fault current $\underline{I}_A$ (i.e., $\underline{I}_B = \underline{I}_C = 0$) during

phase A to ground fault and we set replica impedance, $p\underline{Z}_{1R}$, equal to the positive-sequence impedance, $p\underline{Z}_{1L}$, then $\underline{IZ}$ is stated as:

$$\underline{I}_A = \underline{I}_{1s} + \underline{I}_{2s} + \underline{I}_{0s}, \tag{2.17}$$

$$\underline{IZ} = \underline{I}_A p\underline{Z}_{1R} = \left(\underline{I}_{1s} + \underline{I}_{2s}\right) p\underline{Z}_{1L} + p\underline{Z}_{1L}\underline{I}_{0s}. \tag{2.18}$$

Replica impedance, $\underline{IZ}$, is not equal to the voltage drop $\underline{V}_S$, since $p\underline{Z}_{1L} \neq p\underline{Z}_{0L}$. To be equal to $\underline{V}_S$, the zero-sequence current is multiplied by the ratio of the zero-sequence impedance to the positive-sequence impedance. Hence, Equation (2.17) could be restated as:

$$\underline{I}_A^C = \underline{I}_{1s} + \underline{I}_{2s} + \underline{k}_0\underline{I}_{0s}, \tag{2.19}$$

then

$$\underline{IZ} = \underline{I}_A^C p\underline{Z}_{1R} = \left(\underline{I}_{1s} + \underline{I}_{2s}\right) p\underline{Z}_{1L} + \underline{k}_0\, p\underline{Z}_{1L}\underline{I}_{0s}, \tag{2.20}$$

$$\underline{IZ} = \left(\underline{I}_{1s} + \underline{I}_{2s}\right) p\underline{Z}_{1L} + p\underline{Z}_{0L}\underline{I}_{0s}.$$

Therefore, the operating quantity, $\underline{S}_{op}$, is calculated as:

$$\begin{aligned}\underline{S}_{op} &= \underline{I}_A^C p\underline{Z}_{1R} - \underline{V}_S = \left\{\left(\underline{I}_{1s} + \underline{I}_{2s}\right) p\underline{Z}_{1L} + p\underline{Z}_{0L}\underline{I}_{0s}\right\} - \underline{V}_S, \\ &= \left\{\left(\underline{I}_{1s} + \underline{I}_{2s}\right) p\underline{Z}_{1L} + p\underline{Z}_{0L}\underline{I}_0\right\} - \left(\underline{I}_{1S} + \underline{I}_{2S}\right)p\underline{Z}_{1L} + \underline{I}_{0S}p\underline{Z}_{0L} = 0.\end{aligned} \tag{2.21}$$

In this case, $\underline{I}_A^C\, p\underline{Z}_{1R} = \underline{S}_{op}$, and $\underline{k}_0$, is reffered to zero-sequence current compensation which is used to match the zero sequence impedance of the line. Therefore, the apparent measured impedance, $p\underline{Z}_{1R}$, is stated as the ratio of the measured voltage at the relaying point to the compensated measured current:

$$\frac{\underline{V}_S}{\underline{I}_A^C} = \frac{\left(\underline{I}_{1s} + \underline{I}_{2s}\right) p\underline{Z}_{1L} + p\underline{Z}_{0L}\underline{I}_{0s}}{\underline{I}_{1s} + \underline{I}_{2s} + \underline{k}_0\underline{I}_{0s}} = p\underline{Z}_{1L}\frac{\left\{\underline{I}_{1s} + \underline{I}_{2s} + \left(p\underline{Z}_{0L}/\, p\underline{Z}_{1L}\right)\underline{I}_{0s}\right\}}{\left\{\underline{I}_{1s} + \underline{I}_{2s} + \left(p\underline{Z}_{0L}/\, p\underline{Z}_{1L}\right)\underline{I}_{0s}\right\}} = p\underline{Z}_{1L} \tag{2.22}$$

From Equation (2.22), zero-sequence current, $\underline{k}_0$, is used to match the zero-sequence impedance of the line. This allows the measurement of impedance unit of the distance relay to use the positive-sequence impedance as a measured fault impedance value [26]. Furthermore, the zero-sequence current compensation, $\underline{k}_0$, could also be stated as:

$$\underline{k}_0 = \frac{\underline{Z}_{0L} - \underline{Z}_{1L}}{\underline{Z}_{1L}} \tag{2.23}$$

Performance Evaluation

Evaluating the performance of the impedance unit is necessary to investigate the accuracy of the faulted transmission line impedance calculation. The performance evaluation method reveals the accuracy of the relay algorithm models, and does not include any error introduced from others block functions in Figure 2.10. For evaluation purposes, this thesis investigates through simulation, a number of factors used in different fault scenarios to determine the performance of the IED.

Performance evaluation is stated as the absolute value of error estimation which is expressed as a percentage error in fault impedance calculated on the total line length [35]. This definition is expressed as follow:

$$error_{(SS)}\ (\%) = \frac{\left|\underline{Z}_{est} - \underline{Z}_{act}\right|}{\underline{Z}_{tot}} x\ 100\ \%\,, \tag{2.24}$$

where:

$\underline{Z}_{est}$, $\underline{Z}_{act}$, estimated and actual fault impedance to the fault location (in Ω),

$\underline{Z}_{tot}$, total line impedance (in Ω).

The percentage error of fault impedance in Equation (2.24) is calculated in the steady-state line simulation program, and is developed using the DPL script program which is provided by DIgSILENT. The parameters of the system in Appendix A, Table A.1, and Figure 2.8, demonstrates the performance of the impedance unit of the distance relay for phase A to ground fault simulated at 50% of line length in Figure 2.1. The automation tasks for simulating and calculating the measured steady state error (i.e., performance indices) is developed using the DPL program provided by DIgSILENT.

In this thesis, evaluation of the impedance unit performance considers a number of factors that are simulated simultaneously for different fault scenarios. The factors considered are as follow:

- Fault resistance (R_F).
- Pre-fault power flow angle (δ_F).

- Data inaccuracy of line impedance $(\underline{Z}_L)$.
- Data inaccuracy of source impedance $(\text{e.g., } \underline{Z}_S)$.
- Presence of series compensation (SCs) equipped with Metal Oxide Varistor (MOVs).
- Effect of error in setting zero-sequence current compensation $(\underline{k}_0)$.
- Effect of zero-sequence current on parallel line $\underline{I}_{0p}$ (i.e., effect of mutual coupling).
- Effect of the tapping line for multi-terminal line.

The steady state error calculation enables the investigation of all factors that contribute to the accuracy of the relay algorithm. The sensitivity analysis, which is calculated using SIMLAB, is a method that investigates the effect of individual factors as well as the interaction between factors. This technique reveals the particular factor that most influences the performance of relay algorithm, and therefore, considered for further analysis.

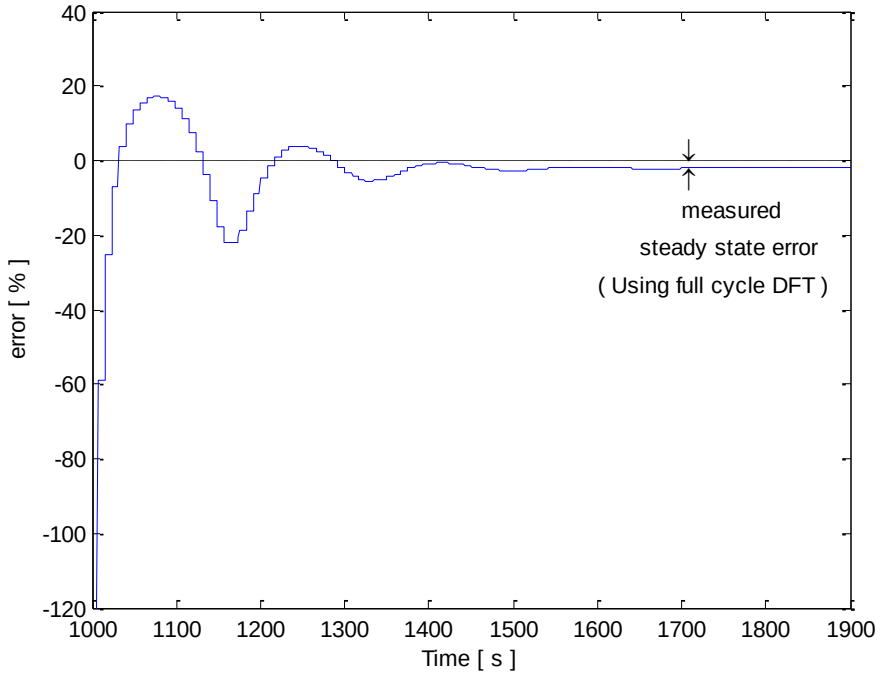

Figure 2.8: Steady state error of fault impedance measurement: fault at 50% of $\underline{Z}_L$, R_F = 10 Ω.

2.3. Generalized Protection Relay Structure

This section develops an understanding of the basic concepts of IED functions. The main standard elements of an IED are organized systematically to model the physical distance relaying systems. Relaying models are developed to verify the performance of the impedance unit in measuring fault impedance during phase A to ground fault condition through off-line tests. To achieve this goal, the fault data obtained from the EMT (Electromagnetic Transient) simulation requires two steps of relaying algorithm investigation: 1) obtain data of voltages, $\underline{v}_s(t)$, and current, $\underline{i}_s(t)$, signals for different case studies (i.e., by simulating the different fault scenarios of different circuits using the power system tool software package), 2) simulate the impedance unit algorithm to measure the performance (i.e., % error estimation) using phasor measured fault data of voltage and current. All steps are processed sequentially.

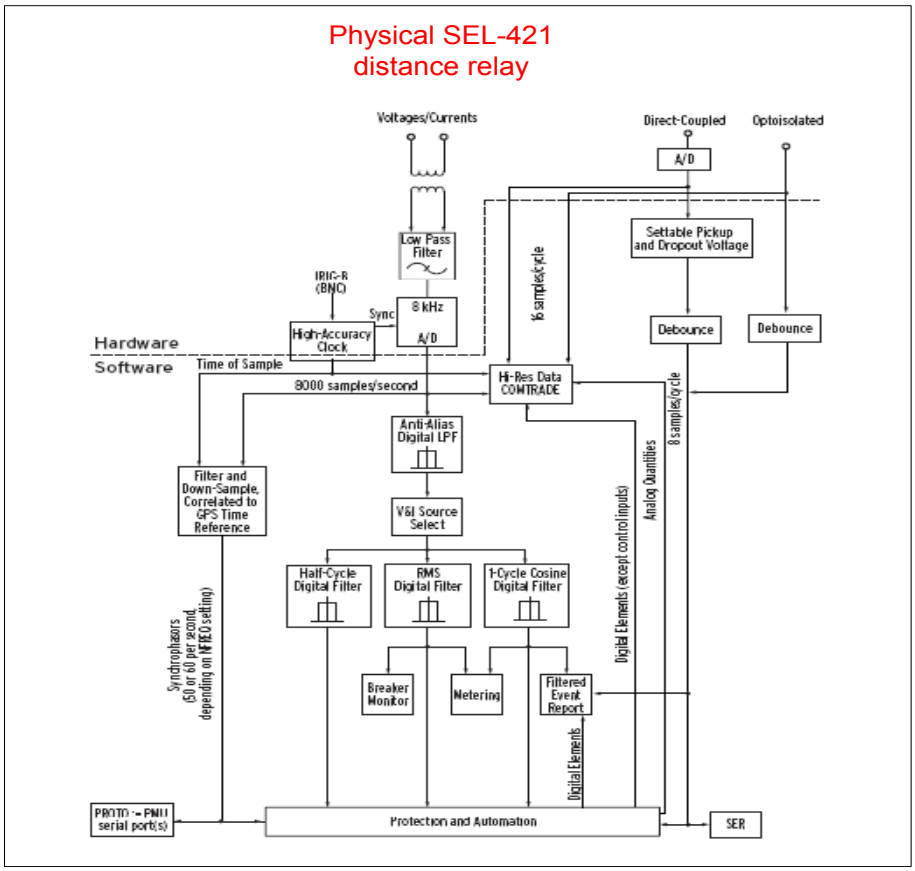

Figure 2.9: Physical model of IED (i.e., SEL-421 distance relay) [15].

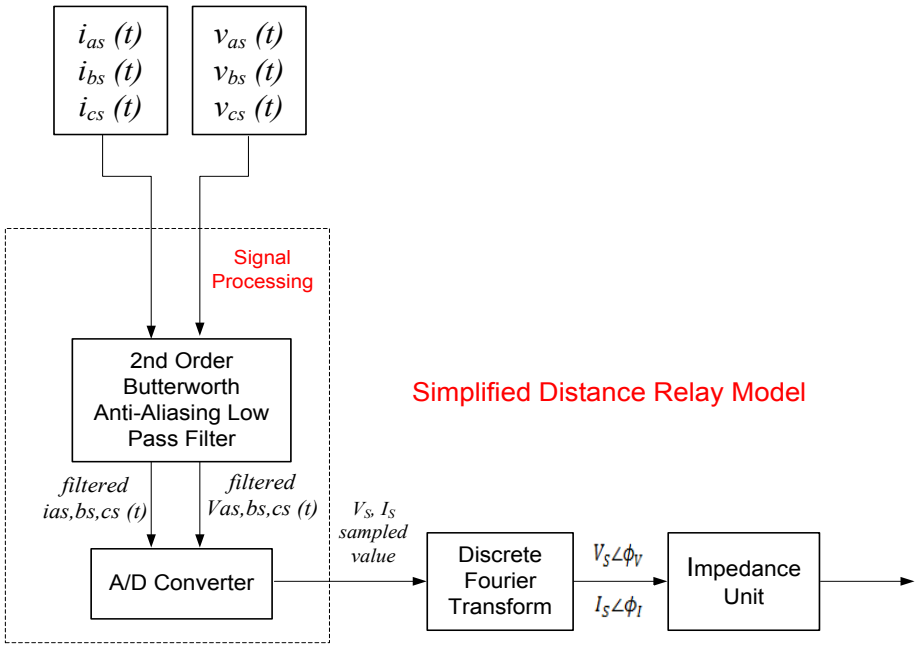

Figure 2.10: Simplified block diagram of protection scheme.

Figure 2.9 shows a physical model of an IED system which was implemented in a microprocessor and widely used for high speed protecton of a section of a transmission line system [15], while Figure 2.10 is the simplified relaying model of an IED structure for the purpose of investigation. This simplified model makes use of the transient voltage and current signals passed through CVT (capacitor voltage transformer) and CT (current transformer) for calculating the apparent fault impedance of $\underline{Z}_m$. Those transient currents and voltages that occurred during faults are mainly composed of exponential dc-offsets and high frequency [36]. Hence, to reliabily calculate the apparent fault impedance, the signal processing algorithm for the combination of the anti-aliasing low pass filter, and the A/D converter, is used to extract the fundamental component and digitized the voltage and current signal inputs. The Discrete Fourier Transform (DFT) is used to generate a phasor fundamental component of voltages and currents for impedance calculations that are implemented in the impedance unit function. The selected main internal block functions of the relay are discussed in the following section.

2.3.1. Analog Anti Aliasing and DC-Offset Removing Filter

The anti-aliasing low pass filter is used to minimize aliasing by removing the unwanted component of high frequency [36, 37]. The 2nd Order Butterwort filter used in the IED model is designed to have an amplitude response characteristic that is as flat as possible in the lower frequency range (called the pass band filter) and monotonically decreasing with increasing frequency [38, 39]. To avoid the error due to the aliasing effect, sampling should be at least twice the maximum value of the analog signal.

As shown in Figure 2.10, this block receives signals from the current transformer (CT) and voltage transformer (CVT). The signal outputs are then digitalized before being filtered by the DFT digital filter block. The specifications for the filter implemented in this project requires the pass band cutoff frequency to be 70 Hz, and a sampling frequency of 1.2 kHz (20 samples/cycle), in order to avoid aliasing. To meet this requirement, the proposed filter preserves the steady state components by rejecting the other components.

The general expression for a normalized transfer function of an *n*th-order Butterworth low-pass filter is given by [38]:

$$H(s) = \frac{1}{\prod_{i=1}^{n}(s - s_i)} = \frac{1}{(s - s_1)(s - s_2)\dots(s - s_n)}\ , \tag{2.25}$$

where the poles of that transfer function are determined as:

$$S_i = e^{j\pi[(2i+n-1)/2n]} = \cos\left(\pi\frac{2i+n-1}{2n}\right) + j\sin\left(\pi\frac{2i+n-1}{2n}\right), k = 1,2,\dots,n. \tag{2.26}$$

However, the abnormal components of the current and voltage signals are not only affected by high frequency but also by the dc-offset component. The aliasing filter only removes the high frequency components but not the dc-offset effect [36, 40]. The dc-offset component is of an exponential form and may occure when a fault occurs. The following equations are derived to remove the dc-offset component. The dc-offset is assumed to be an exponential component when a fault occurs, and is stated as [36]:

$$x_k = \sum_{n=1}^{\infty} X_n \sin\left(\frac{2\pi nk}{N}\right) + Aexp\left(\frac{-k\Delta t}{\tau}\right). \tag{2.27}$$

Equation (2.28) is the output signal with the dc-offset contained in the signal x_k of Equation (2.27) is removed.

$$y_k = x_k - x_{k-1}/\exp(\Delta t/\tau)\,. \tag{2.28}$$

By substituting Equation (2.27) into Equation (2.28), the signal after the dc-offset removal is stated as:

$$y_k = \sum_{n=1}^{\infty} X_n a_n \sin\left(\frac{2\pi nk}{N} + \varphi n\right), \tag{2.29}$$

where:

Δt = sampling interval,

τ = time constant,

N = number of samples per period,

$E_n = 1 - [1/exp(\Delta t/\tau)] \cos\left(\frac{2\pi n}{N}\right)$,

$F_n = [1/exp(\Delta t/\tau)] \sin\left(\frac{2\pi n}{N}\right)$,

$a_n = \sqrt{E_n^2 + F_n^2}$,

$\varphi_n = tan^{-1}(F_n/E_n)$.

2.3.2. Digital Filtering

The DFT digital filter removes non-fundamental frequencies and provides fundamental phasor information [36]. The extracted fundamental voltage and current, in phasor form, is used by the impedance unit to calculate the apparent impedance from the relaying point to the faulted point (see Figure 2.10).

Furthermore, in Figure 2.11, the DIgSILENT software tool allows the use of a variety of Fourier transforms, such as full and half Discrete Fourier Transform (DFT), Fast Fourier Transform, and Cosine Fourier Transform. In this project, we only use the full Discrete Fourier Transform in a number of case studies.

The extraction of the fundamental frequency component via DFT is described as follows [36, 41]:

We assume that the sinusoidal voltage form when the fault occurs is stated as:

$$\underline{v}(t) = \underline{V}_{peak} \sin(\omega t + \theta), \tag{2.30}$$

The equation is expanded as

$$\underline{v}(t) = \underline{V}_{peak} \sin(\omega t) \cos(\theta_v) + \underline{V}_{peak} \sin(\theta_v) \cos(\omega t)\,. \tag{2.31}$$

When $\underline{v}(t)$ is sampled, the resulting samples values are denoted as $\underline{S}_k$. Since $\underline{S}_k$ represents sampled values of sinusoidal voltage with a fixed sample rate of *N* samples per cycle (i.e., $= 20$), the Discrete Fourier Transform calculation of the fundamental components can be defined by the following equations:

$$\underline{V}_{real} = \left(\frac{2}{N}\right) \sum_{k-1}^{N} \left| \underline{S}_k sin\left(2\pi \frac{k}{N}\right) \right|, \tag{2.32}$$

$$\underline{V}_{imag} = \left(\frac{2}{N}\right) \sum_{k-1}^{N} \left| \underline{S}_k cos\left(2\pi \frac{k}{N}\right) \right|. \tag{2.33}$$

Applying Equations (2.32), and (2.33) to (2.30) will result in the following expressions:

$$\underline{V}_{real} = \underline{V}_{peak} cos(\theta_v), \tag{2.34}$$

$$\underline{V}_{imag} = \underline{V}_{peak} sin(\theta_v). \tag{2.35}$$

The magnitude and phase of the voltage phasor can be calculated sequentially by the following equations:

$$\underline{V}_{mag} = \sqrt{\underline{V}_{real}^2 + \underline{V}_{imag}^2}, \tag{2.36}$$

$$\underline{V}_{angle} = arc \tan\left(\underline{V}_{imag} / \underline{V}_{real}\right). \tag{2.37}$$

Equations (2.36) and (2.37) are of the form when the magnitude and phase angle define the phasor of the sinusoidal voltage in Equation (2.30).

A measuring block using DFT calculations determines the real and imaginary parts of each current and voltages. This means that each current and voltage sample is multipled by a sine factor to obtain the real component and by a cosine factor to obtain the imaginary component. These quantities are summed over N consecutive samples to obtain the actual components.

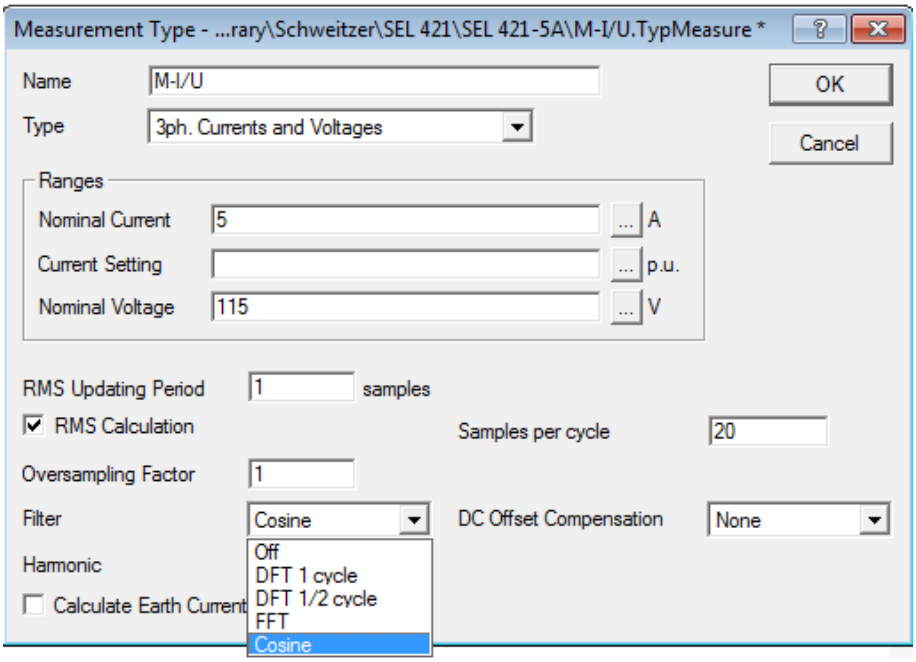

Figure 2.11: The "Measuring" type dialog with the available filtering methods [17].

2.3.3. Impedance Unit

The impedance Unit is an IED block function designed to perform an impedance calculation [42]. The IED relaying scheme makes use of voltage and current passed to the impedance unit trough the CT and CVT for the calculation of impedance. Accuracy is very important since the IED relaying method that relies on the accuracy of estimation could result in revenue loss due to outages. A lot of research has been done to investigate IED performance including the work in this thesis, where the systematic analysis using a combination of several tools and methods is used to analyse the performance of one-ended impedance methods. We describe and examine the impedance-based calculation for a number of different system faults and analyse their performance by considering some possible sources of error (e.g., inaccuracy of calculating and setting system parameters, and fault resistance).

Table 2.1 shows a simple positive-sequence impedance algorithm for calculating positive sequence fault impedance of $p\underline{Z}_{1L}$ [19]. In relation to Figure 2.1, this formula is applicable if the fault resistance R_F, is assumed to be zero, and zero-sequence impedance ,$\underline{Z}_0$, is known, so that the zero-sequence current compensation, $\underline{k}_0 = (\underline{Z}_{OL} - \underline{Z}_{1L})/\underline{Z}_{1L}$), can be applied to compensate the zero-sequence current, $\underline{I}_0$.

Table 2.1: Simple Impedance Equation [19].

Fault Type	Positive-Sequence Impedance Equation ($p\underline{Z}_{1L}$)
A-ground	$\underline{V}_{AS}/(\underline{I}_{AS}+3\underline{k}_0\underline{I}_0)$
B-ground	$\underline{V}_{BS}/(\underline{I}_{BS}+3\underline{k}_0\underline{I}_0)$
C-ground	$\underline{V}_{CS}/(\underline{I}_{CS}+3\underline{k}_0\underline{I}_0)$
A-B or A-B-G	$\underline{V}_{ABS}/\underline{I}_{ABS}$
B-C or B-C-G	$\underline{V}_{BCS}/\underline{I}_{BCS}$
C-A or C-A-G	$\underline{V}_{CAS}/\underline{I}_{CAS}$
A-B-C	can use any of the following: $\underline{V}_{ABS}/\underline{I}_{ABS}$, $\underline{V}_{BCS}/\underline{I}_{BCS}$, $\underline{V}_{CAS}/\underline{I}_{CAS}$

In order to use various impedance-based methods for the impedance algorithm, various steps must first be taken [19], such as: measuring the voltage and current phasor (i.e., $\underline{V}_S(t)$, $\underline{I}_S(t)$), extract the fundamental component (i.e., using anti-aliasing low pass filter), and determining the phasor value of voltage and current $\underline{V}_S\angle\varphi_v$ and $\underline{I}_S\angle\varphi_I$ (i.e., using DFT).

The relay algorithm is analysed by using the existing model, SEL-421 distance relay, provided by DIgSILENT. The "polarizing" type relay dialog of Figure 2.12 provides access to more functions for setting the model. Different types of possible settings for zero-sequence current compensation, type of polarizing unit, and polarizing method, can be set using the polarizing unit combo box.

2.4. Possible Effects on Fault Impedance Calculation

For correct operation during a fault, the IED must have the capability to measure the fault impedance accurately. To enable this, it is necessary to provide the correct measured quantities of voltage and current fault signals to the measurement elements (i.e., impedance unit). However, use of voltage and current for the fault impedance calculation does not

always give a correct result. Several factors need to be considered since they will introduce errors into the fault impedance calculation.

Underreaching and overreaching are two such practical problems. The IED is said to be underreaching when the impedance presented to it is apparently greater than the impedance to the fault. The main cause of this is the effect of fault current infeed [2]. The overreach problem occurs when the apparent impedance presented to it is less than the impedance to the fault. This is caused when the IED is applied on parallel lines where one line is taken out of service and earthed at each end. The following sections will introduce more detail for the possible effects of factors on the performance of the IED impedance unit.

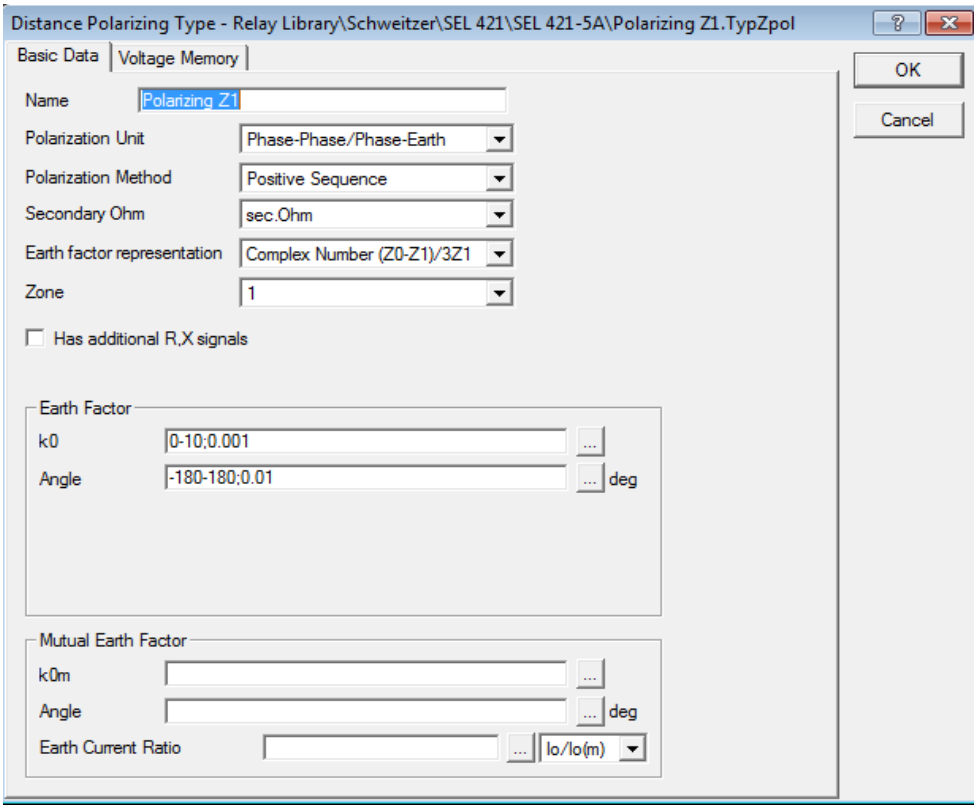

Figure 2.12: The “Polarizing” type dialog [17].

2.4.1. Effect of Combination between Fault Resistance and Power Flow Angle

The combined effect of fault resistance, R_F, and load flow angle, δ_F, that is known as the reactance effect will significantly influence to the operation of the IED [43-45]. The reactance effect has a large impact on calculating the fault impedance. This is due to potential changes in line reactance. To observe the effect of R_F and δ_F, the ground short circuit, that will usually involve the fault resistance, is simulated between two sources of equivalent systems.

Figure 2.13 shows a single circuit interconnection where the single phase to ground fault with a fault resistance is simulated between two sources of equivalent Thevenin circuits. The fault resistance, R_F, is composed of the ground wire, tower footing resistance, trees growing around the line, etc. During a phase to ground fault, the linear characteristic of resistance results in the voltage drop, $\underline{V}_F$, across the fault resistance, R_F, being proportional to the total fault current, $\underline{I}_F$ [24]. In this case, the accuracy of the relaying point used to measure the fault impedance depends on the variation of fault current, $\underline{I}_F$, where the power flow angle, δ_F, may contribute to the variability of $\underline{I}_F$.

The source impedance, $\underline{Z}_S$, non-homogeneity of line impedance, $\underline{Z}_L$, and current infeed are factors that can vary the fault current, $\underline{I}_F$, during fault condition. However, the contribution of the combination of R_F and power flow angle, δ_F, are dominant factors for all fault simulations along the protected transmission line [1].

The effect of R_F is magnified by the value of the fault current, $\underline{I}_F$. Consequently, it impacts the performance of the apparent fault impedance measurement, $\underline{Z}_m$. The following describes how the effect of $\underline{I}_F$ in relation with the variability of power flow angle, δ_F, is investigated. We assume in Figure 2.13 that the fault located at F is simulated between terminal S and R. The fault impedance calculated by the impedance unit is derived as follows [20, 46, 47]:

$$\underline{V}_S = \underline{I}_S p \underline{Z}_{1L} + \underline{I}_F R_F, \tag{2.38}$$

$$\underline{Z}_m = \frac{\underline{V}_S}{\underline{I}_S} = p\underline{Z}_L + \frac{\underline{I}_F}{\underline{I}_S} R_F, \tag{2.39}$$

where:

p - fault distance from the bus S to the fault point F,

$\underline{V}_S, \underline{I}_S$ - voltage and current measured from the relaying point at bus S,

$\underline{I}_F$ - total fault current flowing through the fault resistance ($\underline{I}_F = \underline{I}_S + \underline{I}_R$).

From Equation (2.39), it can be seen that $\underline{Z}_m = p\underline{Z}_L$ if $R_F = 0$ (strictly measure the distance to the fault). Otherwise, the fault resistance is seen by the relay as a certain impedance:

$$R'_F = \frac{\underline{I}_S + \underline{I}_R}{\underline{I}_S} R_F, \tag{2.40}$$

Equation (2.40) shows that the value of impedance, R'_F, will depend on the value of current, $\underline{I}_S$ (i.e., $\underline{I}_S = \underline{I}_{AS} + \underline{k}_0\underline{I}_0$). Figure 2.14 shows the effect of the power flow angle, δ_F, and fault resistance, R_F, to the apparent fault impedance [9]. Without the influence of R_F and δ_F ($R_F = 0$), the impedance is seen by the relay as $p\underline{Z}_{1L}$ (i.e., the line impedance located at F). With the $R_F \neq 0$, the impedance seen by the relay is denoted by point <1>, $R'_F =$ purely resistance. At this point, the real part (R) of impedance is increased while the imaginary part (X) remains constant. Points <2> and <3> represent the cases involving R_F and varying δ_F. The effect of δ_F is to shift R_F to point <2>, when δ_F is positive (i.e., power flows from left to right side), $R'_F =$ resistance and capacitive reactance. In contrast, point <3> shows the impedance seen for the fault when δ_F is negative, $R'_F =$ resistance and inductive reactance.

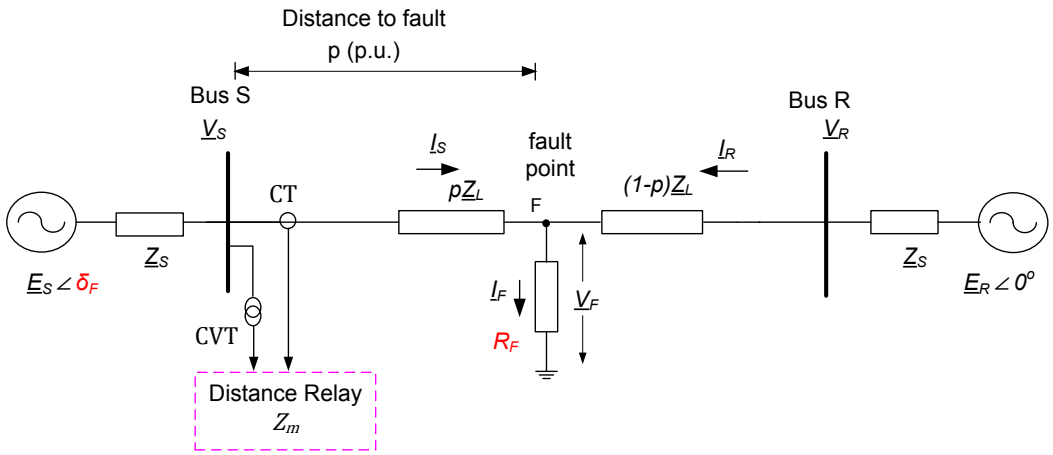

Figure 2.13: Typical phases to ground fault.

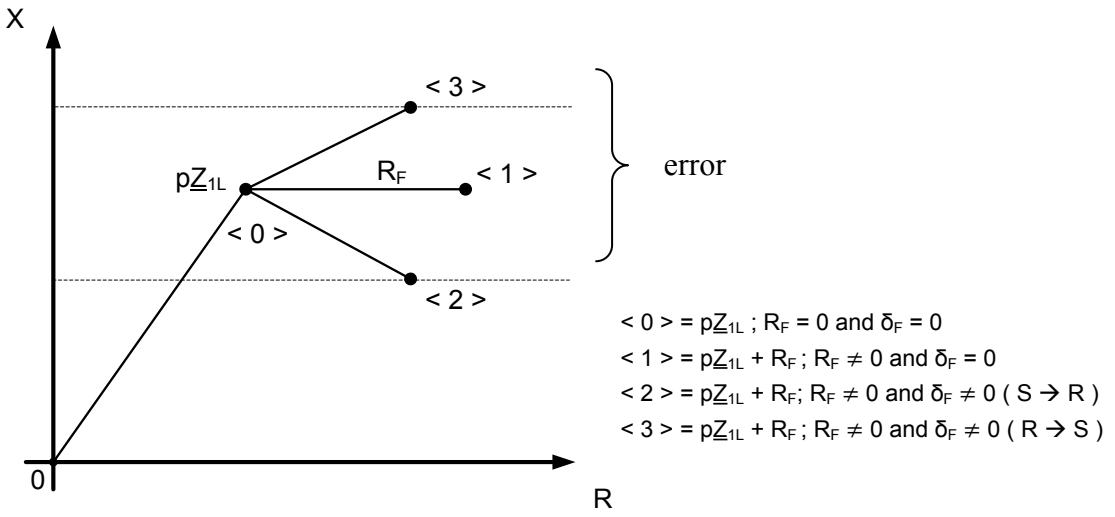

Figure 2.14: Effect of Fault Resistance, R_F, and Power Flow Angle, δ_F.

2.4.2. Effect of Applying Series Compensation

Using series compensation is an alternative solution in which the addition of a series capacitor in line with the transmission line will increase the line's power transfer capability while improving system stability [48]. This is due to the series capacitor reducing the resulting reactance of the transmission line, sequently increasing its transmission capacity. Additionally, it is more economical to use a series capacitor rather than building a new transmission line [49]. The series capacitors can also be used to regulate the power flow in the network by switching them in and out.

However, the addition of a series capacitor in line with the transmission line may present an array of new problems for the impedance based line protection. Some of the problems that are presented to the impedance based relay scheme are [28, 48, 49]: reduced fault reactance, voltage inversion, Zone 1 overreach, sub-harmonic-frequency oscillations.

Reduced fault reactance

The use of series compensation on transmission lines results in a decrease of the apparent impedance that is "seen" by the relaying point. The transmission line thus appears electrically shorter, since the added capacitive reactance due to the inserted series

capacitor, X_{CO}, compensates the line's inductive reactance, X_L. Hence, the apparent line impedance would be $pX_L = X_L - X_{CO}$. This net of reactance seen by the relaying point at terminal S could be capacitive, and would affect the correct measurement of the fault impedance [48-50].

Figure 2.15 shows a schematic diagram of a series compensated line where the series capacitors SCs compensated with Metal Oxide Varistors (MOVs) are inserted into the middle of line S-R. A fault may occur at the fault location of F_1 and F_2. If a fault at F_2 has a positive total fault reactance from the relaying point of S to fault location F_2, the current will lag the voltage in the entire loop. In this case, the voltage at the capacitor has a positive voltage increment and the value of the line reactance, X_L, has been reduced by the capacitor reactance, X_{CO}. For example, Figure 2.16 shows the IED's characteristic of Zone 1, where the measured impedance is not influenced by the series capacitor when the fault is in front of SCs (i.e., the fault located at F_1), since the series capacitor SCs is not included in calculating the fault impedance. The situation is different when the faults occur behind SCs (i.e., the fault is located at F_2), in which the addition of SCs (i.e., capacitor reactance X_{CO}) may reduce the line inductive reactance, X_L, and consequently affect the accuracy of the measured fault impedance, $\underline{Z}_m$.

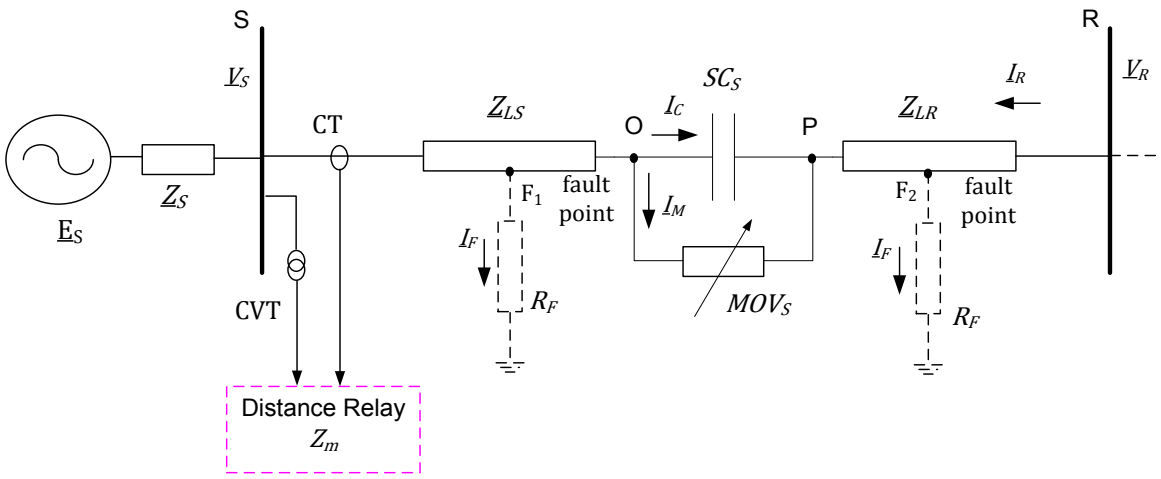

Figure 2.15: Schematic diagram of the series compensated line: F_1, fault in front of SCs and F_2, fault behind SCs.

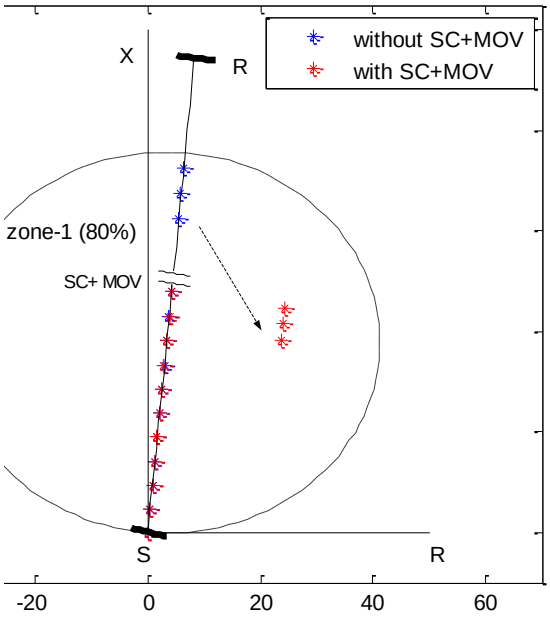

Figure 2.16: Effect of reduced fault reactance due to series capacitor.

Voltage Reversal

Voltage reversal is another problem faced by the IED when the protected line is compensated by SCs as shown in Figure 2.17, with $\underline{V}_{LS}$ and $\underline{V}_{LR}$ 180^0 out of phase. This may occur if the negative capacitor reactance, X_{CO}, is greater than the positive line reactance, pX_L, during a fault at F_2. In this case, the IED will correctly measure the faulted line impedance, $\underline{Z}_m$, when the line voltage information, $\underline{V}_{LR}$, is applied for forward line faults [48] (see Figure 2.17 curve (a)). However, in real conditions where the bus voltage, $\underline{V}_S$, is utilized by the IED, the error of the fault impedance calculation will be produced for the fault located at F_2 [1]. Futher analysis shows, in Figure 2.17 curve (b), that when total reactance of the fault loop is positive due to greater than the negative reactance, the voltage at the relaying point, $\underline{V}_S$, will still remain positive [50] as well as for the fault at F_1. The IED will have correct information for $\underline{V}_S$ for calculating the forward fault impedance located at F_1 (see Figure 2.17 curve (c)).

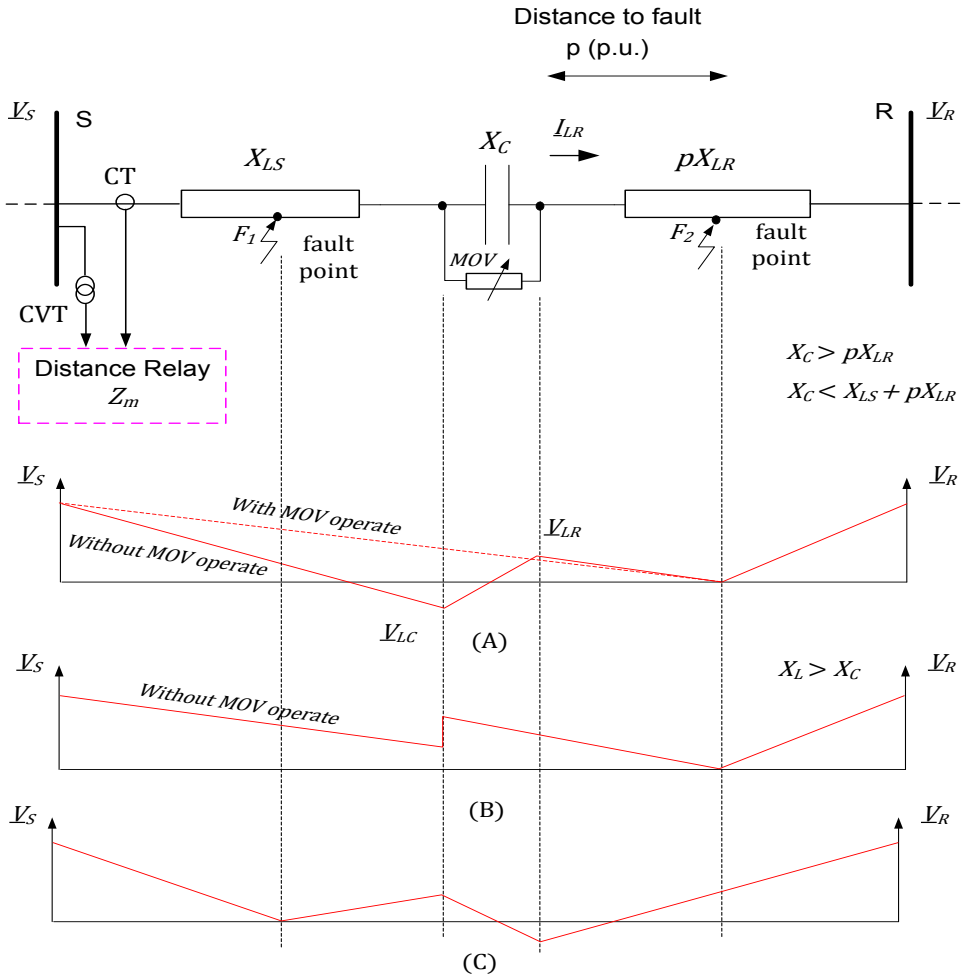

Figure 2.17: Voltage profile and phasor diagram for a forward fault.

2.4.3. Effect of Mutual Coupling on Distance Relay Operation

The main problem faced in measuring fault impedance when the conventional IED is applied on a parallel line is the mutual coupling effect between two lines [30]. Investigations have shown that the effect of positive- and negative-sequence of mutual coupling is small and can be neglected, but the effect of zero-sequence mutual coupling is not small and will vary with line operation and fault conditions [30, 51]. If the zero-sequence mutual coupling, $\underline{Z}_{0M}$, is not compensated, serious problem in measuring fault impedance may occur, especially under different possible configurations such as when two lines are in operation or one line is switched off and grounded at two ends [18].

The different possible configurations of parallel lines, combined with the effect of mutual coupling, $\underline{Z}_{0M}$, have complicated network analysis and setting of line protective

relays. Figure 2.18 shows a simple parallel circuit with the fault simulated at F. Mutual coupling between parallel lines can cause severe underreaching and overreaching errors for the distance relay [30, 52]. Additionally, fault resistance, inaccuracy of measuring instruments, and line parameters also need to be considered as they will impact on the fault impedance calculation [53].

As shown in Figure 2.19, the parallel line system can have many different parallel-line operation modes; for example: (a) both lines are in operation, and (b) one line switched off and grounded at both ends.

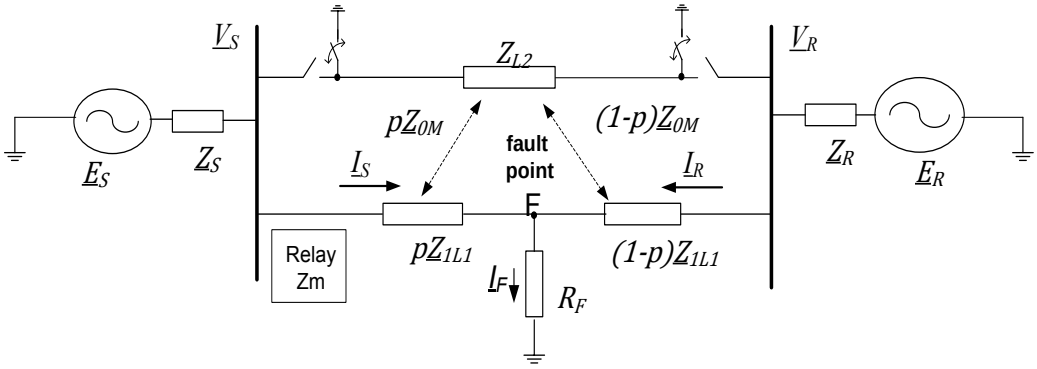

Figure 2.18: Typical Parallel-Line System.

An example of phase A to ground fault is simulated at Figure 2.18. The mutual coupling effect between two parallel lines will influence the accuracy of measured impedance, $\underline{Z}_m$, calculated by the conventional distance relay located at terminal S. If a fault resistance, R_F, is assumed to be zero, then the measured fault impedance, $\underline{Z}_m$, for phase A to ground fault located at F is derived as follows [30]:

$$\underline{Z}_m = \frac{\underline{V}_{AS}}{\underline{I}_{AS} + \underline{k}_0\,\underline{I}_0} = p\underline{Z}_{1L} + \Delta\underline{Z}_{1L}, \tag{2.41}$$

where

$$\underline{V}_{AS} = p\underline{Z}_{1L}\underline{I}_{AS}^{C} + p\underline{Z}_{0M}\underline{I}_{0P}, \tag{2.42}$$

$$\Delta\underline{Z}_{1L} = \frac{p\left(\underline{Z}_{0M}/\underline{Z}_{1L}\right)\underline{I}_{0P}}{\underline{I}_{AS} + \underline{k}_0\underline{I}_0}. \tag{2.43}$$

$\underline{V}_{AS}$ is the post-fault voltage for phase A to ground fault measured by the conventional relay located at the relaying point, while $\underline{I}_{AS}^{C}$ is a zero-current compensation of fault current in phase A. The per unit distance relay error, Δ, in the term of $\underline{Z}_{L1}$ depends upon to the ratio

between the parallel line's zero-sequence current, $\underline{I}_{0P}$, and phase A current fault with zero-sequence current compensation (i.e., $\underline{I}_{AS}^{C} = \underline{I}_{AS} + \underline{k}_0\underline{I}_0$).

Figure 2.19 shows the zero-sequence component system of the parallel line circuit in Figure 2.18 when (a) both lines are in operation and (b) one line is switched off and grounded at both ends.

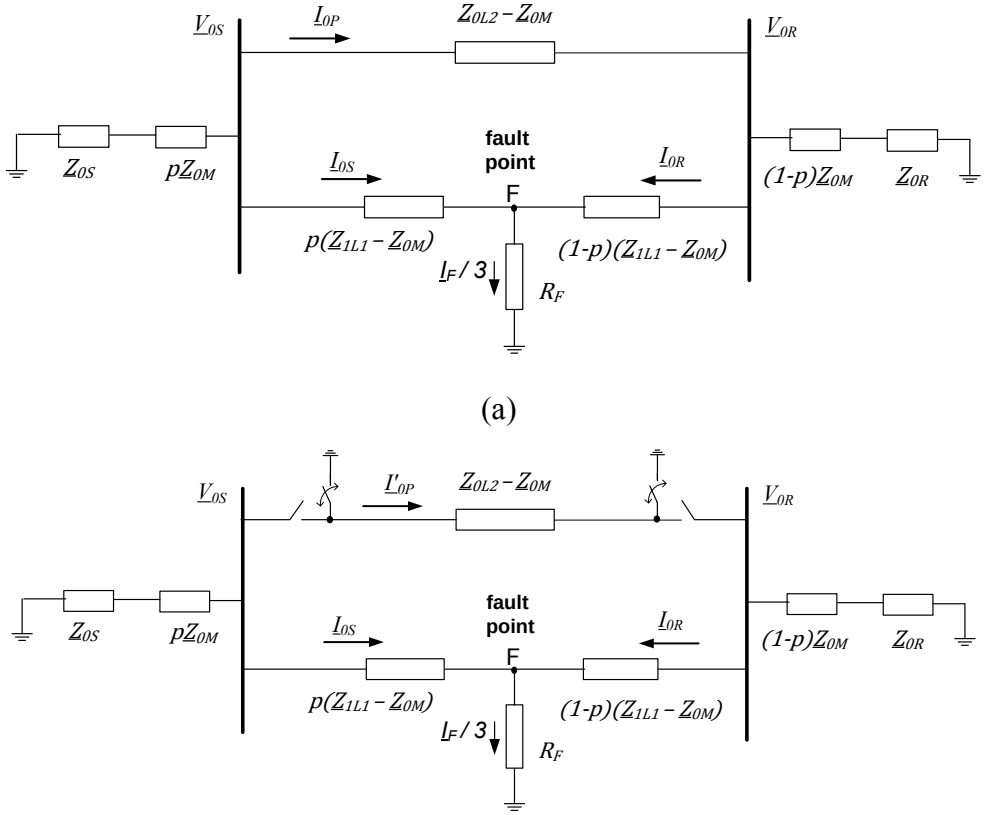

Figure 2.19: Zero-sequence component system of parallel line circuit: (a) Two lines are active, (b) One line is switched off and grounded at both ends.

The zero-sequence of current parallel line, $\underline{I}_{0P}$, when both line in operation, expressed in Equation (2.44), or the zero-sequence of current parallel line, $\underline{I}'_{0P}$, when the circuit SR is disconnected and grounded at both ends, expressed in Equation (2.45), can be derived mathematically as follows [30, 54]:

$$\underline{I}_{0P} = \frac{p\underline{Z}_{0R} - (1-p)\underline{Z}_{0S}}{(2-p)\underline{Z}_{0R} + (1-p)\left(\underline{Z}_{0S} + \underline{Z}_{0L2} + \underline{Z}_{0M}\right)}\underline{I}_0, \tag{2.44}$$

$$\underline{I}'_{0P} = \frac{\underline{Z}_{0M}\{(1-p)\underline{Z}_{0S} - p\underline{Z}_{0R}\}}{\underline{Z}_{0L1}\{(1-p)\underline{Z}_{0L1} - \underline{Z}_{0R}\} - (1-p)\underline{Z}_{0M}^2}\underline{I}_0. \quad (2.45)$$

From Equation (2.44) and Equation (2.45), the modified compensation factor (MCF), is calculated as follows [54]:

$$\underline{k}_{0(mod)} = \underline{k}_0 + \underline{k}_{0M}\underline{I}_{0P}, \quad (2.46)$$

$$\underline{k}'_{0(mod)} = \underline{k}_0 + \underline{k}_{0M}\underline{I}'_{0P}. \quad (2.47)$$

MCF is a function of the system impedance, line impedance, mutual coupling, and fault location.

Figure 2.20 shows the fault impedance measurement tracking that is affected by mutual coupling for two different, and typical operating modes. The overreaching distance relay operation, which is indicated by the red line, is due to the parallel line being switched off and grounded at both ends. The underreaching, indicated by the blue line, is due to both lines being in operation.

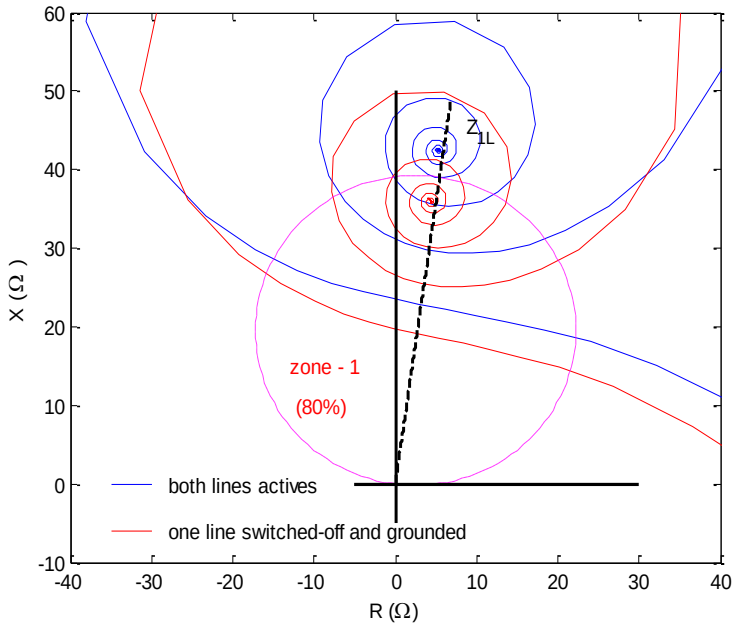

Figure 2.20: Effect of mutual coupling on impedance measurement.

Furthermore, Figure 2.21 shows how a in change in the value of the zero-sequence current setting, $\underline{k}_0$, can reduce the effect of mutual coupling impedance, $\underline{Z}_{0M}$. In this case, a proper

setting of $\underline{k}_0$ will compensate the overreach (red line) and underreach effect (blue line) of the conventional distance relay.

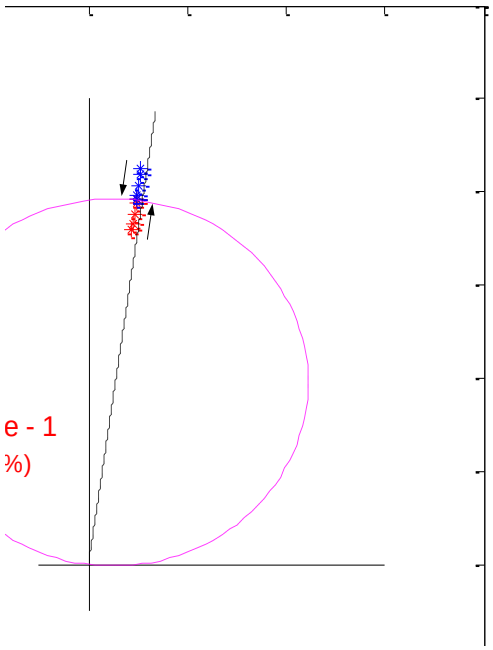

Figure 2.21: Effect of changing value of zero sequence current compensation, $\underline{k}_0$, in impedance measurement.

2.4.4. Effect of Tapped Line on Distance Relay Operation

Figure 2.22 shows the structure of a transmission line with a direct tapping line located between the terminals S and R, and a single phase to ground fault located either in section-1 before tapping (fault location F_1) or section-2 after tapping (fault location F_2). This structure will affect the performance of the non-pilot distance relay located at terminal S, which is originally installed for protecting two-terminal line. There are a number of uncertain parameters, or factors, associated with three-terminal line, that all impact the performance of the distance relay algorithm [8]. However, for a circuit with three terminals in Figure 2.22, more attention needs to be taking into account when single phase to ground fault occurs at F_2. In this case, the presence of a tapping line and high fault resistance will drastically influence the performance of the distance relay [32].

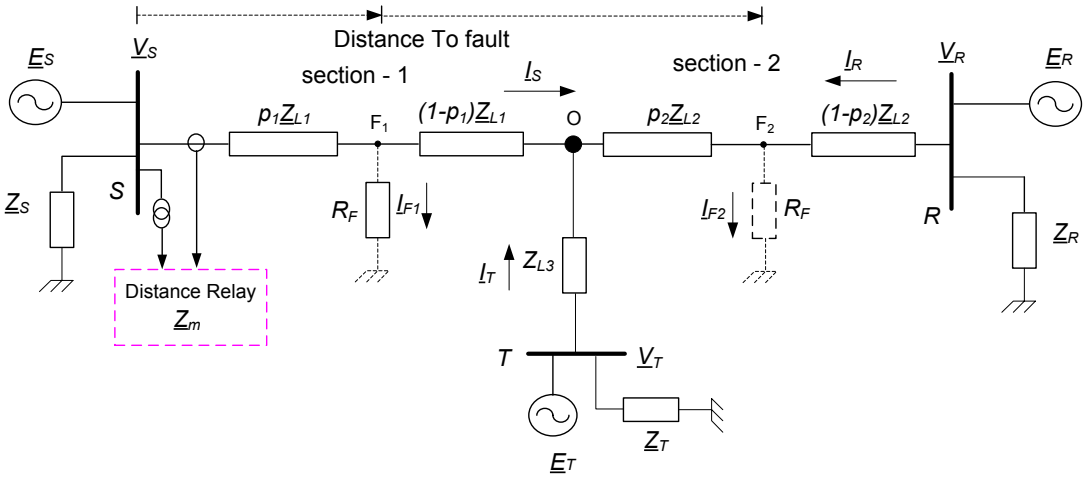

Figure 2.22: The circuit with tapping line.

Distance relays located at terminal S of Figure 2.22 use sampled voltage and current for calculating the apparent fault impedance during fault conditions. The appropriate mho characteristic is used to make a correct decision for protecting the faulted transmission line. The effect of different network conditions corresponds to the different remote-end infeed or outfeed behaviour. As this is not measurable by the distance relay at the located point, the conventional distance relay is subject to underreaching or overreaching [32]. Techniques that use the adaptive concept in [55], or apply a correct setting of the zone reach [56], have been used successfuly. A high fault resistance that occurs during a fault makes the situation more complex [32].

To study the effect of the non-pilot distance relay applied to three-terminal line, we examine the scenario simulated in Figure 2.22. In following analysis we assume that the sources of voltage are equal (i.e., $\underline{E} = \underline{E}_S = \underline{E}_R = \underline{E}_T$) and the fault resistance $R_F = 0$. Hence, from Figure 2.23, the total fault current, $\underline{I}_F$, during a fault at F_2 is made up of two parts and is derived as follows [23]:

$$\begin{aligned} \underline{I}_{F2} &= \underline{I}_R + (\underline{I}_S + \underline{I}_T), \\ &= \underline{I}_R + \underline{I}_{ST}, \end{aligned} \tag{2.48}$$

where $\underline{I}_{ST}$ is stated as

$$\underline{I}_{ST} = \frac{\underline{E}_S}{(1-p_2)\underline{Z}_{L2} + \dfrac{(\underline{Z}_S + \underline{Z}_{L1})(\underline{Z}_T + \underline{Z}_{L3})}{(\underline{Z}_S + \underline{Z}_{L1} + \underline{Z}_T + \underline{Z}_{L3})}}, \tag{2.49}$$

while $\underline{I_S}, \underline{I_T}, \underline{I_R}$ is stated as

$$\underline{I_S} = \frac{\underline{I_{ST}}}{1 + \frac{\underline{Z_S} + \underline{Z_{L1}}}{\underline{Z_T} + \underline{Z_{L3}}}}, \tag{2.50a}$$

$$\underline{I_T} = \frac{\underline{I_{ST}}}{1 + \frac{\underline{Z_T} + \underline{Z_{L3}}}{\underline{Z_S} + \underline{Z_{L1}}}}, \tag{2.50b}$$

$$\underline{I_R} = \left[\frac{(\underline{Z_S} + \underline{Z_{L1}})(\underline{Z_T} + \underline{Z_{L3}})}{(\underline{Z_S} + \underline{Z_{L1}} + \underline{Z_T} + \underline{Z_{L3}})} + (1 - p_2)\underline{Z_{L2}}\right] \frac{\underline{I_{ST}}}{\underline{Z_R} + p_2\underline{Z_{L2}}}. \tag{2.50c}$$

Hence, the relay voltages are computed as

$$\underline{V_S} = \underline{E} - \underline{Z_S}.\underline{I_S}, \tag{2.51a}$$

$$\underline{V_R} = \underline{E} - \underline{Z_R}.\underline{I_R}, \tag{2.51b}$$

$$\underline{V_T} = \underline{E} - \underline{Z_T}.\underline{I_T}. \tag{2.51c}$$

Finally, the fault impedance seen by the relay is computed as follows

$$\underline{Z_{mk}} = \frac{\underline{V_k}}{\underline{I_k}} \;\; ; \;\; k = S, R, T. \tag{2.52}$$

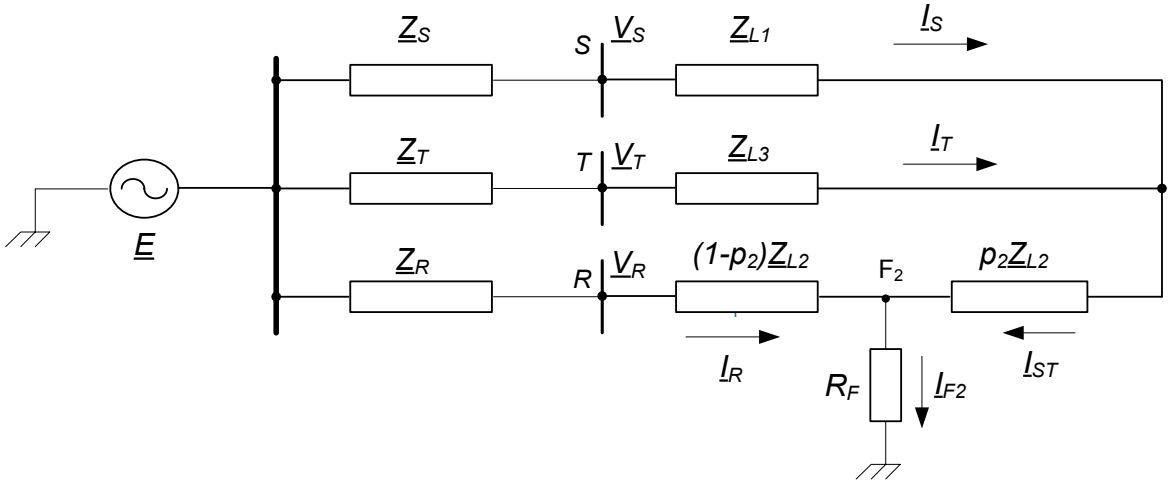

Figure 2.23: Rearrangement of the system of Figure 2.22 [23].

Equations (2.50a, b, and c) show the ratio of the line impedances. It includes the source impedance and the line impedance, and will affect the current flows of $\underline{I_S}$, $\underline{I_T}$, $\underline{I_R}$. Equation (2.52) also shows that this ratio and source impedances will affect the fault impedance measurement. Figure 2.24 and Figure 2.25 demonstrate the effect of the ratios

and variation of $\underline{Z}_{L3}$ on the total fault current value $\underline{I}_{ST}$ and fault impedance measured by the distance relay located at terminal S. The plotted curves are determined using the parameters listed in Table A.3 of Appendix A.

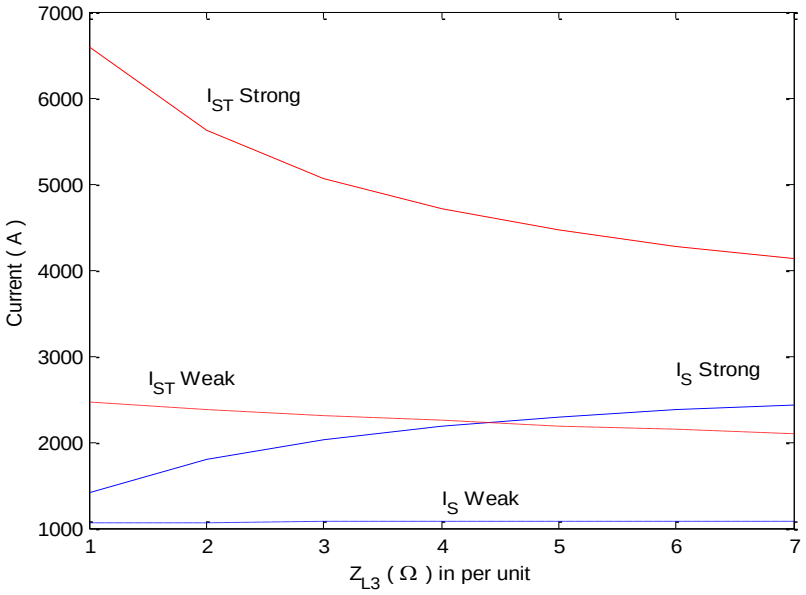

Figure 2.24: Total fault current $\underline{I}_{ST}$ with varying $\underline{Z}_{L3}$.

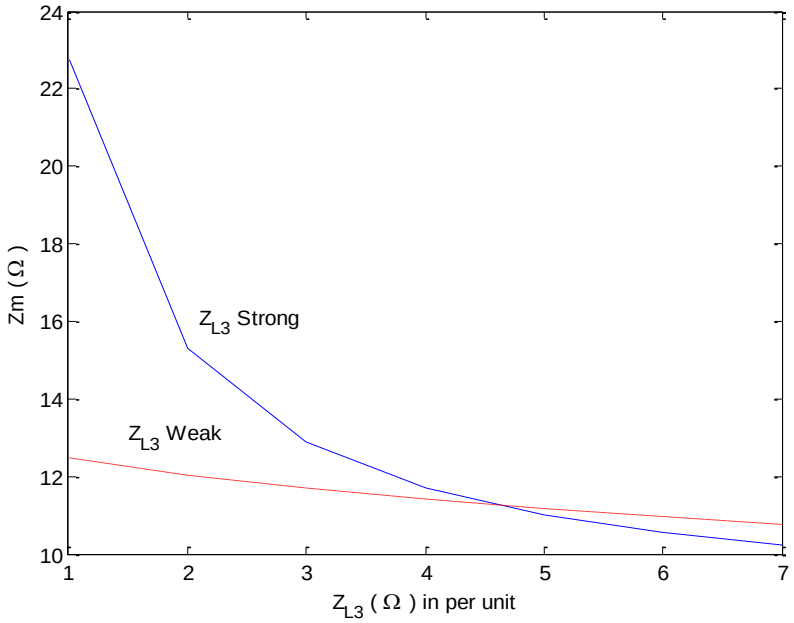

Figure 2.25: Impedance seen by distance relay at terminal S.

Chapter 3

Transmission Network Model for Fault Impedance Calculation

3.1. Introduction

Fault analysis of a power system is required in order to provide information for setting of relays and correctly installing the relay. A power system network is non-static as it changes during operation. To avoid incorrect operation, the relay performance and behaviour needs to be studied under different fault types.

Faults usually occur in a power system due to insulation failure, flashover, physical damage or human error. The types of faults in power system are: three-phase short circuit, phase-to-phase short circuit, two-phase-to-ground short circuit, and one-phase-to-ground short circuit. The resulting challenge is in determining the correct impedance measurement for different types of faults.

In many cases, the network is large, and the number of equations required to describe the network is equal to the number of external ports that must be retained.

To focus only on the effects on the protected transmission line, a reduced network representation is required to simplify the calculations for protection. Multiport equivalent will be used since we are investigating the effect of system infeed on the relay performance.

This thesis only focuses on one-end impedance based fault location calculation and provides simulation results for different faults. The calculation of the fault apparent impedance is obtained by looking into the line from one end of the two-source equivalent system to the fault. In this case no communication channels and remote data are used in the calculation, since only the non-pilot protection relay is used in this experiment.

3.2. Line Impedance Calculation

Investigation of the protective relay algorithm requires the study and calculation of the line impedance. In particular, the line reactance is required. Computation of the line impedance is extensively investigated in [57-60]. Figure 3.1 is used to review how the line impedance is calculated. In this calculation, the line current remains within the conductor, and the line is fabricated with a homogeneous, non-ferromagnetic material (e.g., aluminium and copper).

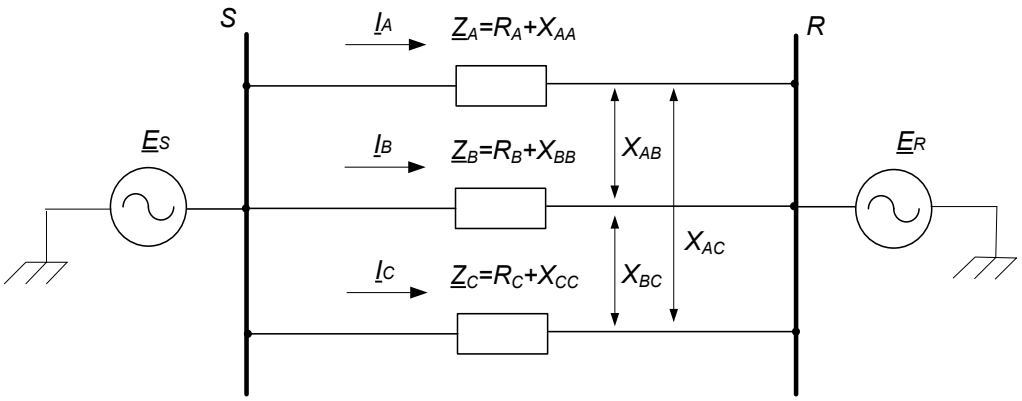

Figure 3.1 Lumped parameter 3 phase Impedance Network.

Figure 3.1 shows the lumped parameter of 3 phase equivalent circuit model. The shunt capacitance, which is affected by the presence of magnetic and electric fields around the conductor [60], is not considered in the model. Assuming that

Figure 3.1 is in a balanced state, the line impedance can be represented using a single phase and is given below [60]:

$$\underline{Z_L} = R_L + jX_L\ \Omega, \tag{3.1a}$$
$$= R_L + j\omega L_{tot},$$

where :

$$R_L = R_{dc} = \frac{\rho l}{A}\ (\Omega/\text{km}), \tag{3.1b}$$

$$L_{tot} = L_{int} + L_{ext}. \tag{3.1c}$$

The series inductance, X_L , consists of two components: internal inductance, $L_{int.}$, and external inductance, L_{ext}, which are due the magnetic flux inside and outside the conductor respectively [58, 60]. While line resistance, R_L, is represented as dc-resistance, R_{dc}, since the frequency of the AC voltage that produces the skin effect on the conductor resistance can be ignored at 50 and/or 60 Hz [57]. In Equation (3.1b), l is the length of the conductor, A is cross-sectional area and, ρ is the resistivity of the conductor. Variations in resistance may be caused by temperature. This resistivity characteristic is based on the material that the conductor is made from, and increases linearly over a normal range of temperature and is stated as [59, 60]:

$$R_{t2} = \frac{M + t_2}{M + t_1} R_{t1}, \tag{3.2}$$

where M is the temperature constant in degrees celcius, R_{t1} is initial resistance at temperature t_1 and R_{t2} is second resistance at t_2.

In a magnetic circuit, a current-carrying conductor, shown in Figure 3.1, produces magnetic flux lines around the conductor. A voltage is induced as the magnetic flux changes due to varying currents. A total series line inductance, as described in Equation (3.1c), depends on the magnetic flux and the line configuration. To determine the total series inductance, some factors such as magnetic intensity, H, magnetic density, B and flux linkage, λ, are used in the equation [58, 60, 61].

Figure 3.2 illustrates how the internal inductance, L_{int}, is calculated. The solid transmission line with radius *r*, carries a current, *I*. The magnetic intensity, H_x, of each point of a closed path at distance *x* from the centre of this conductor is calculated using Ampere's law as:

$$\oint H_x dl = I_x, \tag{3.3a}$$

$$2\pi x H_x = I_x \quad \Longrightarrow \quad H_x = \frac{I_x}{2\pi x}, \tag{3.3b}$$

where dl is a unit vector along that path and I_x is the net current enclosed in the path. If the current is assumed to be distributed uniformly in the conductor, then it can be stated that

$$I_x = \frac{\pi x^2}{\pi r^2} I. \tag{3.4}$$

The magnetic intensity in Equation (3.3b) at radius *x* inside the conductor is then restated as:

$$H_x = \frac{x}{2\pi r^2} I \quad [A/m]. \tag{3.5}$$

From Equation (3.5), the following formula can be derived:

$$B_x = \mu H_x = \frac{\mu x I}{2\pi r^2} \quad [T], \tag{3.6}$$

$$d\emptyset = \frac{\mu x I}{2\pi r^2} dx \quad [Wb/m], \tag{3.7}$$

$$d\lambda = \frac{\pi x^2}{\pi r^2} d\emptyset = \frac{\mu x^3 I}{2\pi r^4} dx \quad [Wb - turns/m]. \tag{3.8}$$

Equation (3.6) defines magnetic flux, and $d\emptyset$ is differential flux enclosed in a ring of thickness *dx* for a 1 meter length conductor. The differential flux linkage in Equation (3.7) is calculated with respect to the area of differential flux. The total internal flux linkage, λ_{int}, is derived as:

$$\lambda_{int} = \int d\lambda = \int_0^r \frac{\mu x^3 I}{2\pi r^4} dx = \frac{\mu I}{8\pi} \quad [Wb - turns/m]. \tag{3.9}$$

Therefore, the internal inductance in Equation (3.1c) is stated as:

$$L_{int} = \frac{\lambda_{int}}{I} = \frac{\mu}{8\pi} \quad [H/m] \tag{3.10}$$

For non-ferromagnetic materials (e.g., copper and aluminium) the relative permeability of the conductor, $\mu_r = 1$. Equation (3.10) can be restated as:

$$L_{int} = \frac{\mu_0}{8\pi} = \frac{4\pi.10^{-7}}{8\pi} = \frac{10^{-7}}{2} \quad [H/m]. \tag{3.11}$$

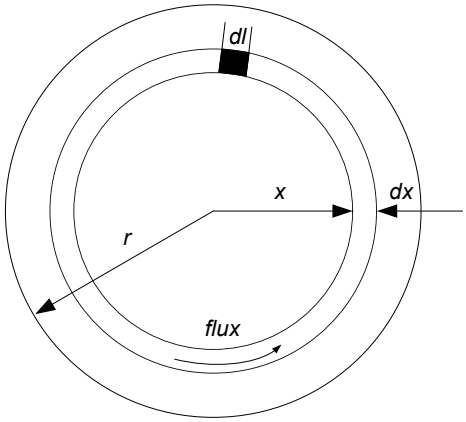

Figure 3.2: The flux linkage on one conductor [61].

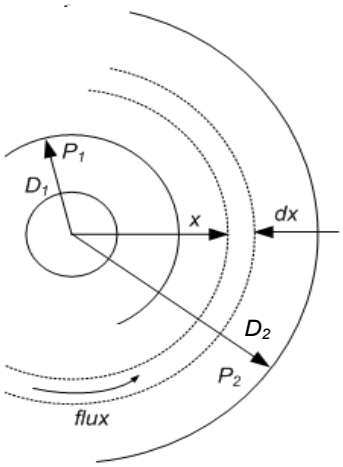

Figure 3.3: The flux linkage between 2 points outside of the line [61].

For the purpose of calculating the external inductance, L_{ext}, we use Figure 3.3 to illustrate the flux linkages between two points, P_1 and P_2, that lie at distance, D_1 and D_2, from the center of the conductor. From Figure 3.3, if the current is within

the tube of the conductor, the magnetic intensity, H_x, and magnetic density, B_x, at a distance x from the centre of conductor is defined as:

$$H_x = \frac{I_x}{2\pi x} = \frac{I}{2\pi x} \quad [A/m], \tag{3.12}$$

$$B_x = \mu H_x = \frac{\mu I}{2\pi x} \quad [T]. \tag{3.13}$$

If the total current, I, flows on the surface of the conductor, then the differential magnetic flux and differential flux linkage contained in a circular tube of thickness dx, and at a distance x from the centre of the conductor is defined as:

$$d\lambda = d\emptyset = \frac{\mu I}{2\pi x} dx \quad [Wb/m]. \tag{3.14}$$

The total external flux linkages per meter can be found by integrating Equation (3.14):

$$\lambda_{ext} = \int_{D_1}^{D_2} d\lambda = \int_{D_1}^{D_2} \frac{\mu I}{2\pi x} dx = \frac{\mu I}{2\pi} \ln \frac{D_1}{D_2} \quad [Wb/m]. \tag{3.15}$$

Finally, the external inductance per meter is stated as:

$$L_{ext} = \frac{\lambda_{ext}}{I} = \frac{\mu}{2\pi} \ln \frac{D_2}{D_1} \quad [H/m]. \tag{3.16}$$

From Equation (3.11) and Equation (3.16), if $r' = D_2 \exp(-1/4) = 0.788\, D_2$ (i.e., geometric mean radius, GMR), then we can formulate L_{tot} as :

$$L_{tot} = L_{int} + L_{ext} = \frac{\mu}{8\pi} + \frac{\mu}{2\pi} \ln \frac{D_2}{D_1}, \tag{3.17}$$

$$= \frac{\mu}{2\pi} \left[\frac{1}{4} + \ln \frac{D_1}{D_2} \right] = (2.10^{-7}) \ln \frac{D_2}{r'}. \tag{3.18}$$

Figure 3.4 shows the three-phase transmission line, where the flux linkages method in one conductor is utilized for calculating the per-phase of inductance reactance, X_L. In this calculation, the locations of overhead transmission conductors are assumed relatively remote from the ground but relatively close to one another. Hence, no currents flow in earth that will change the flux between the conductors.

Formulae similar to Equation (3.18) can be derived for three-phase transmission line and for lines with more phases.

If we assume that the line is symmetrical and transposed, the per-phase inductive reactance, X_L, is assumed equal [58, 60]. Based on lumped parameters approach of Figure 3.1, the inductance reactance of phase A, X_A, is as the summation of the flux from several sources which result the self- and mutual-inductance reactance:

$$\emptyset_A = \emptyset_{AA,self} + \emptyset_{AA,mut} + \emptyset_{AB} + \emptyset_{AC}, \tag{3.19}$$

where flux $\emptyset_{AA,self}$ and $\emptyset_{AA,mut}$ are self flux in phase A due to I_A and another self-flux, but it is a source of mutual impedance which can be seen by phase B and phase C. $\emptyset_{AB}$ and $\emptyset_{AC}$ are the flux due to $\underline{I_B}$ and $\underline{I_C}$ respectively. Using the formula explained above, the average flux linkages for phase A is given as follows:

$$\lambda_A = (2.10^{-7})/3\left[\left(\frac{1}{4}I_a + I_a ln\frac{D_{12}}{D_2} + I_a ln\frac{D_{13}}{D_2} + I_b ln\frac{D_{21}}{D_2} + I_c ln\frac{D_{31}}{D_2}\right) + \ldots\right.$$
$$\left(\frac{1}{4}I_a + I_a ln\frac{D_{21}}{D_2} + I_a ln\frac{D_{23}}{D_2} + I_b ln\frac{D_{32}}{D_2} + I_c ln\frac{D_{12}}{D_2}\right) + \cdots$$
$$\left.\frac{1}{4}I_a + I_a ln\frac{D_{32}}{D_2} + I_a ln\frac{D_{31}}{D_2} + I_b ln\frac{D_{13}}{D_2} + I_c ln\frac{D_{23}}{D_2}\right], \tag{3.20}$$

if $\underline{I_A}+\underline{I_B} + \underline{I_C} = 0$ and $D_{12} = D_{21}, D_{23} = D_{32}, D_{13} = D_{31}$, then Equation (3.20) can be restated as:

$$\lambda_A = \frac{(2.10^{-7})I_A}{3}\left[ln\frac{(D_{12}D_{13}D_{23})}{{D_2}^3} + \frac{3}{4}\right] \ [W/m], \tag{3.21}$$

using $r' = D_2\exp(-3/4)$ (i.e., GMR), and dividing Equation (3.21) with I_A, then the reactance inductive, X_L, per phase is:

$$X_L = \frac{(2.10^{-7})\omega}{3}\left[ln\frac{(D_{12}D_{13}D_{23})^{1/3}}{GMR}\right]. \tag{3.22}$$

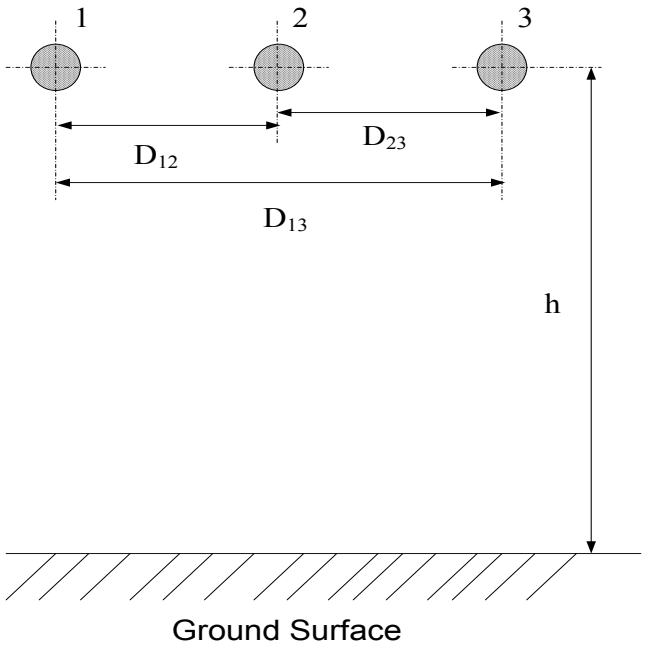

Figure 3.4: Three-phase transmission line.

If as in Figure 3.5, the line conductor is arranged in a bundle, the reactance inductive per phase for this circuit is calculated as [58]:

$$X_L = (2.10^{-7})\omega ln\left(\frac{GMD}{GMR}\right), \tag{3.23}$$

where GMD is expressed as:

$$GMD = (D_{a1b1}D_{a1b2}D_{a1c1}D_{a1c2}D_{b1c1}D_{b1c2})^{1/6}, \tag{3.24}$$

while GMR is GMR of the conductor which is expressed as:

$$GMR = \left(GMR_c{}^3 D_{a1a2}D_{b1b2}D_{c1c2}\right)^{1/6}. \tag{3.25}$$

GMR_c is the GMR of the conductor, and this value depends on the material of the conductor.

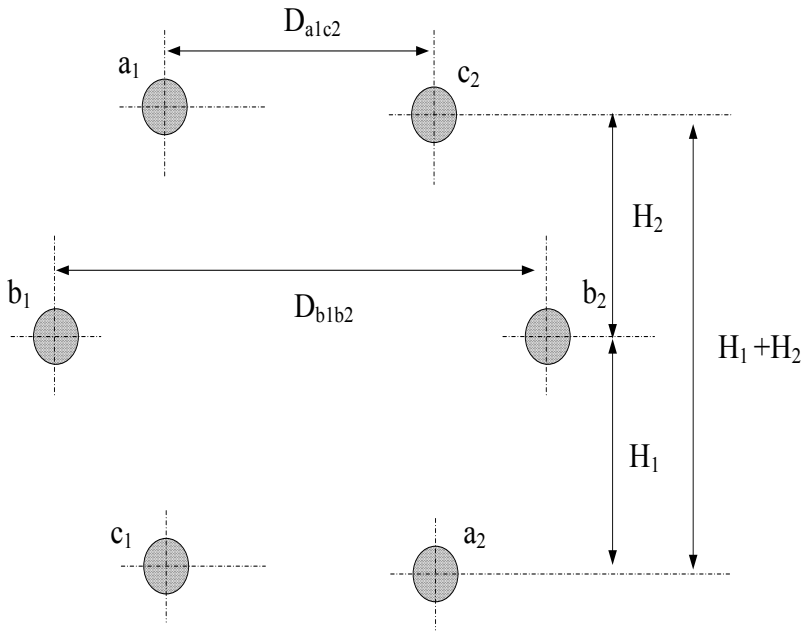

Figure 3.5: Line conductors arranged in a bundle configuration.

In the three phase transmission line of Figure 3.1, each series of line impedance that has been calculated using Equation (3.22) is expressed as:

$$\underline{Z}_L = R_{DC} + jX_L, \tag{3.26}$$

and if the overhead lines are totally transformed, then by Equation (3.20), the self-impedance of each conductor is:

$$Z_{AA} = R_{DC} + j2.10^{-7}\omega\left(\frac{1}{4} + ln\frac{D_{12}}{D_2} + ln\frac{D_{13}}{D_2}\right) = R_{DC} + jX_{AA},$$

$$Z_{BB} = R_{DC} + j2.10^{-7}\omega\left(\frac{1}{4} + ln\frac{D_{21}}{D_2} + ln\frac{D_{23}}{D_2}\right) = R_{DC} + jX_{BB}, \tag{3.27}$$

$$Z_{CC} = R_{DC} + j2.10^{-7}\omega\left(\frac{1}{4} + ln\frac{D_{32}}{D_2} + ln\frac{D_{31}}{D_2}\right) = R_{DC} + jX_{CC},$$

while mutual impedance between conductors of any two conductors is derived as:

$$\underline{Z}_{AB} = j2.10^{-7}\omega\, ln\frac{D_{21}}{D_2} = jX_{AB},$$

$$\underline{Z}_{AC} = j2.10^{-7}\omega\, ln\frac{D_{31}}{D_2} = jX_{AC},$$

$$\underline{Z}_{BA} = j2.10^{-7}\omega\, ln\frac{D_{12}}{D_2} = jX_{BA},$$

$$\underline{Z}_{BC} = j2.10^{-7}\omega\, ln\frac{D_{32}}{D_2} = jX_{BC}, \tag{3.28}$$

$$\underline{Z}_{CA} = j2.10^{-7}\omega\, ln\frac{D_{13}}{D_2} = jX_{CA},$$

$$\underline{Z}_{CB} = j2.10^{-7}\omega\, ln\frac{D_{23}}{D_2} = jX_{CB}.$$

From Equations $(3.27 - 3.28)$, we can state the series impedance matrix of the overhead three-phase transmission line of Figure 3.1 as:

$$\underline{Z}_{ABC} = \begin{bmatrix} \underline{Z}_{AA} & \underline{Z}_{AB} & \underline{Z}_{AC} \\ \underline{Z}_{BA} & \underline{Z}_{BB} & \underline{Z}_{BC} \\ \underline{Z}_{CA} & \underline{Z}_{CB} & \underline{Z}_{CC} \end{bmatrix}, \tag{3.29}$$

where the matrix impedance of Equation (3.29) can also be expressed from Figure 3.1 as follows:

$$\underline{Z}_{AA} = \left(\underline{V}_{AS} - \underline{V}_{AR}\right)/\underline{I}_A \;;\; \underline{Z}_{AB} = \left(\underline{V}_{AS} - \underline{V}_{AR}\right)/\underline{I}_B \;;\; \underline{Z}_{AC} = \left(\underline{V}_{AS} - \underline{V}_{AR}\right)/\underline{I}_C,$$

$$\underline{Z}_{BA} = \left(\underline{V}_{BS} - \underline{V}_{BR}\right)/\underline{I}_A \;;\; \underline{Z}_{BB} = \left(\underline{V}_{BS} - \underline{V}_{BR}\right)/\underline{I}_B \;;\; \underline{Z}_{BC} = \left(\underline{V}_{BS} - \underline{V}_{BR}\right)/\underline{I}_C,$$

$$\underline{Z}_{CA} = \left(\underline{V}_{BS} - \underline{V}_{BR}\right)/\underline{I}_A \;;\; \underline{Z}_{CB} = \left(\underline{V}_{BS} - \underline{V}_{BR}\right)/\underline{I}_B,$$

$$Z_{CC} = \left(\underline{V}_{BS} - \underline{V}_{BR}\right)/\underline{I}_C. \tag{3.30}$$

For balancing three-phase transmission line, both the mutual and self-impedance in Equation (3.29) will be equal. Therefore, the sequence impedance of Equation (3.29) can be expressed as:

$$\underline{Z}_{012} = \begin{bmatrix} \underline{Z}_0 & 0 & 0 \\ 0 & \underline{Z}_1 & 0 \\ 0 & 0 & \underline{Z}_2 \end{bmatrix}, \tag{3.31}$$

where the zero-sequence impedance $\underline{Z}_0 = \underline{Z}_{self} + 2\underline{Z}_{mutual}$, the positive-sequence impedance $\underline{Z}_1 = \underline{Z}_{self} + \underline{Z}_{mutual}$, and the negative-sequence impedance $\underline{Z}_2 = \underline{Z}_{self} + \underline{Z}_{mutual}\underline{Z}_{self}$. The matrix impedance of Equation (3.31) is used in setting the line impedance.

3.3. Network System Models for Protection Study

Since we are only interest in the effect of the power system on the protected component (e.g., transmission line), this reduces the network model and simplifies the equations [23].

In the equivalent networks system, the external systems at the terminal buses are modelled using Thevenin's equivalents which have voltage sources indicated by $\underline{E}_S$, and $\underline{Z}_S$ for the corresponding source impedance. The measured fault impedance of the protected line in that equivalent system is then based on the measured flow of the faulted current, in which the fault current value is affected by the equivalent system. In the following section, we develop the equivalent network model required for the fault impedance calculation.

3.3.1. Two Terminal Network Representing Single-Circuit Line

Figure 3.6(a) shows a simple two-port equivalent with a general equivalent of an external network shown inside the border line [23]. Three nodes in the two-port equivalent are identified with node 1, node 2, and the reference node. The protected component is a transmission line between terminals S and R, with impedance, $\underline{Z}_L$. IED is installed at terminal S, and the fault is occurring on the line at location F.

If the circuits in Figure 3.6(a) are assumed to be linear, then the general scheme of Figure 3.6(a) is equivalent to Figure 3.6(b) [23], where the general equivalent scheme consists of the emf, $\underline{E}_S$, $\underline{E}_R$, and the corresponding impedance sources, $\underline{Z}_S$, $\underline{Z}_R$, $\underline{Z}_E$. Calculation of the source impedances, $\underline{Z}_S$, and $\underline{Z}_R$, derive from the open circuit voltages which are determined by open-circuit tests of the power system at node 1, and node 2. If the protected line, $\underline{Z}_L$, is the only line connecting buses S, and R, then the extra link, $\underline{Z}_E$, as shown in Figure 3.6(c), can be ignored.

In [23], it is shown that the generator, network topology, and load may undergo change, such that the external line, $\underline{Z}_E$, would also change and consequently not be a fixed value. Hence, the source impedances, $\underline{Z}_S$, and $\underline{Z}_R$, which are considered in

the fault impedance calculation process, can be uncertain. This uncertainty impacts the accuracy of the one-end fault impedance calculation algorithm, if that source impedance is used as the input data.

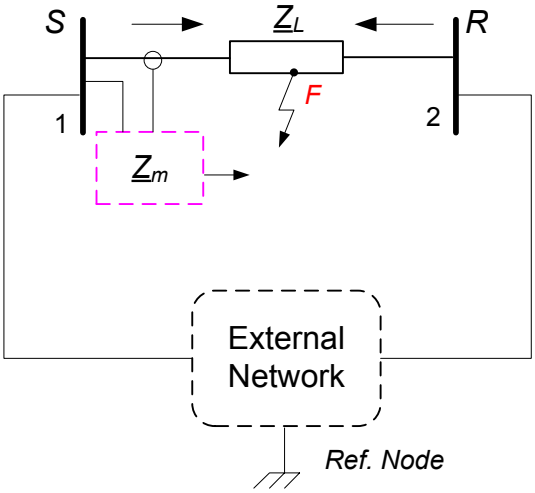

(a)

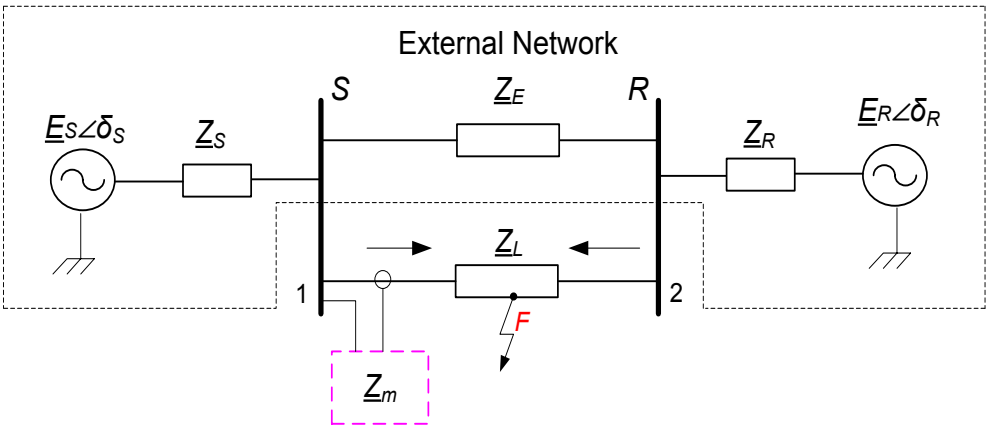

(b)

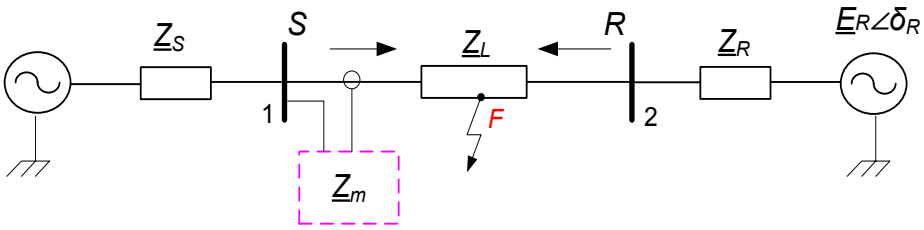

(c)

Figure 3.6: Simple two-port network equivalent:
a) General scheme, b) General equivalent scheme, c) Simplified scheme.

3.3.2. Two Terminal Network Representing Double-Circuit Line

Networks with parallel lines are very common in power networks. They are constructed due to their constant load growth and constraints in getting new right-of-ways. Figure 3.7 shows the equivalent scheme of a power network with parallel lines. The protected line is denoted by $\underline{Z}_{L1}$, while parallel line and zero-sequence mutual coupling are denoted as $\underline{Z}_{L2}$, and $\underline{Z}_{0M}$, respectively.

Operating conditions of a parallel line circuit will change for reasons such as forced outage, load dispatch, and scheduled maintenance. Figure 3.7 shows that the effect of mutual coupling, $\underline{Z}_{0M}$, will depend on the mode operation of parallel line, $\underline{Z}_{L2}$ (i.e., healthy line) [62], which is in parallel with the faulted line, $\underline{Z}_{L1}$.

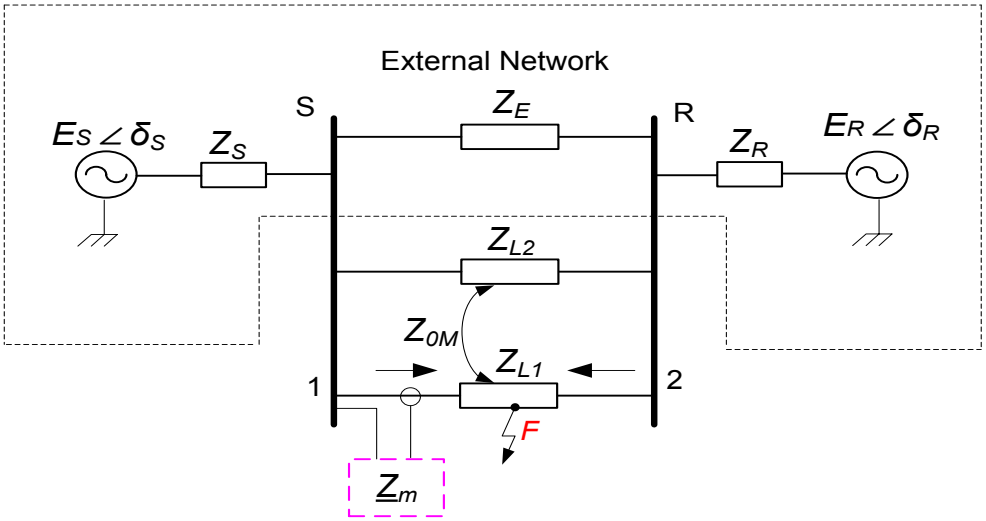

Figure 3.7: Equivalent scheme of power network with parallel line.

Figure 3.8 presents cases for which two modes of parallel circuit lines in which the effect of mutual coupling, $\underline{Z}_{0M}$, needs to be considered [18]. The first cases is when both lines of the parallel circuit are in normal operation (i.e., CB_1, CB_2 close and SW_1, SW_2 open), while the second case is when the parallel line is switched-off and grounded at both ends (i.e., CB_1, CB_2 open and SW_1, SW_2 close). Investigation of the effect of the parallel line status on the fault current requires consideration in the following cases: i) ungrounded parallel line is switched off (e.g., CB_1, CB_2 open and SW_1, SW_2 open), ii) parallel line is switched off at one terminal and

ungrounded (e.g., CB_1 open ,CB_2 close, and SW_1, SW_2 open), and iii) parallel line is switched off and grounded at one end (e.g., CB_1, CB_2 open, and SW_1 close , SW_2 open).

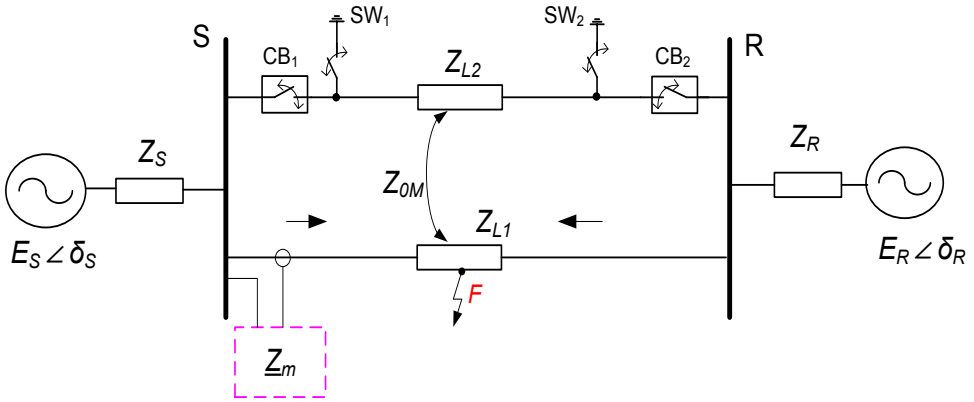

Figure 3.8: Parallel Line Modes.

3.3.3. Multi-terminal Network Representing Tapped Line

The purpose of providing a two terminal method of simplified power system is for the study of faults on the protected line of the network. However, a model of protected line tapped in the middle line is required, but a full switching station is not installed at the tap point. For performance analysis of IEDs in such cases, a multiport equivalent is required.

Figure 3.9 shows a typical configuration of a line with more than two terminals, and with a substantial generator behind them (i.e., a multi-terminal). The number of network elements of a multiport network is given by [23]:

$$N = \frac{n(n-1)}{2}. \tag{3.32}$$

With n = 4 being the number of ports in the protected system, the number of required network elements in the supply system is then calculated as N = 6.

In Figure 3.9(a), the general equivalent scheme consists of emfs, $\underline{E}_S$, $\underline{E}_R$, $\underline{E}_T$, and the corresponding source impedances, $\underline{Z}_S$, $\underline{Z}_R$, $\underline{Z}_T$. The line sections are denoted as $\underline{Z}_{L1}$, $\underline{Z}_{L2}$, $\underline{Z}_{L3}$, while $\underline{Z}_{E1}$, $\underline{Z}_{E2}$, $\underline{Z}_{E3}$ are as the external line that link terminals 1, 2, and 3. If the protected lines $\underline{Z}_{L1}$, and $\underline{Z}_{L2}$, with the fault located at

F_1 and F_2 are the only lines connected to the bus S, and R, and Z_{L3} is indicated as the tapped line in the middle of bus S, and R, then the extra links, $\underline{Z}_{E1}$, $\underline{Z}_{E2}$, and $\underline{Z}_{E3}$, as shown in Figure 3.9(b), can be ignored [23].

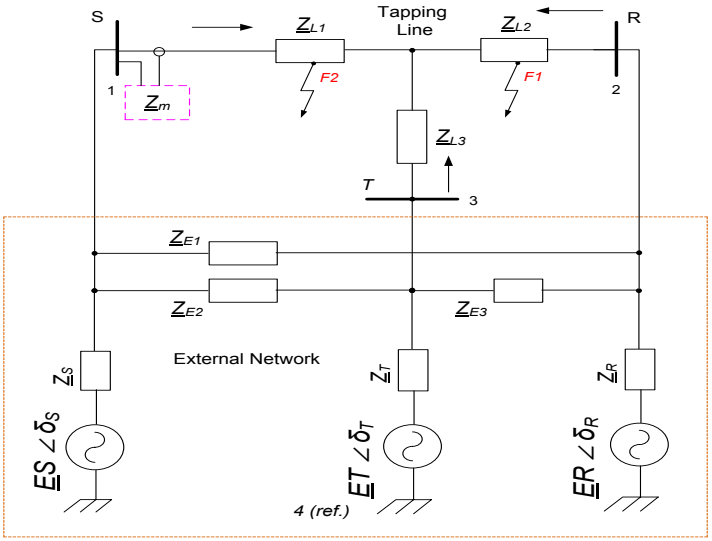

(a)

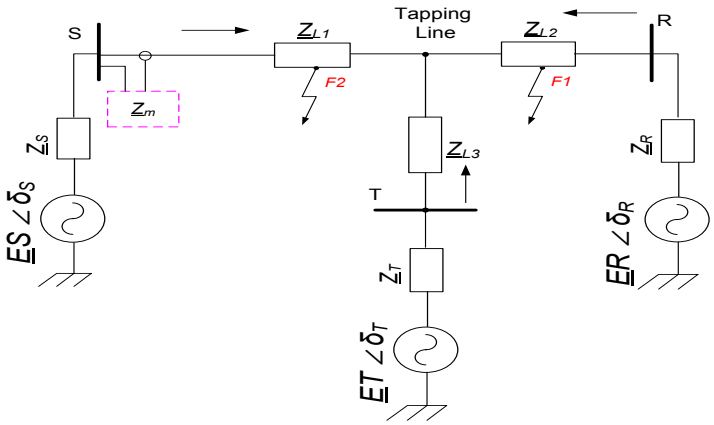

(b)

Figure 3.9: Multi-terminal with tapping line network equivalent:
a) General equivalent scheme, b) Simplified scheme.

3.4. Fault Impedance Calculation and Uncertainty

3.4.1. Fault Impedance Measurement for Line with Sources at Both Ends

This technique uses three-phase voltage and current input signals that are measured by a non-pilot IED located at one-end (terminal S) for calculating the apparent fault impedance, $\underline{Z}_m$. Figure 3.10 shows a single line diagram of a three phase system, where a phase A to ground fault is simulated at F. In this case, the apparent fault impedance measured by the IED is calculated based on the ratio of bus-voltage, $\underline{V}_S$, and current, $\underline{I}_S^c$ (i.e., a measured current, $\underline{I}_S$, during a fault with compensated zero-sequence current), at the distance relay located at terminal S. The apparent fault impedance is formulated as follows [63]:

$$\underline{Z}_m = \frac{\underline{V}_S}{\underline{I}_S^c} = p\underline{Z}_{1L} + \frac{3R_F\underline{I}_F}{\underline{I}_S^c}, \tag{3.33}$$

$$p\underline{Z}_{L1} = \frac{\underline{V}_S}{\underline{I}_S + \underline{k}_0\underline{I}_0}, \tag{3.34}$$

where $\underline{I}_F$ is the total current that is contributed from both ends of the sources. If fault resistance, R_F, is assumed to be zero, then the calculated apparent fault impedance, $\underline{Z}_m$, would be equal to $p\underline{Z}_m$, where p is fault distance between terminal S and fault location F. This is shown in Figure 3.10.

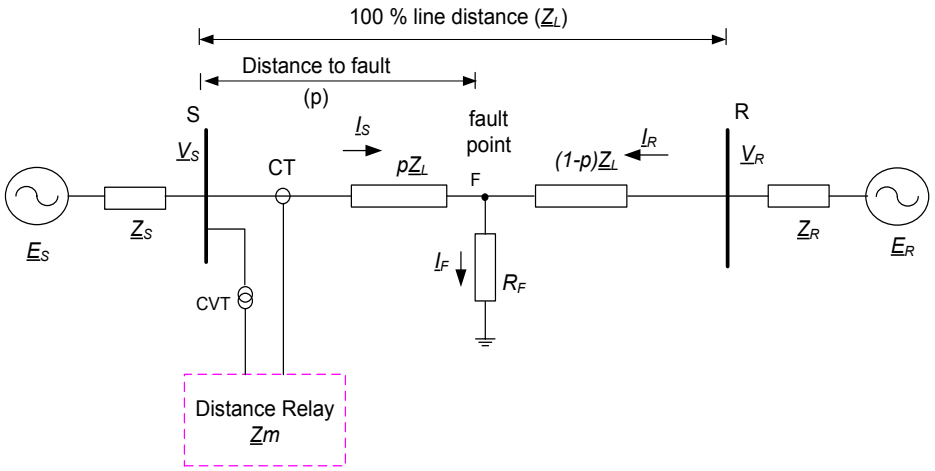

Figure 3.10: A typical single line system.

In Figure 3.11, the fault loop impedance in Equation (3.33) is derived from the relationship between sequence voltages at the fault point, F, as follows:

$$\underline{V_1} + \underline{V_2} + \underline{V_0} = 3R_F\underline{I_F}. \tag{3.35}$$

The sequence voltages in Equation (3.35) can be expressed in terms of the sequence component voltages and currents at the S-side of the line. This leads to the following relation:

$$\begin{aligned}
&\underline{V_{1AS}} - p\underline{Z_{1L}}\underline{I_{1AS}} + \underline{V_{2AS}} - p\underline{Z_{2L}}\underline{I_{2AS}} + \underline{V_{0AS}} - p\underline{Z_{0L}}\underline{I_{0AS}} = 3R_F\underline{I_F}, \qquad (3.36)\\
&\underline{V_{1AS}} + \underline{V_{2AS}} + \underline{V_{0AS}} = p\underline{Z_{1L}}\left(\underline{I_{1AS}} + \underline{I_{2AS}}\right) + p\underline{Z_{0L}}\underline{I_{0AS}} + 3R_F\underline{I_F},\\
&\underline{V_S} = p\underline{Z_{1L}}\left(\underline{I_{1AS}} + \underline{I_{2AS}} + \underline{I_{0AS}}\right) - p\underline{Z_{1L}}\underline{I_{0AS}} + p\underline{Z_{0L}}\underline{I_{0AS}} + 3R_F\underline{I_F},\\
&\underline{V_S} = p\underline{Z_{1L}}\underline{I_S} + p(\underline{Z_{0L}} - p\underline{Z_{1L}})\underline{I_{0AS}} + 3R_F\underline{I_F},
\end{aligned}$$

where

$$\underline{V_S} = \underline{V_{1AS}} + \underline{V_{2AS}} + \underline{V_{0AS}}, \tag{3.37a}$$

$$\underline{I_S} = \underline{I_{1AS}} + \underline{I_{2AS}} + \underline{I_{0AS}}. \tag{3.37b}$$

Using Equation (3.37a) and Equation (3.37b), the total of three sequence voltage networks, defined in Eqution (3.36), can be redefined as

$$\underline{V_S} = p\underline{Z_{1L}}\left[\underline{I_S} + \frac{\underline{Z_{0L}} - \underline{Z_{1L}}}{\underline{Z_{1L}}}\underline{I_{0AS}}\right] + 3R_F\underline{I_F}. \tag{3.38}$$

From Equation (3.38), we can identify the current measured during a fault and compensate for zero-sequence current as:

$$\underline{I_S^c} = \underline{I_S} + \frac{\underline{Z_{0L}} - \underline{Z_{1L}}}{\underline{Z_{1L}}}\underline{I_0}. \tag{3.39}$$

such that the formula for the voltage in faulted phase, in terms of the fault current, is:

$$\underline{V_S} = p\underline{Z_{1L}}\underline{I_S^c} + 3R_F\underline{I_F}. \tag{3.40}$$

Finally, from Equation (3.39) and Equation (3.40), the detailed formula, in Equation (3.33), for phase A to ground could be stated as:

$$\underline{Z}_m = \frac{\underline{V}_S}{\underline{I}_S^c} = \frac{p\underline{Z}_{1L}\underline{I}_S^c + 3R_F\underline{I}_F}{\left(\underline{I}_S + \underline{k}_0\underline{I}_0\right)}. \tag{3.41}$$

If $R_F = 0$, the Equation (3.41) can be redefined as:

$$\underline{Z}_m = \frac{\underline{V}_S}{\underline{I}_S^c} = \frac{\underline{V}_S}{\left(\underline{I}_S + k_0\underline{I}_0\right)} = p\underline{Z}_{1L}, \tag{3.42}$$

where zero-sequence current compensation, $\underline{k}_o$, is required to compensate the residual current, $\underline{I}_o$, is given as:

$$\underline{k}_o = \frac{\left(\underline{Z}_{0L} - \underline{Z}_{1L}\right)}{\underline{Z}_{1L}}. \tag{3.43}$$

It can be seen from Equation (3.39) that the apparent fault impedance, $\underline{Z}_m$, measured at the relaying location, will be affected by the uncertain factors, $\underline{Z}_{0L}$, $\underline{Z}_{1L}$, and R_F . In addition, the fault current, $\underline{I}_F$, is not measured and it depends on load flow angle, δ_F, and other circuit parameters. Since the fault current, $\underline{I}_F$, is fed from both sources, the accuracy of the measured impedance is not only affected by uncertain values of R_F, but from the interaction between R_F and the power flow angle, δ_F [1, 63]. Uncertain values of δ_F, may affect the direction of $\underline{I}_S^c$, and in combination with R_F, will influence the reactance of the measured impedance [1].

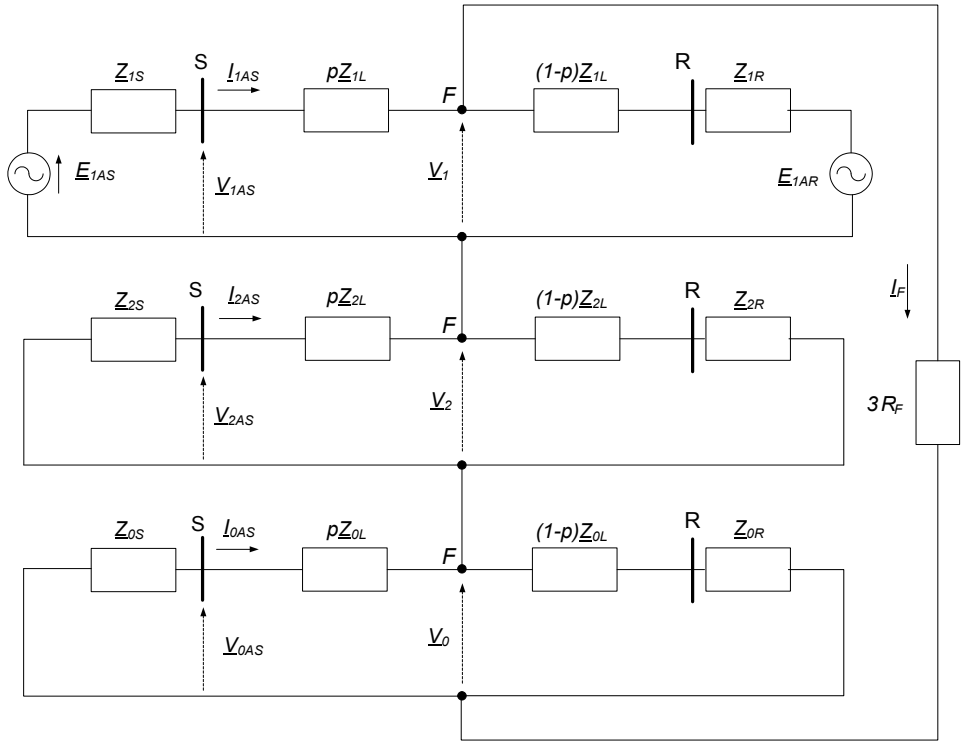

Figure 3.11: Sequence networks for the phase A to ground fault in Figure 3.10.

3.4.2. Fault Impedance Measurement for Double-circuit Line

Zero-sequence current compensation, $\underline{k}_0$, implemented in the non-pilot distance relay, is designed primarily for protecting the single transmission line during a phase A to ground fault. The measured fault impedance, $\underline{Z}_m$, defined in Equation (3.33), is in proportion to the line fault distance with assuming that fault resistance, R_F = 0, and zero-sequence line impedance, $\underline{Z}_{0L}$, can be measured accurately. $\underline{Z}_{0L}$ is not easily measured as it can vary since the value will depend on the soil resistivity [64]. The difficulty could be more severe when non-pilot is used for protecting the line in a parallel circuit. This is due to the IED not having a function to measure the zero-sequence current of a parallel line during a phase to ground fault [15]. For this case, zero-sequence mutual coupling, $\underline{Z}_{0M}$, is not able to be compensated, and will consequently cause additional inaccuracy in the fault impedance calculation [18].

Figure 3.12 shows the same IED using $\underline{k}_0$ to protect phase A to ground faults in a parallel line circuit. The fault impedance given in Equation (3.44) with assumed fault resistance, $R_F = 0$, is derived as follows [62]:

$$\underline{Z}_m = \frac{\underline{V}_S}{\underline{I}_S^c} = \frac{\underline{V}_S}{\underline{I}_S + \underline{k}_0\underline{I}_0} = \frac{p\underline{Z}_{1L}\left(\underline{I}_{1AS} + \underline{I}_{2AS} + \underline{I}_{0AS}\right) + p\underline{Z}_{0M} \times \underline{I}_{0p}}{\underline{I}_S + \underline{k}_0\underline{I}_0}, \tag{3.44}$$

where $p\underline{Z}_{0M}$, is zero-sequence mutual couplings and $\underline{I}_{0p}$, is zero-sequence current of the healthy line (i.e., parallel line). Equation (3.44) shows that mutual coupling, $p\underline{Z}_{0M}$, is an additional factor that is not compensated by the distance relay and will consequently produce an error in calculating the fault impedance.

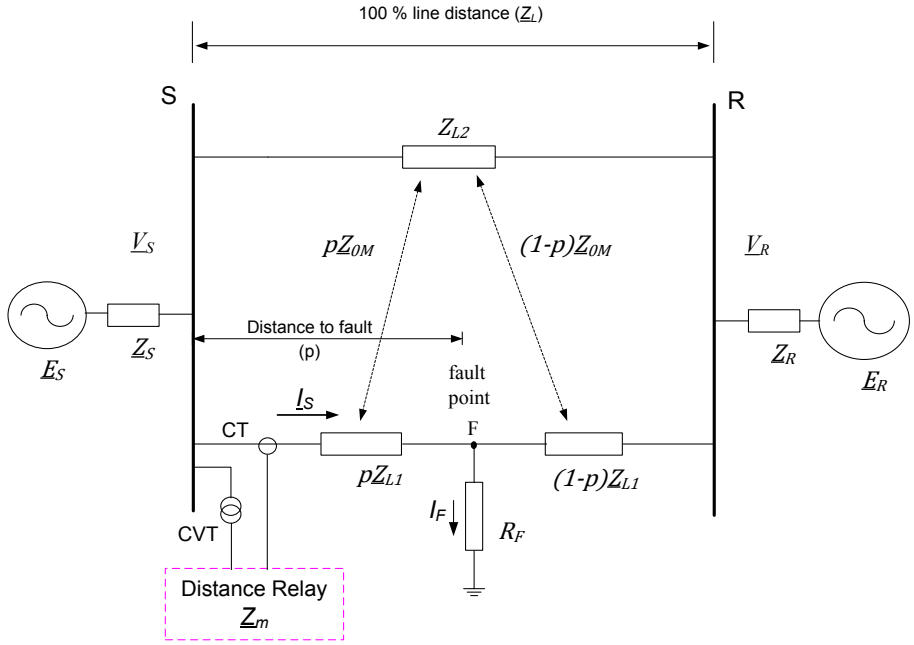

Figure 3.12: Single line diagram for the phase A to ground fault on a parallel line circuits with two sources, $\underline{E}_S$ and $\underline{E}_R$.

To analyse the uncertain factors of impedance measurement for a phase A short circuit at point F, we use the circuit in Figure 3.12, with sequence components circuit in Figure 3.13. Zero sequence mutual coupling, $p\underline{Z}_{0M}$, with another line is modelled in the circuit. The sum of the sequence components votages at the fault point F, is obtained from the circuit in Figure 3.13, such that:

$$\underline{V}_1 + \underline{V}_2 + \underline{V}_0 = 3R_F\underline{I}_F. \tag{3.45}$$

From Figure 3.13, this equation can be resolved as follows:

$$\underline{V}_{1AS} - p\underline{Z}_{1L}\underline{I}_{1AS} + \underline{V}_{2AS} - p\underline{Z}_{2L}\underline{I}_{2AS} + \underline{V}_{0AS} - p\underline{Z}_{0L}\underline{I}_{0AS} \ldots$$
$$-p\underline{Z}_{0M}\underline{I}_{0p} = \ 3R_F\underline{I}_F. \tag{3.46}$$

By representing voltage and current at bus S as:

$$\underline{V}_S = \underline{V}_{1AS} + \underline{V}_{2AS} + \underline{V}_{0AS},$$

$$\underline{I}_S = \underline{I}_{1AS} + \underline{I}_{2AS} + \underline{I}_{0AS},$$

we can write Equation (3.46) in the following form:

$$\underline{V}_S = p\underline{Z}_{1L}\underline{I}_S + p\underline{Z}_{0L}\underline{I}_{0AS} - p\underline{Z}_{2L}I_{2AS} + p\underline{Z}_{0M}\underline{I}_{0p} \ + 3R_F\underline{I}_F, \tag{3.47}$$

$$\underline{V}_S = p\underline{Z}_{1L1}\left[\underline{I}_S + \frac{\underline{Z}_{0L1} - \underline{Z}_{1L1}}{\underline{Z}_{1L1}}\underline{I}_{0AS} + \frac{\underline{Z}_{0M}}{\underline{Z}_{1L1}}\underline{I}_{0p}\right] + 3R_F\underline{I}_F,$$

$$\underline{V}_S = p\underline{Z}_{1L1}\left[\underline{I}_S + \ \underline{k}_0\underline{I}_{0AS} + \underline{k}_{0M}\underline{I}_{0p}\right] + 3R_F\underline{I}_F,$$

where the zero-sequence compensation factors for the faulted line, $\underline{k}_0$, as well as for mutual coupling, $\underline{k}_{0M}$, are stated as:

$$\underline{k}_0 = \frac{\underline{Z}_{0L1} - \underline{Z}_{1L1}}{\underline{Z}_{1L1}} \quad \text{and} \quad \underline{k}_{0M} = \frac{\underline{Z}_{0M}}{\underline{Z}_{1L1}}. \tag{3.48}$$

If the measured fault current with compensated zero sequence is stated as:

$$\underline{I}_S^c = \underline{I}_S + \ \underline{k}_0\underline{I}_{0AS} + \ \underline{k}_{0M}\underline{I}_{0p}, \tag{3.49}$$

the fault impedance, $\underline{Z}_m$, estimated by a relaying algorithm according to Equation (3.47) could be:

$$\underline{Z}_m = \frac{\underline{V}_S}{\underline{I}_S^c} = p\underline{Z}_{1L1} + 3R_F\frac{\underline{I}_F}{\underline{I}_S^c}, \tag{3.50}$$

$$= p\underline{Z}_{1L1} + \Delta\underline{Z}_{1L1}, \tag{3.51}$$

where the error, $\Delta\underline{Z}_{1L1}$, will depend on the additional drop voltage, $p\underline{Z}_{0M}\underline{I}_{0p}$, resulting from the mutual coupling effect of the healthy line's zero-sequence current, $\underline{I}_{0p}$, and also from the following factors, via a nonlinear function f:

$$\Delta \underline{Z}_{1L1} = f\left(\boldsymbol{\underline{P}_E}, \boldsymbol{\underline{P}_S}, R_F, \underline{k}_0\right). \tag{3.52}$$

The factors are grouped in the following vectors:

$$\boldsymbol{\underline{P}_S} = \left[\underline{Z}_{1S}, \underline{Z}_{1R}, \underline{Z}_{0S}, \underline{Z}_{0R}\right]^T \text{ and } \boldsymbol{\underline{P}_E} = \left[\underline{E}_{1S}, \underline{E}_{1R}\right]^T. \tag{3.53}$$

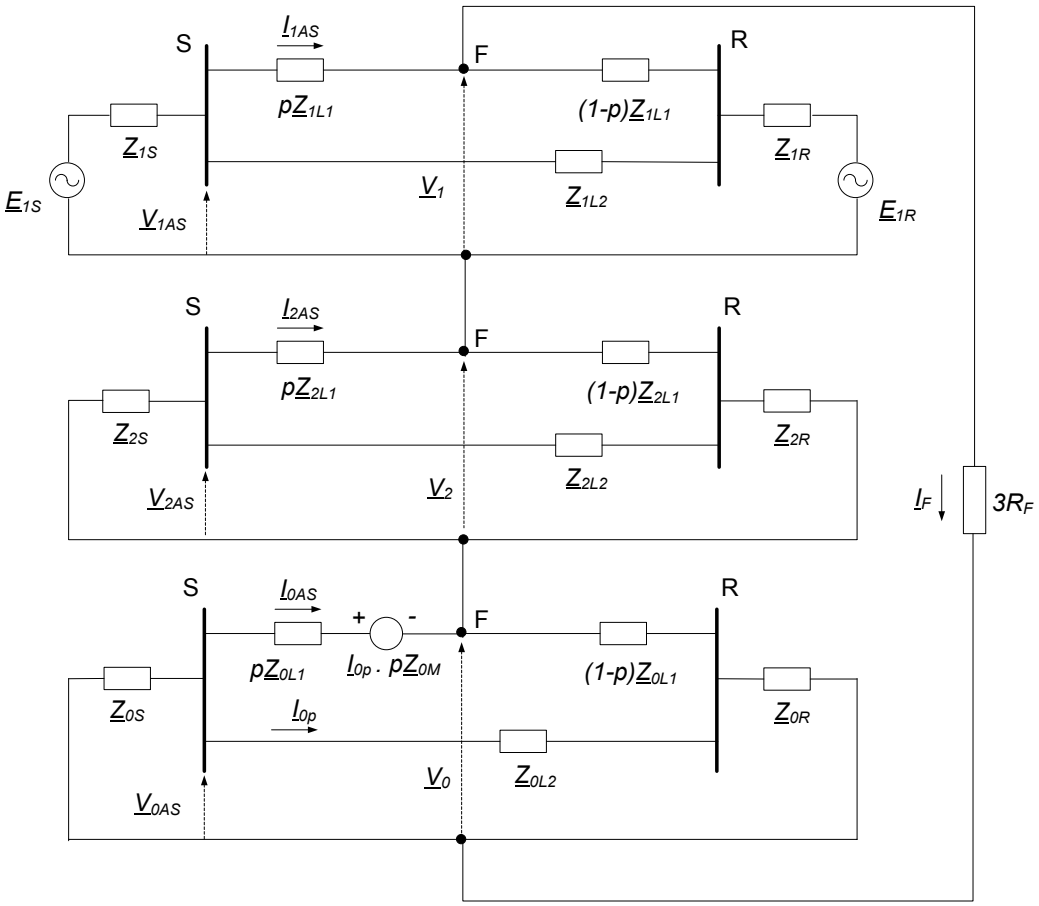

Figure 3.13: Sequence networks for both lines in operation in a phase A to ground fault in Figure 3.12.

3.4.3. Fault Impedance Measurement for Three-Terminal Line

Figure 3.14 shows a faulted three-terminal transmission line and the IED located at terminal S of section 1 (i.e., terminal between S and O). The proposed model determines the performance of calculated fault impedance for phase A to ground

fault with different fault location (F_1 and F_2), and through fault resistance, R_F. These line faults are much more complex to be protected by a distance relay using a one-ended measurement technique since fault resistance is not the only variable that contributes to the error as current infeed from the tapped line will influence the fault impedance calculation [65].

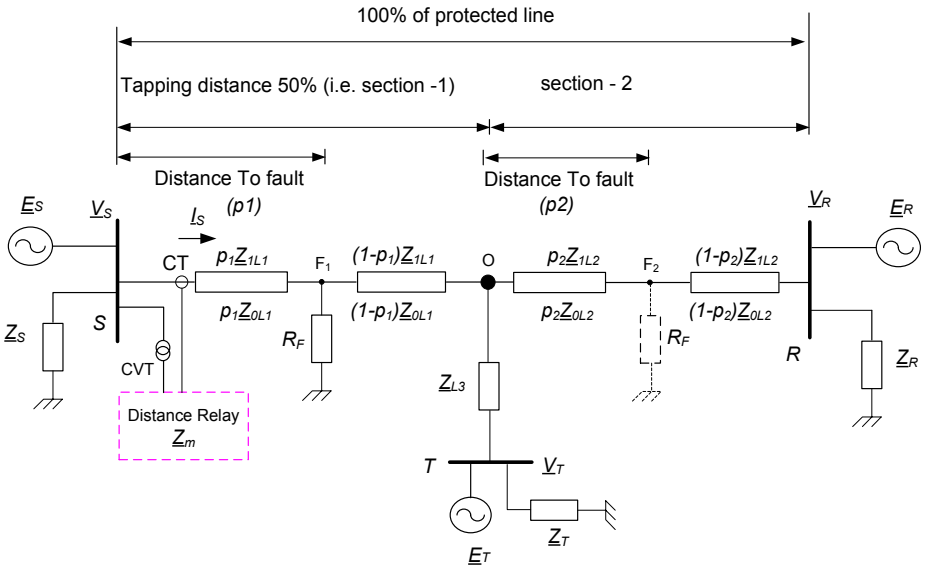

Figure 3.14: Single line diagram for the phase A to ground fault on a three-terminal line.

In the Figure 3.14, the external system is modelled using Thevenin's equivalent having three sources, $\underline{E}_S$, $\underline{E}_R$ and $\underline{E}_T$, with corresponding source impedance, $\underline{Z}_S$, $\underline{Z}_R$ and $\underline{Z}_T$. During the fault, the fault impedance calculated by the relaying point is based on the zero-sequence current compensation method using a factor, $\underline{k}_0$ [66]. The factor $\underline{k}_0$ depends on the zero-sequence impedance, $\underline{Z}_{0L1}$, which is not measured precicely. The fault impedance, $\underline{Z}_m$, measured from the ralaying point to the fault point F_1 (distance p_1 in Figure 3.14), is not always the actual impedance, $p_1\underline{Z}_{1L1}$ [8].

In the case of a single line to ground fault (phase A) in section 1 (fault F_1 in Figure 3.14), the fault impedance $\underline{Z}_m$, estimated by relay algorithm can be stated as [32]:

$$\underline{Z}_m = \frac{\underline{V}_S}{\underline{I}_S^C} = p_1\underline{Z}_{1L1} + \Delta\underline{Z}_{1L1}. \tag{3.54}$$

To specify which factors will affect the error measurement of phase A to ground fault impedance, $\Delta\underline{Z}_{1L1}$, at point F_1, we represent the circuit in Figure 3.14 with sequence components circuit in Figure 3.15.

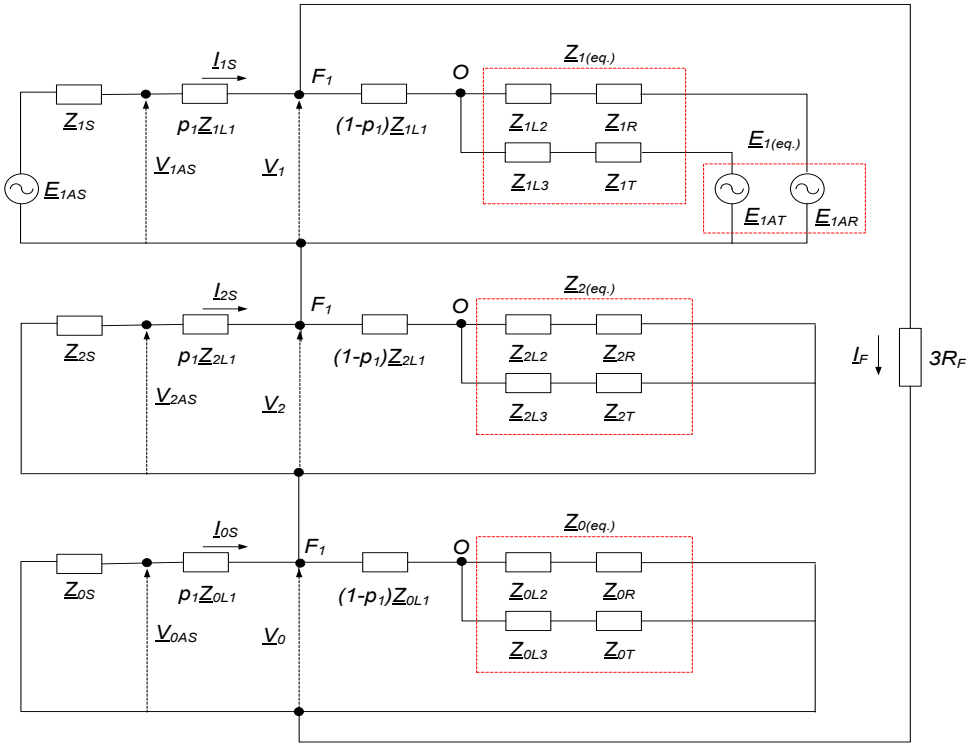

Figure 3.15: Sequence component circuit for the fault at F_1 in Figure 3.14.

The equivalent network of section 2, and section 3, in Figure 3.15 could be derived as follows:

$$\underline{E}_{1(eq.)} = \left(\underline{E}_{1AR} - \underline{E}_{1AT}\right)\frac{\underline{Z}_{1LR}}{\underline{Z}_{1LR} + \underline{Z}_{1LT}}\,, \tag{3.55a}$$

$$\underline{Z}_{1(eq.)} = \frac{\underline{Z}_{1LR}\underline{Z}_{1LT}}{\underline{Z}_{1LR} + \underline{Z}_{1LT}}\,, \tag{3.55b}$$

$$\underline{Z}_{2(eq.)} = \frac{\underline{Z}_{2LR}\underline{Z}_{2LT}}{\underline{Z}_{2LR} + \underline{Z}_{2LT}}, \tag{3.55c}$$

$$\underline{Z}_{0(eq.)} = \frac{\underline{Z}_{0LR}\underline{Z}_{0LT}}{\underline{Z}_{0LR} + \underline{Z}_{0LT}}, \tag{3.55d}$$

where

$$\underline{Z}_{1LR} = \underline{Z}_{1L2} + \underline{Z}_{1R}\ ;\ \underline{Z}_{1LT} = \underline{Z}_{1L3} + \underline{Z}_{1T}\ ;\ \underline{Z}_{2LR} = \underline{Z}_{2L2} + \underline{Z}_{2R}\,,$$
$$\underline{Z}_{2LT} = \underline{Z}_{2L3} + \underline{Z}_{2T}\ ;\ \underline{Z}_{0LR} = \underline{Z}_{0L2} + \underline{Z}_{0R}\ ;\ \underline{Z}_{0LT} = \underline{Z}_{0L3} + \underline{Z}_{0T}\,. \tag{3.55e}$$

The sum of the sequence component voltages at the fault point, F_1, during a phase A to ground fault obtained from the circuit in Figure 3.15, can be written as:

$$\underline{V_1} + \underline{V_2} + \underline{V_0} = 3R_F\underline{I_F}. \tag{3.56}$$

Using Equation (3.56) and $\underline{Z}_{1L1} = \underline{Z}_{2L1}$, we find the measured voltage, $\underline{V_S}$, in phase A at the relay point as follows:

$$\underline{V}_{1AS} - p_1\underline{Z}_{1L1}\underline{I}_{1S} + \underline{V}_{2AS} - p_1\underline{Z}_{2L1}\underline{I}_{2S} + \underline{V}_{0AS} - p_1\underline{Z}_{0L1}\underline{I}_{0S} = 3R_F\underline{I}_F, \tag{3.57}$$

$$\underline{V}_{1AS} + \underline{V}_{2AS} + \underline{V}_{0AS} - p_1\underline{Z}_{1L1}\underline{I}_{1S} - p_1\underline{Z}_{2L1}\underline{I}_{2S} - p_1\underline{Z}_{0L1}\underline{I}_{0S} = 3R_F\underline{I}_F\ , \tag{3.58}$$

$$\begin{aligned}\underline{V_{AS}} = &\quad p_1\underline{Z}_{1L1}\left(\underline{I}_{1S} + \underline{I}_{2S}\right) + p_1\underline{Z}_{0L1}p_1\underline{Z}_{0L1}\underline{I}_{0S} + 3R_F\underline{I}_F, \\ = &\quad p_1\underline{Z}_{1L1}\left(\underline{I}_{1S} + \underline{I}_{2S} + \underline{I}_{0S}\right) - p_1\underline{Z}_{1L1}\underline{I}_{0S} + p_1\underline{Z}_{0L1}\underline{I}_{0S} + 3R_F\underline{I}_F, \\ = &\quad p_1\underline{Z}_{1L1}\underline{I}_{AS} + \left(p_1\underline{Z}_{0L1} - p_1\underline{Z}_{1L1}\right)\underline{I}_{0S} + 3R_F\underline{I}_F,\end{aligned} \tag{3.59}$$

where

$$\underline{V_S} = \underline{V}_{1AS} + \underline{V}_{2AS} + \underline{V}_{0AS}, \tag{3.60}$$

$$\underline{I_S} = \underline{I}_{1S} + \underline{I}_{2S} + \underline{I}_{0S}. \tag{3.61}$$

Finally, the measured voltage in Equation (3.59) is written as:

$$\underline{V_S} = p_1\underline{Z}_{1L1}\left[\underline{I_S} + \frac{\underline{Z}_{0L1} + \underline{Z}_{1L1}}{\underline{Z}_{1L1}}\underline{I}_{0S}\right] + 3R_F\underline{I}_F, \tag{3.62a}$$

$$= p_1\underline{Z}_{1L1}\left[\underline{I_S} + \underline{k}_0\underline{I}_{0S}\right] + 3R_F\underline{I}_F, \tag{3.62b}$$

and the measured impedance for the fault at point F_1, in section 1, is:

$$\underline{Z}_m = \frac{\underline{V_S}}{\underline{I_S^C}} = p_1\underline{Z}_{1L1} + \Delta\underline{Z}_1, \tag{3.63}$$

where $\underline{V_S}$ is the voltage measured in phase A, and $\underline{I_S^C}$ is the current, $\underline{I_S}$, measured in phase A compensated with zero-sequence current, $\underline{I}_{0S}$, and is stated as:

$$\underline{I_S^C} = \underline{I_S} + \underline{k}_0\underline{I}_{0S}. \tag{3.64}$$

The zero-sequence compensation factor, $\underline{k}_0$, is defined as $\underline{k}_0 = \underline{Z}_{0L1} - \underline{Z}_{1L1}/\underline{Z}_{1L1}$.

It can be seen from the detailed analysis of Equation (3.63) that the error in the fault impedance measurement for phase-A to ground fault will depend on the following factors via a nonlinear function f:

$$\Delta \underline{Z}_{1L1} = f\left(\underline{\boldsymbol{P}}_{\boldsymbol{E}}, \underline{\boldsymbol{P}}_{\boldsymbol{S}}, \underline{\boldsymbol{P}}_{\boldsymbol{L}}, R_F, p_1\right), \tag{3.65}$$

where the factors are grouped in the following vectors:

$$\underline{\boldsymbol{P}}_{\boldsymbol{E}} = \left[\underline{E}_S\,, \underline{E}_R\,, \underline{E}_T\right]^T, \tag{3.66a}$$

$$\underline{\boldsymbol{P}}_{\boldsymbol{S}} = \left[\underline{Z}_{1S}\,, \underline{Z}_{1R}\,, \underline{Z}_{1T}\,, \underline{Z}_{0S}\,, \underline{Z}_{0R}\,, \underline{Z}_{0T}\right]^T, \tag{3.66b}$$

$$\underline{\boldsymbol{P}}_{\boldsymbol{L}} = \left[\underline{Z}_{1L1}\,, \underline{Z}_{1L2}, \underline{Z}_{1L3}\,, \underline{Z}_{0L1}\,, \underline{Z}_{0L2}, \underline{Z}_{0L3}\right]^T. \tag{3.66c}$$

A single line to ground fault (phase A) between tapped line and remote end (fault F_2 in Figure 3.14) is more complex due to the current from the tapped line. We use the circuit diagram in Figure 3.16 to show the sequence component networks in order to specify the factors that will impact the impedance measurement. The sum of the sequence component voltages at the fault point, F_2, during phase A to ground fault obtained from the circuit in Figure 3.16, is the same as in Equation (3.56):

$$\underline{V}_1' + \underline{V}_2' + \underline{V}_0' = 3R_F\underline{I}_F. \tag{3.67}$$

The sequence voltages involved in Equation (3.67) can be found in terms of the sequence component voltage and current at the S-side of the line, leading to the following relations:

$$\underline{V}_1' = \underline{V}_{1AS} - \underline{Z}_{1L1}\underline{I}_{1S} - p_2\underline{Z}_{1L2}\left(\underline{I}_{1S} + \underline{I}_{1T}\right), \tag{3.68a}$$

$$\underline{V}_2' = \underline{V}_{2AS} - \underline{Z}_{2L1}\underline{I}_{2S} - p_2\underline{Z}_{2L2}\left(\underline{I}_{2S} + \underline{I}_{2T}\right), \tag{3.68b}$$

$$\underline{V}_0' = \underline{V}_{0AS} - \underline{Z}_{0L1}\underline{I}_{0S} - p_2\underline{Z}_{0L2}\left(\underline{I}_{0S} + \underline{I}_{0T}\right). \tag{3.68c}$$

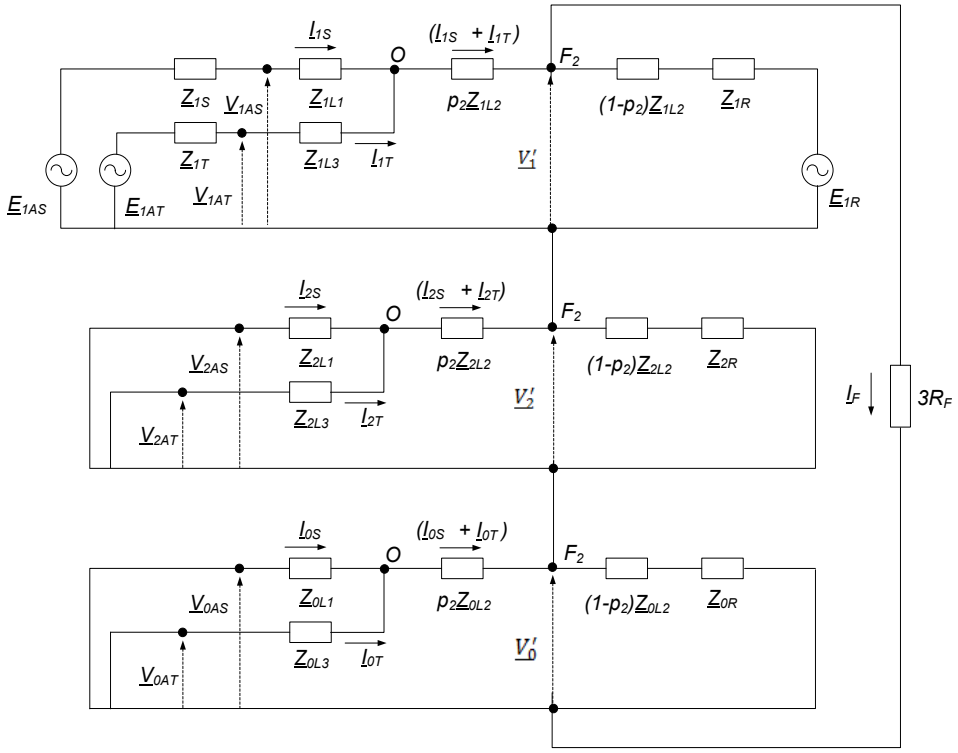

Figure 3.16: Sequence component circuit for the fault at F_2 in Fig 3.14.

Using the expression in Equation (3.68a,b,c), $\underline{Z}_{1L1} = \underline{Z}_{2L1}$, and $\underline{Z}_{1L3} = \underline{Z}_{2L3}$, we can find the measured voltage in phase A at the relay point:

$$\underline{V}_{1AS} - \underline{Z}_{1L1}\underline{I}_{1S} - p_2\underline{Z}_{1L2}\left(\underline{I}_{1S} + \underline{I}_{1T}\right) + \underline{V}_{2AS} - \underline{Z}_{2L1}\underline{I}_{2S} - p_2\underline{Z}_{2L2}\left(\underline{I}_{2S} + \underline{I}_{2T}\right) + \cdots$$

$$\underline{V}_{0AS} - \underline{Z}_{0L1}\underline{I}_{0S} - p_2\underline{Z}_{0L2}\left(\underline{I}_{0S} + \underline{I}_{0T}\right) = 3R_F\underline{I}_F, \tag{3.69}$$

$$\underline{V}_{1AS} + \underline{V}_{2AS} + \underline{V}_{2AS} - \underline{Z}_{1L1}\underline{I}_{1S} - \underline{Z}_{2L1}\underline{I}_{2S} - \underline{Z}_{0L1}\underline{I}_{0S} - p_2\underline{Z}_{1L2}\underline{I}_{1S} - p_2\underline{Z}_{1L2}\underline{I}_{1T} - \ \ldots$$

$$p_2\underline{Z}_{2L2}\underline{I}_{2S} - p_2\underline{Z}_{2L2}\underline{I}_{2T} - p_2\underline{Z}_{0L2}\,\underline{I}_{0S} - p_2\underline{Z}_{0L2}\underline{I}_{0T} = 3R_F\underline{I}_F, \tag{3.70}$$

$$\underline{V}_S = \underline{Z}_{1L1}\left(\underline{I}_{1S} + \underline{I}_{2S}\right) + \underline{Z}_{0L1}\underline{I}_{0S} + p_2\underline{Z}_{1L2}\left(\underline{I}_{1S} + \underline{I}_{1T}\right) + p_2\underline{Z}_{2L2}\left(\underline{I}_{2S} + \underline{I}_{2T}\right) + \ \ldots$$

$$p_2\underline{Z}_{0L2}\left(\underline{I}_{0S} + \underline{I}_{0T}\right) + 3R_F\underline{I}_F, \tag{3.71}$$

$$= \underline{Z}_{1L1}\left(\underline{I}_{1S} + \underline{I}_{2S} + \underline{I}_{0S}\right) + \left(\underline{Z}_{0L1} - \underline{Z}_{1L1}\right)\underline{I}_{0S} + p_2\underline{Z}_{1L2}\Big(\left(\underline{I}_{1S} + \underline{I}_{1T}\right) + \ \ldots$$

$$\left(\underline{I}_{2S} + \underline{I}_{2T}\right) + \left(\underline{I}_{0S} + \underline{I}_{0T}\right)\Big) + \left(p_2\underline{Z}_{0L2} - p_2\underline{Z}_{1L2}\right)\left(\underline{I}_{0S} + \underline{I}_{0T}\right) + \ 3R_F\underline{I}_F,$$

$$\underline{V}_S = \underline{Z}_{1L1}\underline{I}_S + \left(\underline{Z}_{0L1} - \underline{Z}_{1L1}\right)\underline{I}_{0S} + p_2\underline{Z}_{1L2}\left(\underline{I}_{1ST} + \underline{I}_{2ST} + \underline{I}_{0ST}\right) + \ \ldots$$

$$\left(p_2\underline{Z}_{0L2} - p_2\underline{Z}_{1L2}\right)\underline{I}_{0ST} + 3R_F\underline{I}_F,$$

where

$$\underline{V}_S = \underline{V}_{1AS} + \underline{V}_{2AS} + \underline{V}_{2AS} \;;\; \underline{I}_S = \underline{I}_{1S} + \underline{I}_{2S} + \underline{I}_{0S} \;;\; \underline{I}_{1ST} = \underline{I}_{1S} + \underline{I}_{1T},$$
$$\underline{I}_{2ST} = \underline{I}_{2S} + \underline{I}_{2T} \;;\; \underline{I}_{0ST} = \underline{I}_{0S} + \underline{I}_{0T} \;;\; \underline{I}_{ST} = \underline{I}_{1ST} + \underline{I}_{2ST} + \underline{I}_{0ST}. \tag{3.72}$$

Finally, the measured voltage is written as:

$$\underline{V}_S = \underline{Z}_{1L1}\left(\underline{I}_S + \frac{\underline{Z}_{0L1} - \underline{Z}_{1L1}}{\underline{Z}_{1L1}}\underline{I}_{0S}\right) + p_2\underline{Z}_{1L2}\left(\underline{I}_{ST} + \frac{p_2\underline{Z}_{0L2} - p_2\underline{Z}_{1L2}}{p_2\underline{Z}_{1L2}}\underline{I}_{0ST}\right) + 3R_F\underline{I}_F,$$

$$\underline{V}_S = \underline{Z}_{1L1}\underline{I}_S^c + p_2\underline{Z}_{1L2}\underline{I}_S'^c + 3R_F\underline{I}_F, \tag{3.73}$$

and the measured impedance for the fault at point F_2 in section 2 is:

$$\underline{Z}'_m = \frac{\underline{V}_S}{\underline{I}_S^c} = \underline{Z}_{1L1} + p_2\underline{Z}_{1L2}\frac{\underline{I}_S'^c}{\underline{I}_S^c} + 3R_F\underline{I}_F\frac{I_F}{\underline{I}_S^c},$$

$$= \underline{Z}_{1L1} + p_2\underline{Z}_{1L2} + \Delta\underline{Z}_{1L2}. \tag{3.74}$$

In addition to the measured compensated current, in Equation (3.64), we also have in Equation (3.74), the effect of the unmeasured current:

$$\underline{I}_S'^c = \underline{I}_{ST} + k'_0\underline{I}_{0ST}, \tag{3.75}$$

$$\underline{k}'_0 = \frac{p_2\underline{Z}_{0L2} - p_2\underline{Z}_{1L2}}{p_2\underline{Z}_{1L2}}. \tag{3.76}$$

Where $\underline{k}'_0$, in Equation (3.76), is the compensation factor for the second line segment. By further elaborating Equation (3.74), we can define which parameters will impact the measurement error:

$$\Delta\underline{Z}_{1L2} = f\left(\underline{\boldsymbol{P}}_{\boldsymbol{E}}, \underline{\boldsymbol{P}}_{\boldsymbol{S}}, \underline{\boldsymbol{P}}_{\boldsymbol{L}}, R_F, p_2\right), \tag{3.77}$$

where the factors are grouped in the following vectors:

$$\underline{\boldsymbol{P}}_{\boldsymbol{E}} = \left[\underline{E}_S, \underline{E}_R, \underline{E}_T\right]^T, \tag{3.78a}$$

$$\underline{\boldsymbol{P}}_{\boldsymbol{S}} = \left[\underline{Z}_{1S}, \underline{Z}_{1R}, \underline{Z}_{1T}, \underline{Z}_{0S}, \underline{Z}_{0R}, \underline{Z}_{0T}\right]^T, \tag{3.78b}$$

$$\underline{\boldsymbol{P}}_{\boldsymbol{L}} = \left[\underline{Z}_{1L1}, \underline{Z}_{1L2}, \underline{Z}_{1L3}, \underline{Z}_{0L1}, \underline{Z}_{0L2}, \underline{Z}_{0L3}\right]^T. \tag{3.78c}$$

3.4.4. Fault Impedance Measurement for One Line with Series Capacitor

In order to determine the effect of uncertain factors on the fault impedance measurement algorithm with series compensation, we use a faulted two terminal series compensated line and an IED as shown in Figure 3.17. The schematic is modelled using Thevenin's equivalent which has two sources, $\underline{E}_S$, and $\underline{E}_R$, and with corresponding $\underline{Z}_S$, $\underline{Z}_R$. Phase A to ground faults are simulated in different locations, F_1, and F_2, through a fault resistance, R_F. This line fault, for the fault behind the series capacitor located at F_2, is too complex to be protected by a one-ended distance relay since the effect of the series capacitor located in the middle of the line will effect the fault impedance calculation [28].

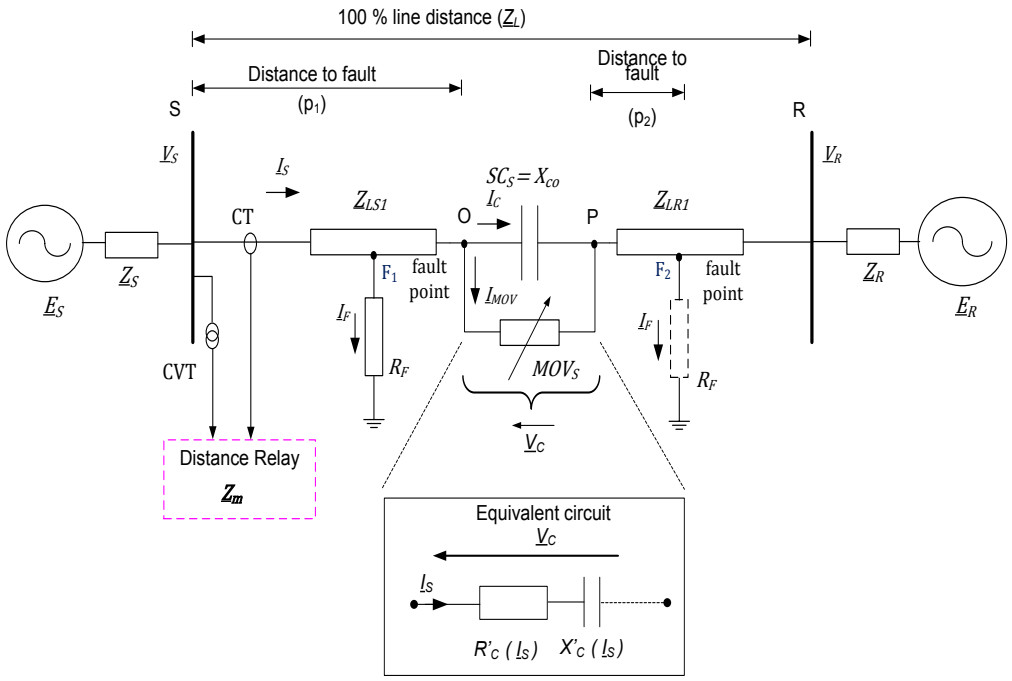

Figure 3.17: Single line diagram for the phase A to ground fault on a transmission line with series compensator: F_1 - fault location in front of SCs, F_2 - fault location behind SCs.

In Figure 3.17, $\underline{V_C}$ is the voltage drop across the parallel connection between the capacitor bank reactance, X_{CO}, and MOVs. The fundamental frequency equivalent is represented with series resistance, R'_C, and the reactance X'_C in Figure 3.17. Both dependend on the current flowing through, $\underline{I_S}$ [67, 68]. Figure 3.18 plots the equivalent resistance and reactance, which is affected by $\underline{I_S}$, using the range of circuit parameters as in [67]. Per unit, P.U., is the ratio between equivalent resistance, R'_C, and reactance, X'_C, to the series capacitor reactance, X_{CO}, respectively, while $\underline{I_{PU}}$ is the per unit value of current, $\underline{I_S}$, with respect to the level of capacitor protective current, $\underline{I_{PR}}$, and is stated as [67]:

$$\underline{I_{PU}} = \frac{\underline{I_S}}{\underline{I_{PR}}} . \tag{3.79}$$

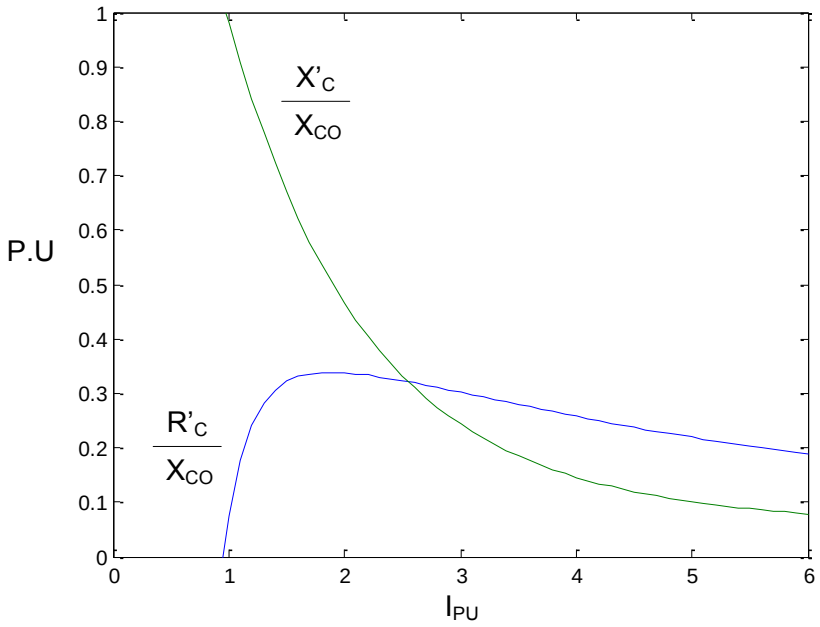

Figure 3.18: Normalized equivalent resistance and reactance vs normalized current

Equations (3.80a,b) are generated via the least-sequares, using data from Figure 3.18, to fit the equivalent values of R'_C, and X'_C, for $\underline{I_{PU}} > 0.98$ [67]:

$$R'_C = X_{CO}\left(0.0745 + 0.49\exp\left(-0.243\underline{I_{PU}}\right) - 35\exp\left(-5\underline{I_{PU}}\right) \ldots \right. \tag{3.80a}$$
$$\left. - 0.6\exp\left(-1.4\underline{I_{PU}}\right)\right)$$

$$X'_C = X_{CO}\left(0.1010 - 0.005749\underline{I}_{PU} + 2.088\exp\left(-0.8566\underline{I}_{PU}\right)\right). \quad (3.80b)$$

The nominal capacitor bank reactance, $X_{CO,}$ and per unit current, $\underline{I}_{PU}$, as defined in Equations (3.80a,b), are the only data required to define the equivalent impedance component of X_C, and R_C.

In the case of a fault at F_1 (fault in the front of SCs), the fault impedance, $\underline{Z}_m^S$, measured at the relaying point, is similar to a fault in an uncompensated line [1]. The procedure for fault impedance calculation is developed for simple two ended sources, without a series compensator. For the fault at F_2 (fault behind SCs), the error analysis should be done since the presence of SCs, as shown in Figure 3.17, will influence the fault impedance calculation. Consequently, the fault impedance, $\underline{Z}_m^R$, measured at the relaying point to F_2 (distance $= p_1 + p_2$) is not always the actual impedance, $\underline{Z}_{1LS} + p_2\underline{Z}_{1LR}$.

A single line to ground fault (phase A) between the series compensator and remote end (fault F_2 in Figure 3.17) is more complicated and so we use the circuit diagram in Figure 3.19, which shows the sequence component networks, to specify which factors will impact the impedance measurement, $\underline{Z}_m^R$. The sum of the sequence component voltages at the fault point, F_2, during a single line to ground fault obtained from the circuit in Figure 3.19 is [69]:

$$\underline{V}_1 + \underline{V}_2 + \underline{V}_0 = 3R_F\underline{I}_F. \quad (3.81)$$

The sequence voltages involved in Equation (3.81) can be determined in terms of the sequence component voltage and current at the S-side of line, leading to the following relation:

$$\underline{V}_1 = \underline{V}_{1AS} - \underline{Z}_{1LS}\underline{I}_{1S} - \underline{V}_{1C} - p_2\underline{Z}_{1LR}\underline{I}_{1S}, \quad (3.82a)$$

$$\underline{V}_2 = \underline{V}_{2AS} - \underline{Z}_{2LS}\underline{I}_{2S} - \underline{V}_{2C} - p_2\underline{Z}_{2LR}\underline{I}_{2S}, \quad (3.82b)$$

$$\underline{V}_0 = \underline{V}_{0AS} - \underline{Z}_{0LS}\underline{I}_{0S} - \underline{V}_{0C} - p_2\underline{Z}_{0LR}\underline{I}_{0S}, \quad (3.82c)$$

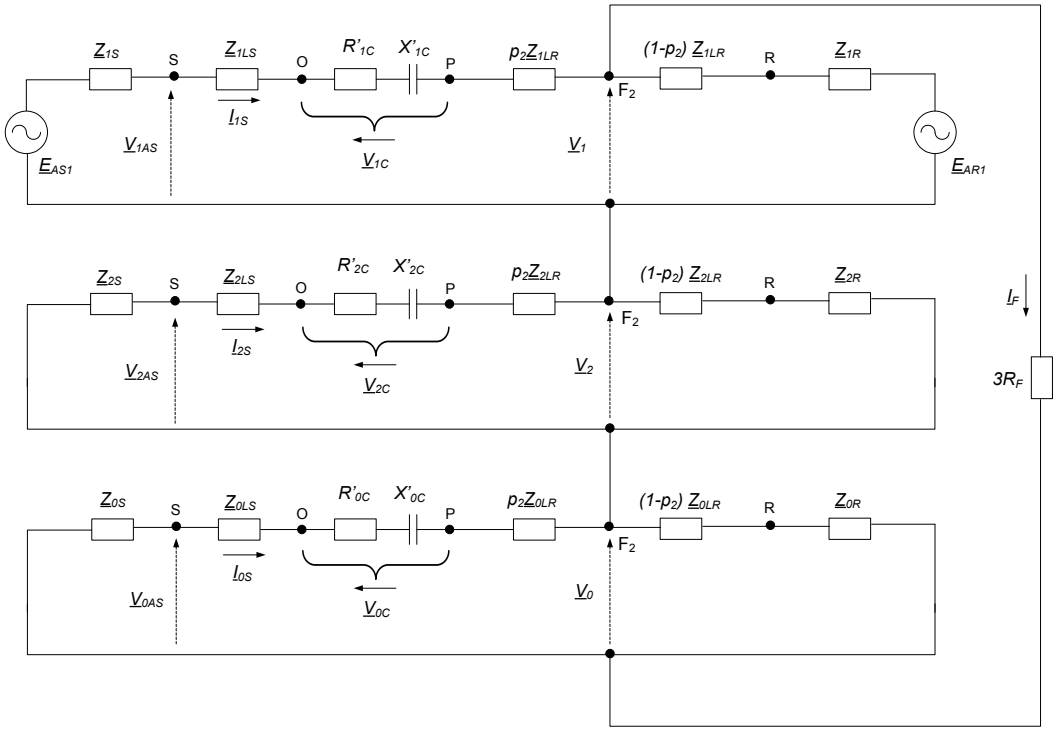

Figure 3.19: Two-Source Symmetrical Component for AG fault at F_2 with fault resistance.

Using the expression in Equations (3.82a, b, c), and assuming that $\underline{Z}_{1LS} = \underline{Z}_{2LS}$, and $\underline{Z}_{1LR} = \underline{Z}_{2LR}$, we can determine the measured voltage in phase A at the relay point:

$$\underline{V}_{1AS} - \underline{Z}_{1LS}\underline{I}_{1S} - \underline{V}_{1C} - p_2\underline{Z}_{1LR}\underline{I}_{1S} + \underline{V}_{2AS} - \underline{Z}_{2LS}\underline{I}_{2S} - \underline{V}_{2C} - p_2\underline{Z}_{2LR}\underline{I}_{2S} + \ \ldots$$

$$\underline{V}_{0AS} - \ \underline{Z}_{0LS}\underline{I}_{0S} - \underline{V}_{0C} - p_2\underline{Z}_{0LR}\underline{I}_{0S} \ = 3R_F\underline{I}_F, \tag{3.83}$$

$$\underline{V}_{1AS} + \underline{V}_{2AS} + \underline{V}_{0AS} - \underline{V}_{1C} - \underline{V}_{2C} - \underline{V}_{0C} - \left(\underline{Z}_{1LS} + \ p_2\underline{Z}_{1LR}\right)\underline{I}_{1S} - \ \ldots$$

$$\left(\underline{Z}_{2LS} + \ p_2\underline{Z}_{2LR}\right)\underline{I}_{2S} - \left(\underline{Z}_{0LS} + \ p_2\underline{Z}_{0LR}\right)\underline{I}_{0S} = 3R_F\underline{I}_F. \tag{3.84}$$

Finally, the measured voltage is written as:

$$\underline{V}_S = \underline{V}_C + \underline{Z}_{1LSR}\left[\underline{I}_S + \frac{\underline{Z}_{0LSR} - \underline{Z}_{1LSR}}{\underline{Z}_{1LSR}}\underline{I}_{0S}\right] + 3R_F\underline{I}_F, \tag{3.85}$$

$$\underline{V}_S = \underline{V}_C + \underline{Z}_{1LSR}\left[\underline{I}_S + \underline{k}_0\underline{I}_{0S}\right] + 3R_F\underline{I}_F,$$

$$= \underline{Z}_{1LSR}\underline{I}_S^C + 3R_F\underline{I}_F + \underline{V}_C,$$

where

$$\underline{V_S} = \underline{V_{1AS}} + \underline{V_{2AS}} + \underline{V_{0AS}} \;;\; \underline{V_C} = \underline{V_{1C}} + \underline{V_{2C}} + \underline{V_{0C}} \;;\; \underline{I_S} = \underline{I_{1S}} + \underline{I_{2S}} + \underline{I_{0S}},$$
$$\underline{Z_{1LSR}} = \underline{Z_{1LS}} + p_2\underline{Z_{1LR}} \;;\; \underline{Z_{2LSR}} = \underline{Z_{2LS}} + p_2\underline{Z_{2LR}} \;;\; \underline{Z_{0LSR}} = \underline{Z_{0LS}} + p_2\underline{Z_{0LR}}, \tag{3.86}$$

p_2 is the distance from the point O to the fault point F_2, and the measured impedance for the fault at point F_2 behind series capacitor is:

$$\underline{Z_m^R} = \frac{\underline{V_S}}{\underline{I_S^C}} = \underline{Z_{1LSR}} + \frac{3R_F\underline{I_F} + \underline{V_C}}{\underline{I_S^C}}, \tag{3.87}$$
$$= \underline{Z_{LSR1}} + \Delta\underline{Z_{LSR1}},$$

where $\underline{V_{AS}}$ is the voltage measured in phase A to ground, and $\underline{I_S^C}$ is the current, $\underline{I_{AS}}$, measured in phase A compensated with zero-sequence current, $\underline{I_{0S}}$, and is stated as:

$$\underline{I_S^C} = \underline{I_S} + \underline{k}_0\underline{I_{0S}}. \tag{3.88}$$

The zero-sequence compensation factor, $\underline{k}_0$, in Equation (3.85), is defined as,

$$\underline{k}_0 = \frac{\underline{Z_{0LSR}} - \underline{Z_{1LSR}}}{\underline{Z_{1LSR}}}. \tag{3.89}$$

It can be seen from a detailed analysis of Equation (3.87) that the error in the fault impedance measurement for phase A to ground fault behind SCs + MOVs will depend on the following factors via a nonlinear function f:

$$\Delta\underline{Z_{LSR1}} = f\left(\underline{\boldsymbol{P_E}}, \underline{\boldsymbol{P_S}}, \underline{\boldsymbol{P_L}}, R_F, p, X_{CO}\right), \tag{3.90}$$

where the factors are grouped in the following vectors:

$$\underline{\boldsymbol{P_E}} = \left[\underline{E_S}\,, \underline{E_R}\,\right]^T, \tag{3.91a}$$

$$\underline{\boldsymbol{P_S}} = \left[\underline{Z_{1S}}\,, \underline{Z_{1R}}\,, \underline{Z_{0S}}\,, \underline{Z_{0R}}\,\right]^T, \tag{3.91b}$$

$$\underline{\boldsymbol{P_L}} = \left[\underline{Z_{1LS}}, \underline{Z_{1LR}}, \underline{Z_{0LS}}\,, \underline{Z_{0LR}}\,\right]^T. \tag{3.91c}$$

Chapter 4

Sensitivity Analysis for Impedance Measurement Algorithm of Distance Relay

4.1. Introduction

A sensitivity analysis (SA) is a tool aimed at revealing the dependency of the model output, y, on the set of model input, $\boldsymbol{x}$. This is one of the accepted alternative methods for analyzing the nonlinear function $f(\boldsymbol{x})$, and has been used in this thesis. In the analysis, $f(\boldsymbol{x})$ is assumed to be a black box function where k is a dimension of input factors $\boldsymbol{x} = (x_1, x_2, \dots x_k)$, and a single output value y:

$$y = y(\boldsymbol{x}) = f(x_1, x_2, \dots x_k). \tag{4.1}$$

The classical approach, using the local sensitivity analysis method, has also been applied in this analysis. The local method, which requires much fewer samples, is based on varying one factor at a time while the other factors are kept constant at their nominal values. However, this local method of analysis is not practical as the multidimensional factor

space, which requires a large number of samples, is analysed simultaneously using the global sensitivity method.

The objective of SA testing of the IED is to measure the dependency of the relay algorithm to the input factors. To study the performance of the model, DIgSILENT PowerFactory is used in this work.

4.2. Sensitivity Analysis Techniques

Performance of the impedance measurement algorithm is quantified via the performance index, and is defined as the absolute difference between the true value and the estimated value as defined in Equation (2.24). This measure is a nonlinear function of uncertain factors and is denoted as $f(\boldsymbol{x})$. In a sampling based technique all factors are varied simultaneously, within their respective intervals of variation based on either pseudo-random or quasi-random sequence. This multidimensional factor space requires a large number of samples and is therefore not practical. The classical approach, which requires much fewer samples, is based on varying one factor at a time while the other factors are kept constant at their nominal values. This approach can be used to rank factors according to their importance but it is not suitable for complete uncertainty and sensitivity analysis. Therefore, a hybrid approach is used where the most influential factors are identified via the local sensitivity method. This reduces the dimension of the factor space so that the global approach, based on sampling, will work with practically achievable number of samples.

Assessing the impact of these factors enables measuring of the sensitivity of the model in calculating the apparent fault impedance, $\underline{Z}_m$. For this purpose, some techniques for sensitivity analysis, as described above for local and global sensitivity analysis, are applied to the models. Two groups of sensitivity analysis using Morris [70] and variance-based Monte-Carlo methods are described in the following subsection.

4.2.1. Morris Method

The local method we use in the project is known as the Morris method. It is a unique randomized scheme that varies one factor at a time. The index used by the Morris method

is called the 'elementary effect', and is used to rank factors. For each factor, i, it is computed by varying this factor only [16] as described in Equation (4.2) below:

$$E_i = \frac{1}{\Delta}[\, f(x_1, x_2, \dots, x_i + \Delta, \dots, x_n) - f(x_1, x_2, \dots, x_i, \dots, x_n)\,]. \tag{4.2}$$

where $\Delta = d/2(d-1)$ is the pre-determined variation of the i^{th} factor, and d is the number of discretization grid levels. The selection of the factor to change is random. For each factor variation, the fault impedance, Z_m, is estimated, and the performance index of model output, $f(\boldsymbol{x})$, and the elementary effect, Equation (4.2), are calculated where $\boldsymbol{x} = (x_1, x_2, \dots, x_i, \dots, x_n)$ is a selected n-dimension of random parameter values in the unit hypercube of Ω. For a number of random variations the computation of statistics using mean, μ, and standard deviation, σ, are calculated and used to measure relative importance of all parameters. A high mean indicates that the total effect of a parameter is important and a high standard deviation means that a parameter impact is produced through interaction with other parameters.

4.2.2. Variance Based Sensitivity using Sobol Method

The GSA with QMC (i.e., use of quasi-random sampling) is well suited for small dimension factor spaces [1]. After reducing the dimension of the original factor space using the Morris method, the sensitivity analysis procedure can proceed with the GSA based on sampling. Uncertainty of the performance index, $f(\boldsymbol{x})$, is measured using variance. To assess the importance of a factor, x_i, we can use the part of the performance index variance that is contributed by uncertainty of this factor. This is calculated by taking the average over all sampled parameter variations, except x_i, which is kept fixed for single calculations. By repeating this computation for different fixed values of x_i we can compute variance over x_i as shown in Equation (4.3). This measure can be indicated as the imporantance effect of x_i on output variance y, or the sensitivity of model output y to input factor x_i ,

$$V_i = V\{E\{f(\mathbf{x})|x_i\}\}. \tag{4.3}$$

The required expectation operator, $E\{*\}$, is computed by solving the corresponding multidimensional integral using the QMC approach with Sobol's quasi random sequences as shown in Equation (4.8).

In real conditions, we do not know the exact value of x_i, hence the expectation value of output variance for possible value $\boldsymbol{x}$ to input factor x_i is $E\{V(f(\boldsymbol{x})|x_i)\}$. In Equation (4.3), the total variance, $V(f(\boldsymbol{x}))$, as the performance index is calculated with numerical integration using QMC and is performed as follows:

$$V\big(f(\mathbf{x})\big) = V\big\{E\{f(\mathbf{x})|x_i\}\big\} + E\{V(f(\mathbf{x})|x_i)\}. \tag{4.4}$$

From Equation (4.3) and Equation (4.4), the global sensitivity measure that describes the main effect of a parameter, x_i, on the performance index, $f(\boldsymbol{x})$, is defined as:

$$S_i = \frac{V\big\{E\{f(\boldsymbol{x})|x_i\}\big\}}{V\big(f(\boldsymbol{x})\big)}. \tag{4.5}$$

We can name Equation (4.5) as the first order of the sensitivity indices [71]. If the sum of all S_i do not sum to one, the performance index variance, $V\big(f(\boldsymbol{x})\big)$, is not only described by individual effects of parameters but also by their interactions. The interaction effect of two independent factors, x_i and x_j, can be defined as the conditional variance:

$$V_{ij} = V\Big\{E\big\{f(\boldsymbol{x})\big|x_i, x_j\big\}\Big\} - V\big\{E\{f(\boldsymbol{x})|x_i\}\big\} - V\Big\{E\big\{f(\boldsymbol{x})\big|x_j\big\}\Big\}, \tag{4.6}$$

where $V\Big\{E\big\{f(\mathbf{x})\big|x_i, x_j\big\}\Big\}$ describes the interaction effect between x_i, and x_j, on the output model y. This interaction effect, shown in Equation (4.6), is named the secondary-order effect, and the same procedure could be developed for a higher-order effect (i.e., $n \geq 3$). Finally, for n significant parameters, the total performance index variance can be decomposed as shown in [16], the so-called Analysis of Variance (ANOVA) decomposition:

$$V\big(f(\boldsymbol{x})\big) = \sum_{\mathrm{i}=1}^{\mathrm{n}} V_i + \sum_{i=1}^{n-1}\sum_{j=i+1}^{n} V_{ij} + \cdots + V_{1,2,\cdots,n}. \tag{4.7}$$

In Sobol's technique, the expected value of model output, $E\{f(\mathbf{x})\}$, in Equation (4.3) is calculated as an n- multidimensional integral:

$$E\{f(\boldsymbol{x})\} = \int_{\Omega^n} f(\boldsymbol{x})p(\boldsymbol{x})d\boldsymbol{x} = \int_{\Omega^n} f(\boldsymbol{x})d\boldsymbol{x}, \tag{4.8}$$

where $p(\boldsymbol{x}) \equiv 1$ (i.e., joint probability density function, $\boldsymbol{x} = (x_1, x_2, \dots, x_i, \dots, x_n)$ assumed uniform). Using ANOVA decomposition, the model function, $f(\boldsymbol{x})$, could be:

$$f(\boldsymbol{x}) = f_0 + \sum_{\mathrm{i}=1}^{\mathrm{n}} f_i(x_i) + \sum_{i=1}^{n-1}\sum_{j=i+1}^{n} f_{ij}(x_i, x_j) + \cdots + f_{1,2,\cdots,n}(x_1, x_2, \dots, x_i, \dots, x_n), \tag{4.9}$$

where the expected value of model output, $E\{f(\boldsymbol{x})\} = f_0$, is equal to Equation (4.8).
Total variance in Equation (4.4) is rewritten as:

$$V\big(f(\mathbf{x})\big) = \int_{\Omega^n} f^2(\mathbf{x})d\boldsymbol{x} - {f_0}^2, \tag{4.10}$$

while the variances of Equation (4.9) are derived as follows:

$$V_i\big(f(\mathbf{x})\big) = \int_{\Omega^n} f^2(\mathbf{x})d\boldsymbol{x}_{\sim \boldsymbol{i}} - {f_0}^2\,, \tag{4.11}$$

$$V_{ij}\big(f(\mathbf{x})\big) = \int_{\Omega^n} f^2(\mathbf{x})d\boldsymbol{x}_{\sim (\boldsymbol{ij})} - {f_0}^2 - V_i\big(f(\mathbf{x})\big) - V_j\big(f(\mathbf{x})\big)\,. \tag{4.12}$$

4.3. SIMLAB Tool for Sensitivity Analysis

SIMLAB is a multi-purpose software designed for statistical calculation and sensitivity analysis [72, 73]. It contains the features required for the sensitivity analysis of the external model, such as the protective relay model. This sensitivity analysis tool includes a graphical user interface (GUI) for facilitating the different methods of sensitivity analysis, such as the Morris method, and Sobol's technique.

The main window, shown in Figure 4.1, is the starting point of the tool box. The following three sections provide the functions required for the statistical analysis of the relay model [72]. The functions are:

1. Pre-processing module: this module covers the steps required for selecting a range and distribution of parameter inputs. The module also includes the steps required for generating sequence samples of the selected parameter inputs.

2. The execution module: this module executes a set of external model outputs of the impedance relay algorithm and the sample elements. The evaluation process involves mapping the input space to the space of the result, which is required for the next step of the sensitivity analysis.
3. Post-processor module: this module is for the sensitivity analysis.

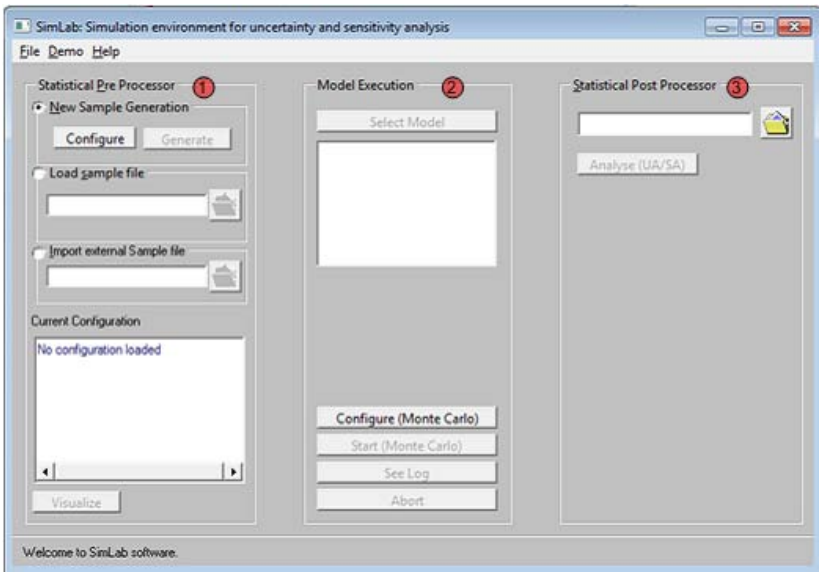

Figure 4.1: Main window of SIMLAB.

Sample Generation

In this work, SIMLAB is used to generate a number of sampled data which is used to study the characteristic of the investigated model. To use this software for the purpose of the sensitivity analysis, we need to generate the input factors using the pre-processing windows shown in Figure 4.2. Several steps to generate a sample of data are demonstrated as follows: 1) Selecting input factors and ranges of their values and distributions (probability distribution functions, or pdfs). 2) Selecting a sampling method among those available such as Morris and Sobol; 3) Generating the actual sample from the input pdfs.

The two different methods for obtaining sampled data, such as Morris and Sobol, are going to be used to investigate the performance of the distance relay model output. These methods are used for different purposes of investigating the relay algorithm output of IED.

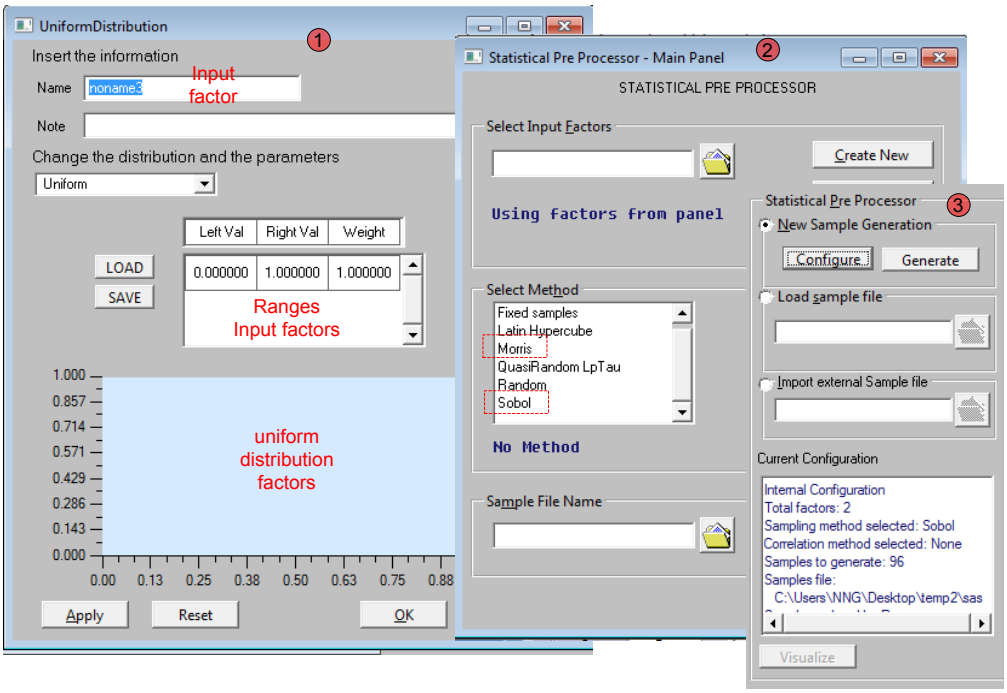

Figure 4.2: Pre-processing frame.

The Morris sample method is used to determine the factors which mostly impact the protective relay model [71, 72]. Pseudo random samples of the desired dimension are generated from the independent input variables. An iteration function is used for generating a random number where user defined starting points. Figure 4.3 shows the following steps used to generate samples of data using the Morris method: 1) Select the advised number value of the seed ≥ 7 digits; 2) Select a number of executions based on the provided list number; 3) Select the number of levels based on the provided list number.

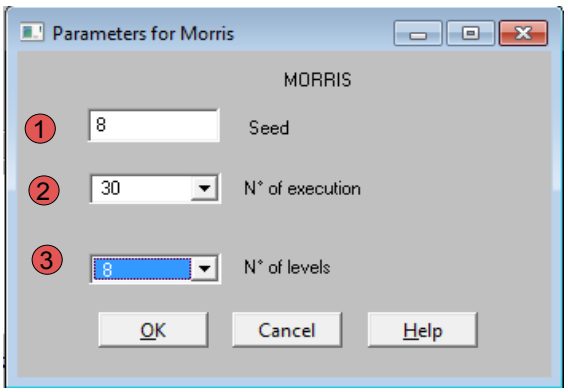

Figure 4.3: Morris Sampling Method.

For variance-based analysis using Sobol's technique, the sampled data is generated using the following steps in Figure 4.4: 1) We select Custom order calculation, since we need to configure the calculation indices; 2) Maximum order of the indices is calculated when the custom option is selected; 3) Select sample size.

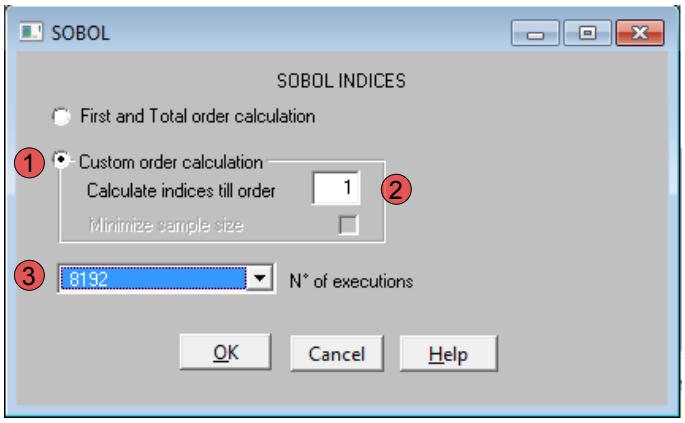

Figure 4.4: Sobol Method Panel.

As shown in Figure 4.2, the last step of the statistical pre-processor is the sample generation. The *Generate* button is used to run the generated samples in which two different methods, such as Morris and Sobol, are applied. Two different formats of the generated sample outputs are saved (*.sam file). The next step of model execution uses two different methods, Morris and Sobol, for the two sampled data evaluation of the external model distance relay algorithm, and is presented in the following section.

External Model Execution

The external model is used since the complex model could not be feasibly executed in the sensitivity analysis software package. The external model of power system fault scenarios, which is implemented in this work, is created in the power system simulator DIgSILENT. To calculate the performance of the model based on the uncertainty values of parameter inputs, sampled parameter data, which are generated using the sensitivity analysis tool, are used in the model. The algorithm for automatic change of parameters and execution is required in this task. The results of performance indices of the model output are then saved for model analysis in the sensitivity analysis tool.

Conceptually, this task is simple. Each element of samples, $x_i = [x_{i1} \dots x_{ik}]$, where $i = 1, \dots, N$, k is the number of independent factors, and N is the sample size, are supplied to the IED and network model in the power system simulator tool as inputs. The performance index is then evaluated as $y_i = f[x_{i1} \dots x_{ik}] = f(\boldsymbol{x}_i)$, where $i = 1, \dots, N$, and is saved for use in model results analysis. The proces of reading a file, fault simulation and producing an output file with performance indices is controlled by an algorithm developed as a DPL script in order to automate the task.

Figure 4.5 shows the steps using the SIMLAB software package required for external model output execution. The following steps are required: Step 1) feed sample elements which are generated in the pre-processor step; Step 2) feed the saved model output (i.e., performance indices of the distance relay algorithm), which is generated in DIgSILENT, through mechanisms using the DPL script program; Step 3) Start button is pressed for the model execution.

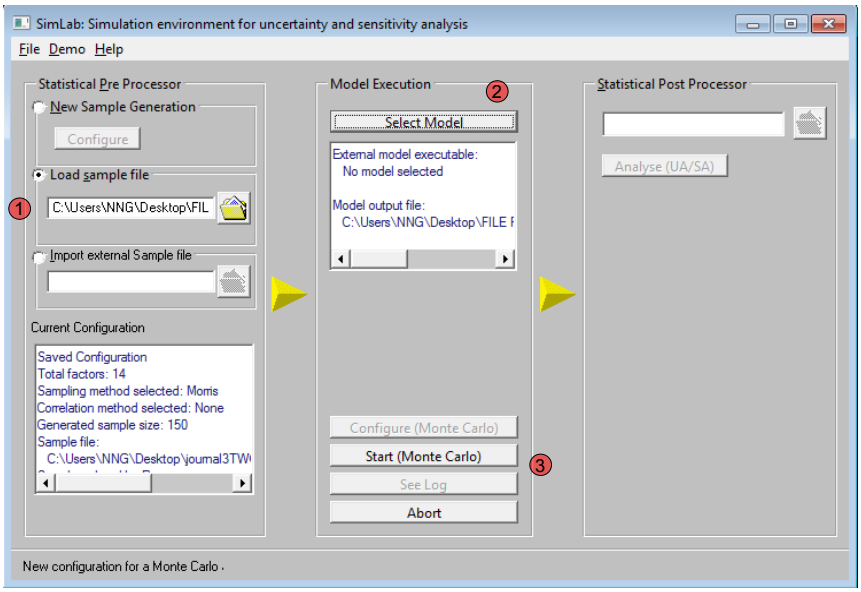

Figure 4.5: Model execution.

Model Result Analysis

In this step, we apply a statistical post processor to perform a sensitivity analysis of the model outcomes (i.e., fault impedance measurement). The purpose of this sensitivity analysis is to determine the impact of the uncertainties of input factors on the algorithm performance, and the variability of model output.

The ‘error’ of the output, when transients initiated by a fault dissaprear, is calculated in steady state. This value is the performance indices of model output are calculated using the DPL script in DIgSILENT. In last step, the sensitivity indices of model output, which are influenced by main factors and interaction between them, can be calculated, as shown in Figure 4.6.

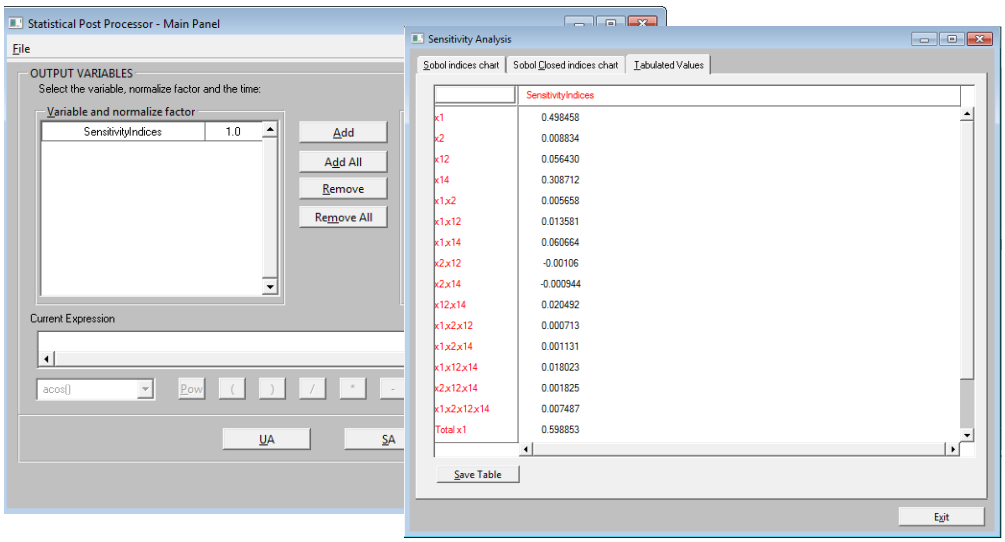

Figure 4.6: Statistical Post-Processor.

Chapter 5

A Proposed Methodology

5.1. Introduction

The relay plays an important role for protecting a power system during a fault. It is designed to detect faults and make decisions locally to isolate faulted power system components from the rest of the system. The correct operation of a protective relay will clear the fault, as well as reduce or eliminate the impact of a disturbance on a power system. On the contrary, unintended or incorrect operation may further deteriorate the system conditions and even jeopardize the stability of the entire system.

Appropriate relay testing helps validate the design of the relay logic, verify the selection of the relay settings, identify vulnerable conditions that cause unintended operation, and carry out fault analysis for understanding unintended or incorrect relay behaviour. The challenge for testing, evaluation tasks, and related methodology, lies in the implementation of large numbers of test and evaluation cases. This requires methods for accurately modelling the power system used for tests, easy simulation of disturbances, facilitating interfacing relays and power system models, automatically executing batch

tests, and collecting relay response events. Testing methods should not only accurately calculate fault impedance but also measure the sensitivity of uncertainty factors during fault conditions.

Studies of fault impedance calculation algorithms and characteristics are based on the use of software for modelling protective relays and power systems. Interfacing digital protective relay models to the power network model allows scenarios to be tested. Since protective relays are modelled with an advanced programming language, the simulation to study the relay algorithm performance is easily implemented. This can also be used as a pre-study tool for selecting specific scenarios of interest so that unnecessary physical relay tests are avoided.

To investigate the characteristics of the relay algorithm during fault conditions, we use the DIgSILENT software package as the power system simulator to develop a new testing methodology for evaluating the power relay. In this work, the software package is used for developing and testing the characteristics of the relay during fault conditions. In terms of global sensitivity analysis, the software is used to create the appropriate power system model and test scenarios required for comprehensive evaluation of the relay design features and performance characteristics that are affected by simultaneous uncertainty factors.

Fault testing methods for various scenarios are generated in an automated way through simulation. Power network models used to simulate disturbance scenarios are addressed including models for the distance relay. Several circuit models are selected as case studies for tests using the new test methodology proposed in this research.

The case study was focused on the performance of the impedance measurement algorithm for the distance relay. Fault scenarios with different fault locations were generated. Several input variables were identified within the model as uncertainty factors. In this work, we identify the test performance requirements of the GSA to examine the effects of varying the uncertainty factors of the relay model algorithm on the impedance measurement result. Understanding the behaviour of the algorithm in response to changes in uncertain factors, that can come from many sources of uncertainty such as errors in measurement network modelling, is of fundamental importance in ensuring correct use of the fault impedance measurement algorithm. In our research, the fault impedance measurement is modelled and implemented in DIgSILENT. The uncertainty value of

factors in the variable power system protection model is manipulated sequentially, while the methodology for sensitivity analyses is developed in SIMLAB.

5.2. Testing Environment

Figure 5.1 shows the implementation of the proposed structure of the testing methodology. This structure is developed for modeling and risk assessment of the IED and is based on the combination of DIgSILENT and SIMLAB. As shown in Figure 5.1, the structure includes a procedure for sensitivity analysis, which is used to assess the effect of variability of model parameters, due to the input factors, on the different simulations of power system protection. The aim of the assessment is to identify which factors have the most impact on the performance of the IED algorithm.

The power system simulator is used to produce the simulated scenario of fault transients for a variety of system configurations and conditions. In this project, the DPL script provides the automation of tasks. The DPL command, which is stored in the script folder in the project directory, is used to take samples of parameter inputs generated using the steps explained in the previous section, pass these variable values to the power system model, and then obtain the output results.

The GSA software package is used for Quasi-Monte Carlo (QMC) based sensitivity analysis. QMC method is used here for quasirandom number generation with emphasis on sampling sets of points from the uniform distribution of samples. QMC-based sensitivity analysis is based on performing the relay mode evaluation with the selected input factors. As shown in Figure 5.1, three modules are involved in the process of calculating the sensitivity analysis using GSA software. The first model, pre-process, is used to execute steps such as range & distribution, and sample generating. The second model, model execution, takes the generated samples and passes them to DIgSILENT. The third model, post-process, evaluates the sensitivity analysis.

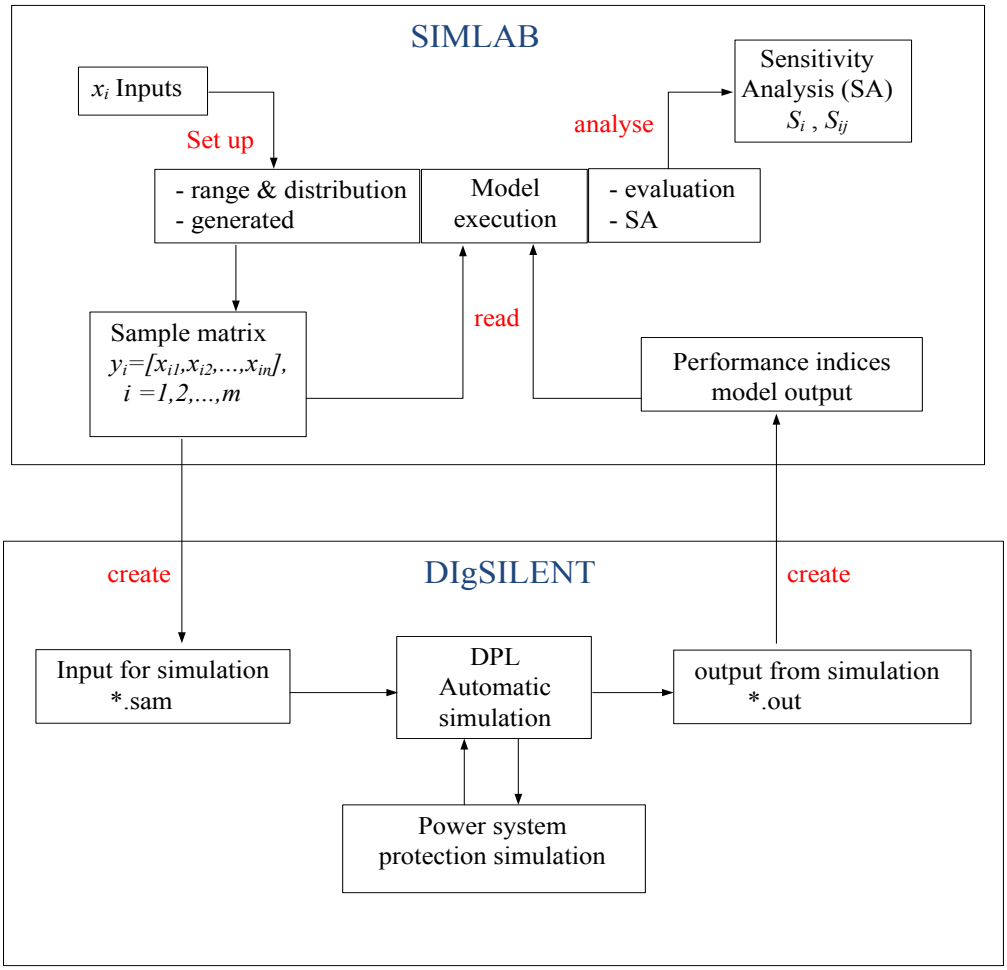

Figure 5.1: The proposed Structure of the Testing Environment.

5.3. Power System Protection Modelling and Simulation in DIgSILENT

The simulation objectives are to evaluate the operating characteristics of the IED model's fault impedance algorithm, and verify its settings. This is achieved through implementation of a comprehensive series of tests. This test assesses the statistical performance related to the relay operating characteristic through the model output. Simulations of batch test scenarios, with a variety of disturbance conditions in different fault locations, are controlled by the algorithm developed in the DPL script.

5.3.1. Simulation Tool - DIgSILENT

The increasing complexity of power system networks and the effects of uncertain factors are challenges faced when using IEDs, especially when non-pilot distance is used to protect the faulted transmission line. To study their performance, computer models of relay protection have been widely used. However, they did not provide access to model parameters that are important for testing the sensitivity of the output to those factors. Sensitivity analysis studies and performance analysis of IEDs requires tools capable of modelling power system protection as well as enabling the implementation of advanced sensitivity analysis methods. DIgSILENT [17] is an example of a standard tool that can be used for the power system protection study.

This power system simulator provides access to the parameters of the power system protection model and also allows simulation of the transient events at same time. These capabilities are very important since GSA is used for performance analysis of the IED model. This experiment requires the selected number of power system protection parameters to be varied using the values (i.e., uncertain values) generated by SIMLAB before each different fault simulation is executed.

In order to get exact simulation results, accurate power system protection models are established. The graphical user interface (GUI) and database manager provided by DIgSILENT are used to create these models and manage the simulation data. The models composed with the power system protection components are used to represent active and passive real elements, such as: power sources, lines, and IED model. These electrical components are built with standard component models and contain parameters that can be accessed and set using the database manager functions. Furthermore, the exact simulation result can be achieved since all components of the models (i.e., the electrical components) interact with the DIgSILENT's modeling library.

Figure 5.2 gives an example of the relationship between the power system and the main parts of the IED relaying model. Instrument transformer (i.e., CT and CVT) are used to link the IED model and electrical network. During a fault, which is simulated in the electrical network, the voltage and current signals measured from secondary parts of instrument transformers are used by the 'polarizing Z1' block for calculating the fault impedance. The existing IED model provided by DIgSILENT is implemented as an object

oriented data structure, in which a multi-level approach using relay type, relay frame, and the relay elements are used in the design of the model.

In the mutlti-level approach of the IED model (shown in Figure 5.2), the three level approach can be defined as follows [17, 74]: 1) Relay frame: in this level the general relay functionality using the block diagram is specified. The main block's function of the IED, such as instrument transformer (i.e., CT, CVT), measurement, and fault impedance calculation, can be defined. This description only defines the number of stages and how the stages interact, no algorithm details are specified in each of the blocks except the number of inputs, outputs, and interconnections between the blocks. 2) Relay type: in this level the mathematical function relating to the relay frame block is defined. In this case, the filter characteristic is defined in the measuring block as well as the mathematical detail for fault impedance measurement and instrument transformers. The relay type contains complete information about the IED and defines the library information for this IED. 3) Relay element: in this level the actual IED model is created by refering to relay type in the library that containt the relay structure including the parameter settings.

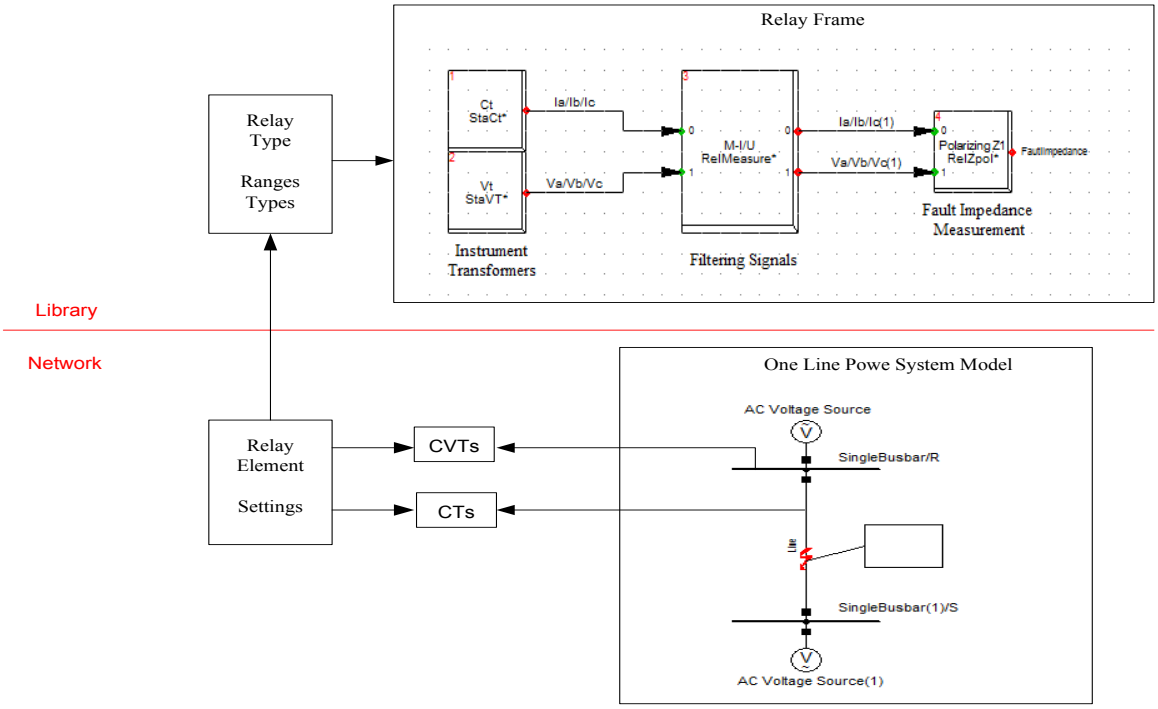

Figure 5.2: Relationship between relay model and power network [74].

5.3.2. Power System Protection Modelling and Data Manipulation

The sensitivity analysis procedure for investigating the IED performance of the Electromagnetic Transient (EMT) model for a specific application requires an impedance measurement function. The EMT model applications include: a faulted transmission line, instrument transformers, and IED (Intelligence Electronic Device). We applied the power system simulation program for modeling the faulted transmission line, current and voltage transformer, and the IED multifunctional relay. Figure 5.3 shows the simple network model which is configured using DIgSILENT, while Figure 5.4 shows the DIgSILENT block representing instrument transformers, blocks for filter modeling, and impedance measurement functions of the IED. The program has models of all standardized protection elements of IEDs, which can be activated via the data manager as shown in Figure 5.5.

In this project, the power system simulator is not only used for power system protection modeling, but also for fault power system simulation and analysis. In this case, the software which has an integrated graphical user interface is able to be used for the IED performance analysis, in which the data entry is accomplished by drawing the power system protection under study.

The data manager allows the features required in testing to be managed. All actions related to modeling and manipulating variability of factors are possible and can be controlled from a single database window. The DPL script can be applied for automatic testing and data manipulation. As SIMLAB may generate thousands of data points, the script enables the data to be automatically read, and vary the uncertainty values of the variables in the model. This feature is very important for global sensitivity analysis and is required for investigating the sensitivity of the IED distance relay model.

Power System Protection Modelling in DIgSILENT

The power system protection models that consist of built-in power system, and relay model, which is presented in this thesis, are implemented in DIgSILENT. This power system simulator has the ability to simulate transient events and calculate fault impedance in the same software environment. Implementation of the global sensitivity analysis is possibile since variable values may be changed in the model and automatic tests using the algorithm can be scripted in DPL.

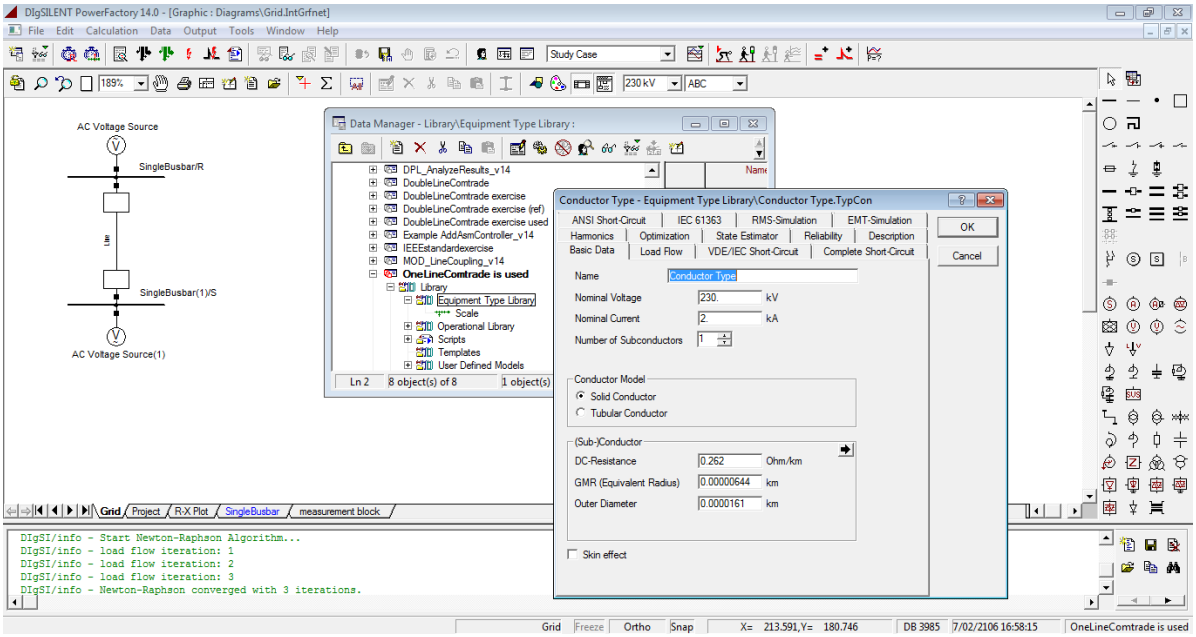

Figure 5.3: Network Model configuring using DIgSILENT.

The SEL-421 multifunctional distance relay models, and current and voltage transformers, were modelled using powerful features of the Dynamic Simulation Language (DSL) provided by DIgSILENT. The full SEL-421 relay model consists of a large number of blocks representing protection elements. However, we are only testing the output of the block used for calculating the fault impedance (block function number 4 in Figure 5.4). This block contains the mathematical function for the fault impedance calculation and some values are required to be set (e.g., the zero-sequence current compensation, $\underline{k}_0$). The main block function of Figure 5.4, as for instrument transformer (i.e., CT/CVT) indicated by number 1 and 2, are connected to the transmission line side. Furthermore, the block function number 3 represents voltage and current input signal channels containing a 2nd order anti-aliasing filter, Analog-to Digital Converter (ADC), and Discrete Fourier Transform (DFT). The block output of block number 3 is a voltage and current phasor which is then used by protection elements and measuring functions of block number 4. The measuring function uses the data obtained from decimated sampled data and is acquired at a frequency of 20 samples per cycle. The earth fault compensation factor, $\underline{k}_0$, is included in this block function, but not for mutual earth compensation, $\underline{k}_{0M}$ (see Figure 5.6).

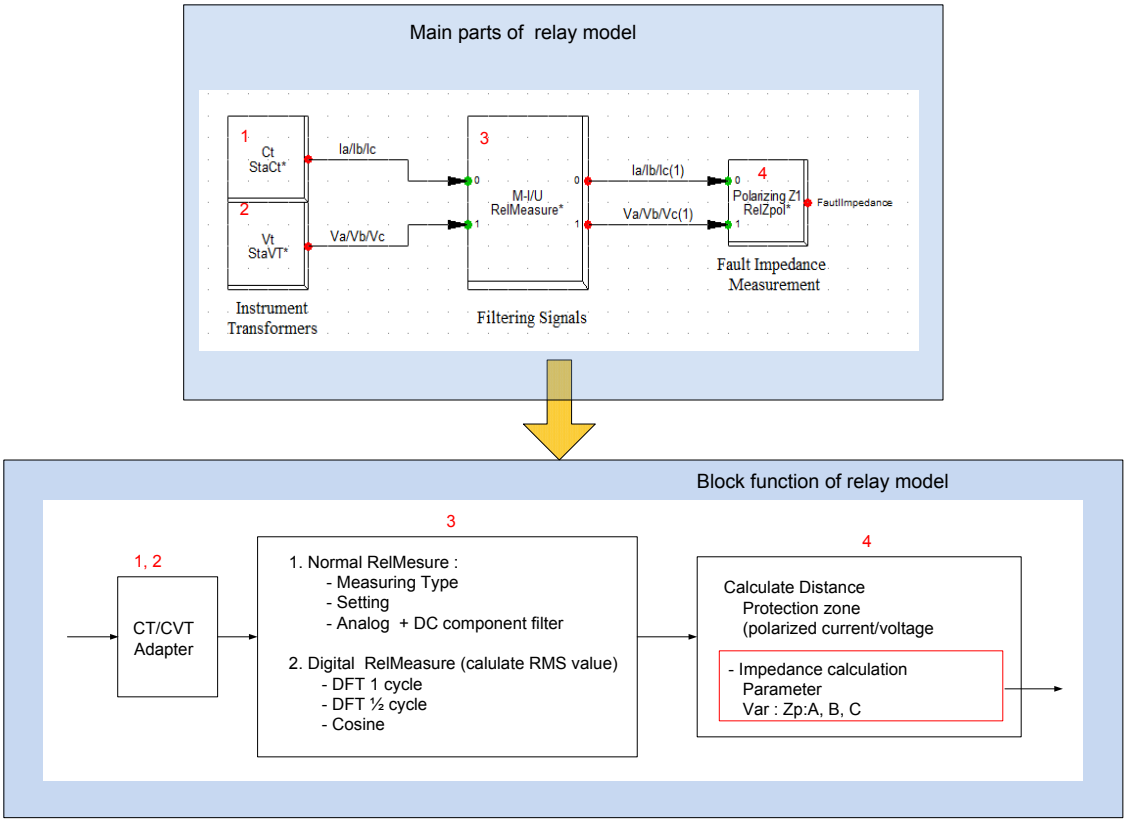

Figure 5.4: The main measurement block of distance relay scheme.

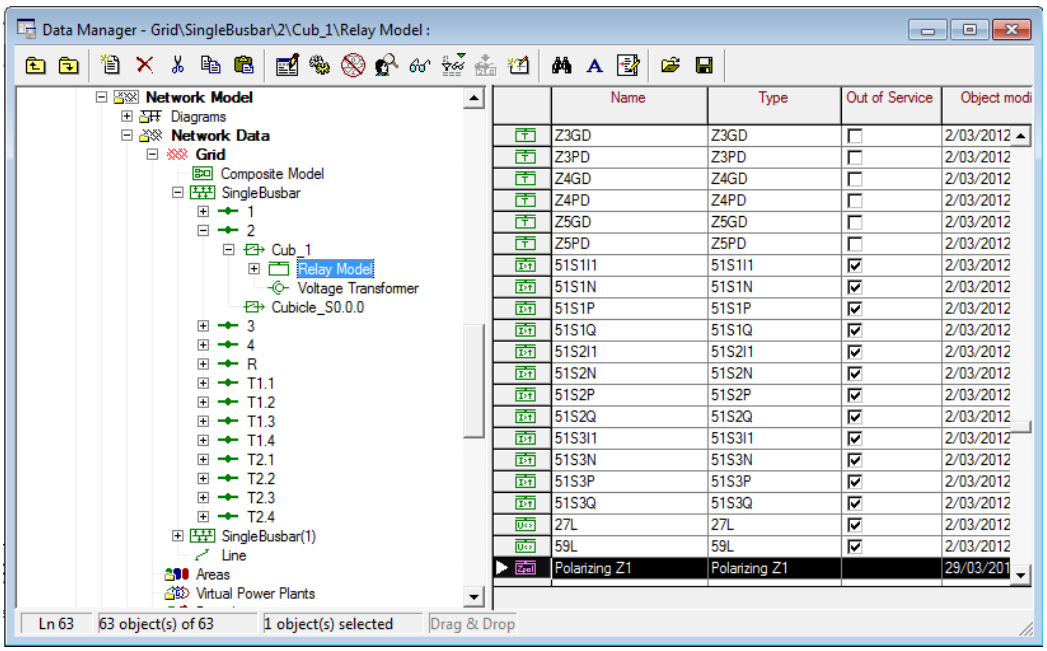

Figure 5.5: DIgSILENT data manager window showing protection elements implemented in the relay model [17].

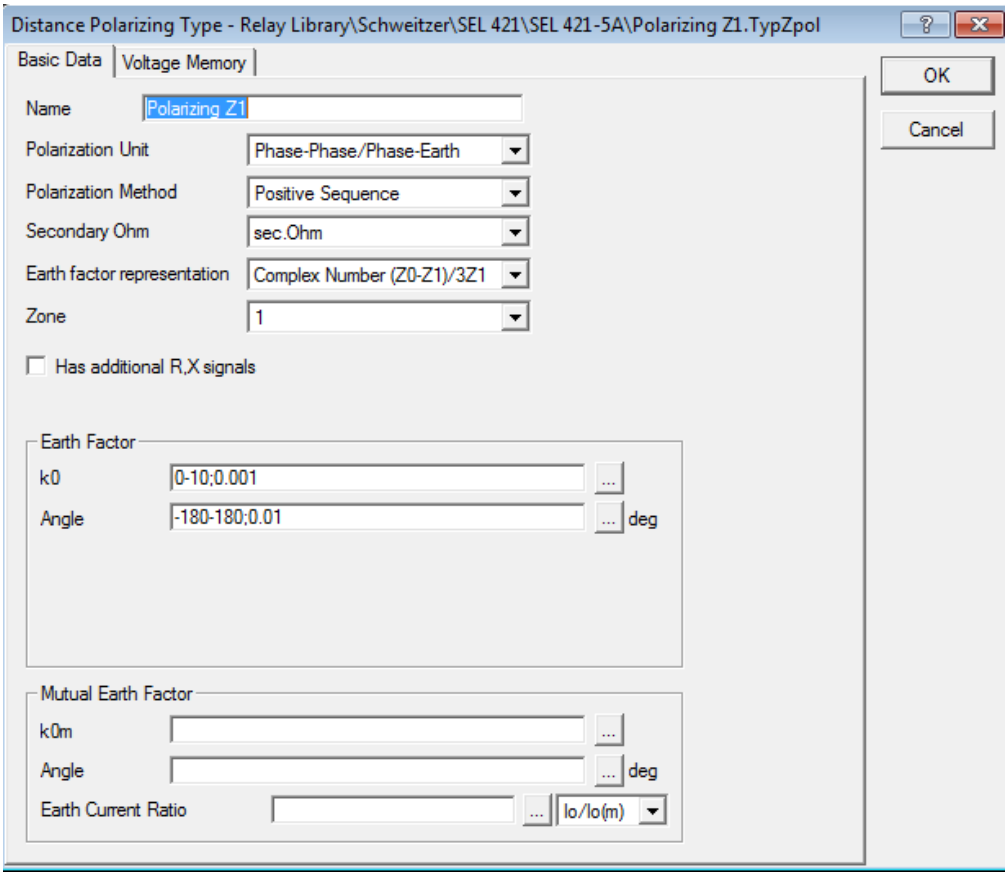

Figure 5.6: The "Polarizing" type dialog [17].

Data Manipulation

For the purpose of global sensitivity analysis some parameters of the protection system model need to change at the same time according to the value of referenced uncertainty factors. The algorithm we developed was applied using DPL to manipulate such factors. DPL is used as an interface for automating tasks in the *PowerFactory* program. Database references that refer to those selected variables are considered in development of the command batch using the DPL script in order to allow for data manipulation as well as for automation of simulation tasks. Figure 5.7 shows how the DPL batch program controls simulation test and data manipulation.

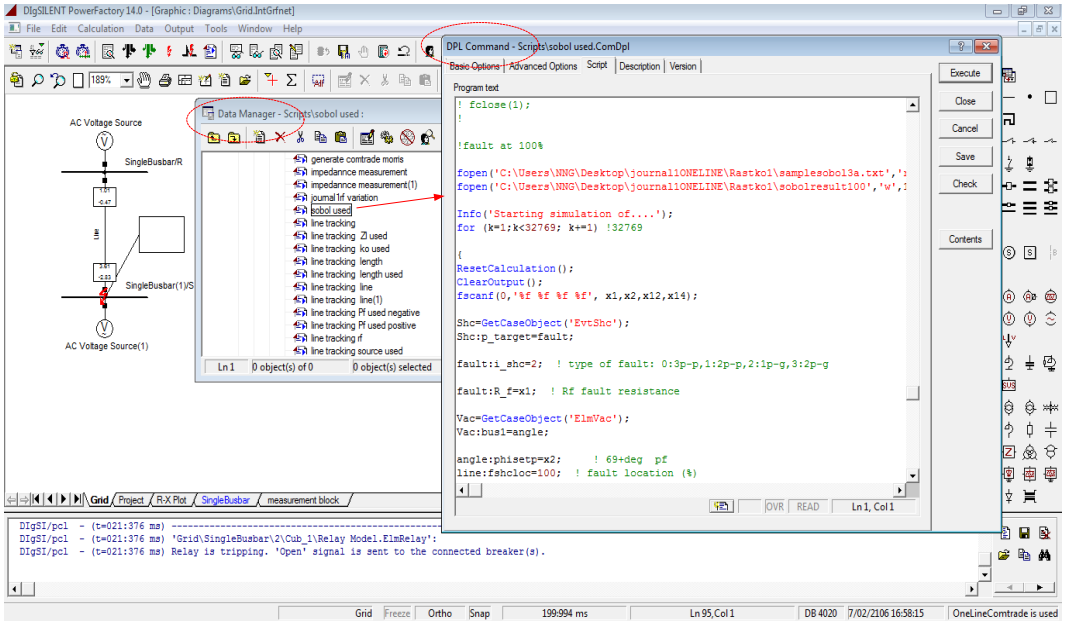

Figure 5.7: Simulation controlled by DPL program.

The structure of the DPL script is presented in Figure 5.8. In the figure, the DPL command object is the central element to link the predefined parameter inputs and set of objects to the results or change parameter values. Internal variables and also internal objects, which include a calculation command, substript, and filter sets, are used by the DPL command object to evaluate the inputs and to produce the results. The DPL command is run in series, and calculations or other functions are started which always communicate with the database to output the results.

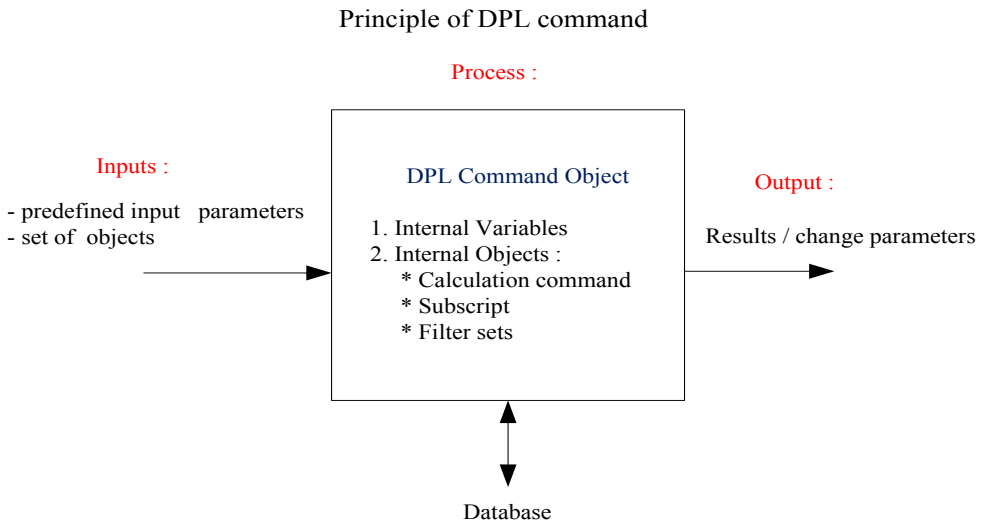

Figure 5.8: Principle of a DPL command.

5.3.3. Protective Distance Relay Simulation

Based on the discussion in previous sections, in Figure 5.9 we can establish the interactive relay test systems by implementing the combination between two software packages DIgSILENT and SIMLAB. The DPL script is used as an interface and for automating the protective relay test. Due to the flexibility of access to the parameters of the models, the DPL script not only gives a command to start the fault simulation system but also to calculate fault impedance at the same time.

DPL runs the process by reading the parameter inputs, which are generated by SIMLAB, then sets and changes the value of simulation system parameters by writing the values of fault resistance, inception angle, fault location, etc. These parameter values are written into the relay and power system network model during simulation while the fault impedance calculation result is read from the 'polarizing block' function based on the voltage and current phasor values generated by the 'measurement block'. Error and corresponding performance indices of the relay for each input factor sample is calculated using the DPL script. Finally, the performance indices of models associated with generated parameter inputs of uncertainty are then transferred to SIMLAB for sensitivity analysis calculation of the relay model.

Figure 5.10 shows a flowchart of testing which has been implemented in all case studies. With this arrangement, the output of testing for different fault scenarios will vary as the sampled data of uncertainty factors. This sensitivity analysis is important in providing a better understanding of IED distance relay model behaviour when applied to different fault scenarios.

The sensitivity measured by SIMLAB on the relay model is able to assess the uncertainties associated with the factors influencing the distance relay. In order to do sensitivity analysis of a relay, we apply two different methods: Morris, and Quasi Monte-Carlo, as described in the previous section. The stored output of the simulation and performance index calculation combined with the generated factor samples, are used as inputs in SIMLAB sensitivity analysis.

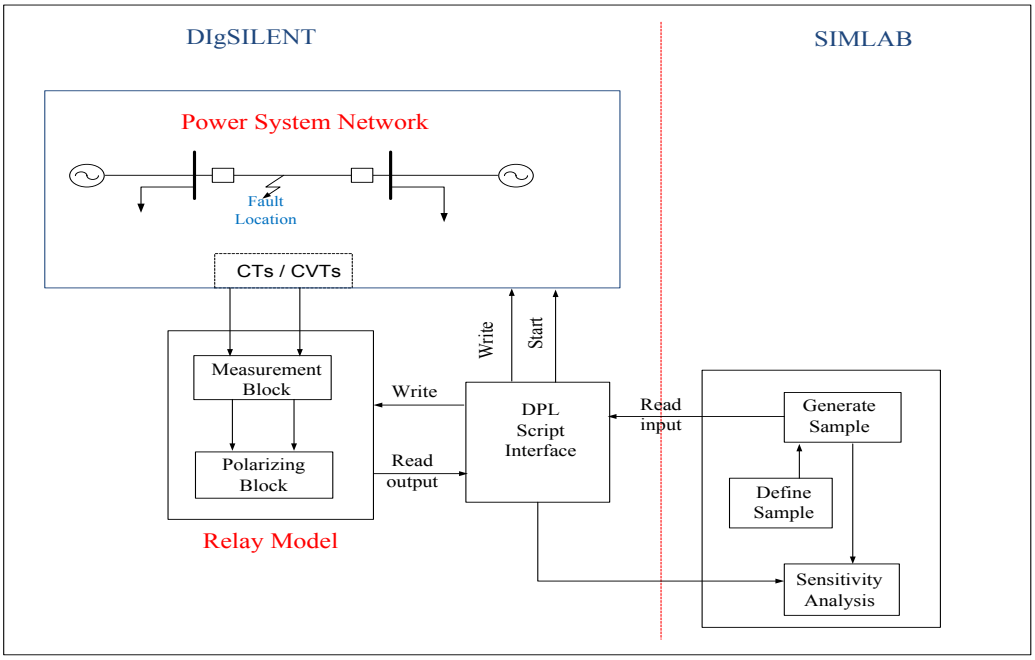

Figure 5.9: Protective relay test systems based on combination between DIgSILENT and SIMLAB.

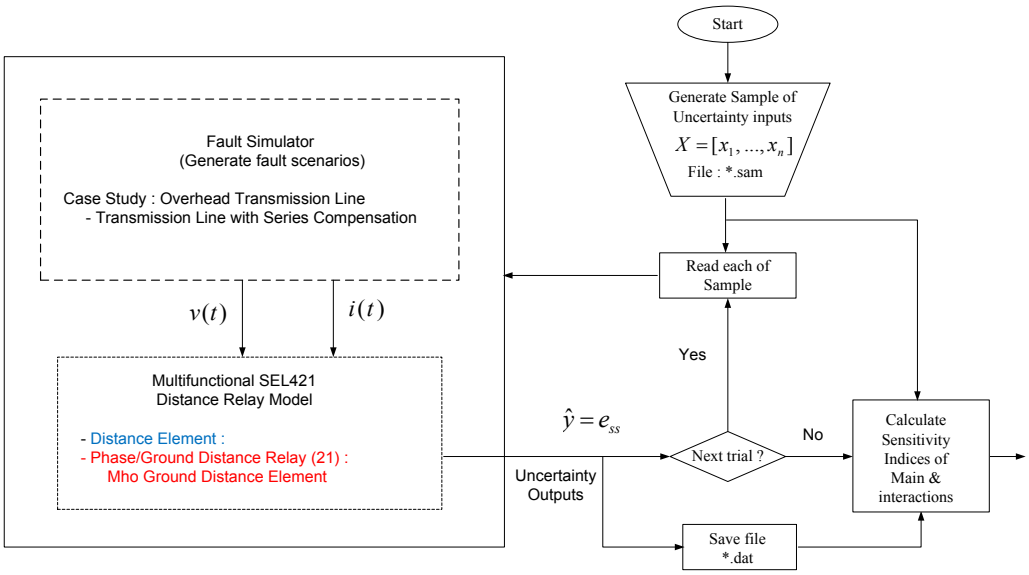

Figure 5.10: Flow chart of Testing.

5.4. Implementation of the Sensitivity Analysis Methodology

The proposed sensitivity analysis methodology is implemented using a combination of three different software programs: DIgSILENT, SIMLAB, and MATLAB. Sensitivity analysis applied in SIMLAB involves four steps [16]: (1) selection of a range and

distribution for each input variable; (2) generating samples from the input variables; (3) propagating the samples through the model under consideration; (4) performance evaluation of sensitivity analysis. However, since there are two methods of sensitivity analysis applied in this project (i.e., Morris and Sobol method), there will be eight steps required for the sensitivity analysis procedure. The procedure is explained using the examples in the case study. Details of the procedure steps shown in Figure 5.11 are given as follows:

The first step is to define the input factors by specifying the interval of variation of each factor, x_i. In this project, we use uniform distribution of data to explore the characteristic of relay model.

The second step is to generate the samples of factor values (i.e., the samples of uncertain inputs) within specified intervals using the factor screening technique based on the Morris method [75-78]. The goal of using this method is to reduce the number of factors before applying full GSA. The method is implemented in the SIMLAB software environment [16]. The result of this step is a sequence of sampled elements of the form

$$\boldsymbol{x}_i = [x_{i1}, x_{i2}, \dots, x_{ik}], \quad i = 1,2, \dots, N. \tag{5.1}$$

Where k is the number of inputs (i.e., sampled variables and N is the sample size).

The third step is to transfer the factors, which are generated in SIMLAB, to DIgSILENT and automatically run simulations of transmission line faults for different values of factors. In the preparation phase, the DIgSILENT model that includes transmission line, instrument transformer (CT/CVT) and the IED of SEL-421 distance relay is prepared and properly parameterized. The automation algorithm, which is developed using the DPL script, changes the parameter values according to the Morris factors sampling plan created in step 2). The simulation is run by passing the current and voltage signals, via instrument transformers, to the IED SEL-421 model, and finally computing the sequence form of errors in measurements of the positive-sequence fault impedance (i.e., the output performance):

$$y_i = f(x_{i1}, x_{i2}, \dots, x_{ik}) = f(\boldsymbol{x}_i), \quad i = 1,2, \dots\dots, N. \tag{5.2}$$

In essence, these model evaluations create a mapping from the analysis inputs, $\boldsymbol{x}_i$, to the analysis results, y_i. Once this mapping is generated and stored, it can be explored in many

ways to determine the sensitivity of model predictions of the IED to the individual input variables.

The fourth step is the sensitivity analysis, which is based on an exploration of the mapping from result defined by the relation in Equation (5.2). The performance results, obtained in DIgSILENT, are passed to SIMLAB where the Morris-based screening algorithm is used to identify important factors. In this way, the dimension of the factor space is reduced before proceeding to the full GSA in the second stage of this procedure.

The fifth step is for the smaller number of factors that is initially specified in step 1). The new samples are generated using Sobol's quasi-random sequence. These samples fill the factor space in the most optimal way and will facilitate computation of the global sensitivity indices [16], which are able to accurately describe the impact of interactions between factors in addition to individual factor effects. The Sobol sequence is generated using the SIMLAB software.

In the sixth step, DIgSILENT reads the factor samples generated in 3) and runs the simulations for all samples. The same DPL script, discussed in 4), is implemented here. The simulation produces fault impedance measurement errors and corresponding performance indices for each input factor sample. These values are transferred to SIMLAB.

In the seventh step, the factor samples generated in 5), and the simulation results produced in 6), are used to calculate global sensitivity indices. The GSA computation is performed according to the Analysis of Variance (ANOVA) procedure implemented in SIMLAB.

Finally, in the eighth step, the sensitivity indices of individual factors, and interactions between factors, are produced and interpreted.

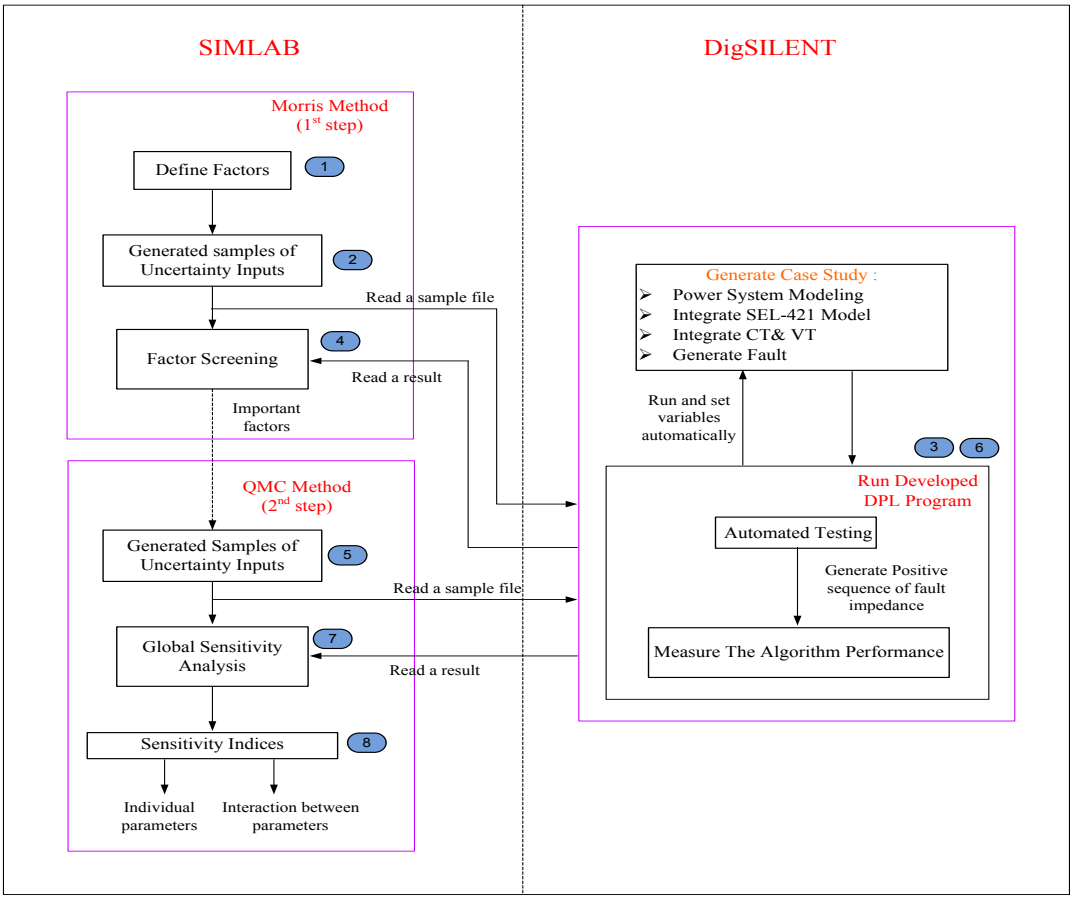

Figure 5.11: The structure of the test software environment.

5.5. Conclusions

This chapter proposes the systematic method based GSA technique for evaluating the IED algorithm in the context of complex transmission line systems, such as a line with two sources, double-line circuits, multi-terminal line, and line series compensation. This systematic methodology has been developed by combining two different software tools, i.e., the power system simulator using DIgSILENT softaware package, and the GSA tool using SIMLAB. Testing is carried out using a script created using DPL, which automates the fault simulation and fault impedance calculation at the same time. Automation is essential since implementing GSA requires large number of fault simulations.

The following main points can be concluded from this chapter:

- The method developed is applicable for automated testing IED algorithms, since the automation tasks of fault simulation, fault impedance calculation,

and the ability to access and vary the parameters values, can be done in the same time.

- Two different software packages, DIgSILENT and SIMLAB, can be integrated. DIgSILENT is a power system tool which can be used effectively for modelling power system protection and simulation. SIMLAB is used to generate the samples and for the sensitivity analysis.
- Two methods of sensitivity analysis techniques are implemented. In the GSA, the QMC sampling strategy, using Sobol sequence as input, is used to investigate effect of the main factors and also the interaction between factors on the performance of the IED algorithm, while the Morris method, is used to pre-screen paremeters, and to eliminate non-influential parameters before applying the GSA.

Chapter 6

Case Studies

This chapter presents four case studies in order to demonstrate the methodology for testing impedance measurement algorithms used in IEDs. The case studies are carried out assuming realistic conditions. The main objective of these case studies is to evaluate the applicability of the global sensitivity method in analyzing the sensitivity of the relay algorithm that is used to protect a range of transmission line configurations.

The case studies are presented in the following order:

I: Line with Sources at Both Ends.

II: Double-Circuit Line.

III: Three-Terminal Line.

IV: One Line with Series Capacitor.

Each case study description contains the information about the model and its application. We then define the uncertainty of factors associated with the protection system model as well as demonstrate the application using different global sensitivity method, i.e., Morris and Sobol's methods. The sensitivity results are then presented graphically.

In these experiments the Morris method is used to remove non-influential factors before applying the QMC to analyse the error variance of the measurement algorithms. The QMC can quantify the influence of the individual factors and their interactions on the measurement algorithm performance. The DIgSILENT PowerFactory is used to simulate transmission line faults with varying uncertainty factors and to run the relay algorithms including estimation of the fault impedance. The DIgSILENT Programming Language (DPL) script is used to automate the tasks required for the assessing performance of the fault impedance estimation algortihm. The SIMLAB software is used to generate factor space samples and to analyse the error variance of the measurement algorithm output.

6.1. Case study I: One Line with Two Sources

6.1.1. Description of the Case Study

This case study presents a method of Global Sensitivity Analysis for testing impedance measurement algorithms of IEDs implemented on a line with sources at both ends of the power system network model. One-ended fault impedance estimation is tested. Figure 6.1 illustrates one line system, showing the uncertainty factors of the system, with the fault simulated at fault location, *F*. Positive sequence fault-loop impedance, looking into the fault located at *F*, is estimated using the method where voltage and current input signals are measured by the IED located at one ended of terminal-S. Conditions that may cause errors for one-ended based fault calculation methods are: combined effect of fault resistance and inception angle, system nonhomogeneity, inaccuracy of line modeling, and setting of zero-sequence impedance.

As shown in Figure 6.1, the following factors will impact the impedance measurement accuracy [1]: fault resistance, R_F, load flow angle, δ_F, inaccurate system parameters, $(\underline{Z}_L, \underline{Z}_S, \underline{Z}_R)$, and k-factor correction, $\underline{k}_o$. In order to determine whether the relay algorithm is sensitive to any of these factors a number of simulation tests are conducted with different fault locations, *F,* and variety of conditions. During simulations the factor values are changed simultaneously. The performance of the relay algorithm is then calculated as a steady-state measurement error. The case study examines the performance of the impedance measurement algorithm of the IED distance relay model.

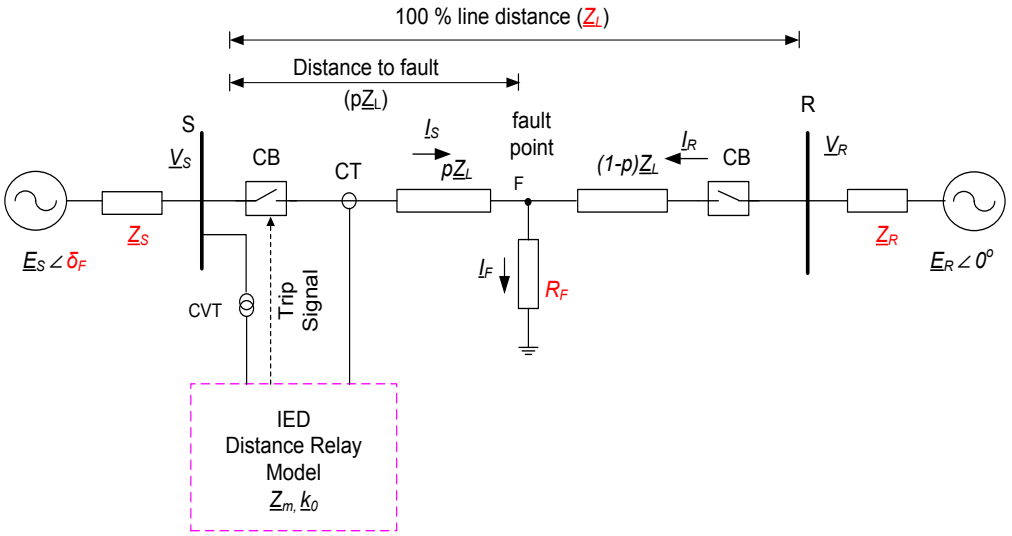

Figure 6.1: Circuit diagram of faulted line with sources at both ends and uncertain factors indicated in red.

The effect of uncertainty of the input parameters on the impedance measurement algorithm (and fault locator) is analysed using the following sensitivity methods: Morris and Quasi-Monte Carlo (QMC) using Sobol's sampling technique. These sensitivity techniques are used to analyse the variability of the algorithm output which is influenced by uncertain inputs (i.e., factors), and are indicated in red on Figure 6.1.

It can be seen from Equation (3.41) that the estimated apparent fault impedance, $\underline{Z}_m$, is linked to measured phasor of the bus voltage, $\underline{V}_S$, and compensated current, $\underline{I}_S^c$, and it can be represented as $\underline{Z}_m = f(\underline{V}_S, \underline{I}_S^c)$, where f is a nonlinear function. Care must be taken because the measured voltage and compensated current can contain uncertain values $\Delta\underline{V}_S$, and $\Delta\underline{I}_S^c$. Based on Equation (3.39) and Equation (3.40), these uncertain values, composed as $\Delta\underline{V}_S = p\underline{I}_S^c + 3R_F\underline{I}_F$, and $\Delta\underline{I}_S^c = \Delta(\underline{I}_S + \underline{k}_0\underline{I}_0)$, are influenced by the uncertain factors. The following section presents an investigation of how the uncertainty factors can impact the performance of the relay algorithm.

6.1.2. Evaluation of Relay Algorithm Performance

The faulted transmission line and IED, as shown in Figure 6.1, are modelled in the DIgSILENT environment. The external system is represented using Thevenin's equivalents comprising of voltage sources, $\underline{E}_S$, $\underline{E}_R$, and their corresponding impedance, $\underline{Z}_S$, and $\underline{Z}_R$. The

transmission line positive sequence impedance is $\underline{Z_L}$. We simulate phase A to ground at point F via resistance R_F. During the fault, the current used in measurement of the impedance between terminal S, and fault at F, is compensated by the relay algorithm for the zero-sequence current using a factor, $\underline{k_o}$ [79]. The factor, $\underline{k_o}$, depends on the zero-sequence impedance, which is not known exactly, and is selected as an uncertain factor for the analysis. Errors in setting this parameter will influence the accuracy of measured fault impedance.

Since the fault current, $\underline{I_F}$, in Figure 6.1 is fed from both sources, the accuracy of measured impedance between terminal S, and fault seen by the IED, is not only affected by the uncertain value of fault resistance, R_F, but also from interactions between R_F, and power flow angle, δ_F [1, 63]. For the purpose of illustrating the effect of R_F and δ_F on the impedance measurement, we simulated the phase A to ground faults at various locations and used the simulated voltages and currents as inputs to the impedance measurement algorithm implemented in the DIgSILENT IED model. The results are demonstrated using the electrical network parameters shown in Tabel A1 of Appendix A.

In Figure 6.2, we illustrate the tracing of measured impedance versus time for the fault at 65% of the line length with $R_F = 10\ \Omega$, and the three-point variation of the load flow angle, $\delta_F = -10^{\circ},\ 0^{\circ},\ +10^{\circ}$. The simulation shows how those two factors impact the measured impedance, $\underline{Z_m}$. Certain value of these factors, $\delta_F = 0^{\circ}$ to -10°, make the relay see the fault in Zone 2. For further illustration, Figure 6.3 shows the effect of δ_F to measurement of $I_m\{\underline{Z_m}\}$, for a fixed value of $R_F = 10\ \Omega$, and for varying fault locations. The error of the reactance measurement increases with the increase of δ_F, and the effect is more pronounced for the faults closed to the remote-side, R, of the transmission line.

It is well known that the ratio of source impedance, $\underline{Z_S}/\underline{Z_R}$, of the Thevenin's equivalent at line-side S and R, in Figure 6.1, will have an effect on impedance measurement [63]. The measurement error will increase with an increase in the ratio $\underline{Z_S}/\underline{Z_R}$, as shown in Figure 6.4. The impact is higher for faults closer to the measurement point.

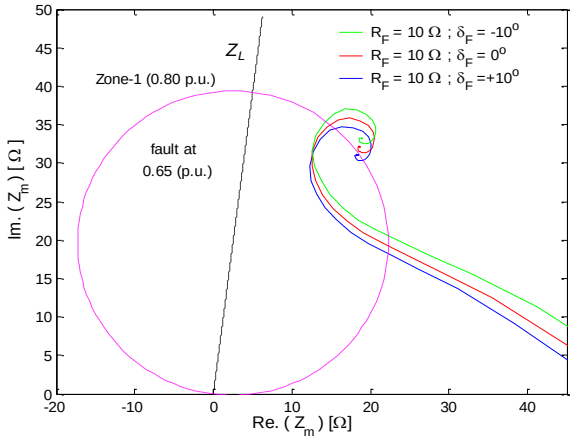

Figure 6.2: Measured impedance trace against IED Mho characteristic for the phase-A to ground fault shown in Figure 6.1.

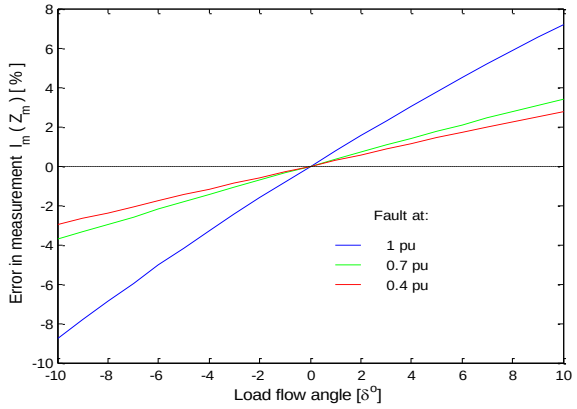

Figure 6.3: Percentage error of the $I_m(\underline{Z}_m)$ measurement as a function of δ_F for resistive faults, R_F = 10 Ω, on the line shown in Figure 6.1 at three locations.

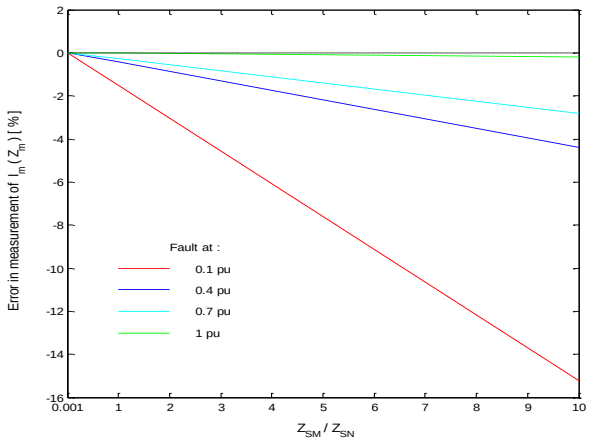

Figure 6.4: Percentage error of the reactance measurement as a function of the ratio, $\underline{Z}_{SM}/\underline{Z}_{SN}$, for the faults in the network in Figure 6.1 at four fault locations, and for fixed parameters, $\delta_F = 0°$ and $R_F = 10\ \Omega$.

Inaccurate relay parameter settings may affect the accuracy of the fault impedance measurement algorithm. In this case, the algorithm is most sensitive to the correction factor, $\underline{k}_0$ (i.e., $\underline{Z}_{0L}$ and $\underline{Z}_{1L}$). Earth resistivity is part of the impedance, $\underline{Z}_{0L}$, and is not known exactly [79]. Figure 6.5 demonstrates the effect of a setting error in $\underline{k}_0$ to the performance of the measurement algorithm. It is apparent that this effect is more pronounced for those faults closer to the remote side, R, of the line. The variation in line geometry and electrical parameters along the line length contribute to errors in setting the value of the positive-sequence line impedance, $\underline{Z}_{1L}$ [35]. This will have considerable effect on the impedance as shown in Figure 6.6. The impact is increasing as the fault location moves towards the remote side of the line.

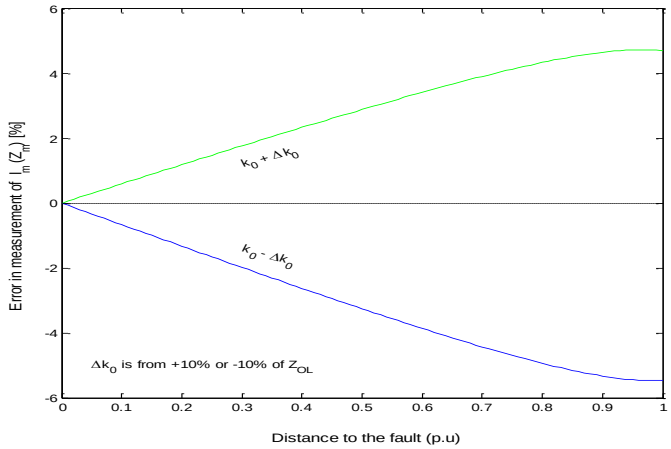

Figure 6.5: Effect of uncertainty of the setting factor $\underline{k}_0$ as a function of distance to fault location for fixed parameters, $R_F = 0\ \Omega$ and $\delta_F = 0°$.

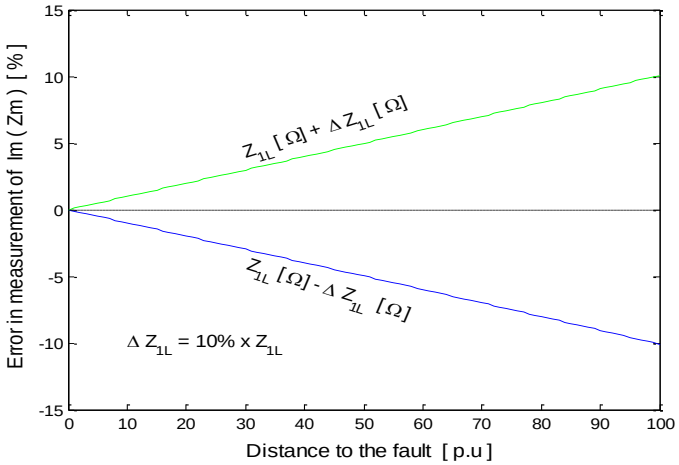

Figure 6.6: Effect of errors in the line positive-sequence impedance setting value, $\underline{Z}_{1L}$, in function of distance to fault for the A-phase to ground faults in the system shown in Figure 6.1. Other factors are kept constant, $R_F = 0\ \Omega$ and $\delta_F = 0°$.

Figure 6.7 shows outputs of the impedance measurement algorithm for all samples of the factors $\mathbf{x} \in \boldsymbol{R}^{14}$, that we have used in the Morris screening method. These uncertain factors are indicated in red in Figure 6.1, and their assumed intervals of variation, that affect the fault impedance measurement are listed in Table 6.1. The outputs are plotted for the three fault locations. It is interesting to note that the measurement output variability increases as the fault location approaches the remote line side. Furthermore, the measured impedance for the fault at 70% of the line length (in Zone 1), for certain values of the factors, can have a value larger than 80% of the line length (in Zone 2). This phenomenon is influenced by uncertain value of $\Delta\underline{V}_S$, $\Delta\underline{I}_S^c$, and fault resistance, R_F, during a fault. In this case, a number of factors listed in Table 6.1, except fault resistance, R_F, will contribute to that random values. For further analysis, the following section will investigate which factors will mostly contribute to that performance.

Table 6.1: Uncertain factors and their assumed intervals of variation that are affecting fault impedance measurements for the single-phase to ground faults in Figure 6.1.

Uncertain parameter	Description	Variation interval
x_1	R_F	[0 ; 10] Ω
x_2	δ_F	[-10 ; 10] deg.
x_3	$Re\{\underline{Z}_{0S}\}$	[2.3535 ; 2.8765]Ω
x_4	$Im\{\underline{Z}_{0S}\}$	[26.901 ; 32.879] Ω
x_5	$Re\{\underline{Z}_{1S}\}$	[1.5678 ; 1.9162] Ω
x_6	$Im\{\underline{Z}_{1S}\}$	[17.9316 ; 21.9164] Ω
x_7	$Re\{\underline{Z}_{0R}\}$	[2.3535 ; 2.8765]Ω
x_8	$Im\{\underline{Z}_{0R}\}$	[26.901 ; 32.879] Ω
x_9	$Re\{\underline{Z}_{1R}\}$	[1.5678 ; 1.9162] Ω
x_{10}	$Im\{\underline{Z}_{1R}\}$	[17.9316 ; 21.9164] Ω
x_{11}	$Re\{\underline{Z}_{1L}\}$	[5.626 ; 6.88] Ω
x_{12}	$Im\{\underline{Z}_{1L}\}$	[44.12 ; 53.93] Ω
x_{13}	$Re\{\underline{Z}_{0L}\}$	[20.781 ; 25.401] Ω
x_{14}	$Im\{\underline{Z}_{0L}\}$	[138.038 ; 168.713] Ω

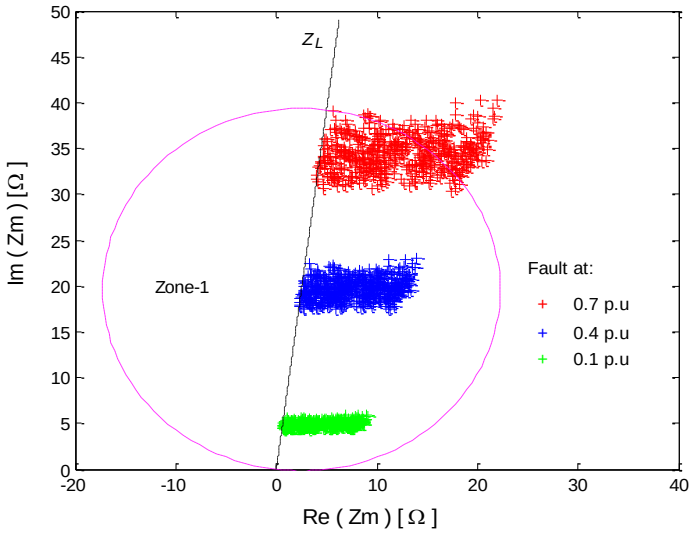

Figure 6.7: Fault impedance measured for all samples of the input factors, $\mathbf{x} \in \boldsymbol{R}^{14}$, generated according to the random sampling method (total of 500 samples) for three different fault locations.

6.1.3. Test Result and Discussion

The DIgSILENT software environment has been used to simulate the phase A to ground faults at different locations in the transmission line shown in Figure 6.1, and for variations of factors specified in Table 6.1. The IED model is implemented in DIgSILENT. The performance of the fault impedance measurement function of this IED was tested for all points in the factor space. These points were designed using the SIMLAB software environment according to the Morris method and Sobol's quasi random sequence. The SIMLAB is also used to compute all statistics and sensitivity measurements according to the GSA methodology.

For the illustration purposes, the results for only one distance to fault location of the Morris factor screening method is shown in Figure 6.8. These results are presented as standard deviation σ, versus mean value, μ, for all elementary effects. These statistics are computed using 150 samples. Large mean values indicate a corresponding factor's importance, while large variance suggests that impact of a factor, together with another factor, is important (i.e., interaction effect). In Figure 6.8, we can identify the following factors as dominant: $x_1(R_F)$, $x_2(\delta_F)$, $x_{12}(Im\{\underline{Z}_{1L}\})$, and $x_{14}(Im\{\underline{Z}_{0L}\})$. Details of the analysis for other fault locations are not reported here but the conclusion is that the selected 4 factors are the most important for all fault locations. The factor x_1, has the

largest mean of its elementary effect, which indicates that the measurement algorithm is the most sensitive to the uncertainty of this factor. In addition x_1 , has large variance of its elementary effect. Therefore, we can conclude that the contribution of x_1 to measurement error variance is not only through its own variability but also via interaction with other factors.

From the figure 6.8, the Morris method reduced the factor space dimension from 14 to 4. This dimension can be successfully handled by the GSA based on quasi-random sampling. We simulated, using DIgSILENT, 5 phase A to ground faults at distances 0.2 p.u., 0.4 p.u., 0.6 p.u., 0.8 p.u. and 1 p.u. of the line in Figure 6.1. For each fault we varied 4 dominant factors a large number of times according to the quasi-random sampling scheme implemented in SIMLAB. For all those simulated cases, we computed the performance index (i.e., absolute value of the difference between true and estimated values). In this experiment the SEL-421 fault impedance measurement function has been tested. The sensitivity indices computed in SIMLAB are shown in Figure 6.9 – Figure 6.10. The conclusions from this analysis are:

- Fault resistance, $R_F(x_1)$, has the highest impact on the uncertainty of the fault impedance measurement for all of the fault locations. The impact is more prominent, relative to the impact of other factors, for faults close to the beginning and at the end of the line.
- Impact of the zero-sequence impedance $Im\{\underline{Z}_{0L}\}$ (x_{14}), is the second largest and it is the highest for the faults in the middle of the line.
- Impact of the load flow angle δ_F(x_2), and the positive-sequence line impedance $Im\{\underline{Z}_{1L}\}$ (x_{12}), will grow as the distance to the fault approaches the remote line end.
- Effect of the interaction between R_F and δ_F is the highest for the faults at the remote line side and the lowest for the faults at the line beginning.
- Effect of the interaction between R_F and $Im\{\underline{Z}_{0L}\}$ is the highest for faults in the middle of the line.

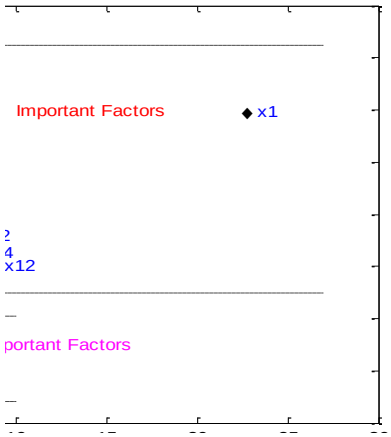

Figure 6.8: Results of the Morris factor screening method for a single-phase short circuit at 80% of the line in Figure 6.1.

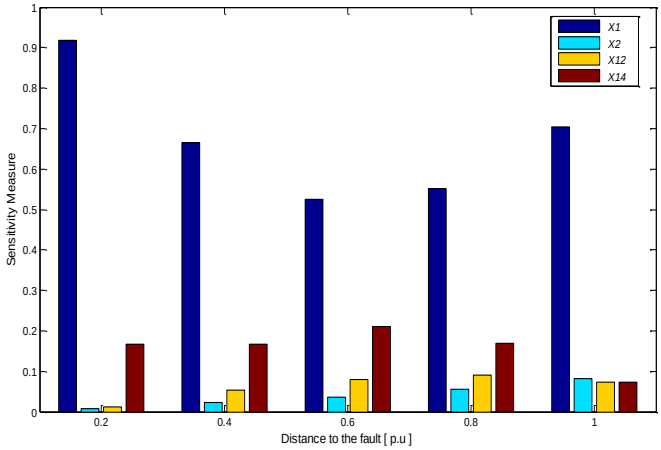

Figure 6.9: Main effects in function of the fault position obtained by using the GSA procedure for four-dimensional factor space.

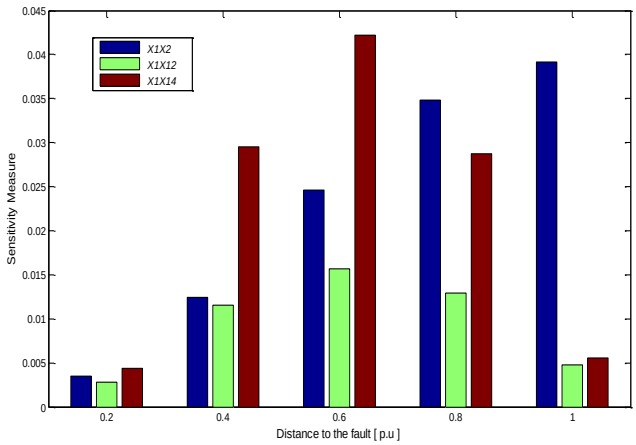

Figure 6.10: Interaction effects in function of the fault position obtained by using the GSA procedure for four-dimensional factor space.

6.2. Case study II: Double Lines with Two Sources Model

6.2.1. Description of the Case Study

This case study presents an application of the GSA method for testing the SEL-421 impedance measurement algorithm implemented on a single transmission line in a system with two lines on the same tower. One-ended fault impedance estimation has been tested. Figure 6.11 shows parallel transmission lines and includes the uncertainty factors of the system with the fault simulated at fault location F. The positive sequence fault-loop impedance, looking into the fault located at F, is estimated where the voltage and current signals are measured by the IED located at one ended, and is used as input to the IED.

In parallel transmission lines significant inductive and capacitive coupling exist between two parallel lines running on the same towers [80]. The coupling effect in those so called "double lines", if not considered appropriately, will introduce additional errors in the impedance measurement at a relay point. Consequently, the distance protection element of the IED can operate improperly, especially for the faults on the border of the protection zone [81]. A systematic methodology is required to test the effect of mutual coupling on the measurement algorithm output

For a single phase to ground fault at the fault point F, in Figure 6.11, a number of factors shown in red, will have impact on the performance of the impedance measurement algorithm and the distance protection element of the SEL-421 IED. These factors are: zero-sequence current compensation factor, $\underline{k}_0$, fault resistance, R_F, S-side sequence-component impedance, $\underline{Z}_S$, R-side sequence-component impedance, $\underline{Z}_R$, and phase angle between S and R sources, δ_F. The individual effects of the mentioned parameters on the relay reach have been studied previously by considering the effect of the uncertainty of one parameter at a time [56, 81]. This approach does not take into account contributions coming from interactions between two or more parameters to the total estimation of error variability. To completely explain the estimation error variability a methodology is required which considers all uncertain parameters taken simultaneously.

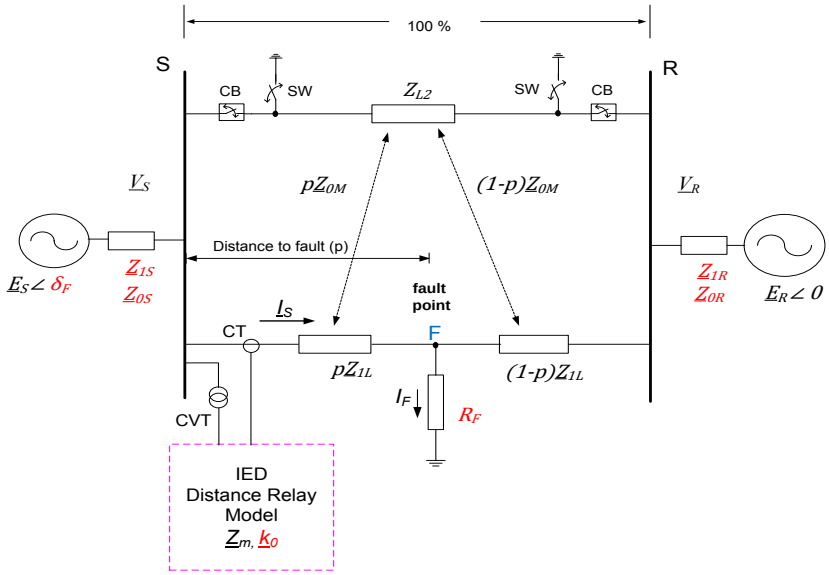

Figure 6.11: Circuit diagram of the faulted system with uncertain factors shown in red.

From Equation (3.50) to Equation (3.53), it can be shown that the measured apparent fault impedance $\underline{Z}_m$, which computed from the measuring phasor of the bus voltage, $\underline{V}_S$, and compensated current, $\underline{I}_S^c$, will contain uncertain values, $\Delta\underline{V}_S$, and $\Delta\underline{I}_S^c$. These random values will impact on the accuracy of the fault impededance calculation, as we can see by analyzing Equation (3.47), and Equation (3.49): $\Delta\underline{V}_S = \Delta\big(p\underline{Z}_{1L}\big[\underline{I}_S + \underline{k}_0\underline{I}_{0AS} + \underline{k}_{0M}\underline{I}_{0p}\big] + 3R_F\underline{I}_F\big)$, and $\Delta\underline{I}_S^c = \Delta\big(\underline{I}_S + \underline{k}_0\underline{I}_{0AS} + \underline{k}_{0M}\underline{I}_{0p}\big)$. A number of uncertain factors, indicated in red in Figure 6.11, and zero-sequence mutual coupling $\underline{Z}_{0M}$, will have impact. The investigation of how the uncertainty factors including zero-sequence mutual coupling $\underline{Z}_{0M}$, will impact the relay algorithm is presented in the following section.

6.2.2. Evaluation of Relay Algorithm Performance

To demonstrate the effect of the uncertain factors on the error in the impedance measurement we simulated a single-phase short circuit in the system of Figure 6.11 at different locations. The parameters for this case study are shown in Table A.2 of Appendix A. The external system is represented using Thevenin's equivalents comprising of voltage sources $\underline{E}_S$, and $\underline{E}_R$, and their corresponding impedances $\underline{Z}_S$, and $\underline{Z}_R$. We simulated phase A to ground fault at point F via resistence R_F.

This case study investigates the fault impedance measurement at terminal S, for the fault at F, based on zero-sequence current compensation (via a factor $\underline{k}_o$). The algorithm setting does not includes the effect of zero-sequence mutual coupling compensation $\underline{k}_{0M}$. To demonstrate the effect of the zero-sequence mutual coupling $\underline{Z}_{0M}$, the impedance measurement error, as a function of distance to fault, and for three different modes of operation, is presented using fixed system parameters and $R_F = 0\ \Omega$. As shown in Figure 6.12, the impedance measurement error depends on the mode of operation of the parallel line and fault location. When the parallel line is disconnected at both ends and not grounded, the zero-sequence current from parallel line $\underline{I}_{0p}$, is zero. Hence, the results are the same as in the case when the two lines are not coupled. However, if both lines are in operation or if the parallel line is not loaded but grounded, the zero-sequence mutual coupling will contribute to the error. It is apparent in the figure that the error will increase as a distance to fault increases.

Figure 6.13 and Figure 6.14 show the impedance measurement error in function of fault resistance R_F, and the correction factor $\underline{k}_o$. These study results are for the mode when both lines are loaded (i.e., both lines are active). The combined effect of fault resistance, R_F, and zero-sequence mutual coupling $\underline{Z}_{0M}$, is shown in Figure 6.13. For high values of fault resistance, the measurement error will increase especially for faults close to the remote side of the transmission line. Measurement error in function of variation of $\underline{k}_o$ in the specified interval (see Table 6.2) is shown in Figure 6.14. It can be seen from Figure 6.14 that for a value smaller than the mean value, the measurement error increases faster with the increase of distance to the fault.

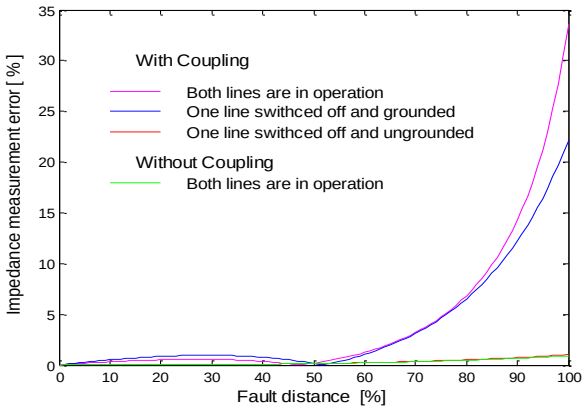

Figure 6.12: Measurement error for three operational modes and different distances of fault location, $R_F = 0\ \Omega$.

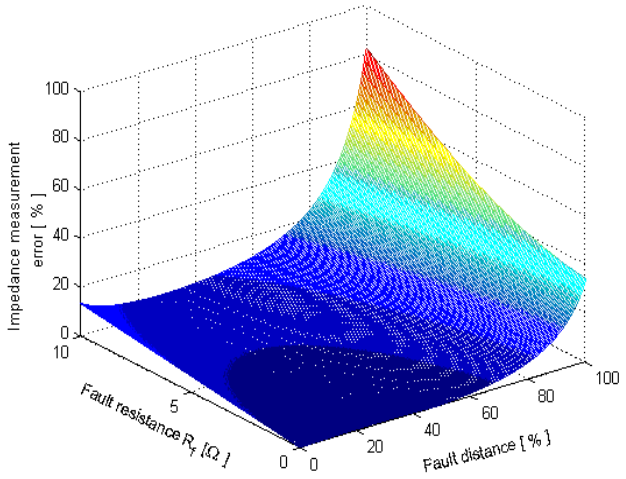

Figure 6.13: Measurement error due to uncertainty of the factor, R_F, and zero-sequence mutual coupling (two line are active).

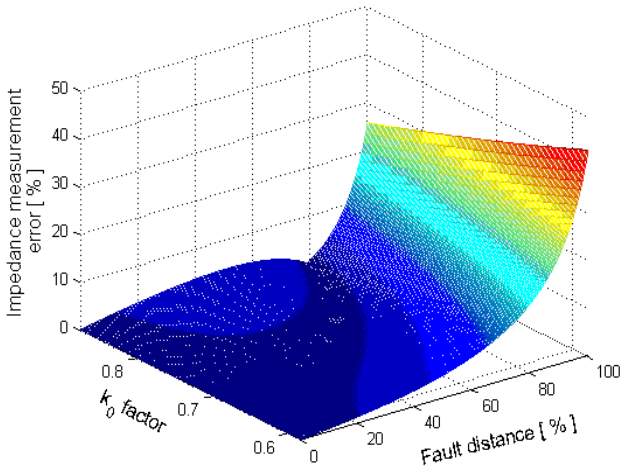

Figure 6.14: Measurement error due to uncertainty of the factor, $\underline{k}_o$, and zero-sequence mutual coupling (two line are active and $R_F = 0\ \Omega$).

As defined in Figure 6.11, we have in total of 11 uncertain factors, and this is considered as a high-dimensional factor space. To illustrate the effect of parameter uncertainty on the algorithm performance, we simulated the faults at different locations and for each fault we draw 500 random samples from the factor space $\mathbf{x} \in \boldsymbol{R}^{11}$, and use them in the Morris screening method. These uncertain factors, which are indicated in red in Figure 6.11, and their assumed intervals of variation that affect the fault impedance measurement, are listed in Table 6.2. For each sample, the SEL-421 IED algorithm estimates the fault impedance. This estimation point is shown using '+' in Figure 6.15(a),

and Figure 6.15(b), when two lines are active and when a parallel line is switched off and ungrounded. The figures show how the uncertainty in the parameters propagate through the algorithm, and as a result, we get uncertainty at the output (shown as clouds of '+'). It is apparent from this figure that the effect of the uncertainty of parameters for the fault at 70% of the line length will make the relay see some faults which are in Zone 2, as faults in Zone 1 (80%).

Table 6.2: Uncertain factors and their assumed intervals of variation that are affecting fault impedance measurements for the single-phase to ground faults in Figure 6.11.

Uncertain parameter	Description	Variation interval
x_1	R_F	[0;10]Ω
x_2	δ_F	[-10;10] deg.
x_3	$\underline{k}_o$	[0.5824; 0.8736]
x_4	$Re\{\underline{Z}_{1S}\}$	[2.3535;2.8765]Ω
x_5	$Im\{\underline{Z}_{1S}\}$	[26.901;32.879]Ω
x_6	$Re\{\underline{Z}_{0S}\}$	[1.5687;1.9173]Ω
x_7	$Im\{\underline{Z}_{0S}\}$	[17.9316;21.9164]Ω
x_8	$Re\{\underline{Z}_{1R}\}$	[2.3535;2.8765]Ω
x_9	$Im\{\underline{Z}_{1R}\}$	[26.901;32.879]Ω
x_{10}	$Re\{\underline{Z}_{0R}\}$	[1.5687;1.9173]Ω
x_{11}	$Im\{\underline{Z}_{0R}\}$	[17.9316;21.9164]Ω

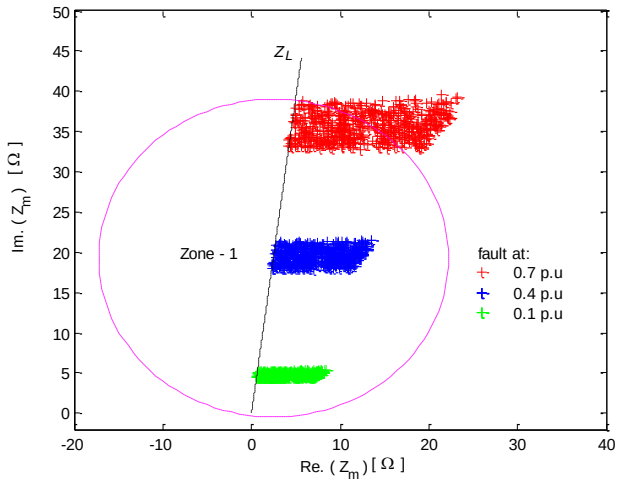

Figure 6.15a: Fault impedance measured for all samples of the input factors, $\mathbf{x} \in \boldsymbol{R}^{11}$, generated according to the random sampling method (total of 500 samples) for three different fault locations (the parallel line is loaded).

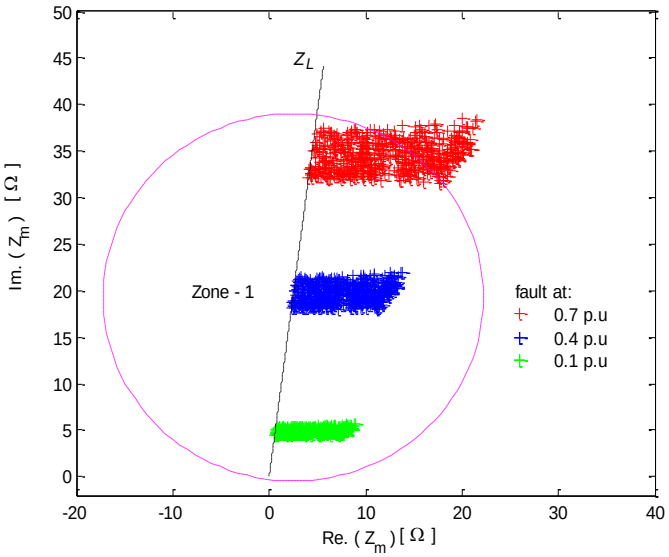

Figure 6.15b Fault impedance measured for all samples of the input factors, $\mathbf{x} \in \boldsymbol{R}^{11}$, generated according to the random sampling method (total of 500 samples) for three different fault locations (the parallel line is not loaded and ungrounded).

6.2.3. Test Result and Discussion

To study the performance of the fault impedance algorithm, we use the DIgSILENT software environment [17] for simulating phase-A to ground faults at different locations on the protected line, as shown in Figure 6.11, and for variations of parameters. We assume that possible values of the parameters are uniformly distributed within the intervals specified in Table 6.2.

Typical results of the factor pre-screening, based on the Morris method, are shown in Figure 6.16. The results are for the fault at the remote end of the line with all three modes of operation of the parallel line.

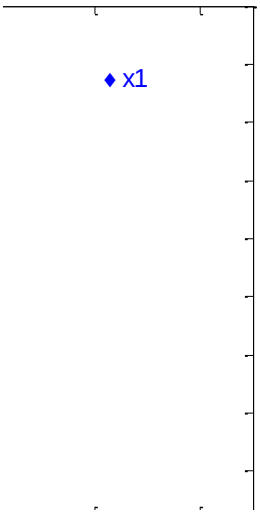

Figure 6.16: Results of the Morris method for all three operational modes of the parallel line.

This method uses the variable of standard deviation versus mean value for all elementary effects. These statistics are computed using 120 samples, which are considered sufficient for this number of factors [16, 76, 77]. A large mean value corresponds to factor importance, and a large variance suggests that the impact of a factor together with another factor is important (i.e., interaction effect). In Figure 6.16, for all three operation modes of parallel line, we can identify the following factors as dominant: x_1 (R_F), x_2 (δ_F), and $x_3(\underline{k}_0)$. Because x_1 has large variance of its elementary effect, we can conclude that the contribution of x_1 to measurement error variance is not only through its own uncertainty but also via interaction with other factors. The identified 3 factors are the most important for all simulated fault locations and all three operational modes of the parallel line.

From the figure, the Morris method reduced the factor space dimension from 11 to 3. This dimension can be successfully handled by the GSA based on quasi-random sampling. We simulated, using DIgSILENT, 5 phase A to ground faults at distances 0.2 p.u., 0.4 p.u., 0.6 p.u., 0.8 p.u., and 1 p.u., of the protected line, S-R, in Figure 6.11. For each fault we varied 3 dominant parameters according to the quasi-random sampling scheme. For all those simulated cases, we compute the performance index for the IED fault impedance measurement function [15]. The sensitivity indices computed in SIMLAB are shown in Figure 6.17 and Figure 6.18. The conclusions from this analysis are:

- The individual effect of fault resistance, $R_F(x_1)$, has the highest impact on the uncertainty of the fault impedance measurement for most of the fault locations and for all three operational modes of the parallel line.
- Impact of $\underline{k}_0$ (x_3) dominates for the faults at 0.6 p.u. of the line.
- Impact of power flow angle, δ_F (x_2), will increase as the fault location moves away from the IED.
- Effect of the interaction between R_F and $\underline{k}_0$ (x_1, x_3) is the highest among interaction effects.
- Interaction impact between R_F and the power flow angle (x_1, x_2) will increase as the fault location moves away from the measurement point S.

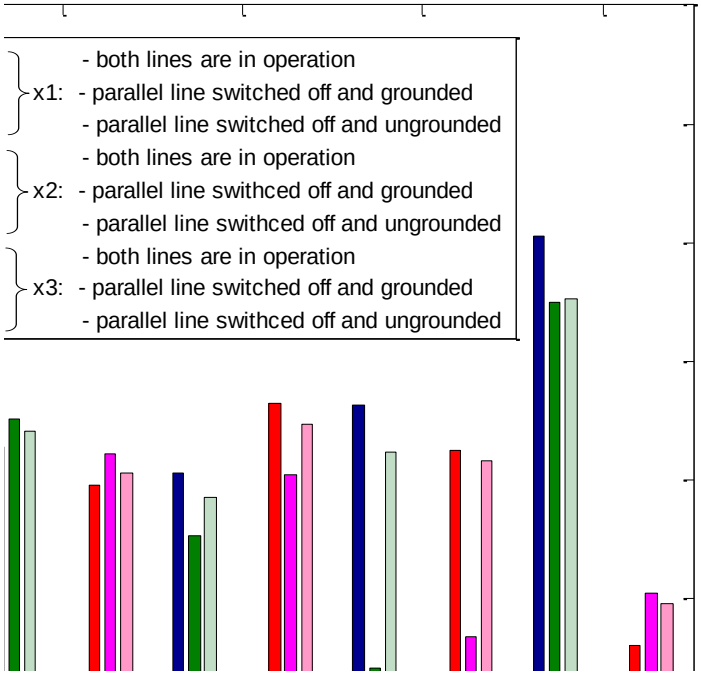

Figure 6.17: Main effects in function of the fault position obtained by using the GSA procedure for three-dimensional factor space.

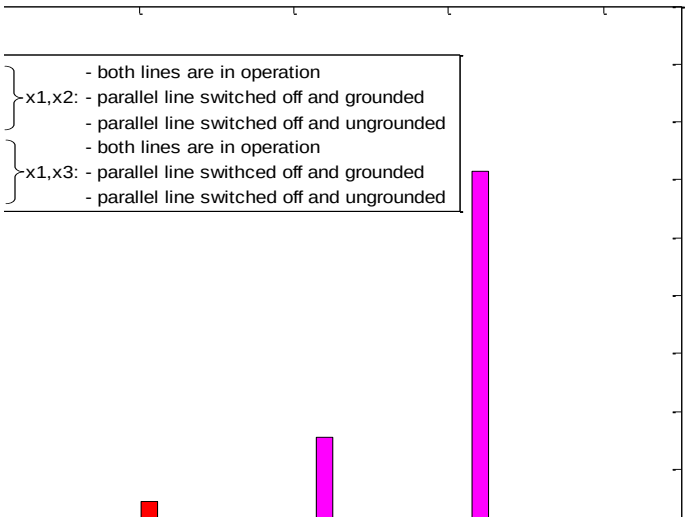

Figure 6.18: Interaction effects in function of the fault position obtained by using the GSA procedure for three-dimensional factor space.

6.3. Case study III: Three-Terminal Line

6.3.1. Description of the Case Study

This case study presents test methodology of one-ended impedance-based fault distance calculation implemented in SEL-421 IED when applied on the three-terminal transmission line. Figure 6.19 illustrates three-terminal lines, including the uncertainty factors of the system, with the faults simulated at fault locations F_1, and F_2. Using the same method as in the previous section, the positive sequence fault-loop impedance, by looking into the fault located at F_1 and F_2, is estimated using voltage and current signals, measured by the IED located at the S-terminal.

Direct tapping of a transmission line is one of the alternatives used in the transmission line circuit and often considered for cost efficiency reason. However, this structure will affect a non-pilot digital distance relay installed for protecting original two-terminal line. Load current from the tapped line, in this case, will impact the fault impedance measurement at a relay point, and as a consequence, relay underreach and overreach situations become possible [80, 82]. Uncertain, and unknown values of some parameters

(e.g., fault resistance, ground resistance) will introduce additional errors in impedance measurement as well as the determination of in which zone the fault lies [56]. The limitations of using a non-pilot distance relaying for three terminal lines has been investigate in [33] using local one factor at the time approach, but a systematic global approach for quantifying these limitations have not been proposed before.

For a single phase to ground fault, shown in Figure 6.19, located either in the first section S-O before the tapped line (fault location F_1), or in the second section O-R after the tapped line (fault location F_2), the various factors, indicated in red in this figure, will influence the fault impedance measurement. Sensitivity analysis can be used to assess the effect of those factors to the performance of a relay measurement algorithm [56]. In this case study, we apply the Global Sensitivity Analysis (GSA) technique based on the estimation of variance through the Quasi-Monte Carlo (QMC) sampling in the multi-dimensional factor space, and is implemented in SIMLAB. A large number of samples are required for the GSA computational process. To speed up computation, pre-processing using the Morris method [70] is required to reduce the factor space dimension. The mathematical model of the three terminal lines under fault conditions, and the fault-loop measurement element, is implemented in the Intelligent Electronic Device (IED). The model of SEL-421 multifunctional IED [15] is implemented using the DIgSILENT *PowerFactory* simulation environment [17]. To implement the GSA, the DIgSILENT scripting language (called DPL) is used to automatically vary the values of the factors in the three-terminal line model and run simulations for each scenario (i.e., sample).

We can find out, using Equation (3.62a) to Equation (3.64), that the apparent fault impedance, $\underline{Z}_m$, is computed using the measured phasor of bus voltage, $\underline{V}_S$, and compensated current, $\underline{I}_S^c$. Based on Figure 6.19, the voltage and compensated current, measured at the relaying point, are not affected by the current from the tapped line when the fault occurs in section 1.

Voltage $\underline{V}_S$, and compensated current $\underline{I}_S^c$, measured at relaying point during a fault in section 1 and section 2 contain random data, which correspond to $\Delta\underline{V}_S$ and $\Delta\underline{I}_S^c$. These random data are affected by the uncertain factors indicated in red in Figure 6.19. For the fault in section 2, where the random data are influenced not only by uncertain factors which are listed in Table 6.3, but also affected by the current infeed from the tapped line, and they can be composed as $\Delta\underline{V}_S = \Delta\left(\underline{Z}_{1L1}\underline{I}_S^c + p_2\underline{Z}_{1L2}\underline{I}_S'^c + 3R_F\underline{I}_F\right)$, and $\Delta\underline{I}_S'^c =$

$\Delta\left(\underline{I}_{ST} + k_0'\underline{I}_{0ST}\right)$. These random data are influenced by the uncertain factors, indicated in red in Figure 6.19, will impact on the accuracy of the fault impedance measurement, $\underline{Z}_m$.

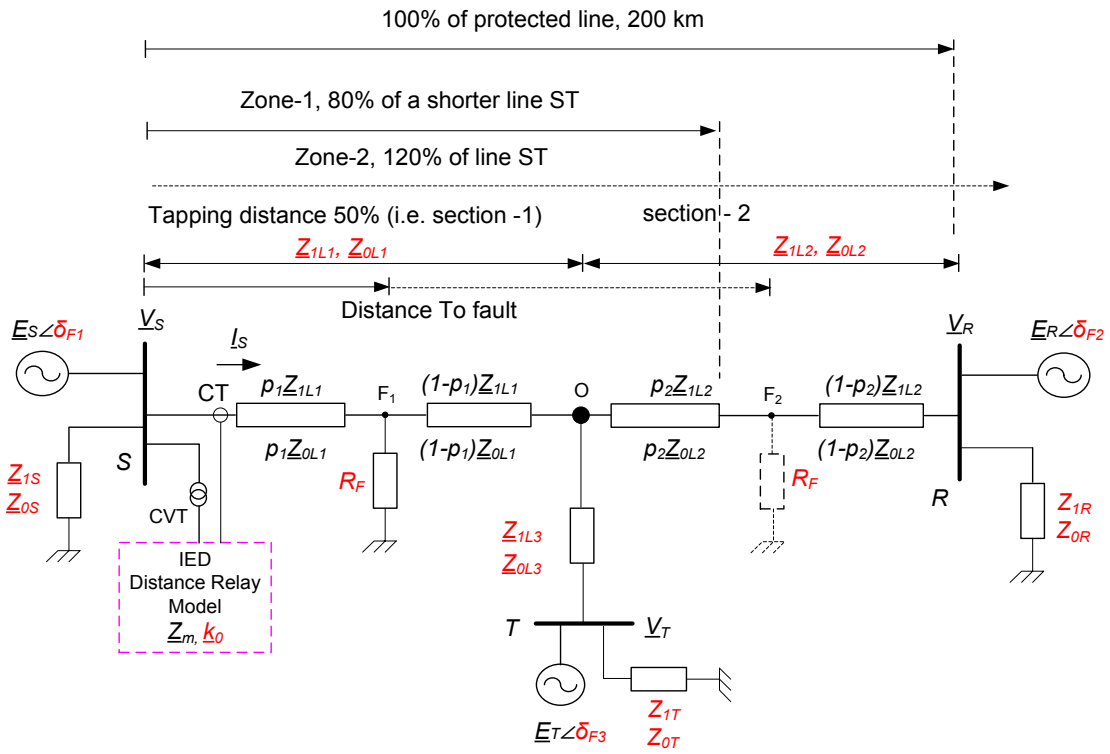

Figure 6.19: Circuit of the faulted system with uncertain factors printed in red.

6.3.2. Evaluation of Relay Algorithm Performance

A faulted three-terminal transmission line and distance relay location is shown in Figure 6.19. All elements in this figure are modelled in the DIgSILENT software environment. The proposed model is used to determine the performance of the distance relay for the phase A to ground with different fault locations F_1, and F_2, and through a fault resistance, R_F. The model includes a set of uncertain factors as indicated in red in Figure 6.19. The performance index values, which are calculated by the impedance measurement algorithm of the IED, are based on the produced signals of the corresponding fault scenarios.

In Figure 6.19, the external system is modelled using Thevenin's equivalent with three sources $\underline{E}_S$, $\underline{E}_R$, and $\underline{E}_T$, and corresponding source impedances $\underline{Z}_S$, $\underline{Z}_R$, and $\underline{Z}_T$. During the fault, the fault impedance calculated by relaying point is based on the zero-sequence

current compensation method using a factor, $\underline{k}_0$ [66]. The factor $\underline{k}_0$, depends on the zero-sequence impedance $\underline{Z}_{0L1}$, which is not known exactly. For the fault in section 2 (between O and R in Figure 6.19), the fault impedance is more complex since the current infeed from tapped line will influence the fault impedance calculation.

The case of a single line to ground fault (phase A) between tapped line and remote end (fault F_2 in Figure 6.19) is more complex. The circuit diagram in Figure 3.16 shows the sequence component networks and specifies which factors will impact the impedance measurement.

To demonstrate the effect of the factors on the error in impedance measurement we simulate different faults in the system in Figure 6.19 using network parameters shown in Table A.3 of Appendix A. Zone 1 is set at 80% of the positive sequence line impedance, comprised of section 1 (between S and O in Figure 6.19), as well as the additional length of the tapped line (section O to T in Figure 6.19). Line impedances per unit length in all sections are equal. This is a typical setting because section O to T is shorter than the segment O to R [15, 83]. Figure 6.20 shows impedance measurement tracking during a single phase short circuit at the border of Zone 1 in the section between O and R in Figure 6.19. In this case, the estimated impedance is not only affected by the fault resistance but also by the infeed current from the tapped line. The effect is quite considerable, as can be seen in Figure 6.20, and the error is higher when the fault is through resistance, $R_F = 10\ \Omega$.

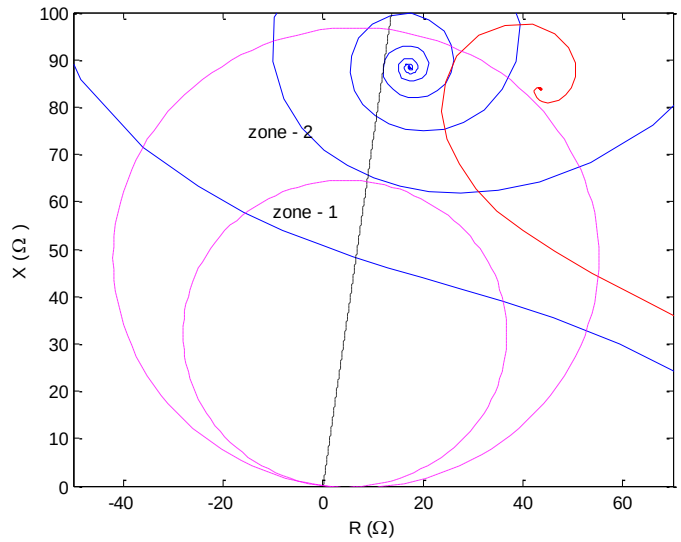

Figure 6.20: Impedance tracking for the fault at the border of Zone 1. The blue line is for the case where $R_F = 0$, and the red line is for the case where $R_F = 10\ \Omega$.

It can be seen in Figure 6.21, when the fault in Figure 6.19 occurs in a deferent section through arc resistance of up to 500 Ω using the same parameters of the system. The apparent impedance is split between measured resistance, *R*, and reactance, *X*. Simulation results indicate that measured *R*, and *X*, are both affected not only by different fault location but also fault resistance, and by changing parameter values of the system. It may be observed, from Figure 6.22, that the effect of the high resistance in different sections places the measured impedance within a different region of the R-X plane.

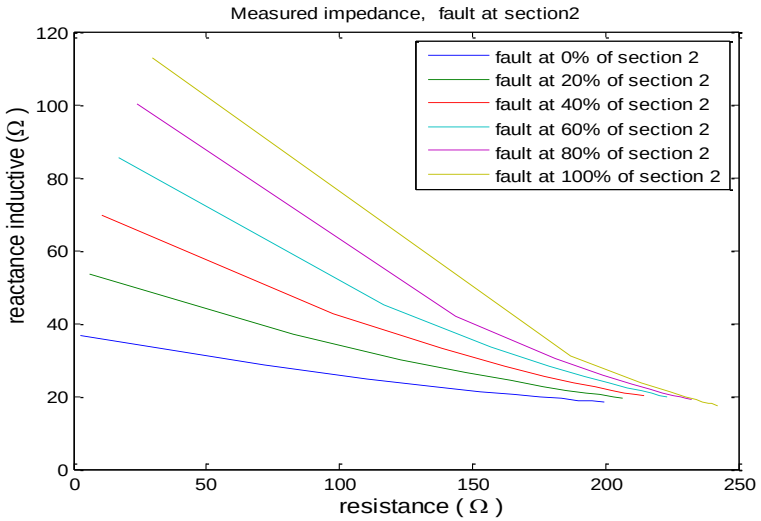

(a)

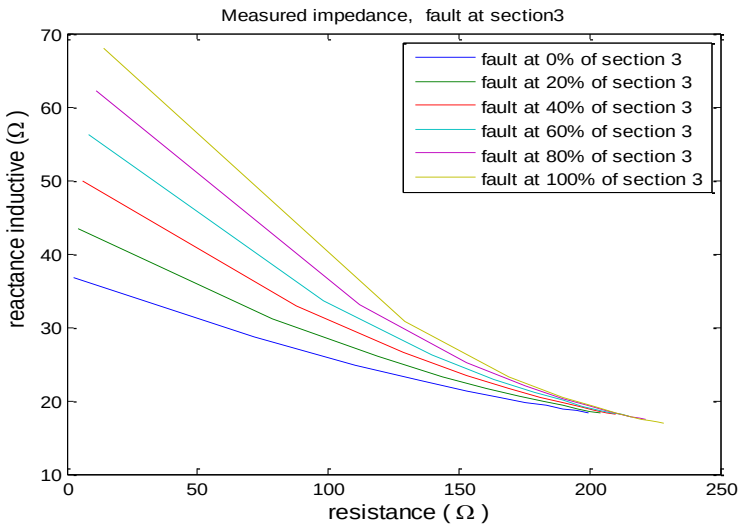

(b)

Figure 6.21: Measured fault impedance from different fault sections:
(a) A fault in section 2 (R_F varying from 0% to 500%),
(b) A fault in section 3 (R_F varying from 0% to 500%).

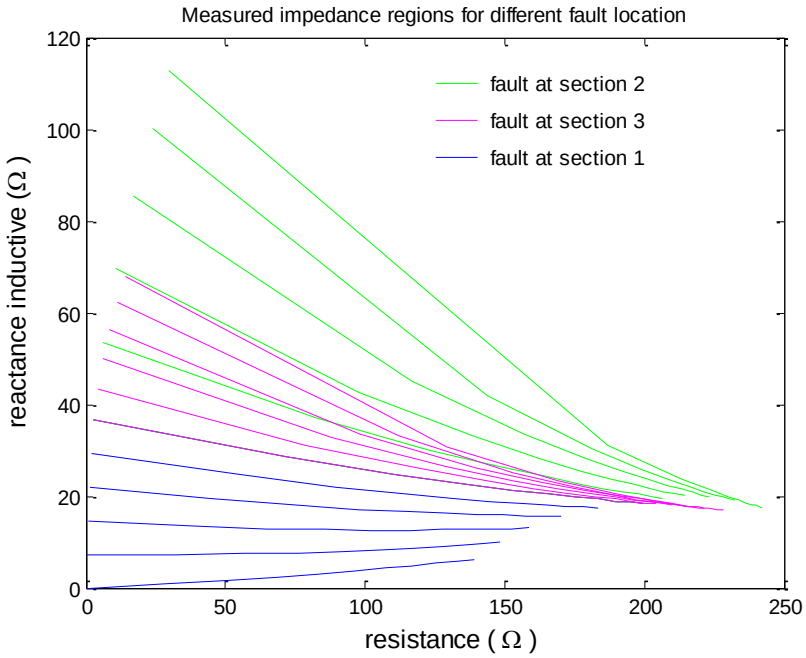

Figure 6.22: Measured impedance region from different fault sections.

In real-life applications the exact parameters are not known. Therefore, Table 6.3 specifies intervals of variation of the selected parameters (i.e., factors) that can affect the performance of the algorithm. In total we have 29 factors, and this is considered a high-dimensional factor space. To illustrate the effect of the parameter uncertainty on the algorithm performance, we simulated three faults at different locations, and for each fault we draw 500 random samples from the factor space. For each sample the IED algorithm estimated the fault impedance. These estimates are shown using '+' in Figure 6.23. The following three fault locations were studied: fault in the section S-O (Figure 6.19) at 40 % of the Zone 1, and two faults in the section O-T at 65 % (just after the point O), and at 80 % of the Zone 1. Figure 6.23 shows how uncertainty in the parameters propagate through the algorithm, and as a result we get uncertainty at the output (shown as clouds of '+'). It is apparent from this figure that the uncertainty of parameters, for this configuration with line tapping, will make the relay see some faults, which are in Zone 1, as faults in Zone 2, and even in Zone 3. There is a systematic error (i.e., bias) which can be corrected by adaptive change of the relay settings and precision error which is a result of unobservable uncertain parameters. In this work, we only discuss precision error.

To quantify the algorithm performance due to uncertainty we will use a sampling based technique to compute estimation error variance and bias. It is important to note that

for the factor space of dimension 29, we require a huge number of samples for accurate variance calculation. Hence, to make this technique practical, we use factor screening with a deterministic sampling scheme to reduce the dimension of the factor space, and then, instead of pseudo-random sampling, we employ more economical quasi-random sampling. In addition, based on the same sampling technique, it is possible to estimate the sensitivity of error to each of the factors as well as to interaction of two or more factors.

Table 6.3: Uncertain factors and their assumed intervals of variation that are affecting fault impedance measurements for the single-phase to ground faults in Figure 6.19.

Uncertain parameter x_i	**Description of x_i**	**Interval of variation**
x_1	R_F	[0;10]Ω
x_2	δ_{F1}	[-10;10] deg.
x_3	δ_{F2}	[-10;10]deg.
x_4	δ_{F3}	[-10;10]deg.
x_5	$\underline{k}_o$	[0.57;0.856]
x_6	$Re\{\underline{Z}_{0SM}\}$	[2.3535;2.8765]Ω
x_7	$Im\{\underline{Z}_{0SM}\}$	[26.901;32.879]Ω
x_8	$Re\{\underline{Z}_{1SM}\}$	[1.5687;1.9173]Ω
x_9	$Im\{\underline{Z}_{1SM}\}$	[17.9316;21.9164]Ω
x_{10}	$Re\{\underline{Z}_{0SN}\}$	[2.3535;2.8765]Ω
x_{11}	$Im\{\underline{Z}_{0SN}\}$	[26.901;32.879]Ω
x_{12}	$Re\{\underline{Z}_{1SN}\}$	[1.5687;1.9173]Ω
x_{13}	$Im\{\underline{Z}_{1SN}\}$	[17.9316;21.9164]Ω
x_{14}	$Re\{\underline{Z}_{0ST}\}$	[2.3535;2.8765]Ω
x_{15}	$Im\{\underline{Z}_{0ST}\}$	[26.901;32.879]Ω
x_{16}	$Re\{\underline{Z}_{1ST}\}$	[1.5687;1.9173]Ω
x_{17}	$Im\{\underline{Z}_{1ST}\}$	[17.9316;21.9164]Ω
x_{18}	$Re\{\underline{Z}_{0L1}\}$	[20.77;25.388]Ω
x_{19}	$Im\{\underline{Z}_{0L1}\}$	[138.024;168.696]Ω
x_{20}	$Re\{\underline{Z}_{1L1}\}$	[5.616;6.864]Ω
x_{21}	$Im\{\underline{Z}_{1L1}\}$	[44.136;53.944]Ω
x_{22}	$Re\{\underline{Z}_{0L2}\}$	[20.77; 25.388]Ω

x_{23}	$Im\{\underline{Z}_{0L2}\}$	[138.024;168.696]Ω
x_{24}	$Re\{\underline{Z}_{1L2}\}$	[5.616; 6.864]Ω
x_{25}	$Im\{\underline{Z}_{1L2}\}$	[44.136; 53.944]Ω
x_{26}	$Re\{\underline{Z}_{0L3}\}$	[14.539;17.7716]Ω
x_{27}	$Im\{\underline{Z}_{0L3}\}$	[96.6168;118.087]Ω
x_{28}	$Re\{\underline{Z}_{1L3}\}$	[3.9312;4.8048]Ω
x_{29}	$Im\{\underline{Z}_{1L3}\}$	[30.8952;37.7608]Ω

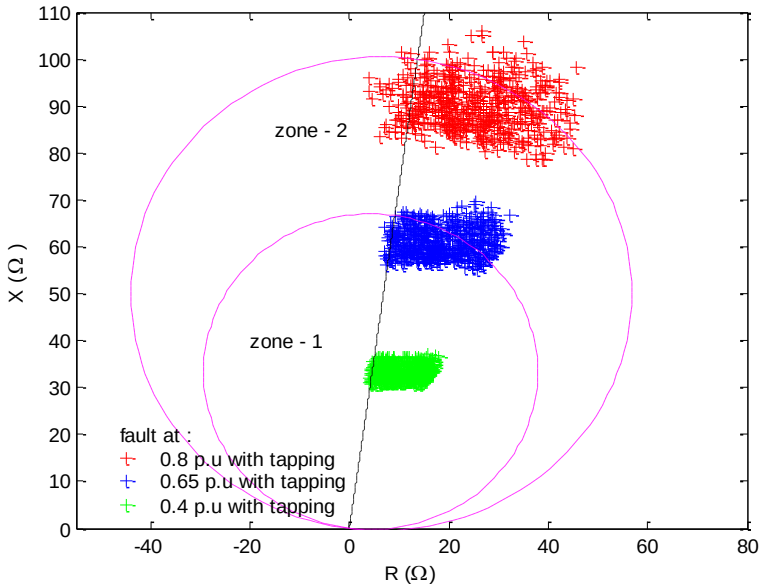

Figure 6.23: Fault impedance measured for all samples of the input factors, $\mathbf{x} \in \boldsymbol{R}^{29}$, generated according to the random sampling method (total of 500 samples) for three different fault locations.

6.3.3. The Test Result and Discussion

Using the DIgSILENT software environment, we simulated phase-A to ground faults at different locations in the system, as shown in Figure 6.19, and for variations of parameters specified in Table 6.3. The faults were simulated in section 1 (S-O in Figure 6.19). We assumed that possible values of the parameters are uniformly distributed within the intervals specified in Table 6.3. The SEL-421 of IED model was implemented in DIgSILENT and the performance of the fault impedance measurement function of this IED was tested for all points in the factor space. These points were designed using the SIMLAB software environment according to Morris and Sobol's quasi-random sequences.

Typical results of the factor pre-screening based on the Morris method are shown in Figure 6.24. These results are presented as standard deviation versus mean value for all elementary effects. These statistics are computed using 120 samples, which is considered sufficient for this number of factors [16]. In Figure 6.24, we can identify the following factors as dominant: x_1 (R_F), x_2 (δ_{F1}), x_3(δ_{F2}), x_4(δ_{F3}), and $x_5(\underline{k}_0)$. Because x_1 has large variance of its elementary effect, we can conclude that the contribution of x_1 to measurement error variance is not only through its own uncertainty but via interaction with other factors. The representative result in Figure 6.24 is for the fault at 1p.u. of the line S-R length. The line S-R, with tap at O, in Figure 6.19 is composed of section 1 (S-O) and section 2 (O-R). The selected 5 factors are the most important for all simulated fault locations.

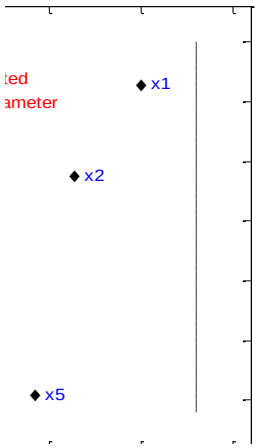

Figure 6.24: The Morris method results for a fault at 1 p.u. of the line S-R in Figure 6.19.

The Morris method reduced the factor space dimension from 29 to 5. This dimension can be successfully handled by the GSA based on quasi-random sampling. The optimal number of samples, according to SIMLAB, for dimension 5 is 65536. So we simulated, using DIgSILENT, 5 phase-A to ground faults at distance 0.2 p.u., 0.4 p.u., 0.6 p.u, 0.8 p.u. and 1 p.u. of the line S-R, and for each fault we varied 5 dominant parameters 65536 times according to the quasi-random sampling. For all those simulated cases, we compute the performance index for the IED fault impedance measurement function. The sensitivity indices computed in SIMLAB are shown in Figure 6.25 and Figure 6.26. The conclusion from this analysis, summarized in Figure 6.25 and Figure 6.26, would be:

- Zero-sequence correction factor $\underline{k}_0(x_5)$, has the highest impact on the uncertainty of the fault impedance measurement for the majority of fault locations.
- Impact of $R_F(x_1)$ and δ_{F1} (x_2) dominate $\underline{k}_0$ (x_5), for the faults on the end R of the line.
- The individual effect of fault resistance, R_F (x_1), is also high for all fault locations. The impact is more prominent, relative to the impact of other factors, close to the beginning of the section 1 (S-O) and at the line end R.
- Impact of power flow angles, $\delta_{F1}, \delta_{F2}, \delta_{F3}$, (x_2, x_3, x_4), will increase as the fault location moves away from the IED.
- Effect of the interaction between R_F and $\underline{k}_0$ (x_1, x_5) is the highest among interaction effects, but it is only dominant for the faults in the line section 1 (S-O).
- Interaction impact between R_F and the power flow angles ($x_1, x_2;$ $x_1, x_3;$ $x_1, x_4;$) will increase as the fault location moves away from the measurement point S.

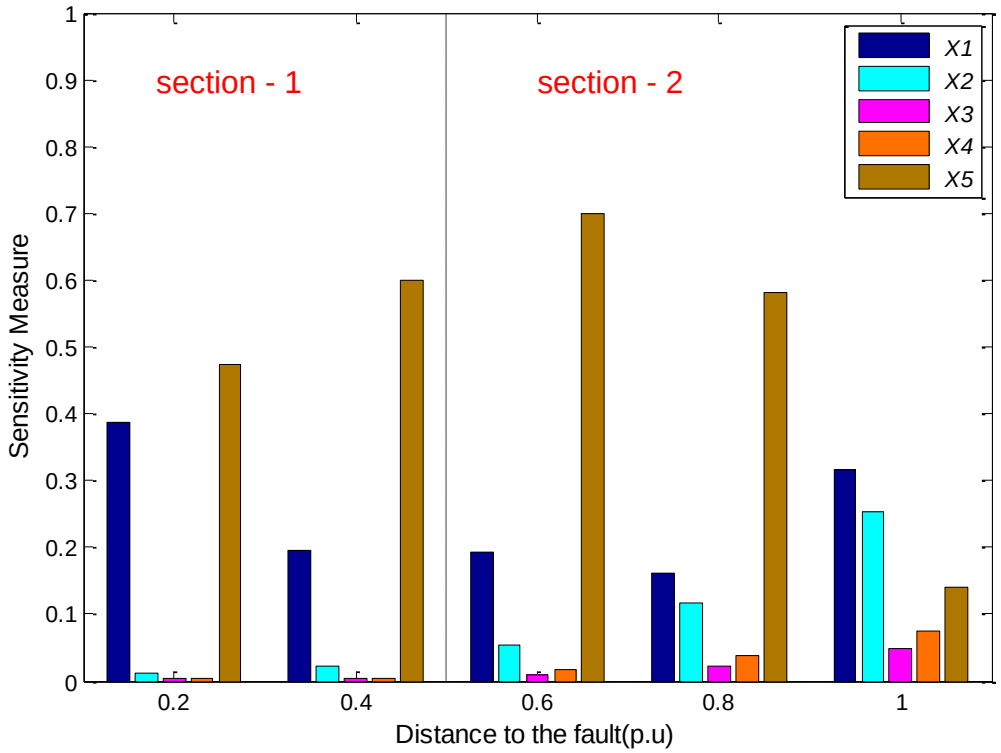

Figure 6.25: Main effects in function of the fault position obtained by using the GSA procedure for five-dimensional factor space.

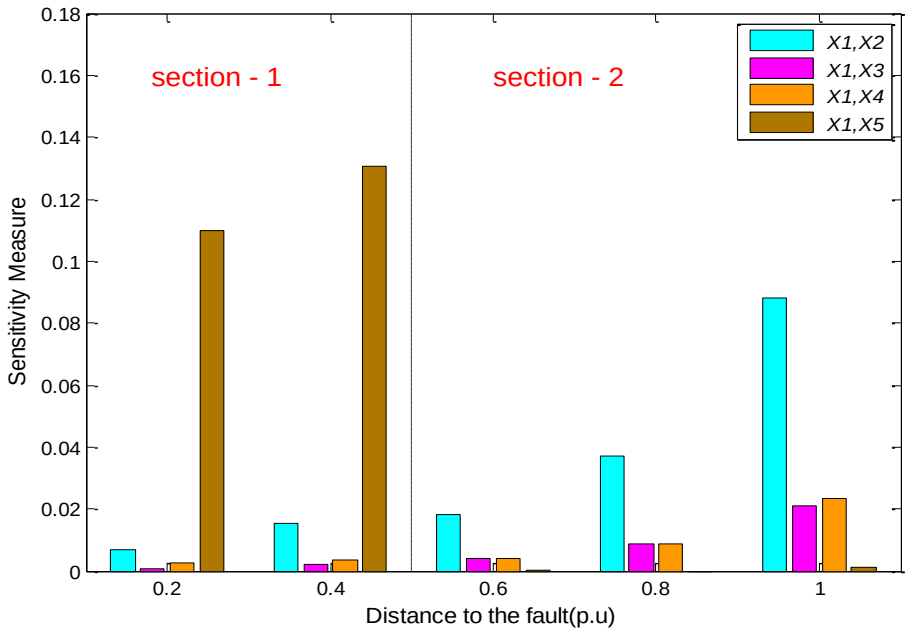

Figure 6.26: Interaction effects in function of the fault position obtained by using the GSA procedure for five-dimensional factor space.

6.4. Case study IV: Two Port of Transmission Line with Series Compensation

6.4.1. Description of the Case Study

Figure 6.27 illustrates the application of series compensation in a two source transmission line and shows the uncertainty factors of the system with the fault simulated at fault location F_1 and F_2. The positive sequence fault impedance is estimated using the voltage and current signals measured by the IED located at terminal S.

The application of series compensation on the transmission line, as shown in Figure 6.27, is one of the alternatives to increase the line's power transfer capability and also to improve system stability [49, 84]. However, the series capacitor, located in series with the protected line, can reduce the line inductance from X_L to the overall series line inductance, $X = X_L - X_C$. The apparent impedance that is seen from the relaying point appears electrically shorter [69].

The presence of series capacitor, SCs, with Metal Oxide Varistors, MOVs, in the protected transmission line create certain problems for relay algorithms for non-pilot distance relays [85]. In this case, the series compensation circuit (i.e., SCs+MOVs) can create unpredictable values of transient response. The status of the capacitors will affect the performance of the relay algorithm for the distance relay [28, 29].

In this section, we will explore the effect of the series capacitor protected with the metal oxide varistors located in the middle of the protected line (see Figure 6.27). Two different faults, located at F_1 and F_2, are simulated to observe the effect of series compensation to the accuracy of the fault impedance measurement. The voltage-current characteristic of MOV presented in Figure 6.28 is approximated as follows [68]:

$$i_{MOV} = P\left(\frac{\underline{V_C}}{\underline{V_{REF}}}\right)^q, \tag{6.1}$$

where:

P - Reference current (P =1000A),

$\underline{V_{REF}}$ - Reference voltage ($\underline{V_{REF}}$: 150 kV),

q - Exponent (q : 23).

During a fault, the MOVs start immediately to protect the series capacitor after the voltage across the capacitor $\underline{V_C}$, exceeds the voltage setting $\underline{V_{REF}}$. If the fault is in front of SCs (i.e., at location F_1), the presence of series-compensation does not affect the relay algorithm, and the fault impedance is measured accurately if the uncertain factors can be ignored. However, when the fault is behind the SCs, care must be taken since the series capacitor will affect the calculation of the apparent fault impedance [1]. Uncertain and unknown values of some parameters (i.e., fault resistance, inception angle, etc.) will introduce additional errors in impedance measurement at a relay point, and as a consequence overreach and underreach may occur during relay operation.

In Figure 6.27, the various factors indicated in red, will influence the fault impedance measurement during the single phase to ground fault located either in section 1 (fault location F_1) or in section 2 (fault location F_2). The sensitivity analysis will be used to assess the effect of those factors on the performance of a relay measurement algorithm. The GSA technique based on the estimation of variance through QMC sampling in the multi-dimensional factor space is applied. A number of samples generated using SIMLAB

are required for the GSA computation process. Pre-processing using the Morris method speeds up computation. It reduces the factor space dimension.

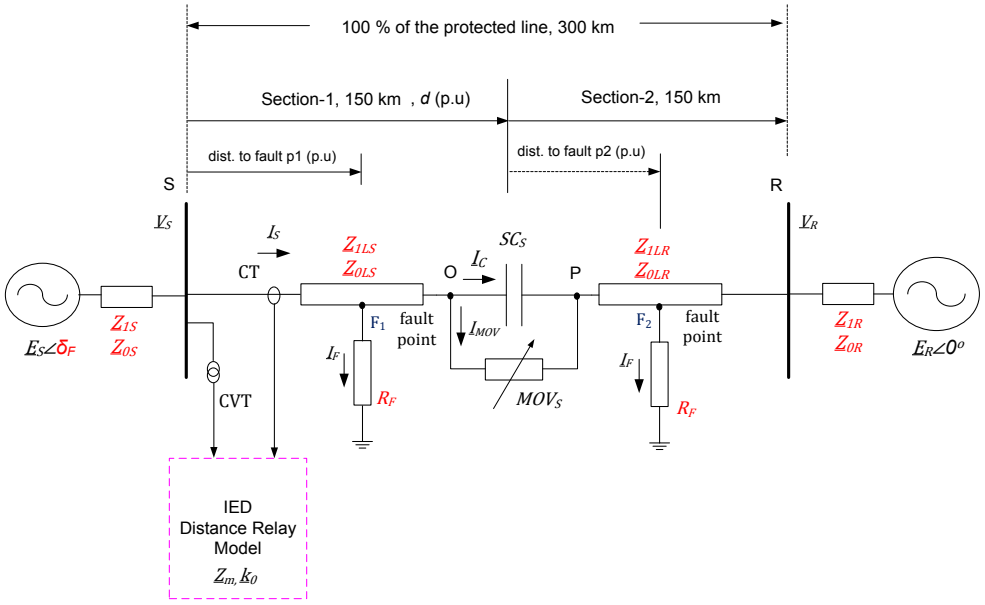

Figure 6.27: Two sources of series compensation with uncertain factors printed in red:
F_1 - fault location in front of $SCs + MOVs$,
F_2 - fault location behind $SCs + MOVs$.

We can conclude, from Equation (3.82a) to Equation (3.88), that the apparent fault impedance $\underline{Z}_m$, is computed using the measured phasor of bus voltage $\underline{V}_S$, and compensated current $\underline{I}_S^c$. In Figure 6.27, the voltage and compensated current measured at the relaying point during a fault in section 1 and section 2 contain uncertain values $\Delta\underline{V}_S$, and $\Delta\underline{I}_S^c$, which can be written as $\Delta\underline{V}_S = \Delta\left(\underline{Z}_{1LSR}\underline{I}_S^C + 3R_F\underline{I}_F + \underline{V}_C\right)$, and $\Delta\underline{I}_S^C = \Delta\left(\underline{I}_S + \underline{k}_0\underline{I}_{0S}\right)$. These random data are influenced by the uncertain factors (indicated in red in Figure 6.27). The series compensation will impact the accuracy of the fault impedance measurement $\underline{Z}_m$ as well. In this section the investigation will be applied to measure the effect of factors including series compensation on the performance of the relay algorithm.

6.4.2. Evaluation of Relay Algorithm Performacne

In Figure 6.29, the circuit diagram demonstrates the effect of fault impedance tracking using the mho characteristic for the phase A to ground fault simulated in front of the series capacitor, F_1, and behind the series capacitor, F_2, through the fault resistance R_F. The

proposed model includes a set of uncertain factors as indicated in red in Figure 6.27. The performance index values are calculated to assess the impedance measurement algorithm performance.

As shown in Figure 6.27, the series capacitor, with 70% of compensation protected with Metal Oxide Varistor (MOVs), is located in the middle of the protected line, and the connection of the series capacitor and MOVs, which can be represented by equivalent resistance, R'_C, and equivalence reactance, X'_C. From that figure, the characteristic of these two values depends on the current reactance $\underline{I_S}$, entering these two components. Two different analyses should be applied for the fault at F_1, and F_2, since the series capacitor system also affects the performance of the relay algorithm function.

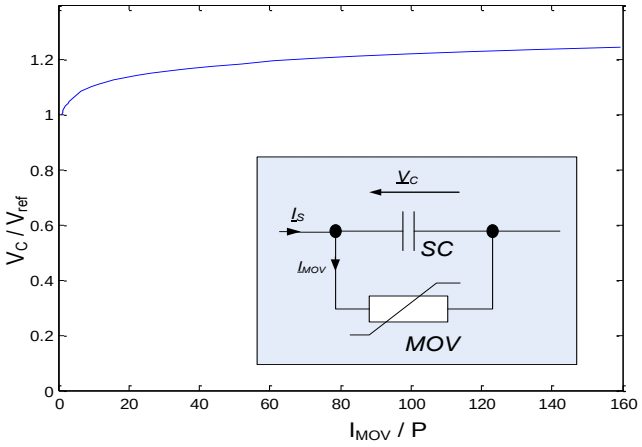

(a)

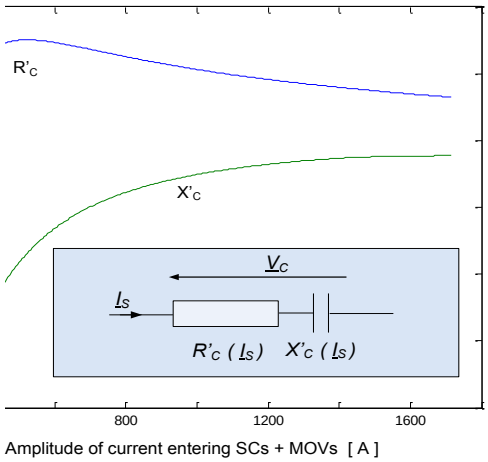

(b)

Figure 6.28: Equivalenting and characteristic of SCs and MOVs:
(a) The original device and $\underline{v}$-$\underline{i}$ characteristic of the MOV, (b) Equivalenting.

Fault in front of the series capacitor

Using the network parameters, as shown in Table A.4, Appendix A, Figure 6.29 shows the tracing, in time, of the measured impedance for the fault simulated in front of SCs located at 0.4 p.u, with $R_F = 10\ \Omega$, and $\delta_F = 0°$. The simulation shows how measured fault loop impedance, $\underline{Z}_m$, is affected by fault resistance, R_F, i.e., deviation from the actual impedance, $p\underline{Z}_{1LS}$. However, since the fault current, $\underline{I}_F$, in Figure 6.27, is fed from the two sources, the measured fault loop impedance, $\underline{Z}_m$, is sensitive to not only R_F, but also power flow angle, δ_F [7, 69].

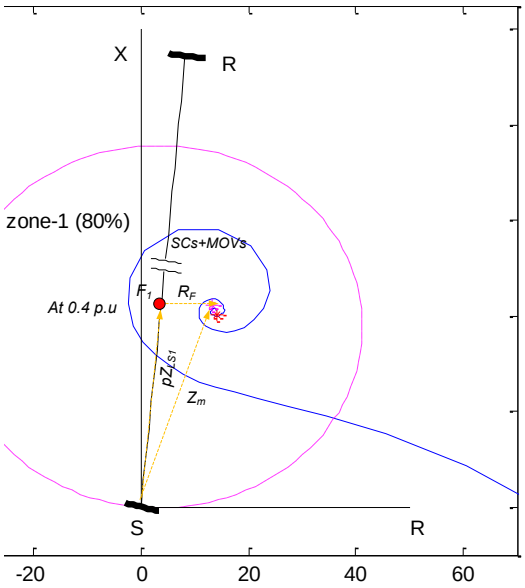

Figure 6.29: Fault Impedance tracking for the fault, F_1 at 0.4 p.u., $R_F = 10\ \Omega$, $\delta_F = 0°$.

Fault behind the series capacitor

Figures 6.30 to 6.33 present the simulation results for the fault behind SCs located at F_2, at 0.6 p.u, with $R_F = 10\ \Omega$, $X_{CO} = 70\%$ of X_L, and $\delta_F = 10°$. Figure 6.30, and Figure 6.31, are the phase voltage, and current, measured at the relaying point. Figure 6.32 presents voltage drops across SCs + MOVs, while Figure 6.33 shows the fault current distribution among the SCs and MOVs branch.

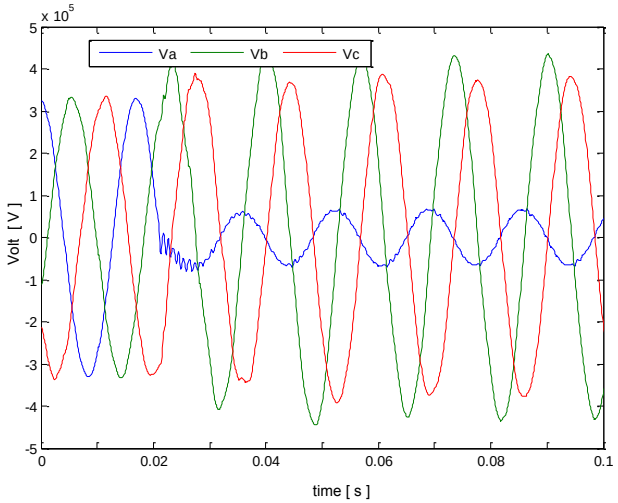

Figure 6.30: Phase voltage at terminal S.

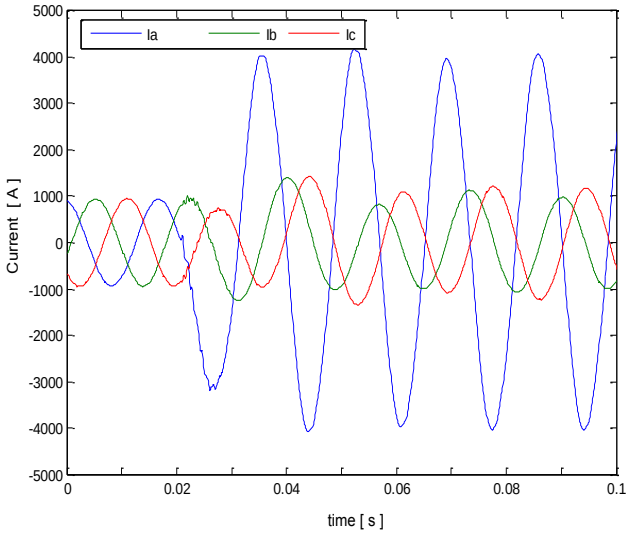

Figure 6.31: Phase current at terminal S.

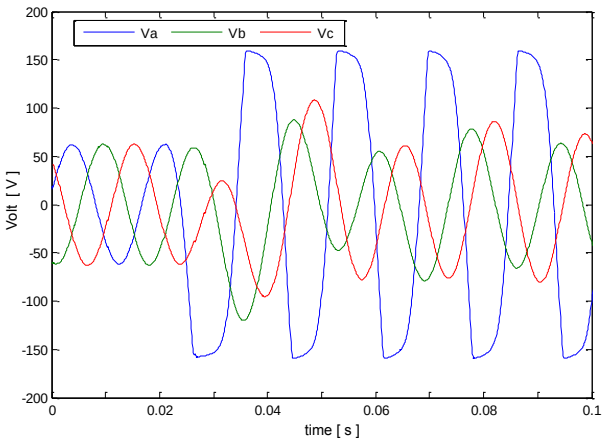

Figure 6.32: Voltage drops across SCs + MOVs.

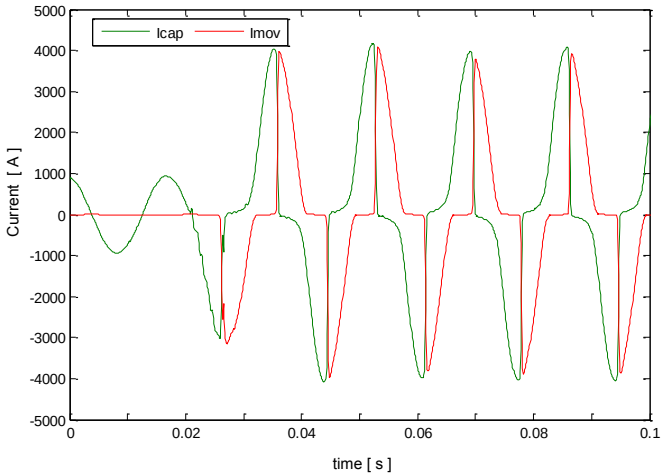

Figure 6.33: Distribution of the phase A fault current among SCs (Icap) and MOVs (Imov) brance.

Figure 6.34 is the tracing, in time, of measured impedance for the fault behind SCs located at F_2, at 0.75 p.u, with $R_F = 10\ \Omega$, and $\delta_F = 0°$. The simulation shows how the error impedance, contributed by SCs and MOVs, also affects the measured fault loop impedance, $\underline{Z}_m$. However, relating to Figure 6.28(b) the calculated fault impedance, $\underline{Z}_m$, at this location could be not fixed, since the value of resistance, R'_C, and X'_C, depends on the current, $\underline{I}_S$. Hence, for the fault simulated at 0.75 p.u., which is close to the border of zone 1, the error will cause the relay to see the fault in zone 2 (see Figure 6.34).

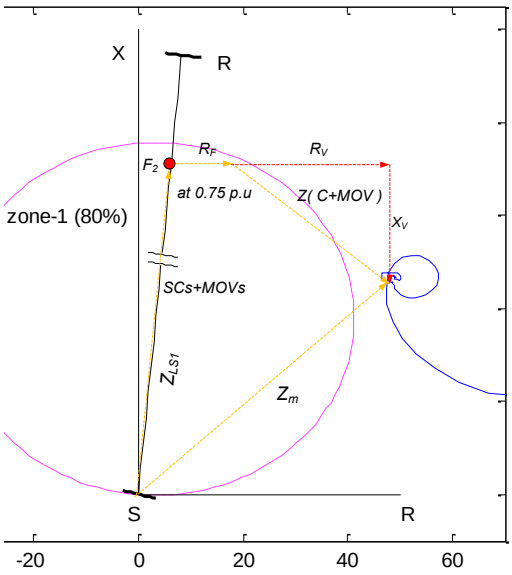

Figure 6.34: Fault Impedance tracking for the fault F_2 at 0.75 p.u., $R_F = 10\ \Omega$, $\delta_F = 0°$.

Due to the impact of uncertain factors, which can lead to uncertainty in the calculation of fault impedance, in Table 6.4 we specify the intervals of variation of the selected parameters. To illustrate the effect of the uncertainty parameter on the algorithm performance, two different fault locations are simulated in front of the SCs and behind the SCs (i.e., the fault at F_1 and F_2) with 500 random samples from the factor space for each fault location. The fault impedance is estimated by the IED algorithm for each sample which is indicated by '+' in Figure 6.35(a), and Figure 6.35(b). The effect of the uncertain factors on the impedance measured in three different locations can be studied as follows: the first three fault locations in 0.1, 0.3, and 0.5 p.u., are the faults simulated in front of the SCs, as shown in Figure 6.35(a). It can be seen how the uncertain factors propagate the fault impedance measurement. The presence of SCs does not affect the fault impedance calculation. However, due to the faults being in front of the SCs, the relaying point still sees the fault in zone 1. However, for the faults behind the SCs, that is, for the second three fault located at 0.6, 0.8, and 1 p.u., the presence of SCs + MOVs will affect the error in the fault impedance measurement. In this condition, the zone 1 setting can be underreaching for the fault simulating in, for example, 0.8 p.u. Effect of uncertain factors on the fault impedance calculations for the faults in 0.8 p.u., shown in blue, indicate that the relaying point can see the fault in zone 2, while for the fault in 1 p.u., the relaying point can see the fault in zone 1, or even in zone 3, for the fault in zone 2.

Table 6.4: Uncertain factors and their assumed intervals of variation that are affecting fault impedance measurements for the single-phase to ground faults in Figure 6.27.

Uncertain parameter	Description	Variation interval
x_1	R_F	[0 ;10] Ω
x_2	δ_F	[-10 ; 10] deg.
x_3	$Re\{\underline{Z}_{0S}\}$	[2.097 ; 2.563] Ω
x_4	$Im\{\underline{Z}_{0S}\}$	[24.12 ; 29.48] Ω
x_5	$Re\{\underline{Z}_{1S}\}$	[1.179 ; 1.441] Ω
x_6	$Im\{\underline{Z}_{1S}\}$	[13.5 ;16.5] Ω
x_7	$Re\{\underline{Z}_{0R}\}$	[2.097 ; 2.563] Ω
x_8	$Im\{\underline{Z}_{0R}\}$	[24.12 ; 29.48] Ω

x_9	$Re\{\underline{Z}_{1R}\}$	[1.179 ; 1.441] Ω
x_{10}	$Im\{\underline{Z}_{1R}\}$	[13.5 ;16.5] Ω
x_{11}	$Re\{\underline{Z}_{1LS}\}$	[3.72 ; 4.53] Ω
x_{12}	$Im\{\underline{Z}_{1LS}\}$	[42.52 ; 51.975] Ω
x_{13}	$Re\{\underline{Z}_{0LS}\}$	[37.125 ; 45.375] Ω
x_{14}	$Im\{\underline{Z}_{0LS}\}$	[138.645 ; 169.455] Ω
x_{15}	$Re\{\underline{Z}_{1LR}\}$	[3.72 ; 4.53] Ω
x_{16}	$Im\{\underline{Z}_{1LR}\}$	[42.52 ; 51.975] Ω
x_{17}	$Re\{\underline{Z}_{0LR}\}$	[37.125 ; 45.375] Ω
x_{18}	$Im\{\underline{Z}_{0LR}\}$	[138.645 ; 169.455] Ω
x_{19}	X_{CO}	[0 ; 66.15] Ω

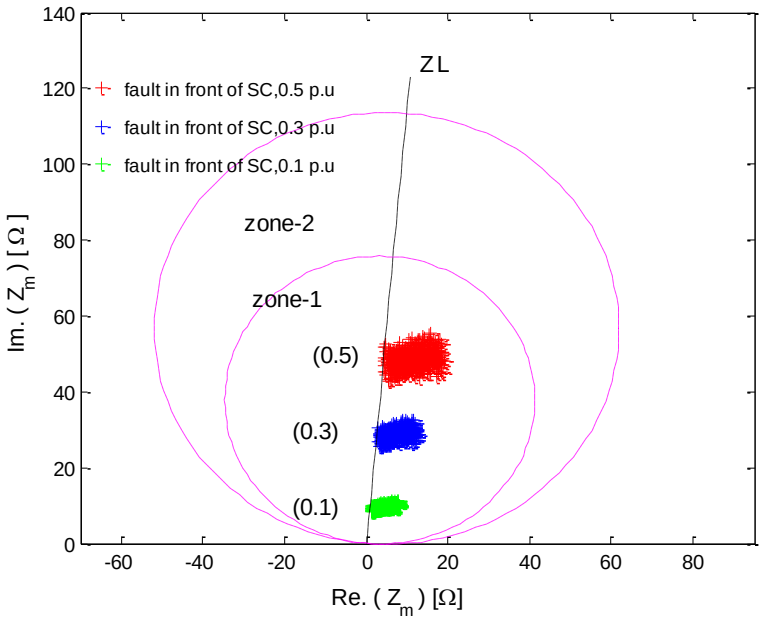

(a)

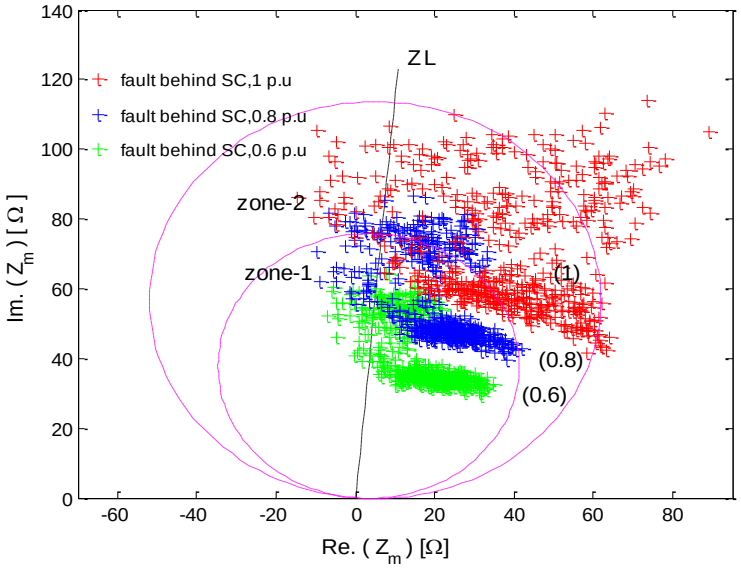

(b)

Figure 6.35: Fault impedance measured for all samples of the input factors, $\mathbf{x} \in \boldsymbol{R}^{19}$, generated according to the random sampling method (total of 500 samples) for three different fault locations (a) when the fault is simulated in front of the SCs, (b) when the fault is simulated behind the SCs.

6.4.3. Test Result and Discussion

Phase A to ground faults have been simulated at different locations in the protected transmission line of Figure 6.27 using the DIgSILENT software environment, and for possible variations of factors, that are assumed uniformly distributed within the interval specified in Table 6.4. The faults were simulated in front of the SCs and behind the SCs. The uniformly distributed points in the factor space were tested to see the performance of the fault impedance measurement function of the IED, and the SEL-421 model, which is implemented in DIgSILENT PowerFactory. These points were designed using the SIMLAB software environment according to the Morris method and Sobol's quasi-random sequence. SIMLAB is also used to compute all statistics and sensitivity measures according to the GSA methodology.

Figure 6.36 is the typical result using the Morris factor screening method for only one distance fault simulated in front of the SCs as well as behind the SCs. These results are presented as standard deviation versus mean value for all elementary effects. These statistics are computed using 190 samples, which is considered sufficient for this number

of factors [16]. A large mean value indicates a corresponding factor's importance, while a large variance suggests that the impact of a factor, together with other factors, is important (i.e., interaction effect). In Figure 6.36(a), we can identify the following factors as dominant: x_1, x_2, x_{12}, x_{14}, and x_{19}, while dominant factors in Figure 6.36(b), are identied as: x_1, x_2, and x_{19}. Details of the analysis for other fault locations are not reported here but the conclusion is that the selected 5 factors for the fault at 0.4 p.u. (i.e., fault in front of the SCs), and 3 factors for the fault at 0.8 p.u. (i.e., fault behind the SCs), are the most important for all fault locations. In Figure 6.36(a), the factor, x_{14}, has the largest mean of its elementary effect, which indicates that the measurement algorithm is most sensitive to the uncertainty of this factor. In addition, x_{14} has large variance of its elementary effect, and therefore, we can conclude that the contribution of x_{14} to the measurement error variance is not only through its own variability but also via its interaction with other factors.

The Morris method reduced the factor space dimension from 19 to 5 for the faults in front of the SCs and from 19 to 3 for the faults behind the SCs. This dimension can be successfully handled by the GSA based on quasi-random sampling. We simulated, using DIgSILENT, 10 phase A to ground faults at distances 0.1 p.u., 0.2 p.u., 0.3 p.u., 0.4 p.u., 0.5 p.u., 0.6 p.u., 0.7 p.u., 0.8 p.u., 0.9 p.u., and 1 p.u., for the protected line in Figure 6.27. For each fault from 0.1 to 0.5 p.u., and from 0.6 to 1 p.u., we varied 5 and 3 dominant factors respectively. A large number of cases are simulated in SIMLAB according to the quasi-random sampling scheme. For those simulated cases, we computed the performance index, i.e., the absolute value of the difference between true and estimated values, for the SEL-412 fault impedance measurement function. The sensitivity indices computed in SIMLAB are shown in Figure 6.37, and Figure 6.38. The conclusions from this analysis are:

- Fault resistance, $R_F(x_1)$, has the highest impact on the uncertainty of the fault impedance measurement for almost all of the fault locations. The impact is more prominent for the faults close to the beginning and end of the line.
- Impact of the zero-sequence impedance, $Im\{\underline{Z}_{0LS}\}$ (x_{14}), is the second largest and it is the highest for the faults around the middle of the line,
- Impact of the load flow angle, δ_F(x_2), the positive-sequence line impedance, $Im\{\underline{Z}_{1LS}\}$ (x_{12}), and capacitive reactance, X_C(x_{19}), will grow as the distance to the

fault approaches the SCs, but for the fault behind the SCs, the effect of the capacitive reactance, $X_C(x_{19})$, is absolutely dominant.

- For the faults in front of the SCs, the effect of all interactions between the factors increase, but the effect is dominated from the interaction between R_F, and $Im\{\underline{Z}_{0LS)}\}$ (x_{14}).
- For the faults behind the SCs, the dominant effect is from the interaction between R_F, and $X_C(x_{19})$. However, this effect will decrease as the distance to the fault approaches the end of the line, except for the fault at 1 p.u., where the interaction between R_F, and $\delta_F(x_2)$, is dominat.

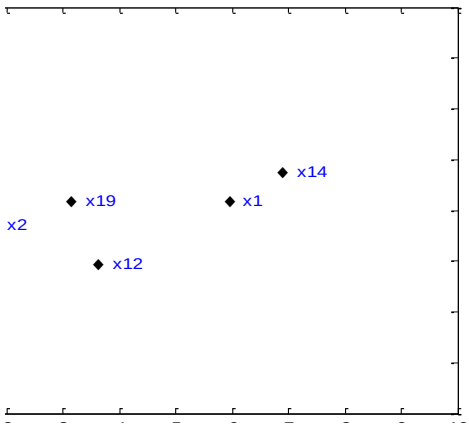

(a)

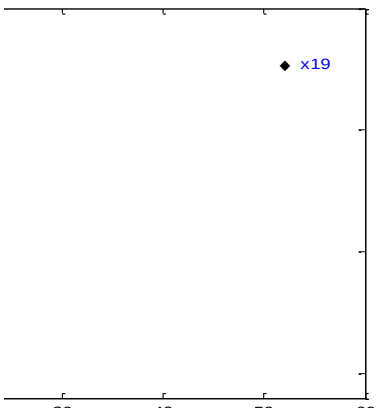

(b)

Figure 6.36: Results of the Morris factor screening method: (a) for a single-phase short circuit at 0.2 p.u. (in front of the SCs), (b) 0.8 p.u. (behind the SCs).

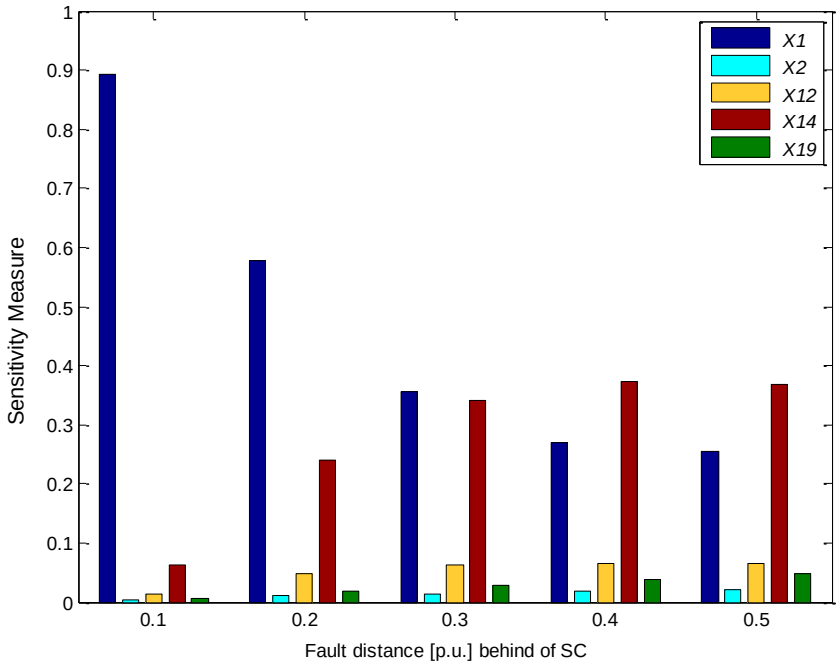

(a)

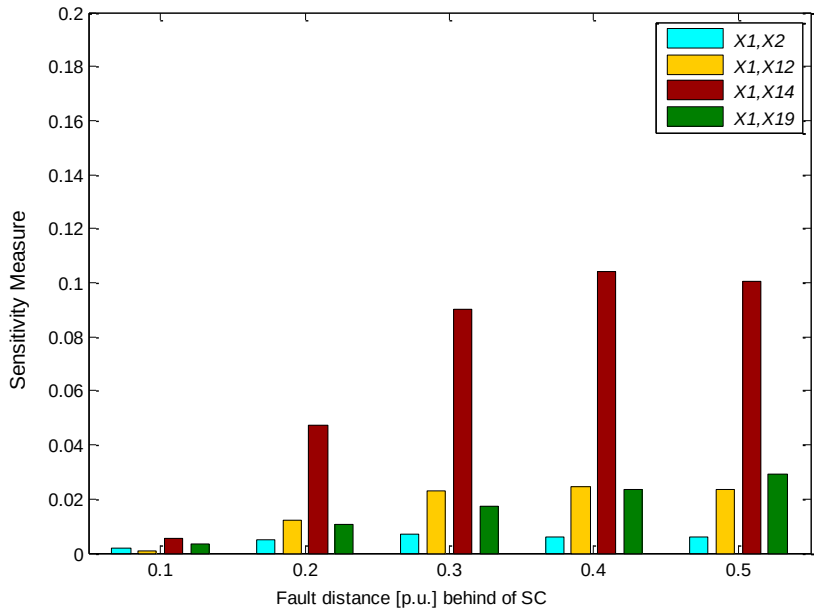

(b)

Figure 6.37: Sensitivity indices in function of the fault position obtained by using the GSA procedure for four-dimensional factor space:
(a) Main effects, (b) Interaction effects.

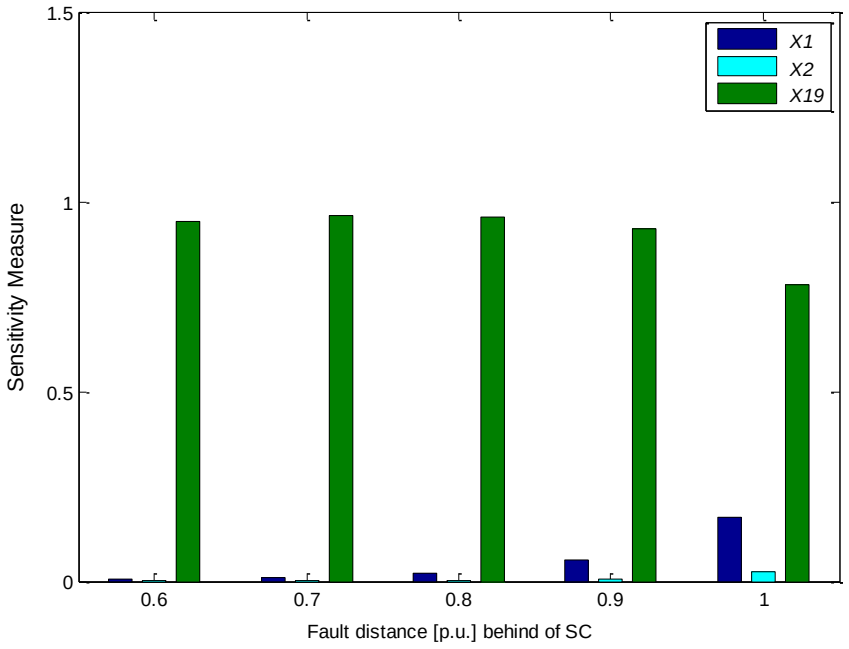

(a)

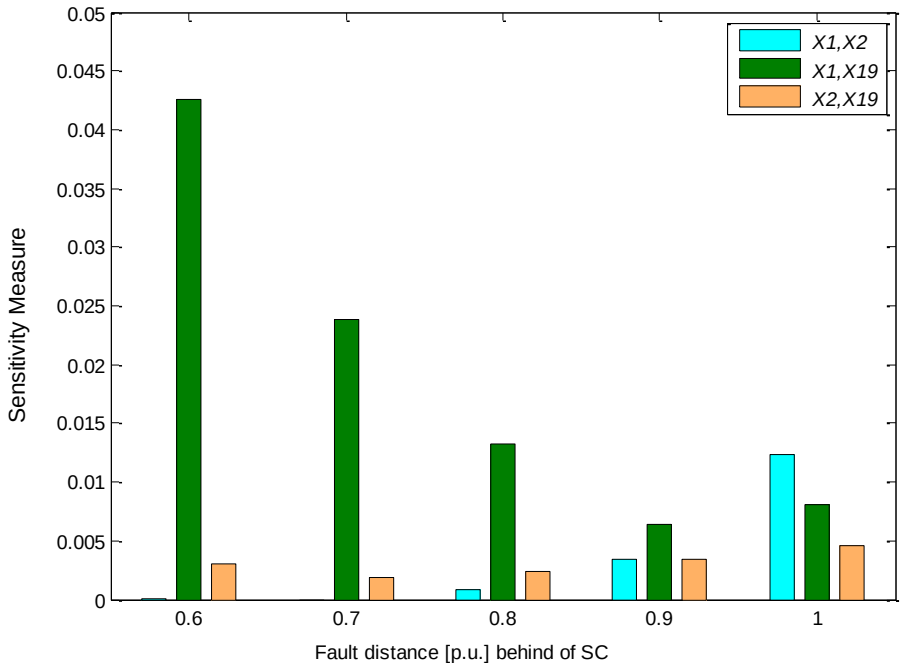

(b)

Figure 6.38: Sensitivity indices in function of the fault position obtained by using the GSA procedure for three-dimensional factor space:
(a) Main effects, (b) Interaction affects.

6.5. Conclusions

In this chapter the systematic method for the sensitivity analysis study of the fault impedance measurement function, in the context of lines with two sources, parallel line circuits, three-line lines, and lines with series compensation, has been presented. The method is based on the analysis of the measuring error variance of the IED algorithm, which is affected by the uncertainty of numerous parameters (i.e., factors). The zero-sequence mutual coupling in parallel line-circuits, remote current infeed in three-terminal line, and the effect of series compensation in lines with a series capacitor are treated as additional problem in assessing the relay performance.

The main important points that can be concluded from this chapter are:

- One-ended impedance-based fault distance calculations produce intolerable errors in some cases. This error could be caused by factors that impact the calculation of the apparent fault impedance. The factors are: fault resistance, inception angle, system infeed, line impedance, source impedance, and zero-sequence compensation.
- Fault resistance R_F, nearly has the highest impact on the uncertainty of the fault impedance measurement. Furthermore effect of fault resistance interaction with inception angle for the faults close to the remote-side R is significant.
- Additional factors, such as zero-sequence mutual coupling effect, current infeed from the tapped line, and the effect of series compensation, will contribute to the performance of fault impedance measurement.
- The Morris factor screening method has been used to eliminate non-influential factors, and the dimension of the factor space was reduced for the presented case studies. The full GSA, based on quasi-random sampling of the factor space, was performed afterwards to clearly identify which factors and their interactions will affect the impedance measurements for single phase short-circuits on various locations and in different case studies.
- The testing methodology was implemented in two software environments: DIgSILENT, where all system simulations and measurements were carried out, and

IEDs defined using SEL-421 functions; SIMLAB, where sampling sequences were generated and sensitivity measures calculated. The proposed methodology is very useful in application testing when performance of different IEDs needs to be compared.

Chapter 7

Conclusions

The development of the fault impedance measurement algorithms for transmission line protection has been a subject of interest. The fault impedance algorithm uses as inputs voltage and current signals measured from secondary parts of CT and CVT located at local terminals on the line. This is a difficult task since the apparent fault impedance, calculated using the one-ended technique (i.e. non-pilot distance relay), could be influenced by factors such as fault resistance, inception angles, variations in the parameters of the line, and so on. Additional factors may also contribute, for example: the mutual coupling in parallel lines, the current infeeds from the multiterminal systems, and a transmission line with series capacitor. These factors may contribute additionaly to the fault impedance calculation error.

A comprehensive, high-quality, performance evaluation of power system protection has been provided using a computer simulation, which combines the power system and relay protection algorithms. A protection system simulation is a valuable preliminary step for investigating the relay performance, using statistical and sensitivity analysis due to input factor uncertainty.

DIgSILENT and SIMLAB are two software tools used in development of the methodology proposed in this thesis. DIgSILENT is applicable for power system protection and distance relay modelling and provides the ability to vary the value of model parameters during the power system simulation. On the other hand, SIMLAB is used to generate the uncertain parameters samples and to calculate the sensitivity indices for the performance analysis of fault impedance estimation algorithms. Another important tool that makes the automated analysis feasible is the use of DPL scripting language provided by DIgSILENT. It is used to interface DIgSILENT and SIMLAB and to automate all simulation tasks. This thesis accomplished the following objectives:

1. The first objective was to design a systematic method for testing the distance relay function. The method is based on the combination between two software packages, DIgSILENT, and SIMLAB. The performance of the distance relay function, which is affected by uncertain factors, and the complexity of the power network, where the distance relay is implemented, is measured based on the analysis of variance for the output of the model. For analysis purposes, a statistical approach is required for calculating the sensitivity indices of the distance relay function.
2. The second objective was to implement the global sensitivity technique, to analyse performance of the measurement algorithm. The Sobol's technique allows investigation of the effects of the main factors, and the interactions between factors, on the performance of the model, while the Morris method is used prior to the Sobol's technique in order to remove unimportant factors.
3. The third objective was to model the power system and integrate the distance relay model in DIgSILENT. The flexibility of the parametrized model, and the ability to use the SEL-421 distance relay model, are the main reasons for using this tool.
4. The fourth objective was to integrate the two tools, DIgSILENT and SIMLAB. The various functions of the tools are required in this project to enable systematic testing. The DPL scripting language is used to interface the two tools. DPL scripting was used to automate the simulation by reading samples and calculating the performance indices.

This thesis proposes a novel systematic sensitivity analysis of an impedance measurement function implemented in an IED. The intention is to use this analysis as a part of the

application testing procedure. It is well known that the fault impedance measurement is affected by a number of uncertain factors, such as fault resistance, and inception angle, etc. as well as the additional impact from zero-sequence mutual coupling, current infeed from the tapped line, and the effect from series compensation.

Until now, the impact of these factors has been investigated by varying one factor at a time, and keeping all other factors fixed at some nominal value. As an improvement to this approach, we proposed a sensitivity analysis based on simultaneously varying all factors, i.e., we explore the factor space completely by using a realistic values in the range of distribution for the factors. In this way, we are able to analyse not only the measurement function sensitivity to individual factors but also sensitivity to the combined uncertainty of two or more factors. To span the whole factor space, as required in the analysis, we use multidimensional sampling based on the Sobol's Quasi-Random sequence. This approach converges faster than pseudorandom sampling. Still, the number of samples required to obtain accurate sensitivity measures will be prohibitively high for high dimensions of factor space. Therefore, we initially perform the procedure, one factor at a time, to identify factors with no impact and reduce the dimension of the factor space. Such a hybrid approach makes the procedure feasible, not only for testing of a simulated IED measurement function (as shown in the thesis), but also for the physical testing of an IED using an injection test set.

The thesis describes the software environment required to perform the proposed analysis and uses specific examples of different networks (e.g. a single line with two sources, parallel circuits, transmission lines with a tapping line, and lines with series compensation) to demonstrate how to perform the analysis and what kind of results we can obtain. The procedure is fully automated by using the DIgSILENT Programming Language (DPL). The DIgSILENT EMT transmission line simulation is integrated with the SIMLAB software, which generates quasi-random samples and performs analysis of output variance. The variance is used to compute sensitivity measures. To conclude: the proposed analysis is able to enhance the IED testing procedure, and therefore, is useful when selecting new IEDs for specific applications, and for performance investigations of existing IEDs.

Appendix A

Transmission Data

Investigating the performance of IED in different condition of circuits and factors have been tested and evaluated with the fault data (i.e., voltage and current signals) obtained from DIgSILENT PowerFactory to calculate the fault loop impedance measurement. The simulations for different faults location are tested in one line with two sources at both ends, double line, multiterminal line and line with series compensation. System parameters for different networks are gathered from the following Tables:

Table A.1: System parameters of the test one line with sources at both ends.

Equivalent system at terminal S ($\varphi = \delta_F°$)	$\underline{Z}_{1S}$	(1.74 + j19.92) Ω
	$\underline{Z}_{0S}$	(2.615 + j29.89) Ω
Equivalent system at terminal R ($\varphi = 0°$)	$\underline{Z}_{1R}$	(1.74 + j19.92) Ω
	$\underline{Z}_{0R}$	(2.615 + j29.89) Ω
Line SR	$\underline{Z}_{1L}$	(0.062 + j0.49) Ω/km
	$\underline{Z}_{0L}$	(0.23 + j1.53) Ω/km
	C_{1L}	8.9 nF/km

	C_{0L}	5 nF/km
Line length		100 km
System Voltage		400 kV
System frequency		50 Hz

Table A.2: System parameters of the test double-circuit line with sources at both ends.

Equivalent system impedance at terminal S ($\varphi = \delta_F$)	$\underline{Z}_{1S}$	(1.74 + j19.92) Ω
	$\underline{Z}_{0S}$	(2.615 + j29.89) Ω
Equivalent system impedance at terminal R ($\varphi = 0°$)	$\underline{Z}_{1R}$	(1.74 + j19.92) Ω
	$\underline{Z}_{0R}$	(2.615 + j29.89) Ω
Line impedance:	$\underline{Z}_{1L}$	(0.062 + j0.49) Ω/km
	$\underline{Z}_{0L}$	(0.23 + j1.53) Ω/km
	C_{1L}	8.9 nF/km
	C_{0L}	5 nF/km
Line length		100 km
System Voltage		400 kV
System frequency		50 Hz

Table A.3: System parameters of the test three-terminal line.

Equivalent system impedance at terminal S ($\varphi = \delta_F$)	$\underline{Z}_{1S}$	(1.74 + j19.92) Ω
	$\underline{Z}_{0S}$	(2.615 + j29.89) Ω
Equivalent system impedance at terminal R ($\varphi = 0°$)	$\underline{Z}_{1R}$	(1.74 + j19.92) Ω
	$\underline{Z}_{0R}$	(2.615 + j29.89) Ω
Equivalent system impedance at terminal T ($\varphi = 0°$)	$\underline{Z}_{1T}$	(1.74 + j19.92) Ω
	$\underline{Z}_{0T}$	(2.615 + j29.89) Ω
Line impedance:	$\underline{Z}_{1L}$	(0.062 + j0.49) Ω/km
	$\underline{Z}_{0L}$	(0.23 + j1.53) Ω/km
	C_{1L}	8.9 nF/km
	C_{0L}	5 nF/km
Line length : Line-1, Line-2, Line-3		100 km, 100 km, 70 km
Tapped line location		0.5 p.u.
System Voltage		400 kV
System frequency		50 Hz

Table A.4: System parameters of the test one line with series compensation.

Equivalent system impedance at terminal S ($\varphi = \delta_F$)	$\underline{Z}_{1S}$	(1.31 + j15) Ω
	$\underline{Z}_{0S}$	(2.33 + j26.8) Ω
Equivalent system impedance at terminal R ($\varphi = 0°$)	$\underline{Z}_{1R}$	(1.31 + j15) Ω
	$\underline{Z}_{0R}$	(2.33 + j26.8) Ω
	$\underline{Z}_{0T}$	(2.615 + j29.89) Ω
Line impedance	$\underline{Z}_{1L}$	(0.03+ j0.315) Ω/km
	$\underline{Z}_{0L}$	(0.275 + j1.027) Ω/km
	C_{1L}	13 nF/km
	C_{0L}	8.5 nF/km
Series Compensation	Series Capacitor	0.7 X_{1L}
	Position of The compensation bank	0.5 p.u.
MOV characteristic: $i_{MOV} = P\left(\frac{\underline{V}_V}{\underline{V}_{REF}}\right)^q$	P	1 kA
	$\underline{V}_{REF}$	150 kV
	q	23
Line length : Line-1, Line-2, Line-3		100 km, 100 km, 70 km
Line line location		0.5 p.u.
System Voltage		400 kV
System frequency		50 Hz

Appendix B

DPL Implemention in DIgSILENT

B.1. The DPL Script Program

The DPL script program listed below is very important for automating tasks of simulation and fault impedance calculation. This developed script program serves the purpose of offering an interface between a power system simulation tool and GSA software.

!**!

The following script DPL program is for general purpose. The conten could be adjusted for the specific purpose such as for sensitivity analysis using Morris and Sobol's technique, and also for analysing the characteristic of the IED which is applied in different network condition.

!**!

object obj, res,Inc,Sim,Shc,Vac,ld,Comtrd,file;

double
x,A,D,B,C,E,pf,rf,F,B1,load,x1,x2,x3,x4,x5,x6,x7,x8,x9,x10,x11,x12,x13,x14,x15,x16,x17

```
,A1,A2,A3,AA,loc,zs,ko,rearth11,erpha11,zsr11,zsx11,zsro1,zsxo1,zrr11,zrx11,zrro1,zrxo
1,tower2;

int  Nvar, Nval, ix,iy,ires,D10,D20,D30,D40,D50,D60,D70,D80,D90,D100,R,error,k;
string  str;

D10=4.9313*1;
D20=4.9313*2;
D30=4.9313*3;
D40=4.9313*4;
D50=4.9313*5;
D60=4.9313*6;
D70=4.9313*7;
D80=4.9313*8;
D90=4.9313*9;
D100=4.9313*10;

R=D100;

!*** starting to simulate a fault located at 20% of the protected line *****!
fopen('C:\Users\NNG\Desktop\sample.txt','r',0);  ! read the sampled data
fopen('C:\Users\NNG\Desktop\result20','w',1);    ! save result

Info('Starting simulation of....');
for (k=1;k<501; k+=1)  !501 = example of a number of samples
{
ResetCalculation();
ClearOutput();

fscanf(0,'%f %f %f %f %f %f %f %f %f %f %f', x1,x2,x3,x4,x5,x6,x7,x8,x9,x10,x11);
                ! This command is to scan the parameters input, the number of parameters
                correspond to parameters that want to be investigated
Shc=GetCaseObject('EvtShc');
Shc:p_target=fault;
fault:i_shc=2;          ! type of fault: 0=3p-p,  1=2p-p,  2=1p-g,  3=2p-g
fault:i_pspgf=2;        ! 0 = phase a to g
fault:R_f=x1;           !  fault resistance
angle:phisetp=x2;       ! inception angle
zero:k0=x3;             ! zero sequence compensator

!source impedance zero sequence-S
zsro:R1=x4;
zsxo:X1=x5;
zsro:R0=x6;
zsxo:X0=x7;
zsro:R2=x4;
zsxo:X2=x5;
```

```
!source impedance zero sequence-R
zrro:R1=x8;  !positive sequence
zrxo:X1=x9;
zrro:R0=x10; ! zero sequnce
zrxo:X0=x11;
zrro:R2=x8;  !negative sequence
zrxo:X2=x9;

line:fshcloc=20;  ! fault location (%)

Inc=GetCaseObject('ComInc');
Inc.Execute();

Sim=GetCaseObject('ComSim');
Sim.Execute();

obj = GetCaseCommand('ComInc');
res = obj:p_resvar;
LoadResData(res);
Nvar = ResNvars(res);
Nval = ResNval(res,0);
!printf('Nvar=%d Nval=%d', Nvar, Nval);
iy = 0;
!iy1 = 1;
!iy 2= 2;
!iy 3= 3;
!iy 3= 4;
ix = 0;
while (ix<Nval) {            ! Nvar=2
GetResData(x, res,ix,iy);
!GetResData(x1, res,ix,iy1);
!GetResData(x2 res,ix,iy2);
!GetResData(x3, res,ix,iy3);
!GetResData(x4, res,ix,iy4);
ix += 1;
!fprintf(1,'%f' %f' %f  ...',x,x1,x2, ...);
}
error=abs(x-D20)*100/R;
fprintf(1,'%f',error);     ! print last value of all cycles
 }
fclose(0);
fclose(1);

!*** starting to simulate a fault located at 40% of the protected line *****!
fopen('C:\Users\NNG\Desktop\sample.txt','r',0);  ! read the sampled data
fopen('C:\Users\NNG\Desktop\result40','w',1);    ! save result

Info('Starting simulation of....');
```

```
for (k=1;k<121; k+=1)  !121 = example of a number of samples

{
ResetCalculation();
ClearOutput();

fscanf(0,'%f %f %f %f %f %f %f %f %f %f %f', x1,x2,x3,x4,x5,x6,x7,x8,x9,x10,x11);
Shc=GetCaseObject('EvtShc');
Shc:p_target=fault;
fault:i_shc=2;  ! type of fault: 0=3p-p,  1=2p-p,  2=1p-g,  3=2p-g
fault:i_pspgf=2;      ! 0 = phase a to g
fault:R_f=x1;         ! Rf fault resistance
angle:phisetp=x2;     ! inception angle
zero:k0=x3;           ! zero sequence compensator

!source impedance zero sequence-S
zsro:R1=x4;
zsxo:X1=x5;
zsro:R0=x6;
zsxo:X0=x7;
zsro:R2=x4;
zsxo:X2=x5;

!source impedance zero sequence-R
zrro:R1=x8;  !positive sequence
zrxo:X1=x9;
zrro:R0=x10; ! zero sequnce
zrxo:X0=x11;
zrro:R2=x8;  !negative sequence
zrxo:X2=x9;

line:fshcloc=40;  ! fault location (%)

Inc=GetCaseObject('ComInc');
Inc.Execute();

Sim=GetCaseObject('ComSim');
Sim.Execute();

obj = GetCaseCommand('ComInc');
res = obj:p_resvar;
LoadResData(res);
Nvar = ResNvars(res);
Nval = ResNval(res,0);
!printf('Nvar=%d Nval=%d', Nvar, Nval);
iy = 0;
!iy1 = 1;
!iy 2= 2;
```

```
!iy 3= 3;
!iy 3= 4;
ix = 0;
while (ix<Nval) {            ! Nvar=2
GetResData(x, res,ix,iy);
!GetResData(x1, res,ix,iy1);
!GetResData(x2 res,ix,iy2);
!GetResData(x3, res,ix,iy3);
!GetResData(x4, res,ix,iy4);
ix += 1;
!fprintf(1,'%f' %f' %f  ...',x,x1,x2, ...);
}
error=abs(x-D40)*100/R;
fprintf(1,'%f',error);     ! print last value of all cycles
 }
fclose(0);
fclose(1);
```

!*** the comment can be continued for the next fault location ****!

B.2. The DPL Command Object

The DPL command object is to hold a reference to a remote DPL command when it is not a root command. Figure B2 shows an example of a referring command, since its"DPL script" reference is to remote command.

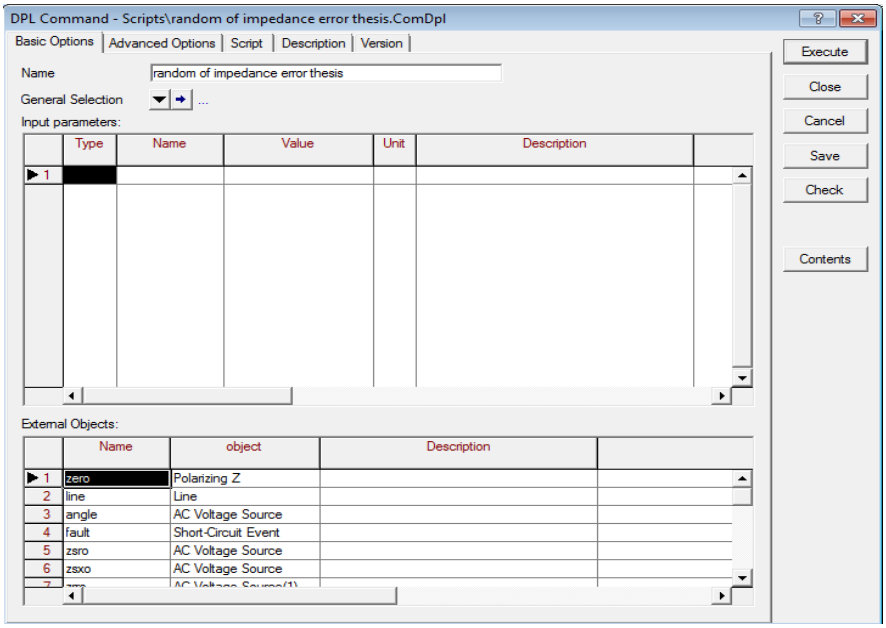

Figure B2: A DPL export script.

Appendix C

Sample File

This appendix is to show an example of the uncertain factors (i.e., sample) which is generated by SIMLAB.

```
0
190   ---   indicated a number of  total executions
18    ---   a total of factors to be executed
0
5.625    1.25      2.359125          29.145   1.228125
27.135   1.293625          14.06250.0251375         0.2874375
1.0141625         0.0271625         0.3189375         0.2578125

0.625    1.25      2.359125          29.145   1.228125
27.135   1.293625          14.06250.0251375         0.2874375
1.0141625         0.0271625         0.3189375         0.2578125
        ....
        ....
        ....
        ....
        ....

        18 Distributions:
        Uniform  ---  type of distribution facto value
        x1           ---  name of factor

        1 1
```

One group data to be executed

Second group data

```
0 10        1  ---  range of distributed factor value

Uniform
x2

1 1
-10         10         1

Uniform
x3

1 1
2.097       2.563      1
....
....
....
```

References

[1] N. Rohadi and R. Živanović, "A Method for Sensitivity Analysis of Impedance Measurement," *Journal of Electrical Engineering, Springer,* 2013.

[2] L. C. Wu, *et al.*, "Modeling and Testing of a Digital Distance Relay MATLAB/SIMULINK," in *Power Symposium*, Proceeding of *37th Annual,* North America, Oct. 2005, pp. 253-259.

[3] M. Kezunovic and J. Ren, "New Test Methodology for Evaluating Protective Relay Security and Dependability," in *IEEE Power and Energy Society General Meeting-Conversion and Delivery of Electrical Energy in the 21st Century*, 2008, pp. 1-6.

[4] M. Kezunovic and B. Kasztenny, "Design Optimization and Performance Evaluation of the Relaying Algorithms, Relays and Protective Systems Using Advanced Testing Tools," in *IEEE International Conference on Power Industry Computer Applications*, 1999, pp. 309-314.

[5] J. Schilleci, *et al.*, "Use of Advanced Digital Simulators for Distance Relay Design and Application Testing," in *Texas A&M 54 th Annual Relay Conference for Protective Relay Engineers*, College Station, TX, 2001.

[6] M. Kezunovic, *et al.*, "An advanced Method for Testing of Distance Relay Operating Characteristic," *Power Delivery, IEEE Transactions on,* vol. 11, 1996, pp. 149-157.

[7] N. Rohadi and R. Zivanovic, "Sensitivity Analysis of Impedance Measurement Alogrithms Used in Distance Protection," in *TENCON 2011, IEEE Region 10 Conference*, 2011, pp. 995-998.

[8] N. Rohadi and R. Zivanovic, "Sensitivity Analysis of Fault Impedance Measurement Algorithm Used in Protection of Three-Terminal Lines," in *AUPEC 2012-IEEE*, Bali, Indonesia, 2012, pp. 1-6.

[9] M. N. Ibrahim, *et al.*, "Methodology for Automated Testing of Transmission Line Fault Locator Algorithms," in *Power Engineering Conference, 2009. AUPEC 2009. Australasian Universities*, 2009, pp. 1-4.

[10] R. Zivanovic, "Evaluation of Transmission Line Fault-Locating Techniques Using Variance-based Sensitivity Measures," Presented at *The 16th Power System Computation Conference (PSCC'2000)*, Glasgow, Scotland, July 2008.

[11] M. Sachdev and T. Sidhu, "Modelling Relays for Use in Power System Protection Studies," *Proceedings of IEE Development in Power System Protection*, 2001, pp. 523-526.

[12] A.Apostolov and B.Vandiver, "Testing of Multifunctional Distance Protection Relays," Presented at *The IEEE Power Engineering Society General Meeting*, Tampa, FL, 24-28 June 2007.

[13] N. Zhang, *et al.*, "Transient Based Relay Testing: A New Scope and Methodology," Presented at *The 13th IEEE Mediteranean Electrotechnical Conf.*, Torremolinos, Spain, May 2006, pp. 1110-1113.

[14] A. Saltelli, *Global Sensitivity Analysis: The Primer*. Wiley-Interscience, 2008.

[15] Schweitzer Engineering Laboraroties, *SEL-421 Relay Protection and Automation System User's Guide,*. USA, 2007. [Online]. Available: http://www.selinc.com.

[16] A. Saltelli, *Sensitivity Analysis in Practice: A Guide to Assessing Scientific Models*: John Wiley & Sons Inc, 2004. [Online]. Available: http://www.jrc.ec.europa.eu/.

[17] DIgSILENT, *User' Manual*, DIgSILENT PowerFactory Version 14.0, Gomaringen, Germany, 2008. [Online]. Available: http://www.digsilent.de.

[18] N. Rohadi and R. Živanović, "Sensitivity Analysis of A Fault Impedance Measurement Algorithm Applied in Protection of Parallel Transmission Lines," in *APSCOM -2012, The 9th International Conference on Advances in Power System Control, Operation and Management,* Hongkong , Nov. 2012.

[19] K. Zimmerman and D. Costello, "Impedance-based fault location experience," in *2005 58th Annual Conference for Protective Relay Engineers* 2005, pp. 211-226.

[20] J. Roberts, *et al.*, "Z= V/I does not make a distance relay," in *Schweitzer engineering laboratories, inc. Pullman, Washington. 20th Annual Western Protective Conference*, 1993, pp. 19-21.

[21] S. Nikolovski, *et al.*, "Numerical Simulation of Distance Protection on Three Terminal High Voltage Transmission Lines," *Advanced Engineering,* vol. 2, 2009.

[22] G. Alsthom, "Protection Relays Application Guide," *GEC Alsthom Measurement limited, Erlangen, GEC Englang, Third edition,* 1990.

[23] P. M. Anderson, *Power System Protection*: McGraw-Hill, IEEE Press, 1999.

[24] G. E. Alexander, *et al.*, "Ground Distance Relaying: Problems and Principles," in *Nineteenth Annual Western Protective Relaying Conference*, Spokane, Washington, October, 1991.

[25] E.O.Schweitzer and j.Robert III, "Distance Relay Element Design," in *in 19th Annual Western Protection Relay Conference*, Spokane, WA, 1992.

[26] J. Andrichak and G. Alexander, "Distance Relay Fundamentals," *General Electric Co Technical Papers,* 1998.

[27] ALSTOM T&D Energy Automation & Information, "Alstom," *T&D Energy Automation and Information,* 2002.

[28] D. Novosel*, et al.*, "Problems and Solutions for Microprocessor Protection of Series Compensated Lines," in *Sixth Internation Conference on Development in Power System Protection*, Nottingham, UK, 1997, pp. 18-23.

[29] H. J. Altuve*, et al.*, "Advances in Series-Compensated Line Protection," in *Protective Relay Engineers, 2009 62nd Annual Conference for*, 2009, pp. 263-275.

[30] Y. Hu*, et al.*, "An Adaptive Scheme for Parallel-line Distance Protection," *Power Delivery, IEEE Transactions on,* vol. 17, 2002, pp. 105-110.

[31] A. Jongepier and L. Van der Sluis, "Adaptive Distance Protection of A Double-circuit Line," *Power Delivery, IEEE Transactions on,* vol. 9, 1994, pp. 1289-1297.

[32] Y. Xia*, et al.*, "High-resistance Faults on A Multi-terminal Line: Analysis, Simulated Studies and An Adaptive Distance Relaying Scheme," *IEEE Transactions on Power Delivery,* vol. 9, 1994, pp. 492-500.

[33] I. W. Group, "Protection Aspects of Multi-terminal Lines," *IEEE Special Publication,* vol. 79, 1979.

[34] W.-K. Chen, *The Circuits and Filters Handbook, (Five Volume Slipcase Set)*: CRC, 2002.

[35] A. Johns and S. Jamali, "Accurate Fault Location Technique for Power Transmission Lines," in *Generation, Transmission and Distribution [see also IEE Proceedings-Generation, Transmission and Distribution], IEE Proceedings*, 1990, pp. 395-402.

[36] C.-H. Kim, *et al.*, "Educational Use of EMTP MODELS for The Study of A Distance Relaying Algorithm for Protecting Transmission Lines," *Power Systems, IEEE Transactions on,* vol. 15, 2000, pp. 9-15.

[37] DIgSILENT, "Measurement Filter Description," *DIgSILENT Technical Document,* March 2007.

[38] C. B. Rorabaugh, "Digital Filter Designer's Handbook," *New York: McGraw-Hill, Inc.,* 1993.

[39] B. Porat, *A Course in Digital Signal Processing* vol. 1: Wiley, 1997.

[40] M. S. Thomas and A. Prakash, "Modeling and Testing of Protection Relay IED," in *Power System Technology and IEEE Power India Conference, 2008. POWERCON 2008. Joint International Conference on*, 2008, pp. 1-5.

[41] DIgSILENT, "Digital measurement block," *DIgSILENT Technical Document,* December 2003.

[42] DIgSILENT, "Polarizing block," *DIgSILENT Technical Document,* March 2007.

[43] V. Cook, "Fundamental Aspects of Fault Location Algorithms Used in Distance Protection," in *Generation, Transmission and Distribution, IEE Proceedings C*, 1986, pp. 359-368.

[44] L. Eriksson, *et al.*, "An Accurate Fault Locator with Compensation for Apparent Reactance in The Fault Resistance Resulting from Remote-end Infeed," *Power Apparatus and Systems, IEEE Transactions on,* 1985, pp. 423-436.

[45] A. Wiszniewski, "Accurate Fault Impedance Locating Algorithm," in *Generation, Transmission and Distribution, IEE Proceedings C*, 1983, pp. 311-314.

[46] A. Wiszniewski, "Accurate Fault Impedance Locating Algortihm," *IEE Proceedings. Part C, Generation, Transmission and Distribution,* vol. 130, No.6, Nov.1983, p. 311-314.

[47] N. El Halabi, *et al.*, "Application of A Distance Relaying Scheme to Compensate Fault Location Errors due to Fault Resistance," *Electric power systems research,* vol. 81 , 2011, pp. 1681-1687.

[48] H.J. Altuve, *et al.*, "Advances in Series-compensated Line Protection," *35th Annual Western Protective Relay Conference,*Spokane, WA, Oct. 2009.

[49] M. Zellagui and A. Chaghi, "Impact of Series Compensation Insertion in Double HV Transmission Line on the Settings of Distance Protection," *International Journal of Scientific & Engineering Research*, Vol.2, Aug. 2011.

[50] J. L. V. D. Berg, "Protection Problems and Solutions Accociated with Series Compensated Transmission Lines," *Industrial Project IV*, Tech. Rep.,Technikon Pretoria.

[51] M. Sanaye-Pasand and H. Seyedi, "Simulation, Analysis and Setting of Distance Relays on Double Circuit Transmission Lines," in *Australasian Universities Power Engineering Conference, AUPEC*, 2003, pp. 177-183.

[52] D. Spoor and J. Zhu, "Selection of Distance Relaying Schemes when Protecting Dual Circuit Lines," in *Proc. Australasian Power Engineering Conf.,* Christchurch, New Zealand, 2003.

[53] A. Apostolov, *et al.*, "Protection of Double Circuit Transmission Lines," in *Proc. 60th Annu. Conf. Protective Relay Engineers*, 2007, pp.85-101.

[54] B. R. Bhalja and R. P. Maheshwari, "High-resistance faults on two terminal parallel transmission line: analysis, simulation studies, and an adaptive distance relaying scheme," *Power Delivery, IEEE Transactions on,* vol. 22, 2007, pp. 801-812.

[55] G. D. Rockefeller, *et al.*, "Adaptive Transmission Relaying Concepts for Improved Performance," *IEEE Transactions on Power Delivery,* vol. 3, Oct. 1988, pp. 1446-1458.

[56] M. Mir and M. Hasan Imam, "Limits to Zones of Simultaneous Tripping in Multi-Terminal Lines," in *Fourth International Conference on Developments in Power Protection*, Edinburgh, Apr. 1989, pp. 326-330.

[57] J. Horak, "Zero Sequence Impedance of Overhead Transmission Lines," in *Protective Relay Engineers, 2006. 59th Annual Conference for*, 2006, p. 11 pp.

[58] R. A. Rivas, "Overhead Transmission Lines and Underground Cables," Section 9, 2004. [Online]. Available: http:// www.magergy.com.

[59] H. El-Tamaly and H. Ziedan, "Sequence Impedances of Overhead Transmission Lines Carson's Method Versus Rudenberg's Method," in *Universities Power Engineering Conference, 2006. UPEC'06. Proceedings of the 41st International*, 2006, pp. 298-302.

[60] M. Reta-Herna´ndez, "Transmission Line Parameters,″ chapter 13, 2006. [Online]. Available: http://www.unioviedo.es/pcasielles/uploads/proyectantes/cosas_lineas.pdf.

[61] G. V. Tcheslavski, " Transmission Lines, " Lecture 9, 2008. [Online]. Available: http://www.ee.lamar.edu/gleb/power/Lecture%2009%20-%20Transmission%20lines.ppt

[62] Y. Hu*, et al.*, "Improving parallel line distance protection with adaptive techniques," in *Proc. 2000 Power Engineering Society Winter Meeting,*vol.3,Jan. 2000,. pp. 1973-1978.

[63] A. Funk and O. Malik, "Impedance Estimation Including Ground Fault Resistance Error Correction for Distance Protection," in *International Journal of Eelectrical Power & Energy Systems*, 2000, pp. 59-66.

[64] IEEE Strandard PC37.114, "Draft Guide For Determining Fault Location on AC Transmission and Distribution Lines," 2004.

[65] D. A. Tziouvaras, *et al.*, "New Multi-ended Fault Location Design for Two-or Three-terminal Lines," *Inst. Elect. Eng. Developments in Power System Protection*, no.479, 2001, pp. 395-398.

[66] L. Hulka, *et al.*, "Measurement of Line Impedance and Mutual Coupling of Parallel Lines to Improve The Protection System," in *20th International Conference on Electricity Distribution (CIRED)*, Prague, Czech Republic, 2009.

[67] D. L. Goldsworthy, "A linearized Model for MOV-protected Series Capacitors," *Power Systems, IEEE Transactions on,* vol. 2, 1987, pp. 953-957.

[68] J. Izykowski, *et al.*, "Fundamental Frequency Equivalenting of Series Capacitors Equipped with MOVs Under Fault Condition of A Series-compensated Line," in *Proceeding of the 8th International Symposium on Short-Circuit Currents in Power Systems*, Brussels, Belgium, October, 1998, pp. 13-18.

[69] J. Izykowski, *et al.*, "ATP-EMTP Investigation of Detection of Fault Position with Respect to The Compensating Bank in Series Compensated Line by Determining The Contents of DC Components in Phase Currents," in *International Conference on Power Systems Transients (IPST'09,),* Kyoto, Japan on June, 2009, pp. 3-6.

[70] M. D. Morris, "Factorial Sampling Plans for Preliminary Computational Experiments," *Technometrics,* vol.33, 1991, pp. 161-174.

[71] I. M. Sobol, "Sensitivity analysis for non-linear mathematical models," *Mathematical Modelling and Computational Experiment,* vol. 1, 1993, pp. 407–414.

[72] V. SIMLAB, "2.2, Simulation environment for Uncertainty and Sensitivity Analysis," *Developed by the Joint Research Center of the European Commission,* 2004.

[73] K. Petr, *et al.*, "Technique of uncertainty and sensitivity analysis for sustainable building energy systems performance calculations," in *Proc. of the 10th IBPSA Building Simulation Conf.*, Sept. 2007, pp. 629-636

[74] M. Poller, *et al.*, "Simulating The Steady State and Transient Response of Protective Relays," in *Developments in Power System Protection, 7th International Conf. on (IEE)*, 2001, pp.267-370.

[75] F. Campolongo, *et al.*, "An effective screening design for sensitivity analysis of large models," in *Environmental Modelling & Software*, 2007, pp. 1509-1518.

[76] M. N. Ibrahim and R. Zivanovic, "Factor-space dimension reduction for sensitivity analysis of intelligent electronic devices," in *TENCON 2011*, Bali, 2011, pp. 1035-1039.

[77] M. D. Morris, "Factorial sampling plans for preliminary computational experiments," *Technometrics,* vol. 33, 1991, pp. 161-174.

[78] F. Campolongo, *et al.*, "Enhancing the Morris Method, paper presented at Sensitivity Analysis of Model Output," 2005, pp. 369-379.

[79] L. Hulka, *et al.*, "Measurement of line impedance and mutual coupling of parallel lines to improve the protection system," in *20 th International Conference on Electricity Distribution (CIRED)*, Prague, Czech Republic, 2009, pp. 1-4.

[80] P. M. Anderson, "Transmission Line Mutual Inductance," in *Power system protection*, Wiley-IEEE Press, 1999.

[81] M.Mir and M.Imam, "A mathematical technique for the optimum reach setting of distance relays considering system uncertainties," *Electric power systems research,* 1989, pp. 101-108.

[82] K. Silva, *et al.*, "EMTP Applied to Evaluate Three-Terminal Line Distance Protection Schemes," in *International Conference on Power System Transients*, Lion, France, June 2007.

[83] G. Alexander and J. Andrichak, "Application of phase and ground distance relays to three terminal lines " *GE Protection and Control, Malvern, PA, GE-3964,* 1996.

[84] A. A. Cuello-Reyna*, et al.*, "Transient Performance for a Series-Compensation in a High Voltage Transmission System." [Online]. Available: http:// ece.uprm.edu

[85] J. Iżykowski, *Fault location on power transmission lines*: Oficyna Wydawnicza Politechniki Wrocławskiej, 2008.